

A

N72-10945

**NASA CONTRACTOR
REPORT**



NASA CR-1899

NASA CR-1899

**DEVELOPMENT OF CONTROL SYSTEMS
FOR SPACE SHUTTLE VEHICLES**

Volume I

*by C. R. Stone, T. W. Chase, B. M. Kiziloz,
E. D. Skelley, G. Stein, and M. D. Ward*

Prepared by

HONEYWELL, INC.

SYSTEMS AND RESEARCH CENTER

Minneapolis, Minn.

for George C. Marshall Space Flight Center

1. REPORT NO. NASA CR-1899	2. GOVERNMENT ACCESSION NO.	3. RECIPIENT'S CATALOG NO.	
4. TITLE AND SUBTITLE DEVELOPMENT OF CONTROL SYSTEMS FOR SPACE SHUTTLE VEHICLES Volume I		5. REPORT DATE October 1971	6. PERFORMING ORGANIZATION CODE
		8. PERFORMING ORGANIZATION REPORT # 14257-FR	
7. AUTHOR(S) C. R. Stone, T. W. Chase, B. M. Kiziloz, E. D. Skelley, G. Stein, M. D. Ward		10. WORK UNIT NO.	11. CONTRACT OR GRANT NO. NAS8-25181
9. PERFORMING ORGANIZATION NAME AND ADDRESS Honeywell, Inc. Systems and Research Center Minneapolis, Minnesota		13. TYPE OF REPORT & PERIOD COVERED CONTRACTOR REPORT	
		14. SPONSORING AGENCY CODE	
12. SPONSORING AGENCY NAME AND ADDRESS NASA Washington, D. C. 20546		15. SUPPLEMENTARY NOTES	
16. ABSTRACT <p>Control of winged two-stage space shuttle vehicles was investigated. Control requirements were determined and systems capable of meeting these requirements were synthesized. Control requirements unique to shuttle were identified. It is shown that these requirements can be satisfied by conventional control logics. Linear gain schedule controllers predominate. Actuator saturations require nonlinear compensation in some of the control systems.</p>			
17. KEY WORDS Covariance analysis, entry control system, control surface displacement, dynamic derivatives		18. DISTRIBUTION STATEMENT	
19. SECURITY CLASSIF. (of this report) Unclassified	20. SECURITY CLASSIF. (of this page) Unclassified	21. NO. OF PAGES 254	22. PRICE \$3.00

NOTICE

Because of a waiver initiated and signed in compliance with NASA Policy Directive (NPD) 2220.4, para. 5-b, the International System of Units of measurement has not been used in this document.

FOREWORD

This report fulfills the final reporting requirements for "Development of Control Systems for Space Shuttle Vehicles" performed under National Aeronautics and Space Administration Contract NAS8-25181. The program was conducted under the direction of John M. Livingston of the Aero-Astro Dynamics Laboratory, George C. Marshall Space Flight Center. The Honeywell Systems and Research Center work was managed by Dr. Grant B. Skelton with C. R. Stone as principal investigator. T. W. Chase was co-investigator.

The report is presented in two volumes. Volume I contains the ten sections for the main body of the report. Detailed derivations and data are presented in eight appendixes of Volume II.

Section I was developed by Drs. G. B. Skelton and E. E. Yore and Messrs. J. G. Rupert, T. W. Chase, R. K. Phelps, A. J. Pejsa and C. R. Stone. Sections II and III were prepared by C. R. Stone (covariance analyses) and T. W. Chase (conventional analyses).

M. D. Ward generated the covariance data and performed quadratic syntheses in these sections. T. W. Chase prepared Sections IV, V, and VI and Appendixes B, G, and H. Section VI was adapted from work performed by M. W. Reed. Dr. G. Stein prepared Section VII, C. R. Stone prepared Sections VIII, IX, and X, and Appendixes A, C, D, E, and F. E. D. Skelley synthesized the quadratic controllers and obtained the covariance results of Section XIII.

MSFC provided the trajectory, aerodynamic, and mass properties data for Vehicle B. Data for the North American orbiters 130G and 134C were used without restriction by permission of Mr. A. B. Kehlet of the North American-Rockwell Corporation. Messrs. Stone and Chase and Mrs. B. M. Kizilos estimated missing data by use of the DATCOM Handbook, slender body theory, and impact theory.

CONTENTS

	Page
SECTION I	
SUMMARY	1
Objective	1
Approaches	1
Results	1
Brief Summary	2
Pitch Launch	2
Lateral Launch	2
Orbiter Injection	4
Orbiter Pad Abort	4
In-Flight Orbiter Aborts	4
Orbiter Entry	5
Orbiter Subsonic Flight	5
Unpowered Orbiter Landings	5
Specification Type	5
Non-Specification Type	6
SECTION II	
LAUNCH PHASE PITCH CONTROL	7
Overview	7
Conventional Analyses	18
Covariance Analyses	34
Resolution of the Winds	35
Number of Winds	35
Gimbal Actuators	37
Accelerometer Location	37
Static Derivatives	37
Dynamic Derivatives	37
Gust Penetration	37
Axes	37
Reference Trajectories	38
Bending Moments	38
Conventional Controllers	38
Discussion	38
SECTION III	
LAUNCH PHASE LATERAL AXES CONTROL	50
Overview	51
Conventional Analyses	57
Stability Analyses	57
Analog Simulations	60
Covariance Analysis	80
Number of Winds	83
Gimbal Actuators	83
Gimbal Slewing	83
Accelerometer Location	83

		Page
	Gust Penetration	84
	Euler Angles	84
	Discussion	84
SECTION IV	ORBITER INJECTION	86
	The Models	86
	Discussion	86
SECTION V	DELTA WING ORBITER CONTROL FOR ABORT	86
	Summary and Conclusions	96
	Pad Abort Flyaway	98
	Preliminary Analysis of Abort Trajectories	106
	High Altitude Abort Simulation	106
	Conclusions	125
SECTION VI	DELTA WING ORBITER CONTROLS FOR REENTRY	128
	Summary	128
	Entry Control System (ECS)	128
	ACPS Requirements and Fuel Usage	130
	Effect of Vehicle Parameter Variations	131
	Control Surface Displacement and Rate Requirements	131
	Method for Blending TVC, Aero, and ACPS Control	136
	Concluding Remarks	138
SECTION VII	LATERAL HANDLING QUALITIES CAPABILITIES OF A STRAIGHT-WING ORBITER IN POST-ENTRY FLIGHT	139
	The Basic Airframe	139
	The Augmented Aircraft	142
	Flight Condition 9	157
	Flight Condition 11	157
SECTION VIII	ROLL POWER REQUIREMENTS FOR LANDING	196
	Technical Discussion	198
	Erratum	206
SECTION IX	UNPOWERED SHALLOW FINAL LANDING APPROACHES	210
SECTION X	CONCLUSIONS AND RECOMMENDATIONS	212
	Results	212
	Boost Pitch	212
	Boost Lateral	212
	Orbiter Injection	213
	Orbiter Entry	213

	Page
Pad Abort	213
In-flight Abort	213
Subsonic Lateral Handling Qualities	213
Roll Power Requirements	213
Shallow Approach Landing	214
Recommendations	214
REFERENCES	216

ILLUSTRATIONS

Figure		Page
1	Booster/Orbiter Launch Configuration	9
2	Trim Alpha and Delta	10
3	Maximum Perturbation n , $\bar{q}\alpha$, and δ	
4	Maximum Perturbation Bending Moments	12
5	Terminal Drift Rate	13
6	Terminal Drift	14
7	Sample of Vaughn/Skelton E-W March Wind	15
8	Locus of Short Period Roots	22
9	Eight Conventional Control Systems	24
10	Minimum Drift, Attitude Hold, and Three Load Relief Controls for a Statically Stable Vehicle	27
11	Minimum Drift versus Acceleration Load Relief, Showing Accelerometer Bias Effect	28
12	Minimum Drift and " $q\alpha$ " of Load Relief, with Bias on " $q\alpha$ " Sensor	29
13	Minimum Drift versus Acceleration Limiter for Load Relief	30
14	Bending Moments From Analog Simulations	31
15	Drift and Drift Rate From Analog Simulations	32
16	Angle of Attack and Gimbal Deflection at 64 Seconds From Analog Simulations	33
17	Mean Response	40
18	Response Covariance	43
19	Pitch Axis Gains	46
20	Maximum Gimbal Deflections	52
21	Maximum Inflight Loads	53
22	Terminal Drift Rate	54
23	Terminal Drift	55
24	Performance of Five Control Systems	61
25	Performance of Five Controls	62
26	Effect of Ailerons on Peak Differential Gimbal Deflection (δ_x) Required	64

27	Effect of Wind and Engine Failures with Minimum Drift Rate Control	66
28	Effects of Wind and Engine Failures on Minimum Drift Control	67
29	Effect of Integral Gain (T) on Scheduled Attitude plus Lateral Acceleration Control Response to Left Outboard Engine Failure	68
30	Effects of Integral Gain on Scheduled Attitude plus Lateral Acceleration Control in Wind and Left Outboard Engine Failure	69
31	Effect of Integral Gain (T) on Scheduled Attitude plus Lateral Acceleration Control Response to Right Outboard Engine Failure	70
32	Effects of Integral Gain on Lateral Acceleration Control in Wind and Right Outboard Engine Failure	71
33	Effect of Wind Biasing and Altitude of Peak Gust on Three Controls	72
34	Effect of Wind Biasing and Altitude of Peak Wind on Min Drift and Load Relief Controls	73
35	Effects of Integral and Proportional Gains on Lateral Acceleration Control	75
36	Effect of Integral Control and Accelerometer Gain on Scheduled Attitude plus A_y System	76
37	Effect of Accelerometer Bias on Load Relief Controller	77
38	Scheduled Min Drift $+Y_v$, with Manual Control of the Drift Rate Gain	78
39	Negligible Effect of TWD and DWT on Attitude and Min Drift Controls; No Load Relief	79
40	Three-Engine Orbiter	87
41	NR 134C Orbiter	88
42	Three-Engine Orbiter TVC Controller	89
43	Two-Engine Orbiter TVC Controller	90
44	Altitude/Velocity Profiles Comparing NR's Point Mass Trajectory with Honeywell's 6 Degree of Freedom Response to the Same Steering Commands	97
45	Wind Force on a Straight-Wing Orbiter	100
46	Wind Force on a Delta Wing Orbiter	101
47	Delta Wing Pad Abort with 19,000 lb Nose Thrust	102
48	Straight Wing Pad Abort with 27,000 lb Nose Thrust	103

49	Delta Wing Pad Abort with 4.0 Deg Nose Up Tilt	104
50	Straight Wing Orbiter Pad Abort	105
51	Abort Altitude, Velocity, and Flight Path Angle	107
52	Abort Heading and Range	108
53	Abort Bank Angle, Angle of Attack, and Dynamic Pressure	109
54	Abort Load Factor and Heat Rates	110
55	Inclination of Propellant Surface Due to Aerodynamic Normal Force and Thrust	111
56	Thrust Vector Control	112
57	TVC 11° to $50^\circ \alpha$ Commands at 226,957 feet Velocity 10,308 ft/sec	114
58	TVC - 50° Roll Commands ($\alpha=11^\circ$) at 226,957 feet	115
59	TVC - 50° Roll Commands ($\alpha=50^\circ$) at 226,957 feet	116
60	Programmed Commands for Abort at 226,957 feet, Velocity = 10308 ft/sec, and $\gamma = +6^\circ$	118
61	57° Left Gimbal is not Quite Enough with Right Engine Out	119
62	Abort Near Stage - $\beta_c = +5^\circ$ with No. 2 Engine Out, Normal C.G. Travel ^c	120
63	Abort Near Stage with W_{CG} at Burnout and Entry at 1422 inches from Nose (= Station 1633)	121
64	Abort at 225,000 feet. Sequential Burn of Main and Orbit Maneuver Propellant	122
65	Abort at 225,000 feet with Parallel Burn of Main and Orbit Maneuver Engines	123
66	Effect of AFT CG (Due to on Orbit Propellant) on Aerodynamic Trim Capability of 134-C, D, at Mach 10	124
67	α Control with SAS - No TVC	126
68	SAS - TVC Control	127
69	134D Entry Control System	129
70	North American 130G Straight Wing Orbiter	140
71	FC9 Step Responses - 0.026 Rad Aileron Actuator Input	143
72	FC9 Step Responses 0.015 Rad Rudder Actuator Input	145
73	FC9 Step Responses Max Commands	147
74	FC11 Step Responses 0.015 Rad Aileron Actuator Input	150

75	FC11 Step Responses 0.015 Rad Rudder Actuator Input	152
76	FC11 Step Responses Max Command	154
77	Handling Quality Controller Design Procedure	156
78	Step Responses, FC9 with Aileron/Rudder Control 0.15 Rad Rudder Command	160
79	Step Responses, FC9 with Aileron/Rudder Control 0.030 Rad Lateral Command	163
80	Step Response FC9 Aileron/Rudder Control Maximum Lateral Command	165
81	Step Responses FC9 Spoiler/Rudder Control 0.03 Rad Lateral Command	169
82	Step Responses, FC9 Spoiler/Rudder Control 0.015 Rad Rudder Command	172
83	Step Responses FC9 Spoiler/Rudder Control Maximum Lateral Command	175
84	Step Responses FC11 Aileron/Rudder Control 0.03 Rad Lateral Command	178
85	Step Responses FC11 Aileron/Rudder Control 0.015 Rad Rudder Command	181
86	Step Responses FC11 Aileron/Rudder Control Maximum Lateral Command	184
87	Step Responses, FC11 Spoiler/Rudder Control 0.015 Rad Lateral Command	187
88	Step Responses, FC11 Spoiler/Rudder Control 0.015 Rad Rudder Command	190
89	Step Responses, FC11 Spoiler/Rudder Control Maximum Lateral Command	193
90	North American 134D Orbiter	197
91	Baseline Quadratic Controller System Roots	205
92	Q Controller	207
93	Q Controller $ \delta a \leq 0.05$ $ \dot{\delta} r \leq 0.05$	208

TABLES		Page
Table		
1	Control Requirements Summary	3
2	Maximum Perturbation Responses	17
3	Liftoff Transfer Functions	19
4	High \bar{q} (64 sec) Transfer Functions	20
5	Near-Terminal Flight (160 sec) Transfer Functions	21
6	Shuttle and Saturn Stability	23
7	Simulations Compared	36
8	Controllers Compared	36
9	Five Conventional Lateral Controls	58
10	Simulations Compared	80
11	Controllers Compared	81
12	Stability Derivations	82
13	Maximum Responses	85
14	Equations of Motion	91
15	Vehicle Mass Properties	93
16	Three-Engine Orbiter Stability	94
17	Two-Engine Orbiter Stability	95
18	Effect of Aerodynamic Coefficients on Yaw ACPS Fuel Consumption, 134D Delta-Wing Orbiter in Normal Entry	132
19	Effect of Aerodynamic Coefficient Variations on Roll Maneuvers at Mach 6, 134D Orbiter	134
20	Effect of Aerodynamic Coefficient Variations on Roll Maneuvers at Mach 3, 134D Orbiter	135
21	Lateral Handling Quality Characteristics of Basic Airframe	141

22	Details of the Design Procedure	158
23	Gains and Quadratic Weights	159
24	Baseline Quadratic Controller	201
25	Baseline Quadratic Controller System Roots	202
26	Comparative Performance of Alternative Quadratic Controllers	203
27	Gain Matrices	204

SECTION I SUMMARY

This Space Shuttle control study was motivated by the need to identify any:

- Unique control requirements
- Control system influence on other systems
- Holes in the control technology

early in the shuttle preliminary design.

The benefit of this study is early identification of control issues that affect configuration and control technology drivers.

OBJECTIVE

The fundamental objective to achieve these ends is to identify Space Shuttle control requirements. With well over 20 Shuttle configurations and an infinite number of flight conditions, the split of depth versus breadth was selective. The objective was achieved for typical or promising configurations by considering rigid-body dynamics at the extreme flight regimes.

APPROACHES

Evaluation and judgment decisions of control requirements and control logic were used to achieve the objective. First, the evaluation was done by in-depth analyses of several shuttle configurations throughout the flight regimes to obtain requirements and control logics. These analyses were also used to identify sources of difficulties and solutions. Second, judgment decisions were made of results achieved by other groups working shuttle problems. The experience gained in the in-depth analyses provided both reasonable objectivity and expertise for judging other results. Those cases where judgments are discussed are identified.

Mechanizations meeting control requirements were also designed for many requirements. These demonstrated that the requirements could be met, or point to the difficulty in meeting them. When mechanizations were not defined, either because of finite resources and/or because of deficiencies of basic configuration or control logic, potential mechanizations and/or remedies are discussed. All mechanizations were of low bandwidth so that the rigid-body assumptions were not violated.

RESULTS

To summarize the results of the in-depth evaluation and the broad survey:

- Today's control technologies will design a flyable baseline controller. However, payload is dependent on the quality of control; thus considerable attention to controller design is warranted. Control of flexure and slosh (load alleviation and mode suppression) could yield additional payload. Technology for these designs is ready; however, we need better models than existed at the time of this study.
- Shuttle does have unique control requirements (Table 1). However, these requirements do not appear to demand exotic control logics or control schemes. Gain scheduling on dynamic pressure, Mach number, rocket power level, etc., appear adequate. Since flight control demands are modest, there should be no undue difficulties in implementing them in a central processor.
- The control system does have strong interaction with other systems. Among these are guidance, overall configuration, structure, aerodynamics, weight distribution, gimbal requirements, pilot, etc.

On the one hand there appears to be no fundamental difficulties due to control that will prevent operation of shuttle. This does not imply that considerable labor will not be required to develop viable control systems to attain acceptable vehicle control performance.

BRIEF SUMMARY

The remainder of this section discusses the unique control requirements and an overview of system interactions from the control viewpoint summarized in Table 1. The in-depth discussions are reserved for the technical sections and the Methods and Vehicle Models are in the appendixes. Requirements and interactions for eight flight regimes are summarized: pitch launch, lateral launch, orbiter injection, orbiter pad abort, in-flight orbiter aborts, orbiter entry, orbiter subsonic flight, and unpowered orbiter landings.

Pitch Launch -- Pitch requirements are a strong function of vehicle design. Also in pitch, the perturbation gimbal and terminal drifts are highly (and maybe inflight loads) significant requirements. They have large impacts on shuttle. In Section II we show that diverse and conflicting requirements can be simultaneously achieved by careful attention to controller design. This is in direct conflict with ref. 1 where $\max \dot{q}\alpha$ could be reduced but where simultaneous reduction in maximum bending moments was thought not to be achievable.

Lateral Launch -- Lateral launch results are not as comprehensive as pitch results. With limited resources pitch problems were judged to be drivers and thus received the attention. Lateral requirements are based on judgments of what is achievable. The analyses leading to these judgments are presented in Section III. The tools developed for pitch are ready to use to verify these judgments.

Table 1. Control Requirements Summary

Flight Regime	Problem	Cause	Solution	Remarks	
Pitch Launch	Trim gimbal requirements (up to ± 5 , 5 deg)	Depth-wise center-of-gravity travel	Mount orbiter more forward; increase booster/orbiter mass ratio; reshape trajectory	Up to ± 5 deg to track center of gravity Trajectory shaping may have adverse side effects. Up to $\pm 4, 5$ to compensate for aerodynamics.	
	Perturbation gimbal requirements (up to ± 6 deg)	Aerodynamic forces	Change booster to orbiter to cant angle; tailor booster and/or orbiter aerodynamics		
	Inflight loads	Winds	Control; trajectory shaping; vehicle design	For a statically stable vehicle (which most shuttle configurations appear to be) perturbation gimbal requirements can be required to $\pm 1, 5$ deg.	
	Terminal drift	Winds	Control	Excellent control can generally decrease all inflight loads to 50 percent of those achieved with good control. Forward-body-bending moments can be simultaneously reduced to 25 percent. There is a modest increase in inflight loads as terminal dispersions are reduced from 15,000 ft to 4,000 ft.	
Lateral Launch	Roll gimbal requirements (up to ± 15 deg)	Side winds and rolling moment due to sideslip	Control Allow the vehicle to roll to large angles so the wind is resolved into the pitch plane Use ailerons Change gimbal slewing arrangement Trajectory shaping	It is believed better control can reduce this to 15 deg. Some roll gimbal slewing arrangements increase pitch gimbal requirements. Pilots may object to the large roll angles. It may reduce overall control capabilities because of analytical difficulties. Controller complexity is increased. Aerodynamicists are having difficulties in developing ailerons that are effective in the high-dynamic pressure transonic regime where they are required. Effectiveness of this potential solution is not known. Potential side effects may be adverse. It will only be effective for those configurations using swept-back wings.	
	Yaw gimbal requirements (up to ± 6 deg)	Side winds	Control	C_L can be made zero at a particular point on the trajectory. It is a strong function of the center of gravity, so this reduces rather than eliminates the difficulty. Changing dihedral will have adverse effects in other flight regimes. The decision to provide only ± 7 deg has been made. This will increase roll effectiveness by increasing gimbal moment arms. The drag increase would decrease orbital payloads.	
	Inflight loads	Side winds	Control	It is believed better control can reduce these requirements to ± 3 deg.	
	Terminal drift	Side winds	Control	Increasing directional stability would decrease yaw gimbal requirements. Loads are demonstrated to be sensitive to control policy. It is believed improvements of excellent control over good control would be similar to that achieved for pitch control.	
					This is not a significant problem.
	Orbiter Injection	None			
Orbiter Pad Abort	Collision-free launch	Clearances between booster and launch tower in winds	Nose thruster; orbiter tilt	Weight penalties of additional force procedures; mechanical problems in achieving tilt.	
Orbiter Inflight Abort	Control	Increase inflight envelope	Not fully resolved	Provision for inflight abort of the orbiter has major implications on the orbiter control and guidance. Problems appear to be resolvable without major revisions of the vehicles or their control, but detailed investigations are necessary. Section V of this report examines some of the problems and presents some solutions.	
Orbiter Entry	ACPS fuel consumption	Directional stability of single vertical-tailed orbiters	Control Vehicle design	Guidance demands are small. Controls must be designed to meet minimal requirements to avoid wasting propellant. The twin vertical-tailed orbiters can rely on aerodynamics. They appear to be currently unpopular because of large hinge moments at high-dynamic pressures.	
Orbiter Subsonic Flight	None			Unaugmented airframes have inherently good handling characteristics. Control augmentation to meet handling qualities specifications is minimal.	
Empowered Orbiter Landing	"Spec" type	High landing speeds and large flight path angles	Small vehicle lift-drag ratio and compatibility for manual landing	All known efforts for landing fly a constant-speed approach on the "front side" of the power required curve. This provides the beneficial effects of inherent speed stability and large control power. The adverse effects are steep approach paths (above 10 deg), high approach speeds, and high landing speeds.	
	"Non-spec" type	Manual flight in high winds not possible	Small control surface rate capabilities	For the case of a delta-wing orbiter that is examined in Section VII, aileron and rudder rates can be reduced from 20 deg/sec and 6 deg/sec to 3 deg/sec and 3 deg/sec, respectively. It is believed these reductions imply large increases in orbital payload.	
	Shallow Approaches	Manual flight would be difficult	Pilot has to control both height and speed	Control Approach would be at 3 deg and be compatible with conventional ILS equipment. Approach initiation speed would be very high. Touchdown speed would be close to stall. The lower landing speed would decrease braking requirements and increase orbital payload.	

Work in progress by Honeywell indicates roll gimbal requirements can be markedly reduced by allowing the vehicle to roll to resolve the side wind into the pitch plane.

Orbiter Injection -- Both the control demands and requirements are small, (Section IV). Fixed gain controls provide good control performance for nominal injections.

For a three-engine orbiter, fixed gain controls provide acceptable control performance even under engine-out and reduced power level conditions. Better control performance is easily achievable by adjusting control gains with power level.

For a two-engine orbiter, fixed-gain controls provide acceptable control performance even under engine-out and reduced power level conditions; it is necessary to actuate the roll attitude control propulsion system (ACPS) to achieve roll control.

Orbiter Pad Abort -- Launch of an orbiter directly from the pad to escape from a booster that is about to explode is briefly considered in Section V. Ground winds induce loads that require special provisions to assure a collision-free launch. Nose thrusters on the orbiter or tilting of the orbiter provide potential solutions.

In-Flight Orbiter Aborts -- Considerable effort was devoted to control problems of in-flight abort. Relative to the total effort required to identify and resolve all problems the results are incomplete.

The primary effect of in-flight abort is to increase the flight envelope over nominal conditions. This has tremendous impacts on the vehicle, on control, and on guidance.

One impact on the vehicle, Section V, is a fuel sloshing problem unique to the abort situation. Fuel surface angles change markedly over those normally achieved. This has a direct impact on baffle design and will undoubtedly affect structural loading.

Stringent restrictions are placed on control and guidance.

The operation of both thrust vector control (TVC) and attitude propulsion control systems (ACPS) simultaneously over extremely wide ranges in Mach number and dynamic pressure dictates gain scheduling requirements for control, requires peculiar fuel sequencing procedures, and guidance. Gain scheduling requirements are also going to be dictated by the increased flight envelope. Section V identifies a fuel sequencing requirement that was not obvious prior to making the abort study and shows an example that guidance policies must be carefully matched to control capabilities to avoid destruction of the orbiter.

Orbiter Entry -- Details are presented in Section VI and summarized in Table 1.

Orbiter Subsonic Flight -- If the orbiters are designed toward meeting the objectives of specification handling qualities requirements, subsonic flight presents no difficulties. It appears all orbiters are being designed to meet these objectives.

Section VII examines in detail the lateral handling qualities capabilities of a North American straight-wing orbiter. The unaugmented airframe has good inherent capabilities. Modest augmentation with ailerons and rudder alone brings it up to Level 1 specifications requirements. With rudder and very low-response lateral spoilers, the orbiter can meet Level 3 requirements. Thus the spoilers provide a natural backup lateral control system.

Reference 1 considers both the lateral and longitudinal control capabilities.

Both the results presented here and those of ref. 1 concur on the effectiveness of lateral control by use of ailerons and rudder. The results presented here are more enthusiastic in their recommendation for use of the spoiler and rudder as a backup lateral control system.

Longitudinal control capabilities are shown to be good in ref. 1.

Unpowered Orbiter Landings -- Two aspects of orbiter landing are discussed: "specification type," and "non-specification type." A tradeoff which has not been addressed between these "spec" and "non-spec" landings should be made. The tradeoff study would require both an objective overall systems analysis and subjective judgments. The subjective judgments would involve emotional factors because of the break with tradition. Recommendations for non-spec landings (Section VIII and IX), from the results of this report, would be premature.

Specification Type -- Discussion of "spec" type landings for shuttle is taken from the results of others. Test pilots (ref. 2) at Edwards have made strong recommendations of the steep approach (and relatively severe flare-out) for shuttle based on tests using F-111 and B-52 aircraft. This achieves both inherent speed stability, and for nominal orbiters, lateral control authorities that are compatible with specification handling qualities requirements.

Honeywell, Sperry, and in-house studies at the Manned Spacecraft Center (ref. 1, 3, and 4) are investigating steep-approach automatic landings comparable to those recommended by the pilots. There appear to be no difficulties.

Non-Specification Type -- There are two aspects to the non-spec type. The first aspect is based on analysis described in Section VIII. The other aspect (shallow approaches) is based on judgments.

Section VIII shows that if specifications roll power specs are reduced from those required for manual control for landing to that sufficient to achieve good landings with automatic control, marked reductions in roll authority can be obtained. There is the strong implication this can significantly reduce orbiter weight and thus increase orbital payloads.

Shallow approach landings (Section IX) initiated at high speed and terminating near stall at touchdown appear to provide the same kind of tradeoff as that cited for roll power. The greater capabilities of automatic control would be substituted for manual control. The potential payoffs are reduced orbiter weights, lower landing speeds, and shorter runway requirements. Alternatively, wing size can be reduced and landing speeds maintained.

SECTION II

LAUNCH PHASE PITCH CONTROL

Pitch axis launch-phase control of Shuttle is examined. The objectives are to determine problems unique to the launch phase of large, winged, rocket-powered boosters and to provide potential solutions.

A major problem is the relatively large amount of gimbal deflection required for trim. Much of the trim gimbal requirement is generated by the large depth-wise center-of-mass travel with fuel consumption; the gimbal thrust vector has to generally track the center of mass. Large gimbal trim requirements are also imposed by forces generated by the large wing surfaces.

Gimbal trim requirements are most largely a function of the shuttle configuration design. It is believed that for a given shuttle modest reductions in gimbal trim requirements can be accomplished by trajectory shaping without incurring excessive penalties in payloads. Trajectory shaping was beyond the objectives of this effort.

The primary objectives of this effort are to determine and resolve problems in following a nominal trajectory. It is necessary to achieve small perturbation loads and terminal drift with small amounts of perturbation gimbal control.

Primary objectives have been achieved by designing and evaluating 10 different controllers. In-flight loads, terminal drift, and gimbal requirements are significantly affected by controller type to about the same degree as would be expected from extrapolating experience from Saturn V class vehicles. The major specific difference noted is a modest increase in in-flight loads as terminal drift is reduced from 19,000 feet to 4000 feet. The bending moment at a forward body is less subject to reduction than midbody and aft body bending moments. Good control can be achieved with pitch gimbal deflections of less than ± 1.5 deg perturbation from that required for trim.

Subsequent subsections present an Overview, results of Conventional Analyses, and finally, of Covariance Analyses.

OVERVIEW

Salient results are summarized with minimum attention to technical detail. This serves dual purposes; it makes it possible to obtain the major results quickly and provides an objectivity for interpretation of detailed discussions in subsequent subsections.

Figures 1 through 6 provide the summary.

A three-view of the MSFC in-house Vehicle B shuttle is presented as Figure 1.

Pitch gimbal and angle-of-attack trim requirements for the nominal trajectory are presented in Figure 2. Almost 12 deg of total gimbal deflection are required to meet the trim requirements for this shuttle to fly its nominal trajectory. The figure shows that virtually the entire requirement is imposed by the necessity for tracking the center of mass. There is a large aerodynamic trim requirement between 45 and 70 sec. This has a large impact on roll control discussed in Section III and Appendices B and D. Other shuttle configurations are much less demanding of gimbal trim. Reference 1, (for example) shows that pitch gimbal trim requirements for launch combinations of Convair boosters and North American orbiters typically require about 6 deg of pitch gimbal for trim.

The remainder of this discussion deals only with perturbation variables. These are the additional demands imposed by the necessity of compensating for winds. The effects are shown in Figures 3 through 6.

Figure 3 shows the maximum perturbation values for the acceleration normal to the pilot's seat (n), $\bar{q}\alpha$, and pitch gimbal deflection (δ) achieved with nine different controllers and two types of analyses.

The normal acceleration at the pilot's seat is insignificant compared with the boost axial acceleration. The top portion of Figure 3 shows that the maximum normal acceleration is less than 7 ft/sec². For a 3-g launch (which this is) the tangential acceleration is of the order of 96.5 ft/sec². Vector addition of the two components yields 97 ft/sec². That is, the normal acceleration contributes less than 0.3 percent of the total acceleration felt by the pilot.

Chronologically, controllers 1, 7, 2, 3, 4, 5, and 6 were synthesized first by conventional methodology; i. e., frequency response, root locus, and analog simulations. Controllers 13 and 15 were subsequently synthesized by application of quadratic control theory.

Two kinds of analyses were performed. Covariance analyses of all controllers were performed. These results are indicated by the left sets of bars containing both a clear portion for the mean response and a cross hatched portion for the rms response. A single sample of the random wind model (cf Appendix A) used to generate the covariance analyses was used in the manner of a synthetic wind for the analog analyses. Figure 7 shows this sample; it is a 1 σ wind with a 3 σ peak at 55 seconds. This sample was used in a time-varying analog simulation to develop the conventional analysis results shown by shading.

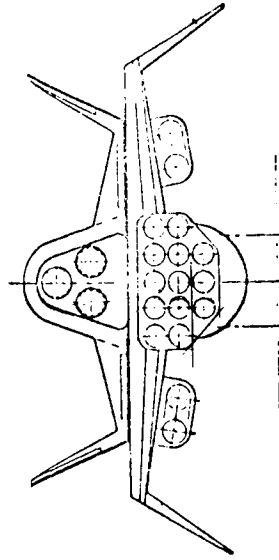
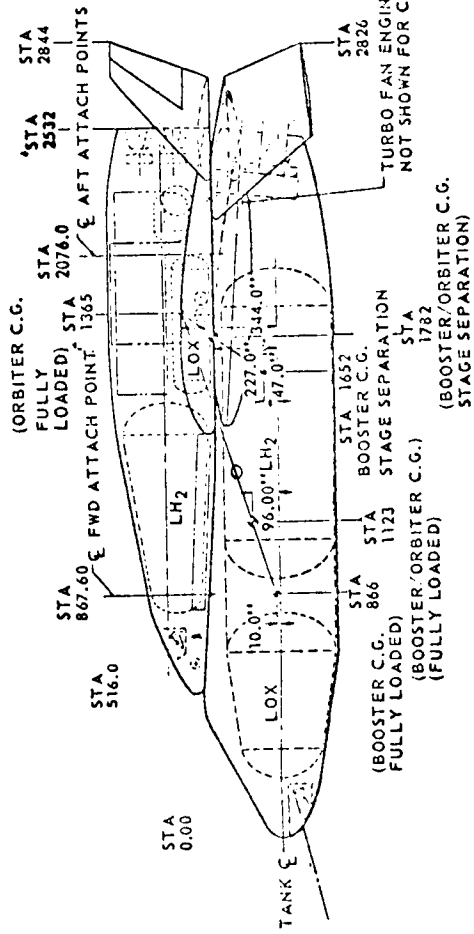
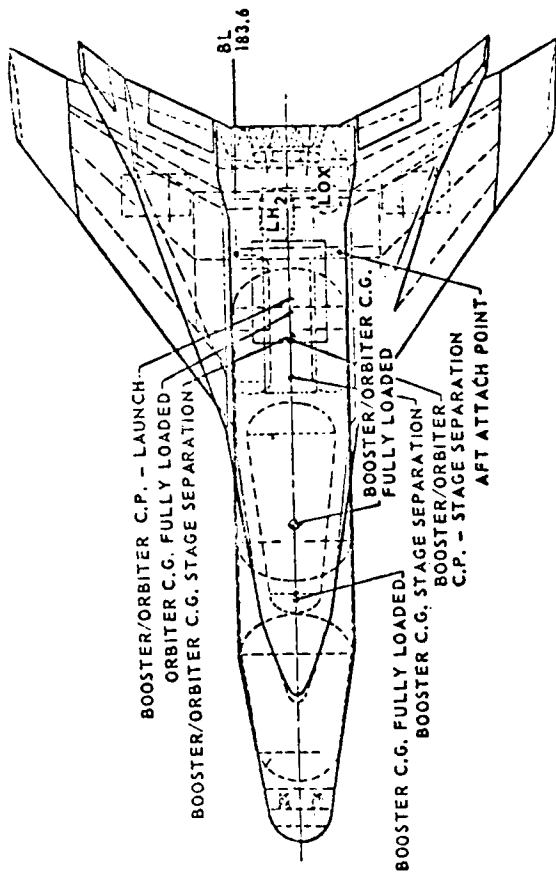


Figure 1. Booster/Orbiter Launch Configuration

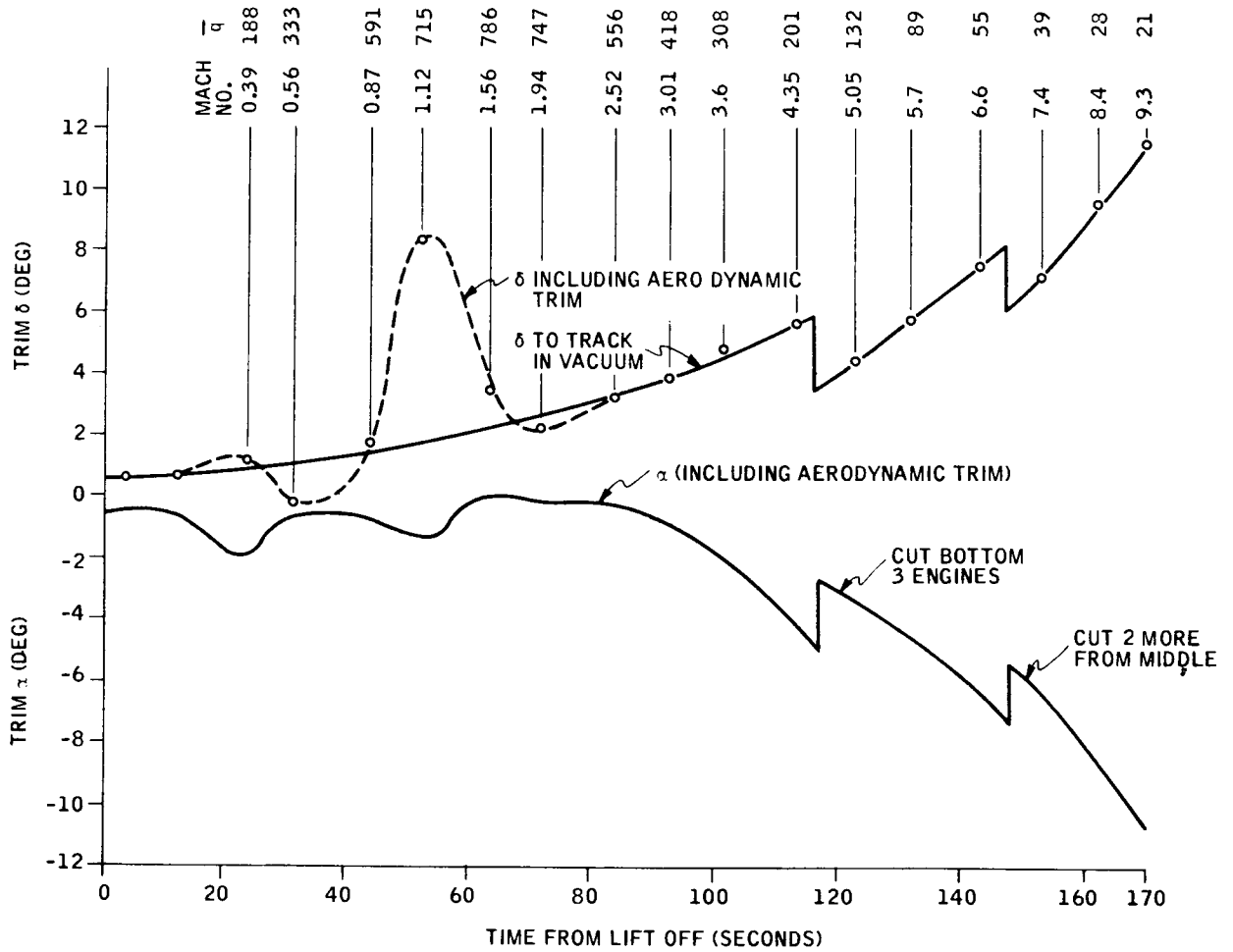


Figure 2. Trim Alpha and Delta

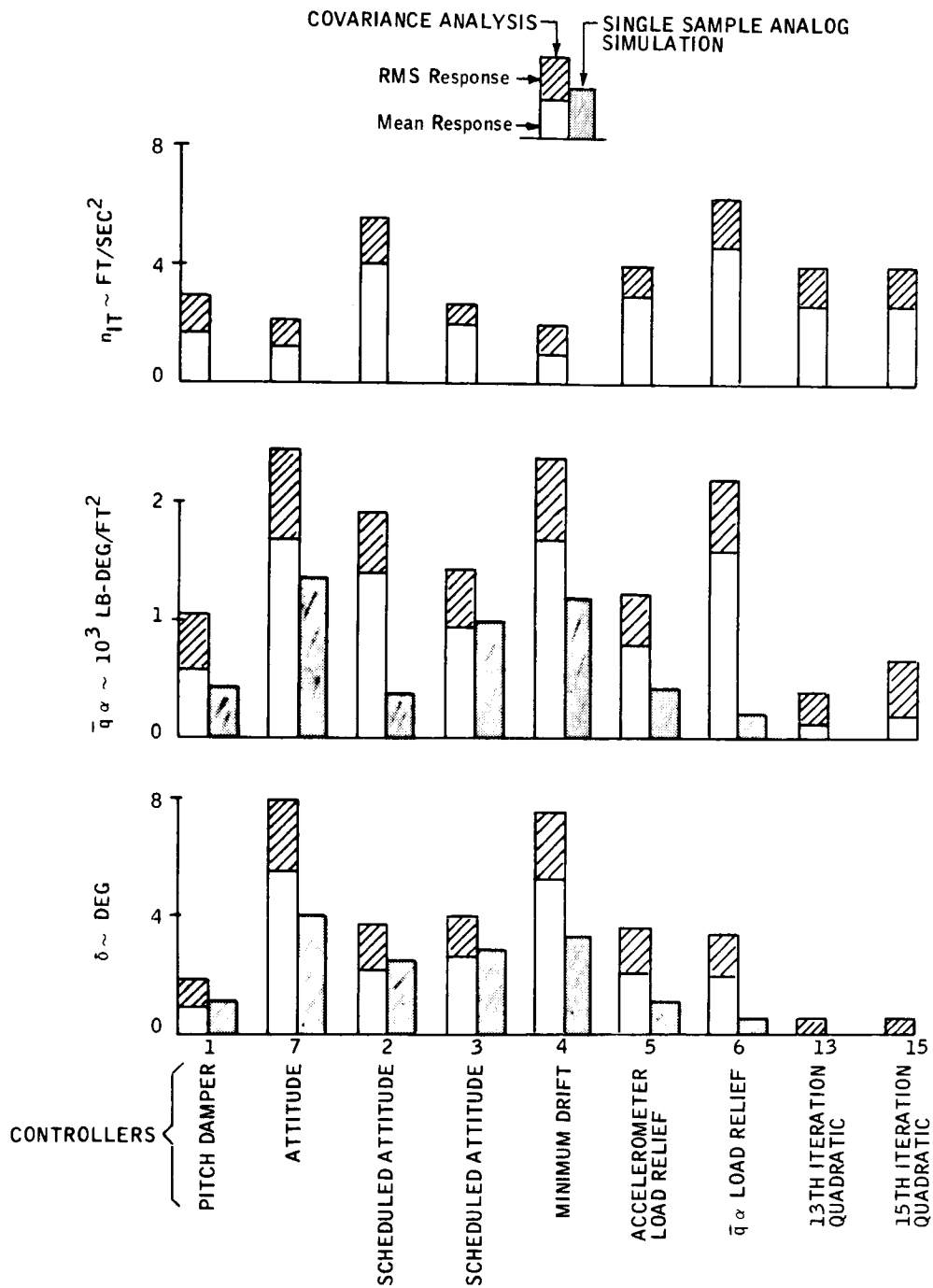


Figure 3. Maximum Perturbation n , \bar{q}_α , and δ

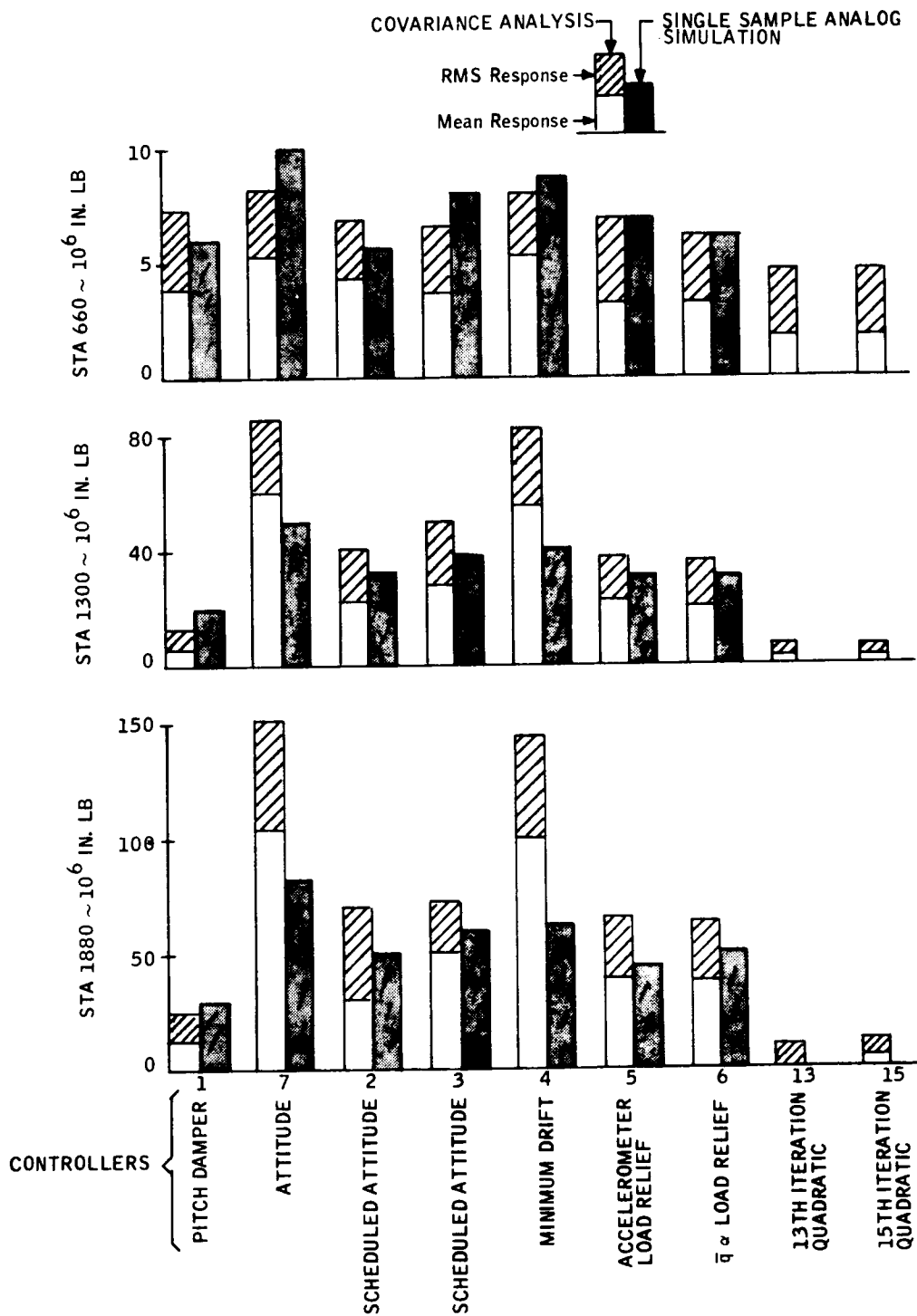


Figure 4. Maximum Perturbation Bending Moments

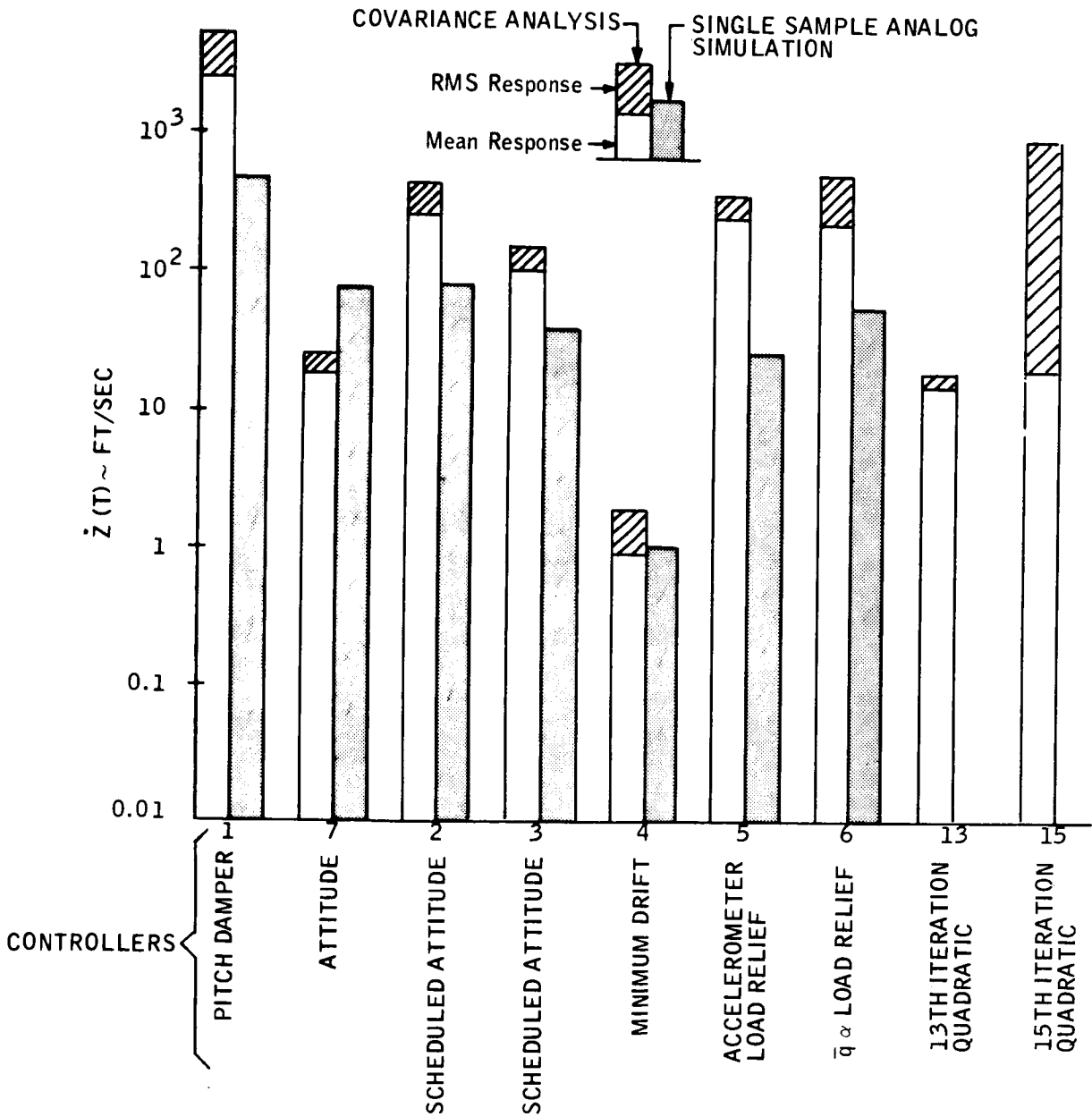


Figure 5. Terminal Drift Rate

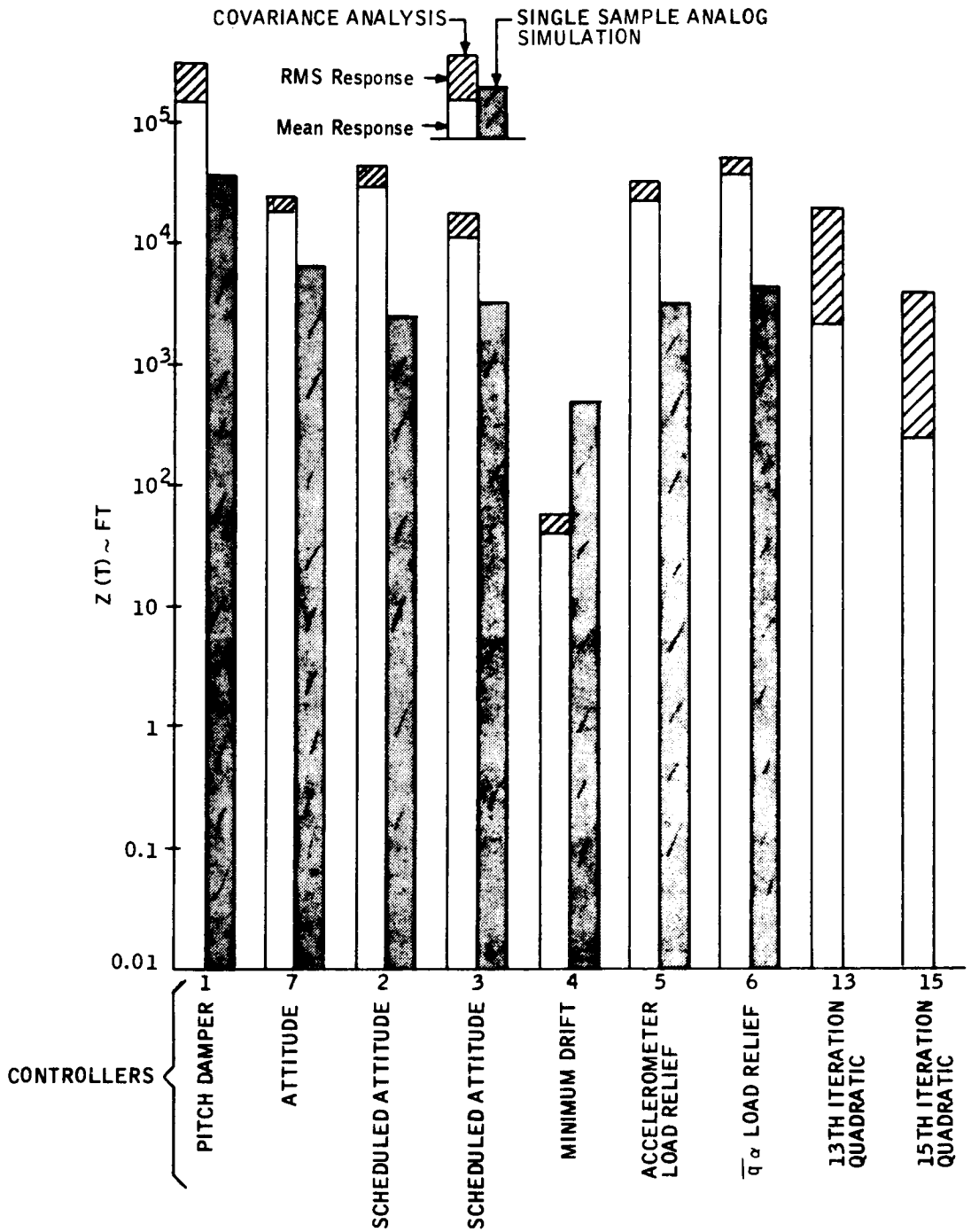


Figure 6. Terminal Drift

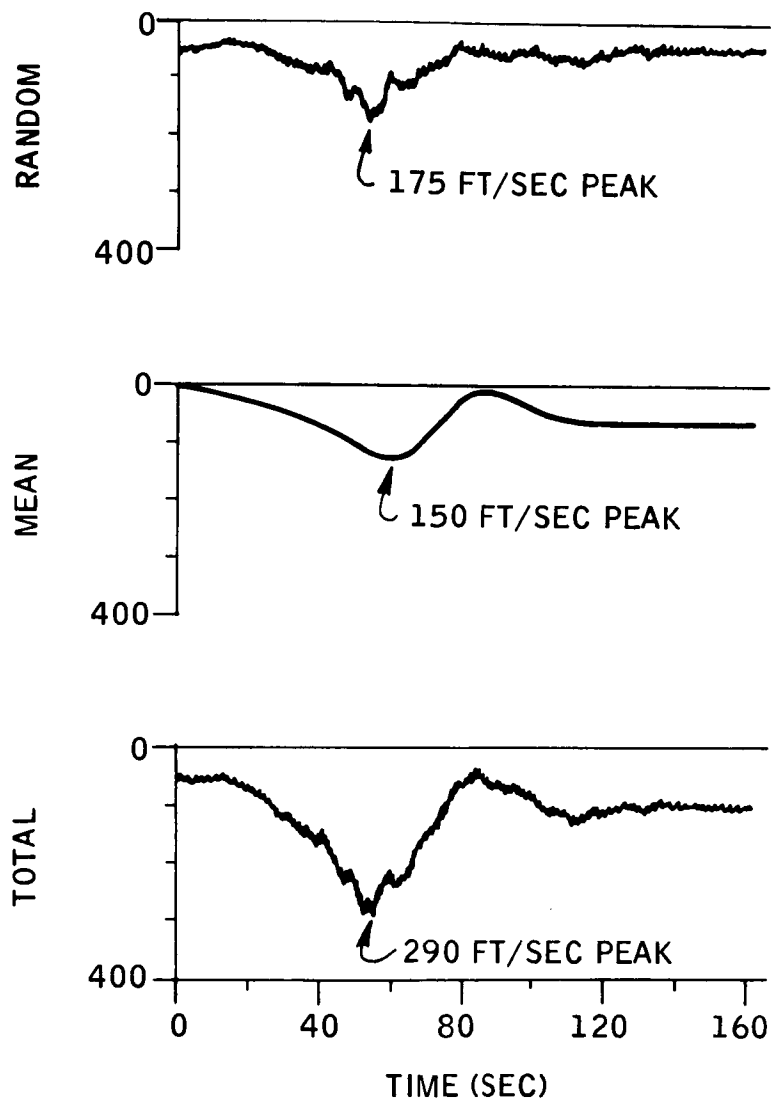


Figure 7. Sample of Vaughan/Skelton E-W March Wind

The results for $\bar{q}\alpha$ (Figure 3) are now discussed. The covariance results are always more severe than those obtained from analog simulation; this is usually true for other response variables. Both the covariance analyses and the analog simulation results show marked differences in load severity with controller types with generally the same trend characteristics. The covariance results for the $\bar{q}\alpha$ load relief controller (6) do not sustain the relative excellence as evaluated by analog simulation. The analog results are optimistic because of particularly favorable interactions between controller gain variations and the selected wind sample.

The $\bar{q}\alpha$ results for controllers 13 and 15 will be discussed after two pieces of background information are provided for perspective.

The MSFC Vehicle B used for this investigation was designed to provide for an assessment of problem areas before good data were available from NASA Phase B Shuttle contracts. The MSFC Vehicle B model does permit the realistic addressment of the problems confronting launch of large rocket-powered winged vehicles. Trend results obtained will be generally applicable to shuttle configurations. There is a difficulty in using the MSFC Vehicle B model but this has been satisfactorily resolved for the study effort involved here. The maximum allowables for response variables (except for gimbals deflection) for this vehicle are not known. This was resolved here by generally requiring improvements in the minimum maximum values (of $\bar{q}\alpha$, δ , three bending moments, terminal drift, and terminal drift rate) from the covariance results for the seven conventional controllers. The conventional controllers were considered to be reasonably good controllers so this provided stringent design objectives. Since the requirements are achieved, it is much more than conjecture to speculate that critical responses for a viable shuttle can be improved by larger percentages.

The second piece of background information deals with the extrapolation of results from Saturn V class vehicles to Shuttle. Previous studies (ref. 6 and 7) at Honeywell have shown that terminal drift and drift rate can be markedly reduced near the end of burnout without significantly increasing in-flight loads. The experience here is that in-flight loads increase as the terminal drift is reduced from 18,810 feet to 3745 feet.

Now $\bar{q}\alpha$ of Figure 3 for controllers 13 and 15 can be discussed. Controller 13 is synthesized to reduce the minimum maximum of the in-flight excursions obtained from the conventional controls. For $\bar{q}\alpha$ (and other in-flight variables) controller 13 achieves a marked reduction. There is an increase in $\bar{q}\alpha$ for controller 15 from that for 13 but the result is still much better than that achieved by the best of the conventional controllers. Subsequent results show that $\bar{q}\alpha$ is by far most adversely affected (relative to the other in-flight constraints) by the reduction in terminal drift. Table 2 (discussed in more detail later) shows why this is true. Controller 15 is unique in that it attains its maximum $\bar{q}\alpha$ at the terminal time.

Table 2. Maximum Perturbation Responses

Item	δ Rad	M_{660} 10^6 in. lb	M_{1300} 10^6 in. lb	M_{1880} 10^6 in. lb	v_{IT} ft/sec	$\bar{q}\alpha$ lb rad/ft ²	$\dot{z}(170)$ 100 ft/sec	$z(170)$ 1000 ft
1 Pitch Damper	-0.0154	-4.03	6.80	13.2	-1.75	9.93	28.1	154.0
	0.0142	3.52	6.65	13.43	1.257	8.00	28.2	158.2
	0.0296	7.55	13.39	26.63	2.997	17.93	56.3	312.2
	60	55	40	60	54	50		
7 Attitude	-0.0957	-5.40	59.2	104.0	1.20	29.8	-0.188	-1.920
	0.0431	2.68	27.0	47.2	0.915	12.58	0.0499	0.616
	0.1388	8.08	86.2	151.0	2.115	42.38	0.2379	2.536
	60	65	60	60	50	65		
2 Scheduled Attitude	-0.0385	-4.28	23.6	41.6	4.08	24.4	2.86	29.90
	0.0257	2.64	16.1	28.1	1.428	8.72	1.082	11.14
	0.0642	6.92	39.7	69.7	5.508	33.12	3.942	41.04
	35	50	35	35	105	100		
3 Schedule Attitude	-0.0466	-3.75	28.1	50.5	1.95	16.4	1.07	12.40
	0.0216	2.89	21.1	21.4	0.695	7.32	0.424	4.72
	0.0682	6.64	49.2	71.9	2.645	23.72	1.494	17.12
	60	55	65	65	100	65		
4 Minimum Drift	-0.0918	5.33	56.7	99.7	1.08	29.4	0.00979	-0.0391
	0.0413	2.65	26.0	45.1	0.896	12.3	0.00816	0.0178
	0.1331	7.98	82.7	144.8	1.976	41.7	0.01795	0.0569
	60	65	60	60	50	65		
5 Accelerometer Load Relief	-0.0364	-3.33	22.00	39.20	2.98	14.1	2.46	25.60
	0.0244	3.57	15.32	26.70	1.02	7.13	0.952	9.75
	0.0608	6.90	37.32	65.90	4.00	21.23	3.412	35.35
	35	55	35	35	110	45		
6 $\bar{q}\alpha$ Load Relief	-0.0347	-3.39	20.9	37.20	4.65	8.10	3.58	37.70
	0.0234	2.70	11.55	25.40	1.66	9.78	1.36	14.18
	0.0581	6.09	35.45	62.60	6.31	37.88	4.94	51.88
	35	50	35	35	105	110		
Q13	0.0002	-1.75	-3.48	-0.45	-2.74	2.33	0.151	-2.130
	0.0076	2.93	3.16	8.05	1.288	4.54	0.0255	16.680
	0.0078	4.68	6.64	8.50	4.088	6.87	0.1765	18.810
	25	55	55	25	65	50		
Q15	0.0007	-1.77	-3.53	-3.61	-2.73	3.56	0.193	-0.245
	0.0092	2.93	3.10	7.21	1.26	7.91	0.735	3.500
	0.0099	4.70	6.63	10.82	3.99	11.47	0.928	3.745
	40	55	55	55	30	170		

NOTES: (for each controller)

Row 1 - $\mu(\tau)$

Row 2 - $\sigma(\tau)$

Row 3 - $\max_t \{ |\mu(t)| + \sigma(t) \}$

Row 4 - τ = time at which row 3 is maximized

The bottom part of Figure 3 presents the perturbation gimbal deflections (δ) for the nine controllers. Comparisons are similar to those obtained for $\bar{q}\alpha$ except there isn't much penalty for the reduction in terminal drift. The most significant observation concerning gimbal deflection is the small values attainable with controllers 13 and 15. Mean values are negligible and rms values are about 0.5 deg. Taking a pessimistic point of view, ± 1.5 deg of pitch perturbation gimbal is sufficient. The small value is attributed to the inherent static stability of this shuttle configuration.

The bending moment summary is presented in Figure 4. For the conventional controllers the results are similar to the comparisons for $\bar{q}\alpha$ and δ . Controllers 13 and 15 reduce both aft bending moments to 50 percent of the best of the conventional. For the forward-bending moment 25 percent was the best that could be obtained (subject to the other constraints) in the time available. Due to the nature of data requirements for Vehicle B, it is not known whether this is serious. The relative importance of the bending moments is not known.

CONVENTIONAL ANALYSES

Eight controllers are synthesized and analyzed to determine their capabilities. The primary objective is to achieve low in-flight loads and small terminal excursions by use of modest control authority. Consideration to practical details (such as sensor bias) is given.

Appendix B presents the vehicle equations, data, and diagrams for their analog simulations. Table B4 presents the plant stability derivatives and frozen point characteristic equations at 19 times over the 170-second trajectory.

Airframe transfer functions are succinctly summarized in Tables 3 through 5. Both tail-wags-dog (TWD) and dog-wags-tail (DWT) effects are estimated. The tables and analog simulations show both TWD and DWT effects to be of negligible importance for the rigid body representations considered here.

Figure 8 shows the short period is stable throughout the flight.

Differences between control requirements for Saturn V class vehicles (ref. 8 and 9) and Shuttle were noted during this Study (Table 6). At maximum dynamic pressure it can be seen that control authorities are comparable but the shuttle is much more stable.

Table 3. Liftoff Transfer Functions

<u>Denominator</u>		
	Without DWT	$(0.001) (S^3) \left(\begin{matrix} \omega = 31.6 \\ \zeta = 0.4 \end{matrix} \right)$
	With DWT	$(0.00095) \left(\begin{matrix} \omega = 31.4 \\ \zeta = 0.42 \end{matrix} \right) S^3$
<u>Numerators</u>		
$\frac{\theta}{\delta_i}$	Without TWD	1.425
	With TWD	$(0.00113) (S) \left(\begin{matrix} \omega = 35.4 \\ \zeta = 0 \end{matrix} \right)$
$\frac{A_{CG}}{\delta_i}$	Without TWD	$48 S^3$
	With TWD	$(0.037) (S^3) \left(\begin{matrix} \omega = 36.0 \\ \zeta = 0 \end{matrix} \right)$
$\frac{w}{\delta_i}$	Without TWD	$48 (S + 0.99) (S - 0.96)$
	With TWD	$(0.037) (S + 0.99) (S - 0.96) \left(\begin{matrix} \omega = 36 \\ \zeta = 0 \end{matrix} \right)$
$\frac{A_z(612)}{\delta_i}$	Without TWD	$-8.8 S^3$
	With TWD	$-0.0082 S^3 \left(\begin{matrix} \omega = 32.8 \\ \zeta = 0 \end{matrix} \right)$

Table 4. High \bar{q} (64 sec) Transfer Functions

<u>Denominators</u>		
	Without DWT	$(0.001) (S - 0.016) \left(\begin{matrix} \omega = 2.60 \\ \zeta = +0.084 \end{matrix} \right) \left(\begin{matrix} \omega = 31.6 \\ \zeta = 0.4 \end{matrix} \right)$
	With DWT	$(0.00093) (S - 0.016) \left(\begin{matrix} \omega = 2.76 \\ \zeta = 0.081 \end{matrix} \right) \left(\begin{matrix} \omega = 31.1 \\ \zeta = 0.43 \end{matrix} \right)$
<u>Numerators</u>		
$\frac{\theta}{\delta_i}$	Without TWD	$1.85 (S + 0.049)$
	With TWD	$(0.0013) (S + 0.049) \left(\begin{matrix} \omega = 37.7 \\ \zeta = 0 \end{matrix} \right)$
$\frac{A_{CG}}{\delta_i}$	Without TWD	$72 (S - 0.016) (S - 1.28) (S + 1.49)$
	With TWD	$(0.049) (S - 0.016) (S - 1.28) (S + 1.49) \left(\begin{matrix} \omega = 38 \\ \zeta = 0 \end{matrix} \right)$
$\frac{w}{\delta_i}$	Without TWD	$72 (S - 0.016) (S + 39.5)$
	With TWD	$(0.049) (S - 0.016) (S + 40) \left(\begin{matrix} \omega = 38 \\ \zeta = 0.008 \end{matrix} \right)$
$\frac{A_z(612)}{\delta_i}$	Without TWD	$-29.8 (S - 0.016) \left(\begin{matrix} \omega = 2.15 \\ \zeta = -0.07 \end{matrix} \right)$
	With TWD	$-0.022 (S - 0.016) \left(\begin{matrix} \omega = 2.15 \\ \zeta = -0.07 \end{matrix} \right) \left(\begin{matrix} \omega = 36.4 \\ \zeta = 0 \end{matrix} \right)$

Table 5. Near-Terminal Flight (160 sec) Transfer Functions

<u>Denominators</u>		
	Without DWT	$(0.001) S^3 \left(\begin{array}{l} \omega = 31.6 \\ \zeta = 0.4 \end{array} \right)$
	With DWT	$(0.00091) S^3 \left(\begin{array}{l} \omega = 31.1 \\ \zeta = 0.44 \end{array} \right)$
<u>Numerators</u>		
$\frac{\theta}{\delta_i}$	Without TWD	3.2S
	With TWD	$(0.0024) \left(\begin{array}{l} \omega = 36.5 \\ \zeta = 0 \end{array} \right) S^2$
$\frac{A_{CG}}{\delta_i}$	Without TWD	$129S^3$
	With FWD	$(0.100) \left(\begin{array}{l} \omega = 35.9 \\ \zeta = 0 \end{array} \right) S$
$\frac{w}{\delta_i}$	Without TWD	$129 (S + 234)S$
	With TWD	$(0.100) (S^3) \left(\begin{array}{l} \omega = 36.5 \\ \zeta = -0.002 \end{array} \right) (S + 226)$
$\frac{A_z(612)}{\delta_i}$	Without TWD	$-194 S^3$
	With TWD	$(-0.142) S^3 \left(\begin{array}{l} \omega = 36.9 \\ \zeta = 0 \end{array} \right)$

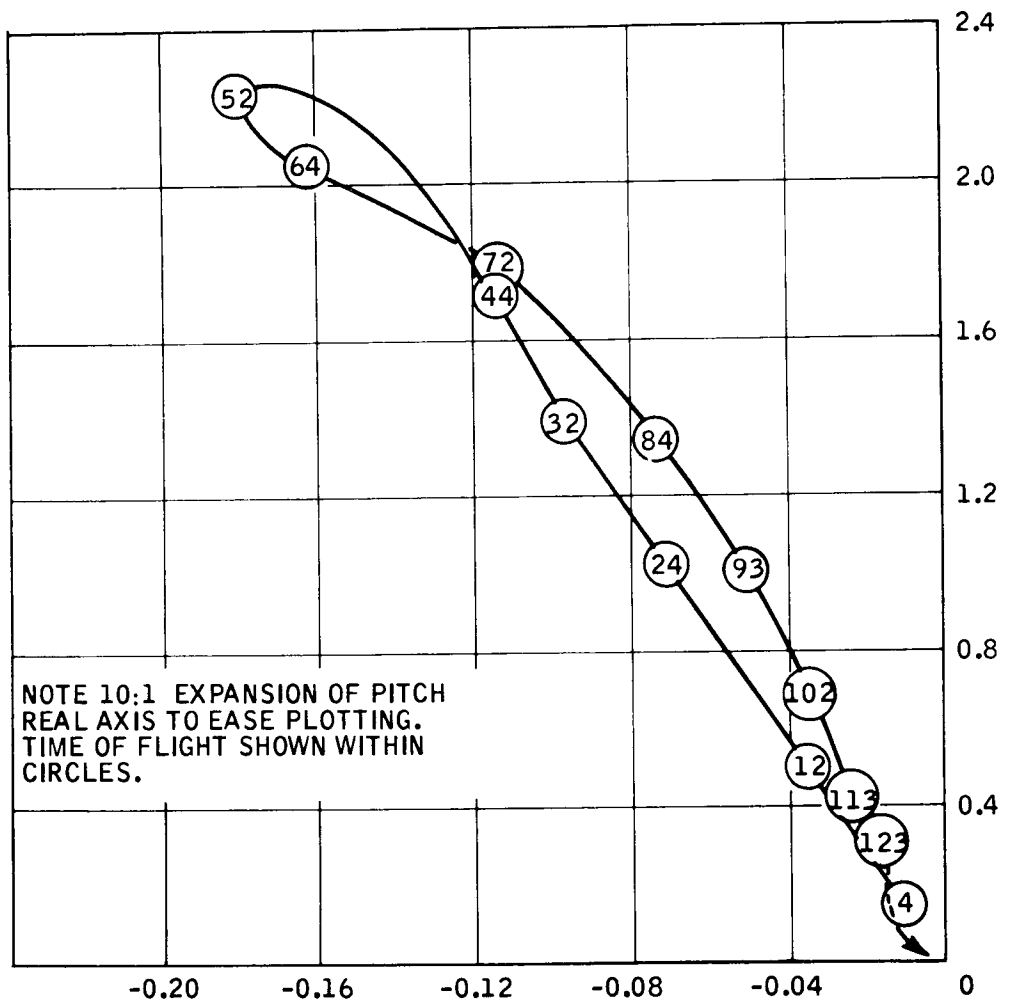


Figure 8. Locus of Short Period Roots

Table 6. Shuttle and Saturn Stability

Stability Derivative	Vehicle	
	Shuttle	Saturn V/Voyager
M_{α}	-4.28	+0.26
M_{δ}	-1.86	-1.21

The controllers are now discussed. Figure 9 presents the eight control equations synthesized, analyzed, and simulated.

Frequency response and root locus analysis were used to determine gains. No attempt was made to optimize gain levels because the vehicle representation contains neither slosh nor flexure dynamics.

Closed-loop roots and stability characteristics for the pitch damper, attitude controller, and accelerometer load relief controllers are discussed.

The pitch damper gimbal command (from Figure 9) is

$$\delta_i = 2.4 q$$

The high-frequency gain margin is ample, providing stiffness closer to that which would be obtained with bending modes added. The closed-loop poles at this gain are

$$\text{Liftoff} \quad (S + 4.2) \left(\begin{array}{l} \omega = 29.6 \\ \zeta = 0.43 \end{array} \right)$$

$$64 \text{ seconds} \quad (S - 0.015) (S + 2.35) (S + 3.95) \left(\begin{array}{l} \omega = 28.7 \\ \zeta = 0.42 \end{array} \right)$$

$$160 \text{ seconds} \quad (S + 10.9) \left(\begin{array}{l} \omega = 26.6 \\ \zeta = 0.41 \end{array} \right)$$

The vehicle is unstable at 64 sec, but the divergence is slow. A higher gain could be used. For example, at a gain of 5, the poles at 160 sec are

$$(S + 27) \left(\begin{array}{l} \omega = 24.9 \\ \zeta = 0.26 \end{array} \right)$$

The actuator damping is deteriorating rapidly. This higher gain does not eliminate the slow divergence at 64 sec.

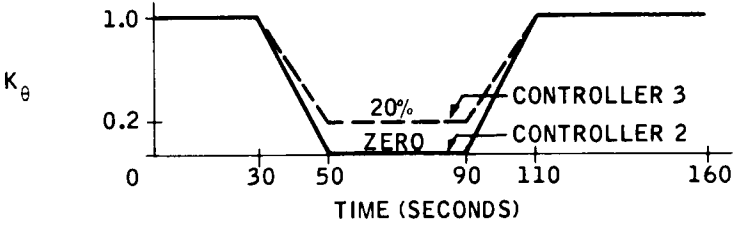
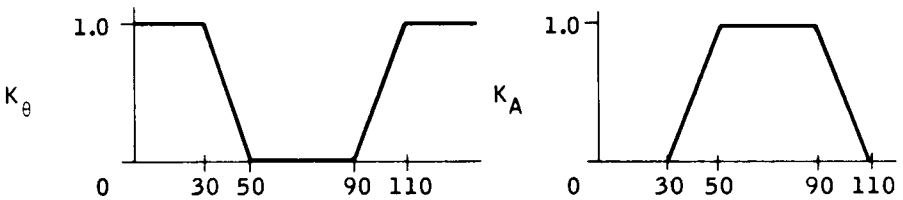
CONTROLLER NUMBER	CONTROLLER NAME AND CONTROL LAW
1	PITCH DAMPER $\delta_i = 2.4q$
2 AND 3	<p>SCHEDULED ATTITUDE $\delta_i = 2.4q + 2.4 K_\theta \theta$, WHERE</p>  <p>The graph shows the gain K_θ on the y-axis (ranging from 0 to 1.0) versus Time (Seconds) on the x-axis (ranging from 0 to 160). Both Controller 2 (solid line) and Controller 3 (dashed line) start at $K_\theta = 1.0$ from 0 to 30 seconds. At 30 seconds, they begin to decrease linearly, reaching $K_\theta = 0.2$ at 50 seconds. From 50 to 90 seconds, the gain is 0.2. At 90 seconds, the gain drops to 0. From 90 to 110 seconds, the gain increases linearly back to 1.0. After 110 seconds, the gain remains at 1.0.</p>
4	MINIMUM DRIFT $\delta_i = 2.4q + 2.4 (\theta - 0.2V_N) (1 + \frac{1}{10S})$
5	<p>ACCELEROMETER LOAD RELIEF</p> $\delta_i = 2.4q + 2.4 \left[K_\theta \theta - \frac{0.01K_A A_z}{S+1} \right]$  <p>The left graph shows K_θ vs Time (Seconds). K_θ is 1.0 from 0 to 30s, drops to 0 at 50s, and returns to 1.0 at 110s. The right graph shows K_A vs Time (Seconds). K_A is 0 until 30s, then rises to 1.0 at 50s and stays there until 90s, then drops to 0 at 110s.</p>
6	<p>q_α LOAD RELIEF</p> $\delta_i = 2.4q + 2.4 \left[K_\theta \theta - 0.0035K_A Z_w w_A \right]$
7	ATTITUDE HOLD $\delta_i = 2.4q + 2.4\theta (1 + \frac{1}{10S})$
8	<p>ACCELERATION LIMITER LOAD RELIEF</p> <p>OFF LIMIT $\delta_i = 2.4q + 2.4\theta (1 + \frac{1}{10S})$</p> <p>ON LIMIT $\delta_i = 2.4q - 0.024 \left[\frac{A_z}{S+1} - \text{LIMIT} \right]$</p> <p>LIMITS = $\pm 0.5, \pm 0.62, \pm 0.75, \pm 1.0$</p>

Figure 9. Eight Conventional Control Systems

The attitude controller (from Figure 9) is

$$\delta_i = 2.4q + 2.4 \left(1 + \frac{1}{10S} \right) \theta$$

The integral control is added so that the cg can be tracked. Figure 2 shows rapidly changing trim requirements between 45 and 65 seconds. The perturbation analysis could not test the system's ability to track this. The final analysis should include programmed gimbal trim as well as integral control.

Again the gain margins are excessive, but, as will be shown subsequently the performance was acceptable. The closed-loop poles at this gain are:

$$\begin{aligned} \text{Liftoff} & \quad (S + 0.11) (S + 2.35) (S + 1.58) \left(\begin{array}{l} \omega = 29.6 \\ \zeta = 0.43 \end{array} \right) \\ 64 \text{ seconds} & \quad \left(\begin{array}{l} \omega = 0.044 \\ \zeta = 0.55 \end{array} \right) \left(\begin{array}{l} \omega = 3.83 \\ \zeta = 0.79 \end{array} \right) \left(\begin{array}{l} \omega = 28.7 \\ \zeta = 0.43 \end{array} \right) \\ 160 \text{ seconds} & \quad (S + 0.11) (S + 1.0) (S + 10.4) \left(\begin{array}{l} \omega = 26.6 \\ \zeta = 0.42 \end{array} \right) \end{aligned}$$

The normal acceleration controller (accelerometer at station 612) is

$$\delta_i = 2.4q + 2.4 \left(K_{\theta_2} \theta - \frac{0.01 K_A}{S + 1} A_Z \right)$$

This loop uses the pitch attitude inner loop. The 1-sec lag anticipates noise and bending problems. The gain margins are ample as is the case with the pitch rate and attitude loops. The closed-loop poles are

$$\begin{aligned} \text{Liftoff} & \quad (S + 0.93) (S + 4.5) \left(\begin{array}{l} \omega = 29.5 \\ \zeta = 0.43 \end{array} \right) \\ 64 \text{ seconds} & \quad (S + 0.033) (S - 0.016) \left(\begin{array}{l} \omega = 1.45 \\ \zeta = 0.72 \end{array} \right) (S + 6.4) \left(\begin{array}{l} \omega = 28.3 \\ \zeta = 0.42 \end{array} \right) \\ 160 \text{ seconds} & \quad (S - 0.0046) (S + 0.0054) (S + 22) (S + 0.64) \left(\begin{array}{l} \omega = 25.1 \\ \zeta = 0.31 \end{array} \right) \end{aligned}$$

The vehicle is stable at liftoff with very slow divergences at 64 seconds and 160 seconds. These instabilities are of minor concern when the load relief control is used for a limited time near maximum dynamic pressure.

Analog simulation results are presented in Figures 10 through 13. The smallest visible division is 2 sec; the smallest distinguishable deviation is 10 sec. All of the runs last at least 130 sec of the 160-sec time of flight. They are often discontinued after everything has subsided.

All four figures include a minimum drift system for reference. This system has no load relief, the control equation being

$$\delta_i = 2.4q + 2.4 \left(\theta - 0.2V_N \right) \left(1 + \frac{1}{10S} \right)$$

It holds the drift rate to zero with a slight drift accumulated; $Z = +5000$ feet (down wind) at cutoff.

Significant data from Figures 10 through 13 are summarized in bar charts:

Figure 14 - Bending moments

Figure 15 - Drift and drift rate at 160 seconds

Figure 16 - Angle of attack and gimbal deflection at 64 seconds

Consider the bending moments in Figure 14. The attitude hold system has higher values than the minimum drift system. Thus, even if no other form of load relief is provided, a guidance system controlling cross-course velocity as well as attitude reduces both bending moments and drift. It is also noted that none of the systems except the pitch damper, which is impractical, show any drastic reduction in bending moments, particularly, at the forward station 660*. In Figures 10 through 13 it can be seen that this moment's mean value is more significantly reduced with load relief systems (compare pitch damper with the minimum drift system in Figure 10), but the severe turbulence produces spikes which the vehicle cannot respond to for the model used for this analog simulation. This part of the analog results would probably be somewhat different had gust penetration been included in the analog. The analog model (Appendix B) uses sudden immersion.

The bar third from the left in Figure 14 is for the scheduled attitude system; it shows reasonable reduction at all stations. This system uses the inherent static stability to weathercock into the wind at the high dynamic

*There is a factor of 10 discrepancy between the results plotted for the forward station bending moment as presented in Figure 4 and Figure 14. The equations used for both the analog and digital covariance analyses have been rechecked, the analog wiring checked, and the digital program reviewed. No errors were found. The magnitudes of gimbal deflection and angle of attack indicate the analog results are low by a factor of 10.

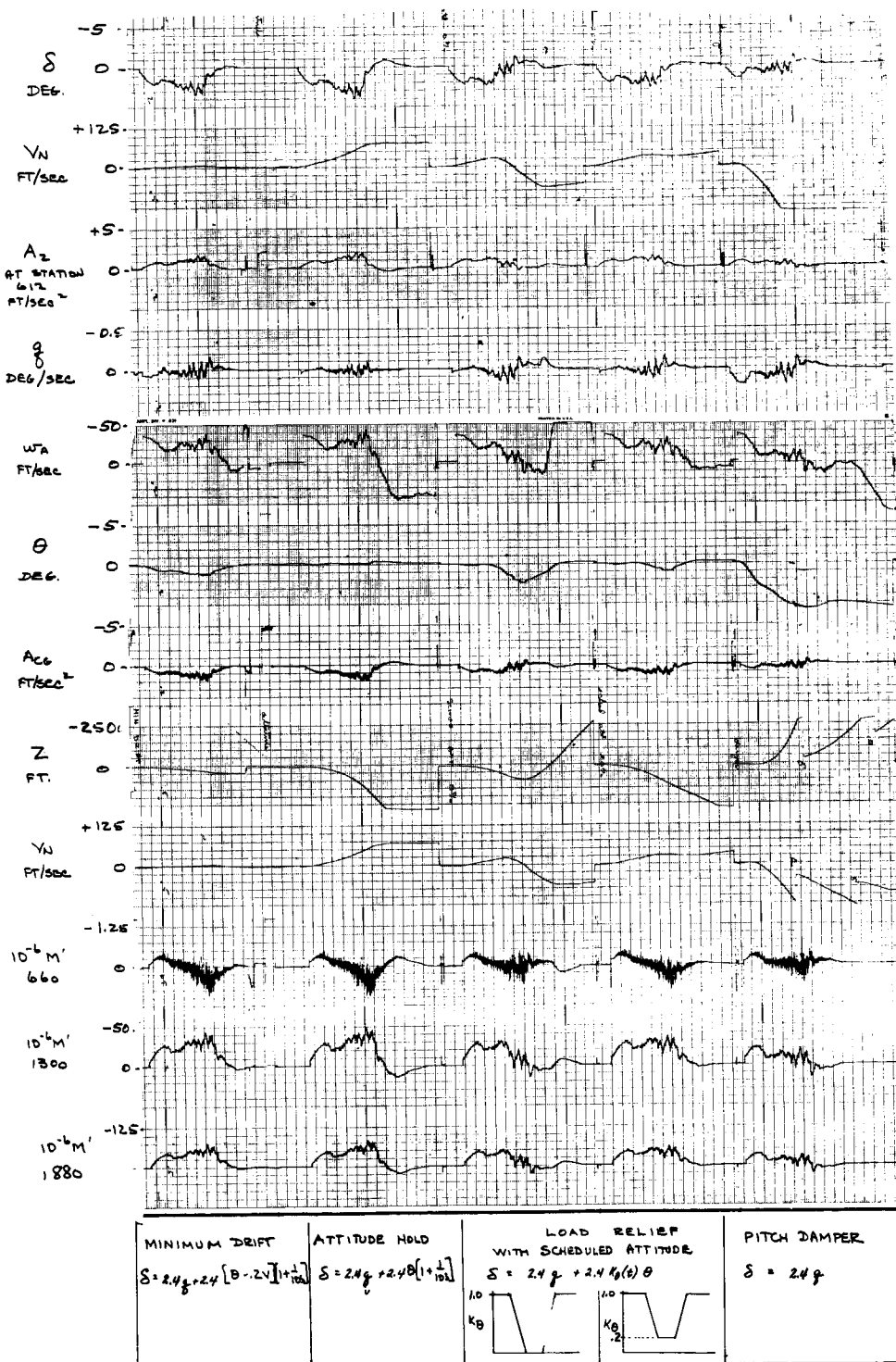
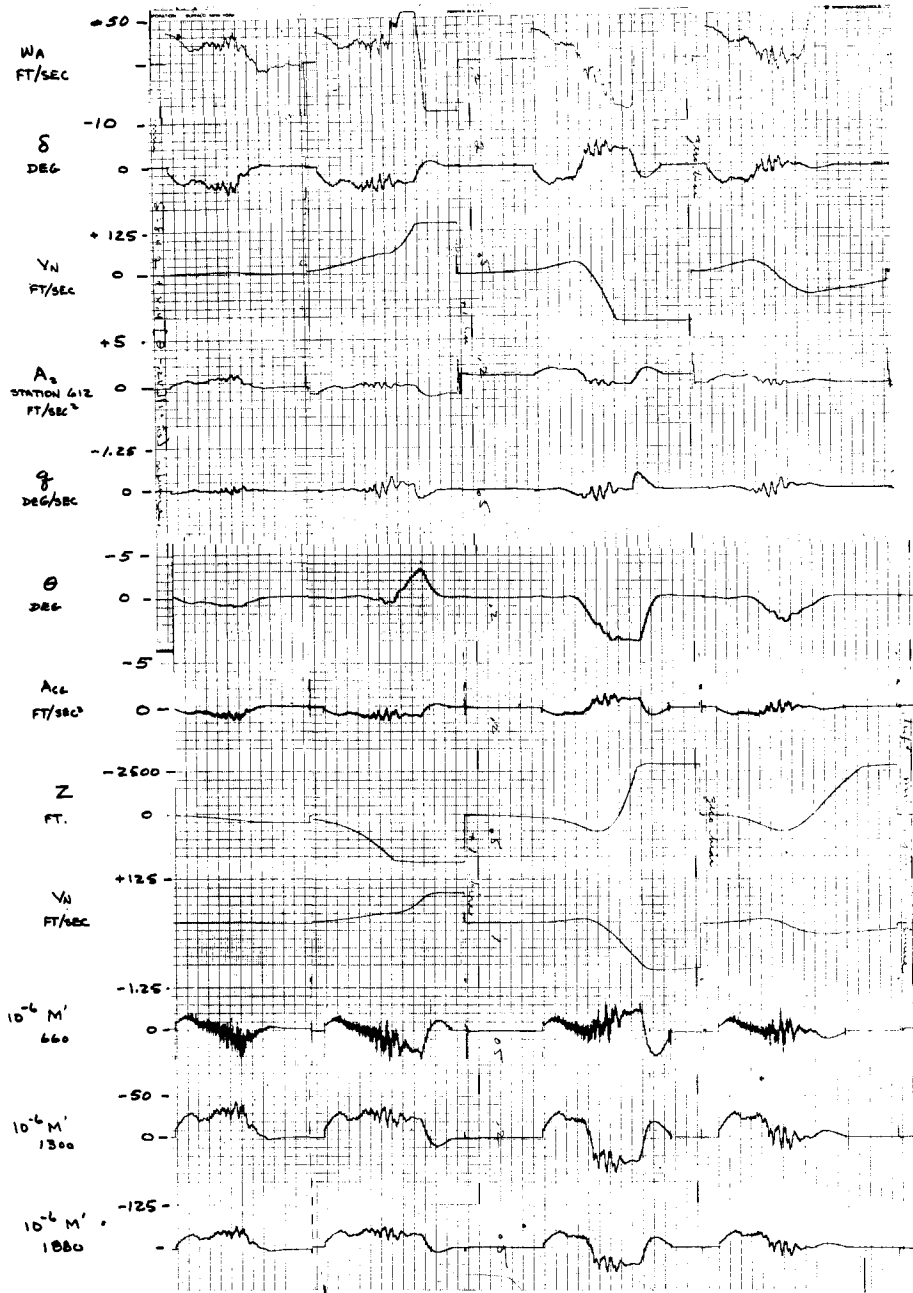


Figure 10. Minimum Drift, Attitude Hold, and Three Load Relief Controls for a Statically Stable Vehicle



MIN DRIFT	LOAD RELIEF
$S = 2.4g + 2.4 \left(1 + \frac{1}{10s}\right) (\theta - 2V)$	$S = 2.4g + 2.4 \left(K_B(\theta)B + \frac{K_A(t)A_1}{S+1}\right)$
ACCELEROMETER BIAS \rightarrow	
-1 FT/SEC ²	+1 FT/SEC ²
	ZERO

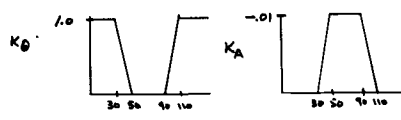


Figure 11. Minimum Drift versus Acceleration Load Relief, Showing Accelerometer Bias Effect

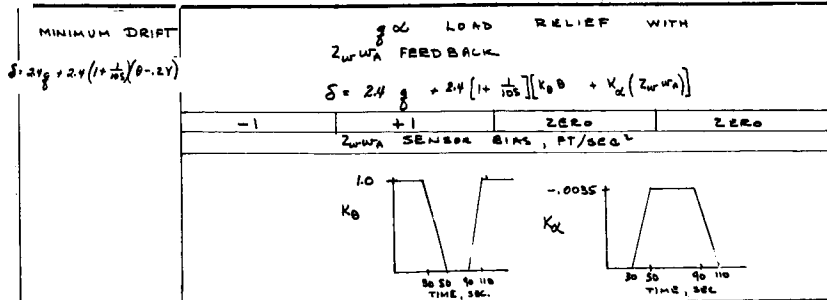
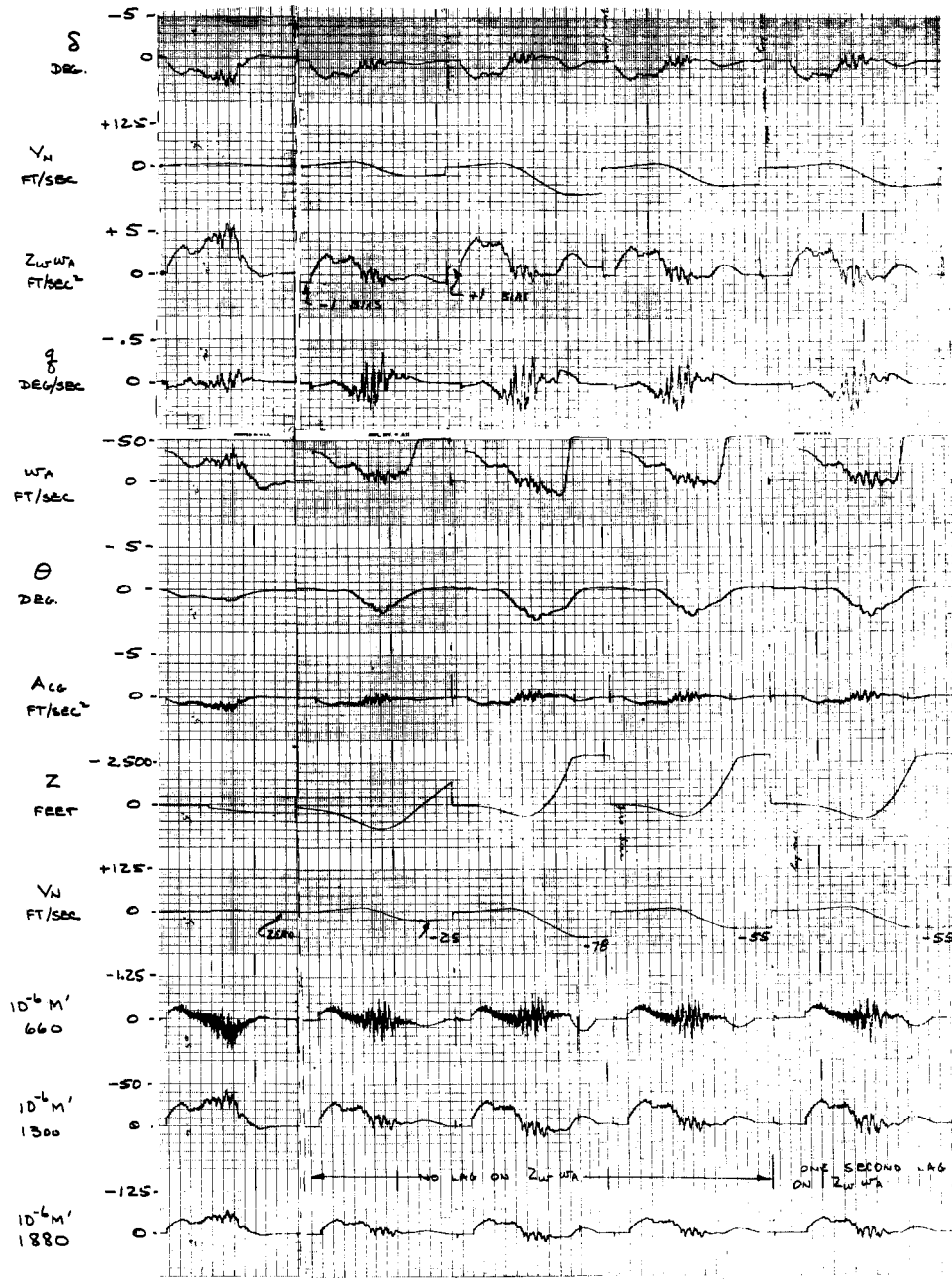


Figure 12. Minimum Drift and "g" of Load Relief, with Bias on "g" Sensor

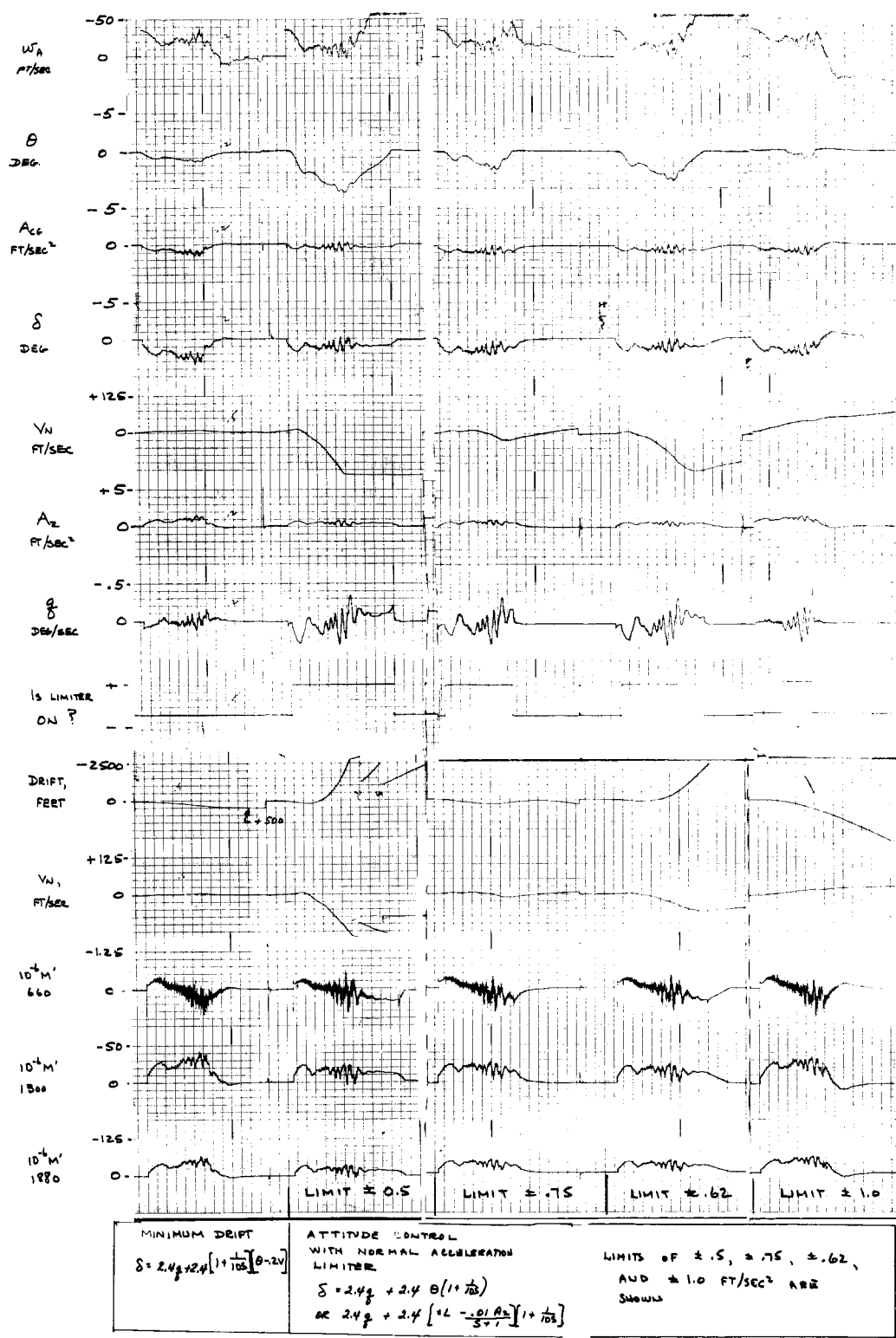


Figure 13. Minimum Drift versus Acceleration Limiter for Load Relief

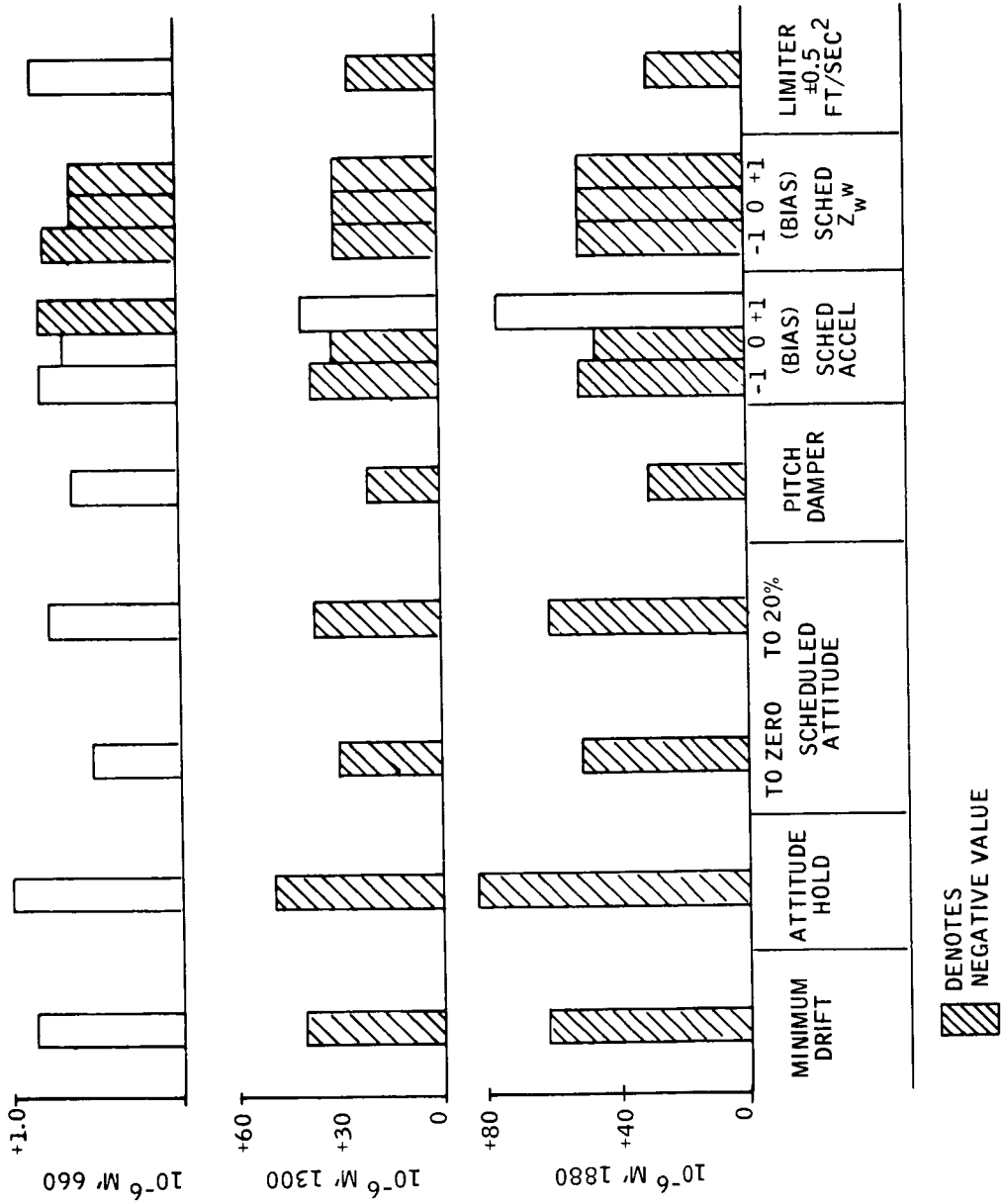


Figure 14. Bending Moments From Analog Simulations

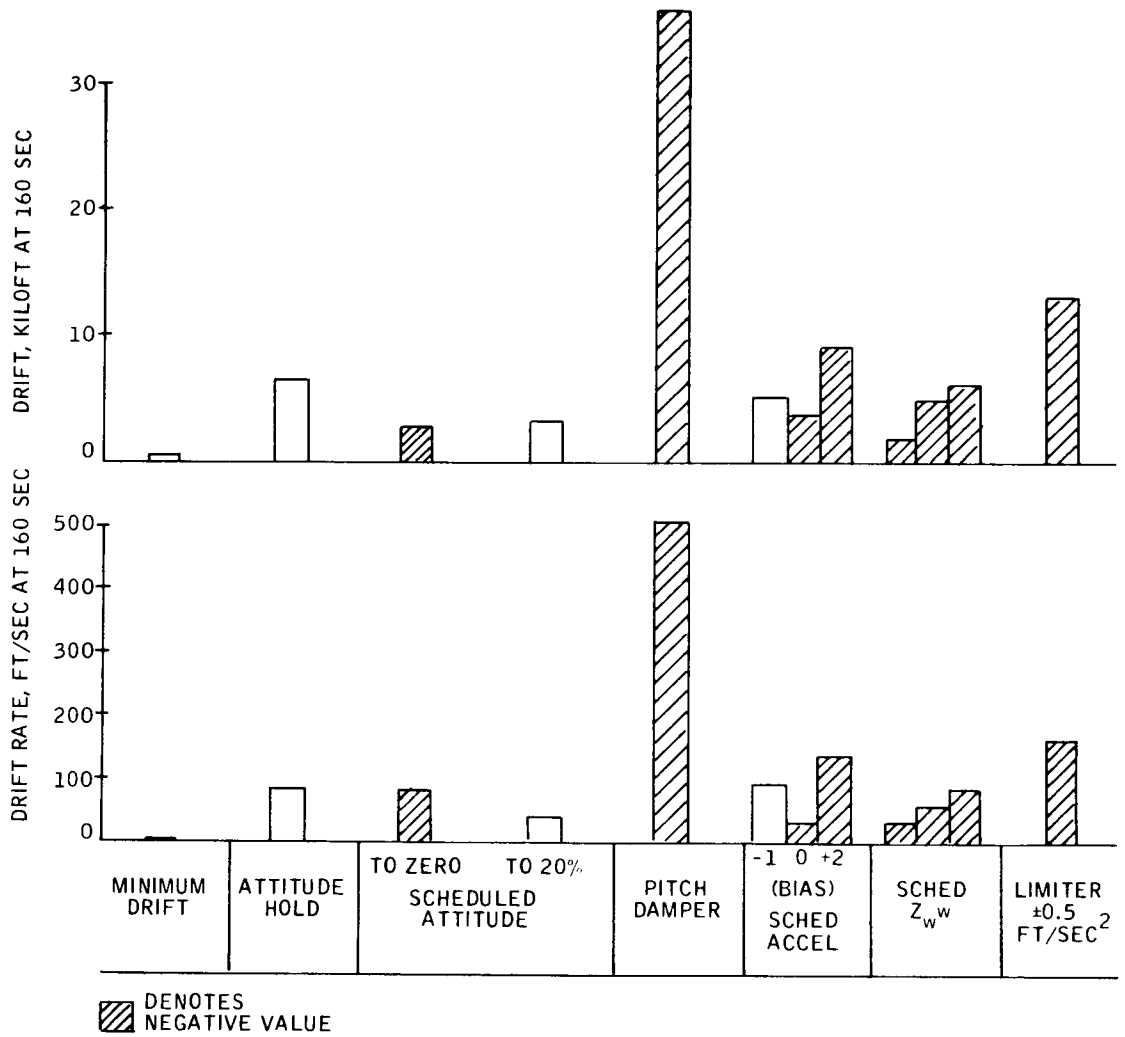


Figure 15. Drift and Drift Rate From Analog Simulations

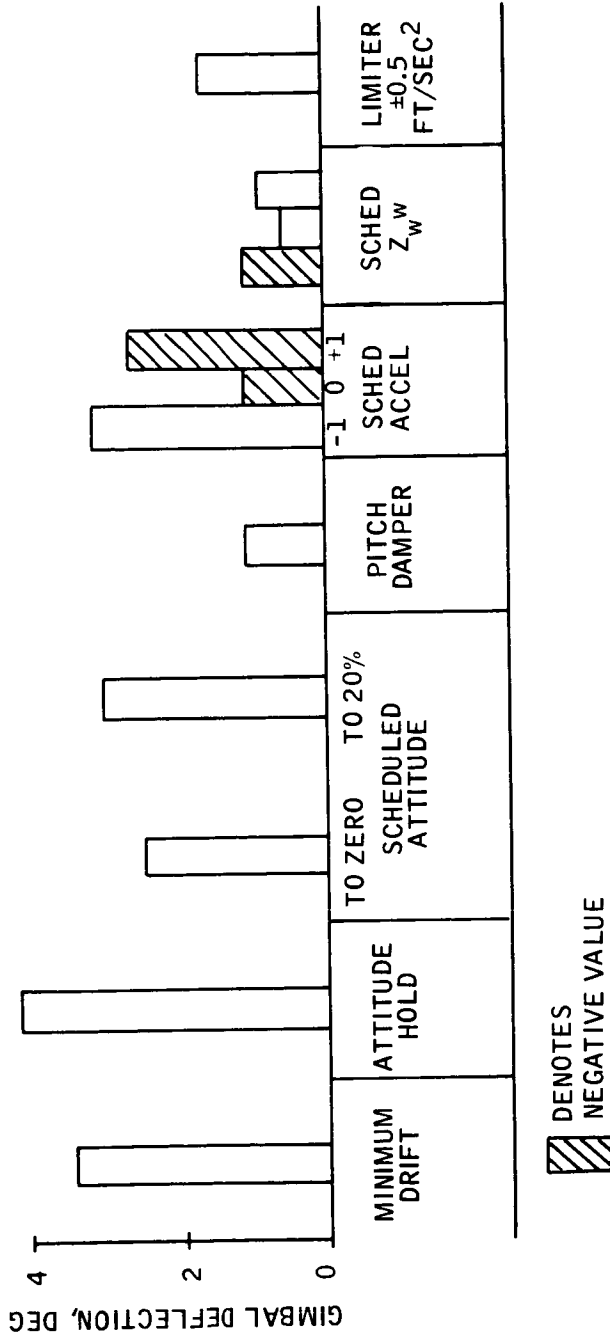
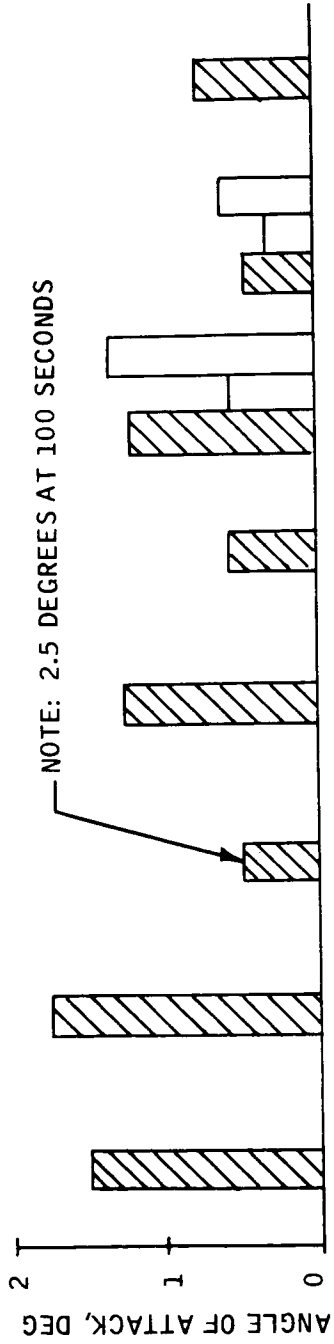


Figure 16. Angle of Attack and Gimbal Deflection at 64 Seconds From Analog Simulations

pressure region. In Figure 15 the drift for the scheduled attitude system is quite low, about 2500 feet up wind.

The pitch damper system shows good load relief, but is impractical because no steering is provided for the entire trajectory.

The scheduled acceleration and attitude systems show good performance when no bias is present; it equals that of the scheduled attitude system. Accelerometer biases of ± 1 ft/sec² cause performance to deteriorate badly. This bias could be produced in a body-mounted accelerometer with a 1-deg error in the predicted gimbal deflection at 64 sec. There is no reason to use an accelerometer for static stability augmentation where the vehicle is inherently stable. The scheduled Z_{ww} feedback system shows reasonable performance, with biases having less effect than in the accelerometer system. Again there appears to be no need with a stable vehicle.

The limiter system is shown on the extreme right in Figures 14 through 16, and recordings in Figure 13. It was devised to provide load relief without time scheduling, which is subject to errors. If, for example, one or two engines fail, it provides reasonable performance. However, it has two major objections:

- The vehicle is on the limit too much of the time. Figure 13 shows 110 sec with the limit set at ± 0.5 ft/sec². In this respect it is much like the pitch damper system; both have unstable (but very small) poles.
- It would be subject to the same accelerometer bias problems as the scheduled accelerometer system.

The results of this subsection indicate:

- The scheduled attitude system is the best of the systems tested. It is simple and provides both load relief and low drift.
- An attitude hold system should not be used even if bending moments are not a severe problem; a minimum drift system results in lower moments and minor guidance errors at cutoff.

COVARIANCE ANALYSES

The two primary objectives of this subsection are to 1) present the comparative analyses of seven of the conventional controllers discussed in the previous subsection; and 2) present results for two additional controllers developed by stochastic optimization techniques.

After discussing the above nine controllers, the results of a check on the validity of the covariance analyses will be presented. The check shows the covariance analyses presented are valid. The check was considered mandatory because of an unexpected difficulty that arose in performing comparable types of covariance analyses for lateral launch (Section III).

The earlier Overview subsection presented the major results; it did not consider the following details.

Figures 3 through 6 present comparisons of the effectiveness of seven conventional controllers as evaluated by analog simulation and by covariance analyses. Appendixes B and C present the plant representations used for the analog and covariance analyses. Table 7 briefly summarizes the major differences between the plant models of Appendixes B and C. Differences in the simulation of controllers are presented in Table 8. The quadratic controllers (Q13) are not tabulated in Table 8. They are state controllers which will be described later.

With a single exception there are good and valid reasons for the differences. In one case (the resolution of the wind) it is due to a lack of coordination between the investigators. That there are differences in models implies that comparisons are not strictly on "apples to apples" bases. To some extent this is desirable; it indicates the sensitivity to procedures and to data.

Immediately following is a discussion of the differences in simulations and data. The major differences are summarized in Tables 7 and 8.

Resolution of the Winds

For the covariance analyses the winds were assumed to be orthogonal to the flight path. For the analog analyses the winds were assumed to be parallel to the earth's surface; only the component normal to the flight path was used. In particular, at the high-dynamic pressure flight condition the flight path angle is 50 deg; the analog wind is 64 percent of the digital wind. This is one reason why the results of the covariance analyses are more severe.

Number of Winds

The covariance results use the Skelton differential equation fit (Appendix A) of the Vaughan (ref. 5), E-W March Kennedy data for the mean and random components of the wind. The entire wind population is used.

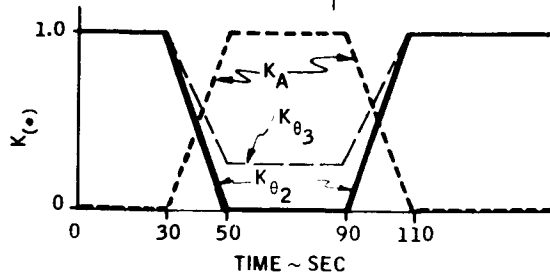
For the analog simulations, the Skelton differential equations were analog simulated. A wind was generated (Figure 7), stored on magnetic tape, and used for all the analog simulations; it is used in the same manner as a synthetic wind.

Table 7. Simulations Compared

Covariance	Conventional
Winds orthogonal to flight path	Winds parallel to earth's surface
All winds used	A single wind sample used
First-order actuators	Second-order actuators, DWT and TWD
Accelerometer at 718	Accelerometer at 612
Violently faired static derivatives	Smoothly faired wind tunnel static derivatives
Contains dynamic derivatives	Omits dynamic derivatives
Contains gust penetration	Omits gust penetration
Wind axes equations	Body axes equations
3-g reference trajectory	4-g reference trajectory
Bending moments for $-a$ only	Bending moments for both Δa and $-\Delta a$

Table 8. Controllers Compared

Covariance	Both	Conventional
$u_1 =$	$2.4 q$	
$u_7 =$	$2.4 q + 2.4 \theta$	
$u_2 =$	$2.4 q + 2.4 K_{\theta_2} \theta$	
$u_3 =$	$2.4 q + 2.4 K_{\theta_3} \theta$	
$u_{4D} = 2.4 q + 2.4 \theta$ $+ \frac{0.048}{57.3} Vy - \frac{0.0048}{57.3} z$		
$u_{4A} =$		$2.4 q + 2.4 \left(\theta - \frac{0.02 \sqrt{N}}{57.3} \right) \left(1 + \frac{1}{10s} \right)$
$u_{5D} = 2.4 q + 2.4 K_{\theta_2} \theta$ $+ 0.024 K_A \eta_{1T}$		
$u_{5A} =$		$2.4 q + 2.4 \left(K_{\theta_2} \theta - \frac{0.01 K_A \Lambda z}{s+1} \right)$
$u_6 =$	$2.4 q + 2.4 (K_{\theta_2} \theta - 0.0035 K_A z_w w_A)$	
η_{1T} @ 718		
A_z @ 612		



Gimbal Actuators

The analog simulations used second-order actuators with both TWD and DWT dynamics. The previous subsection shows that the effects of both TWD and DWT dynamics are negligible. First-order actuators were used for the covariance analyses; both simulations have the same break frequencies.

Accelerometer Location

The accelerometer feedback for the analog simulations had the accelerometer at station 612. For the covariance analyses it was at 718 (the pilot's station). Both stations are well forward of the center of mass so the differences in results should not be marked because of this.

Static Derivatives

The MSFC data package (ref. 10) had wind tunnel values for $C_{L\alpha}$ and $C_{m\alpha}$ at seven different Mach numbers. For the analog simulations a curve was faired through these test points. For the analog simulations some additional points were generated by use of the Datcom handbook (ref. 2).

With feedback control, it is doubtful that these differences are significant.

Dynamic Derivatives

The covariance analyses contained the stability derivatives L_q , L'_α , M_q , and M'_α . For the analog simulations these were taken to be zero.

Gust Penetration

The covariance analyses include gust penetration; the analog uses sudden immersion. For the conventional controller comparisons, the differences should be minor. Gust penetration dynamics are mandatory for synthesis of stochastic controllers by quadratic control methodology (ref. 6 and 7)

Axes

Body axes for the analog simulations and wind axes for the covariance -- there had better not be any significant differences due to these.

The analog drift and drift rate equations are accurate. Relatively simple approximations to drift rate and drift are used for the covariance analyses.

Reference Trajectories

Three-g limit for the covariance and 4-g limit for the analog -- Reference 11 shows there are negligible differences over the most important 120 sec of flight.

Bending Moments

At the high-dynamic pressure flight condition the analog simulations used

$$\Delta M_{1880} = \begin{cases} -22.8 \cdot 10^6 (57.3)\Delta\delta + 5.84 \cdot 10^6 (57.3)\Delta\alpha & \text{for } \Delta\alpha > 0 \\ -22.8 \cdot 10^6 (57.3)\Delta\delta - 10.1 \cdot 10^6 (57.3)\Delta\alpha & \text{for } \Delta\alpha < 0 \end{cases}$$

but the digital took (because $\alpha_{\text{TRIM}} < 0$)

$$\Delta M_{1880} = -22.8 \cdot 10^6 (57.3)\Delta\delta - 10.1 \cdot 10^6 (57.3)\Delta\alpha$$

Similar differences occur in the ΔM_{1300} and ΔM_{660} equations. For the results obtained there are no differences due to this for stations 1300 and 1880, because $\alpha < 0$ for maximum bending moments in the analog simulations.

Conventional Controllers

Table 8 presents the controllers compared. There are no differences between covariance and analog in controllers 1, 7, 2, 3, and 6.

For controller 4, the analog version includes an integration on pitch attitude (θ) not present in the digital simulation.

For controller 5, the accelerometer is lagged in the analog version while it is not in the digital simulation. For the rigid-body representations used here it is believed the differences due to this are small.

Discussion

The comparative performance evaluations of the seven conventional controllers previously discussed in the Overview subsection will now be augmented. Figures 3 through 6 present the comparisons.

The results on these figures from analog simulations are taken directly from the previous subsection (Conventional Analyses)

The covariance differential equations for the plant model of Appendix C were integrated by digital computer. The mean and covariance results for

these integrations are included in Appendix C. These tables were read to determine the maximum response data of Table 2. These data (except for the times at which maxima occur) are presented in Figures 3 through 6.

The synthesis of the quadratic stochastic controllers is discussed in the following paragraphs. The primary objective for this part of the effort is to obtain measures of the percentage gains in load reduction, gimbal deflection, and terminal drift over that attainable with good conventional controls. The effort here terminates after achieving these measures. Termination at this point is an unfortunate necessity imposed by the time and money constraints of a small technology contract effort. It is unfortunate because the improvements in load reduction, gimbal deflection, and drift are demonstrably achieved with controllers requiring not only full state measurement, but also mean wind biasing. These quadratic stochastic controllers are unpalatably complex. Honeywell practical experiences with other vehicles and in-house theoretical studies (partially sponsored by the NASA MSFC) strongly suggest that performance improvements achieved with full state control can be essentially achieved with controllers of acceptable complexity.

The quadratic stochastic controllers were synthesized by the method of ref. 6). Since maximum allowables for the response states are not known for this vehicle, the design objective was to improve all responses over the best attained by conventional control. Table 2 and Figures 3 through 6 present maximum responses for these controllers.

Figures 17 through 19 present the mean responses, covariances, and controller gains for controller Q13. The results of Figure 19 for the gains for Q13 controller are mostly disappointing. Most encouraging is that the gimbal feedback gain implies the closed-loop bandpass is low; i. e., the controller is not likely to excite the flexure modes that have been neglected. The disappointing aspect is in the lack of physical interpretation for the other gains. A very important result of applying the quadratic stochastic design methodology to Saturn V class vehicles in ref. 6 was the obvious physical interpretation attributable to the controller gains. This permitted the results to be used as design guides for conventional synthesis. No such physical interpretation appears from the controller gains of Figure 19.

There were no difficulties in applying the quadratic methodology of ref. 6 and 7, to analysis and synthesis of the pitch plane for shuttle. Subsequently lateral axes launch analyses at first yielded a 0.7-sec-per-cycle divergent oscillation for which it was necessary to decrease the digital time step by a factor of 2.5 to get satisfactory results; an ultraconservative factor of 5 reduction was finally used. This difficulty raised questions as to the validity of the pitch plane results that had already been completed, using a digital time step of 0.1 sec.

A digital time step of 0.02 sec was used to obtain additional covariance results for the conventional attitude controller (C7). These results are presented in Table C17; the response variables of interest differ less than one percent from those in Table C7 obtained using a 0.1-sec time step.

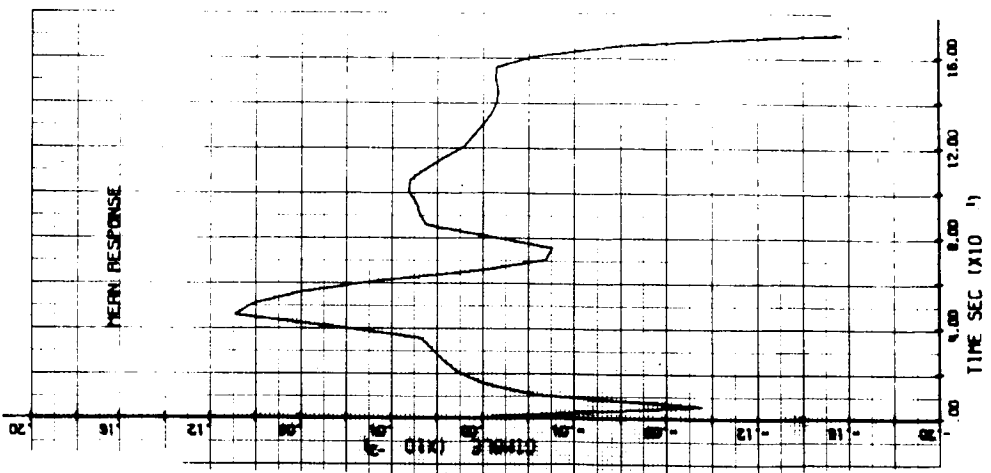
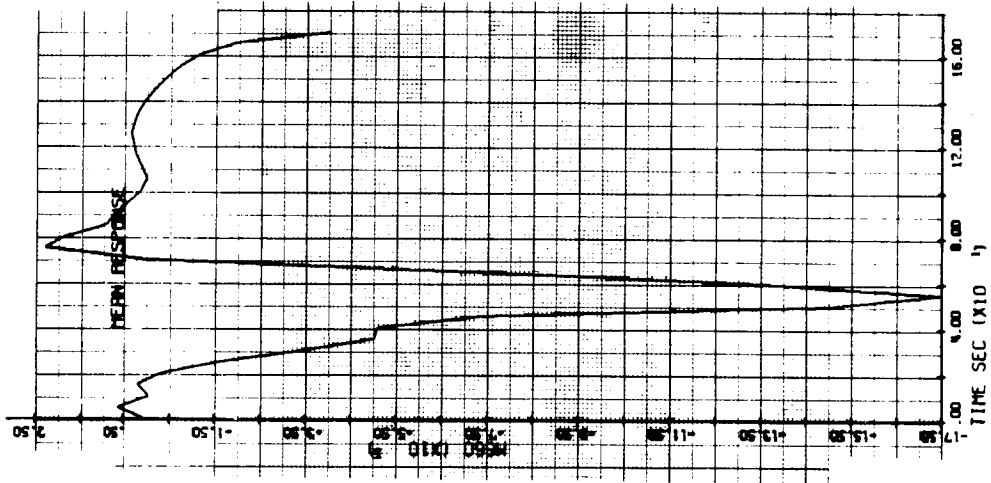
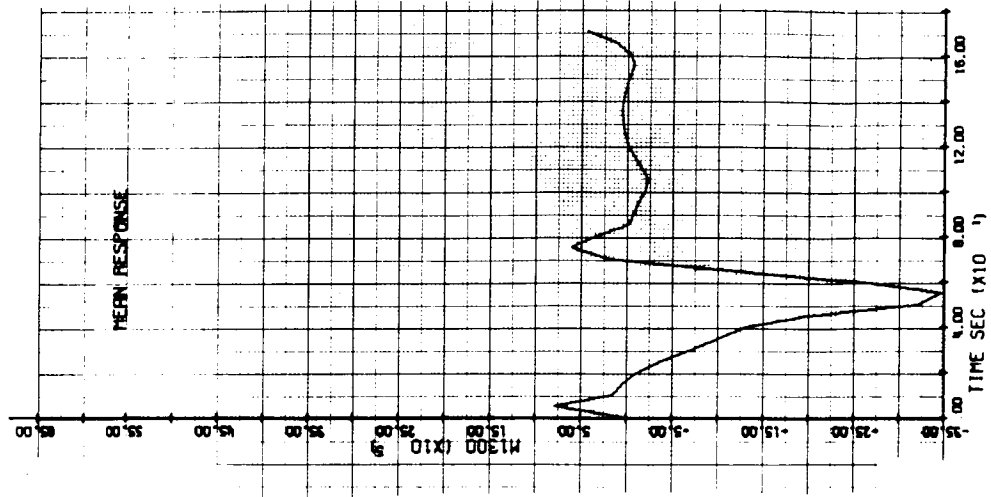


Figure 17. Mean Response

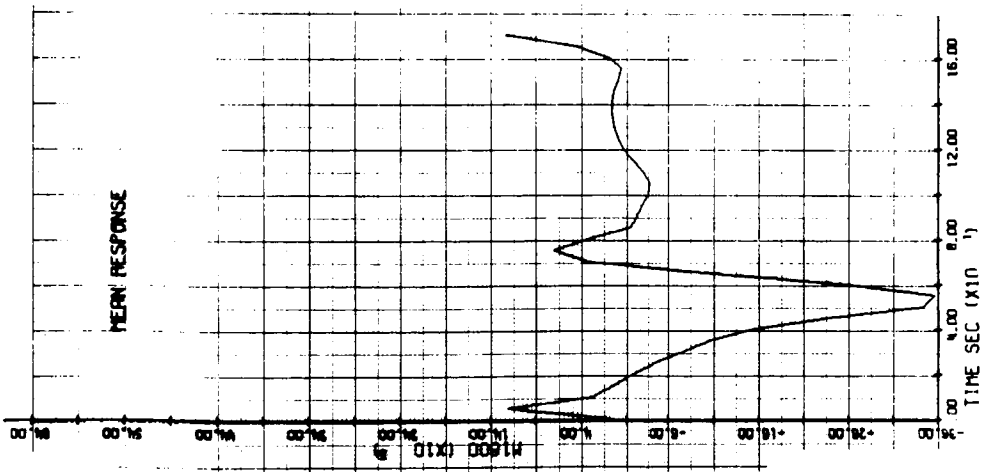
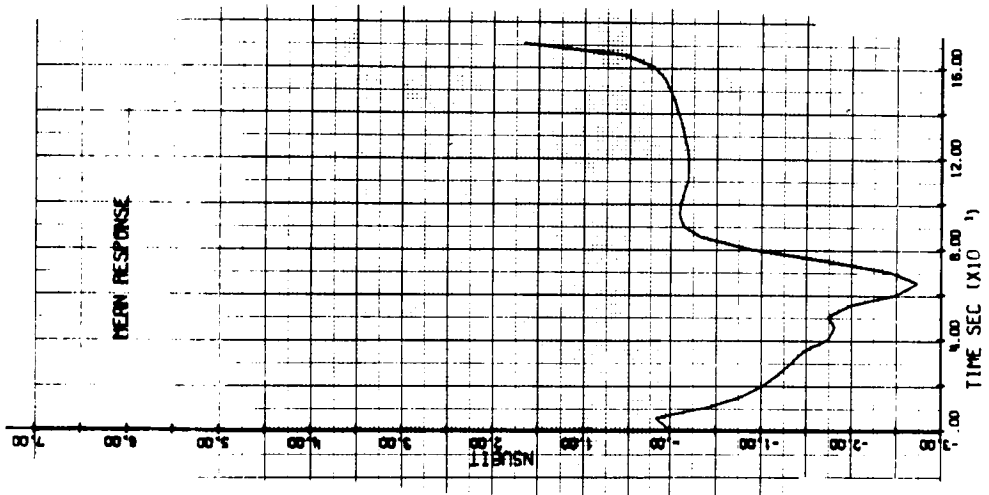
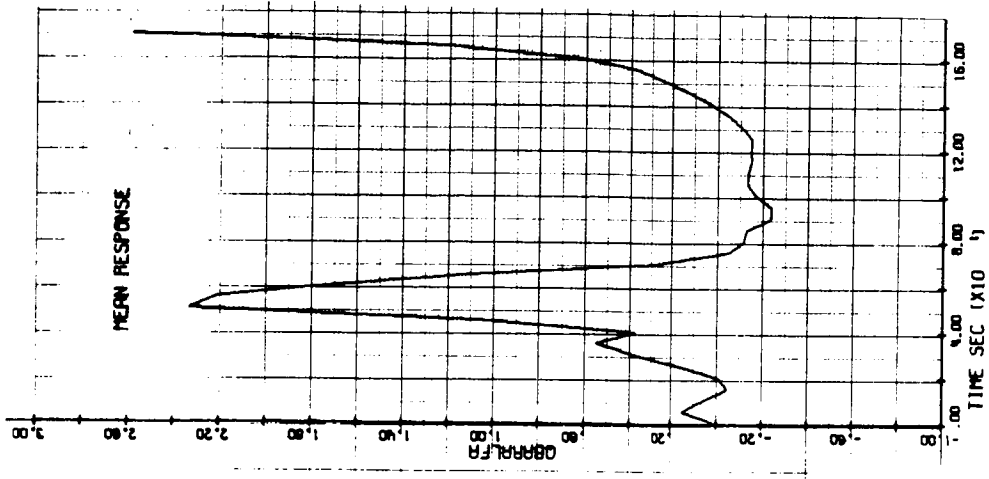


Figure 17. Mean Response (Continued)

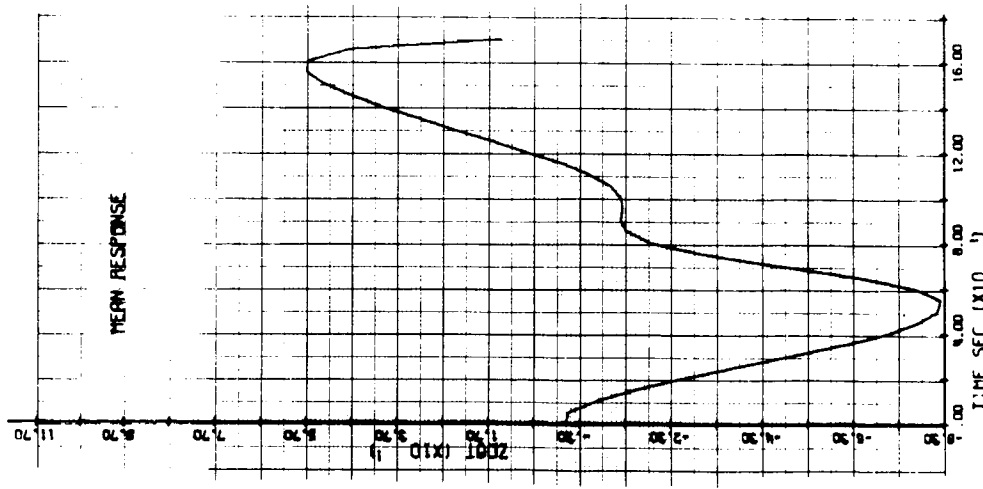
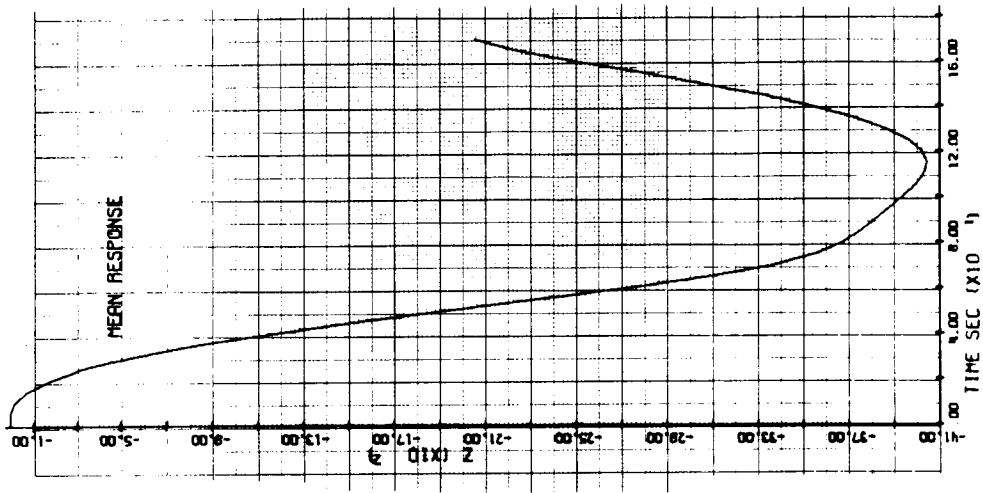


Figure 17. Mean Response (Concluded)

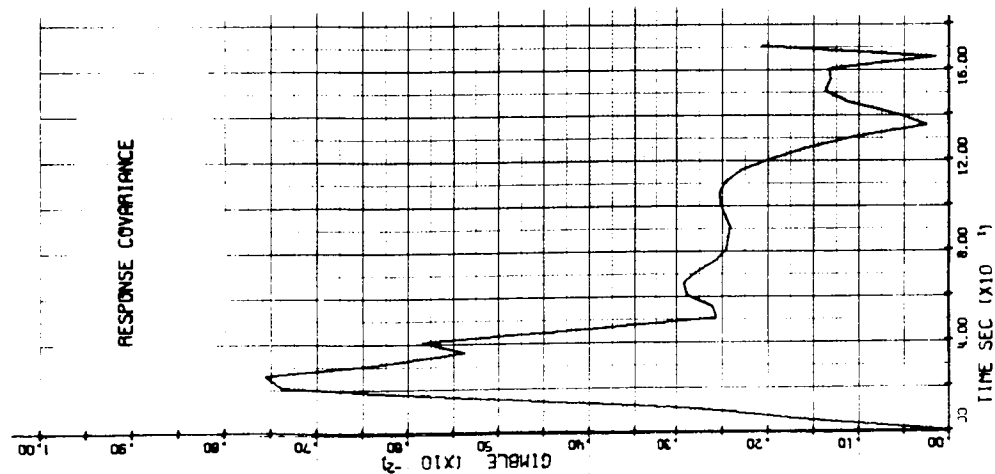
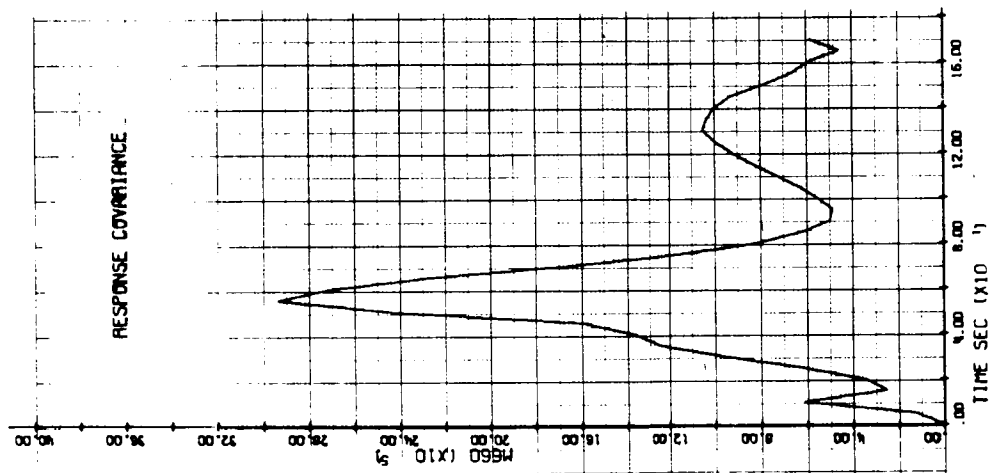
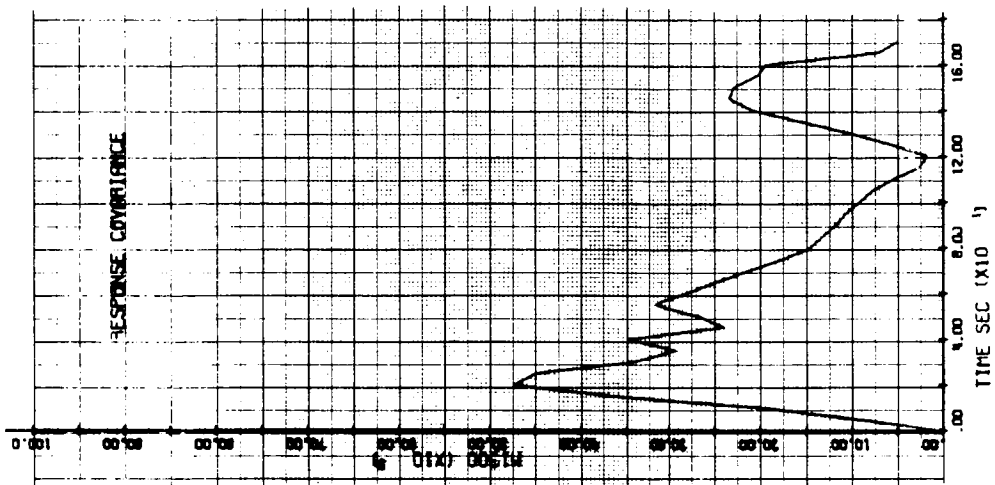


Figure 18. Response Covariance

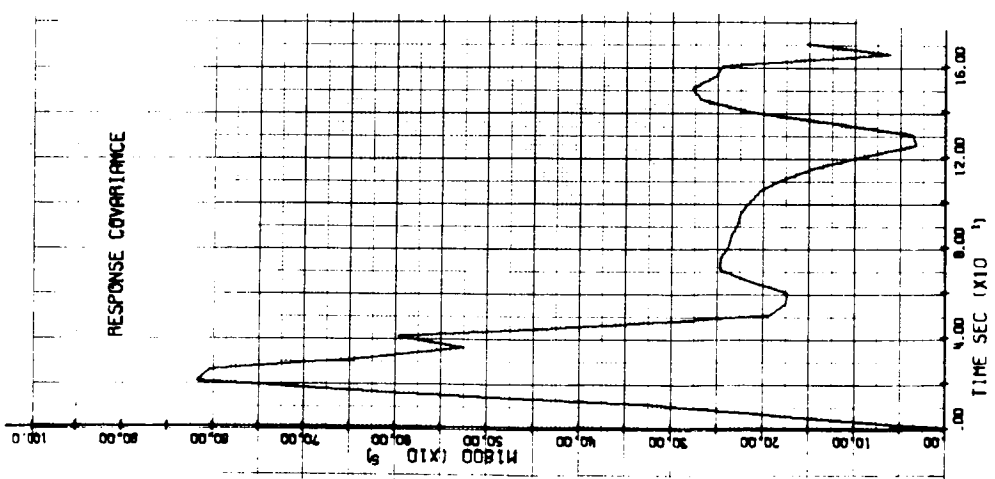
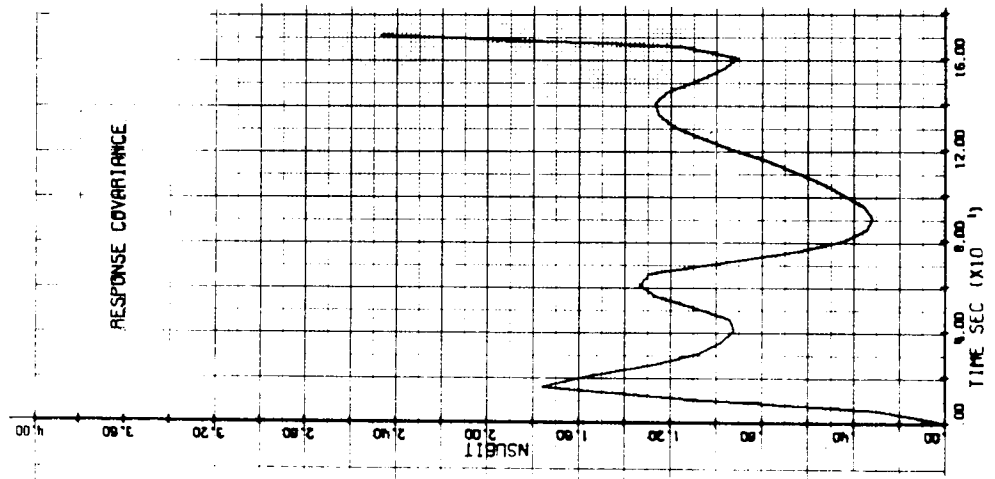
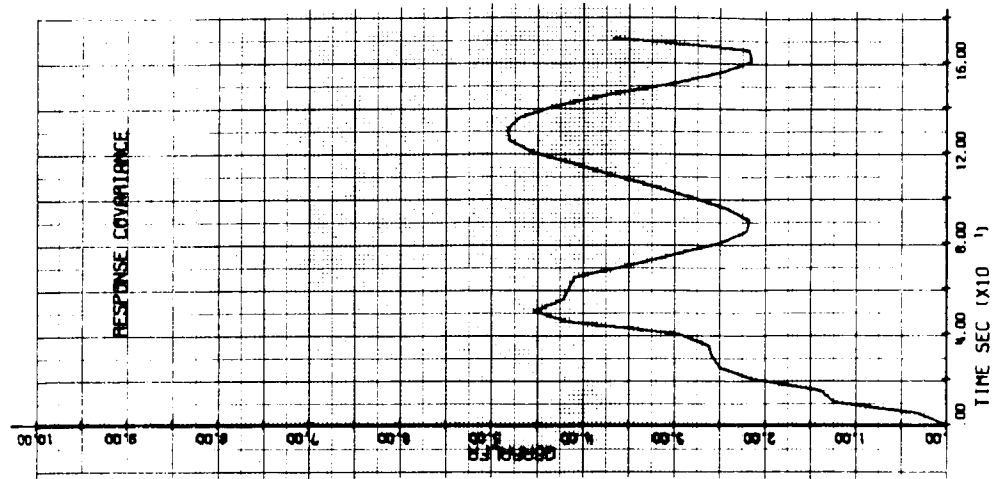


Figure 18. Response Covariance (Continued)

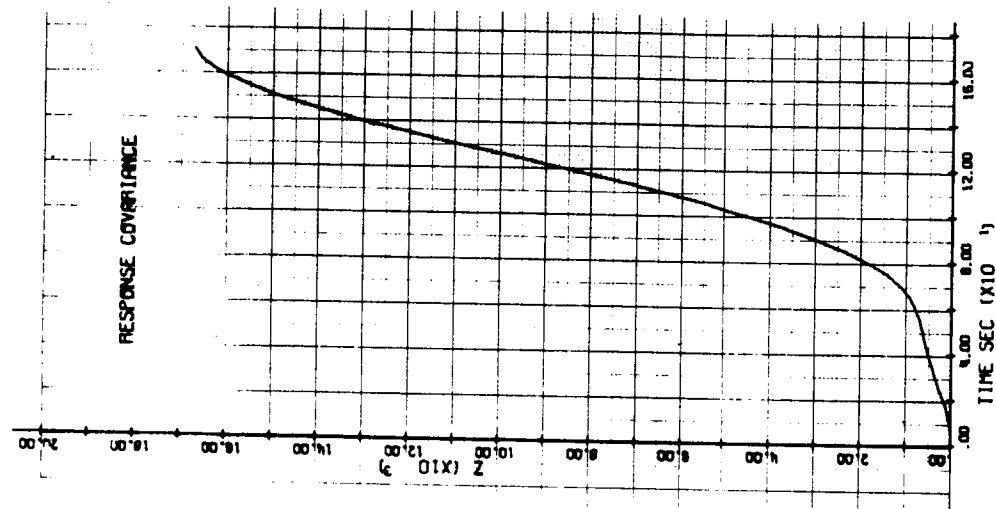
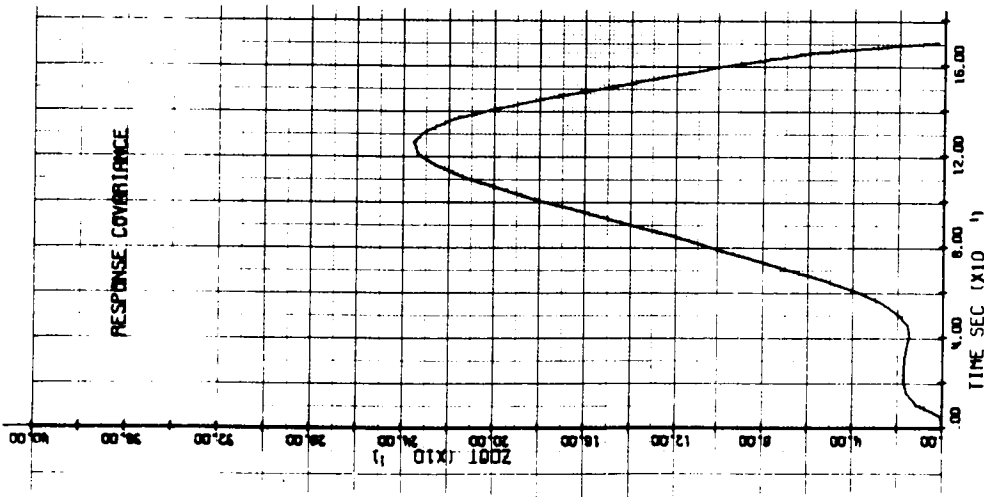


Figure 18. Response Covariance (Concluded)

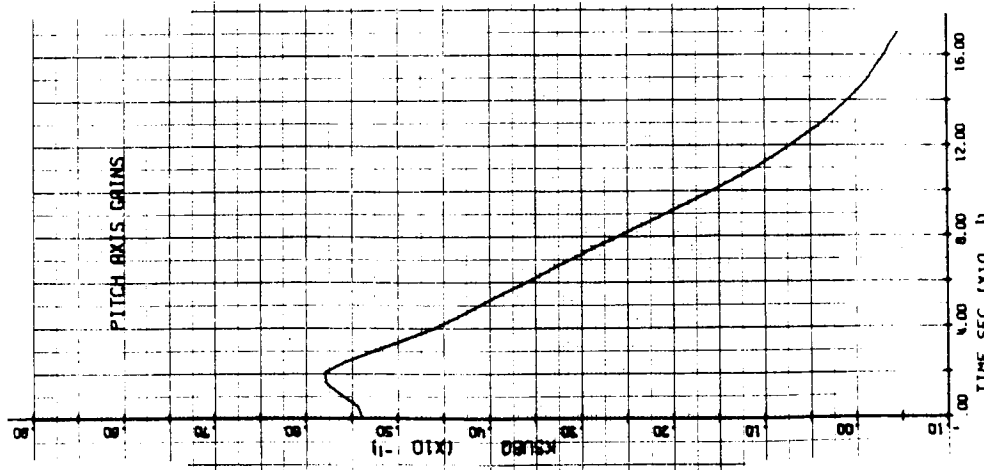
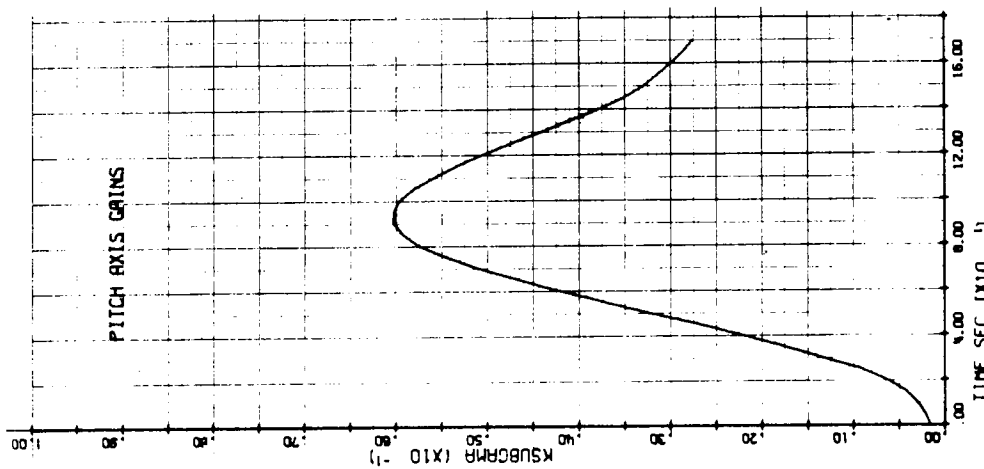
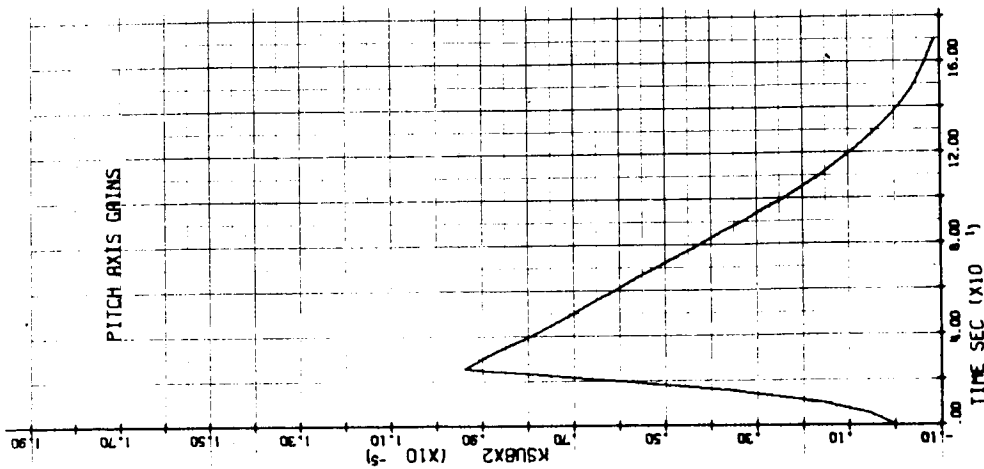


Figure 19. Pitch Axis Gains

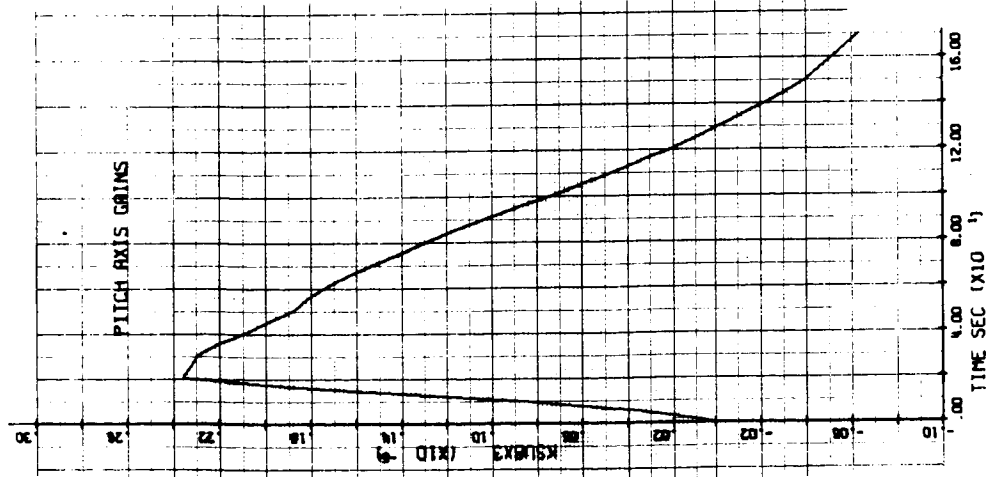
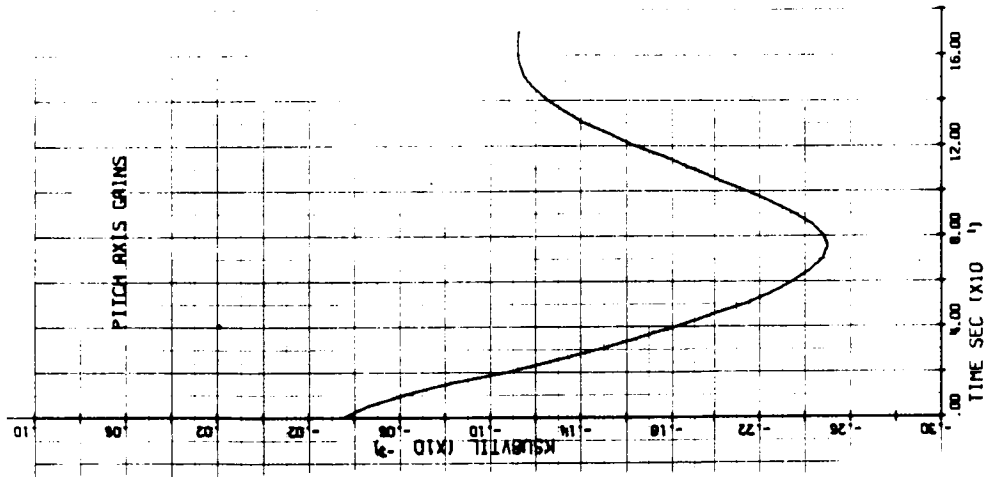
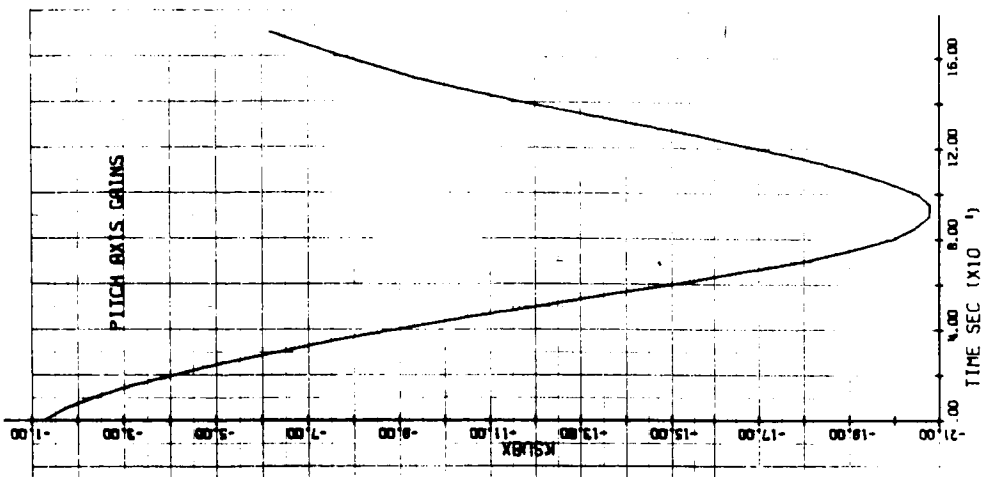


Figure 19. Pitch Axis Gains (Continued)

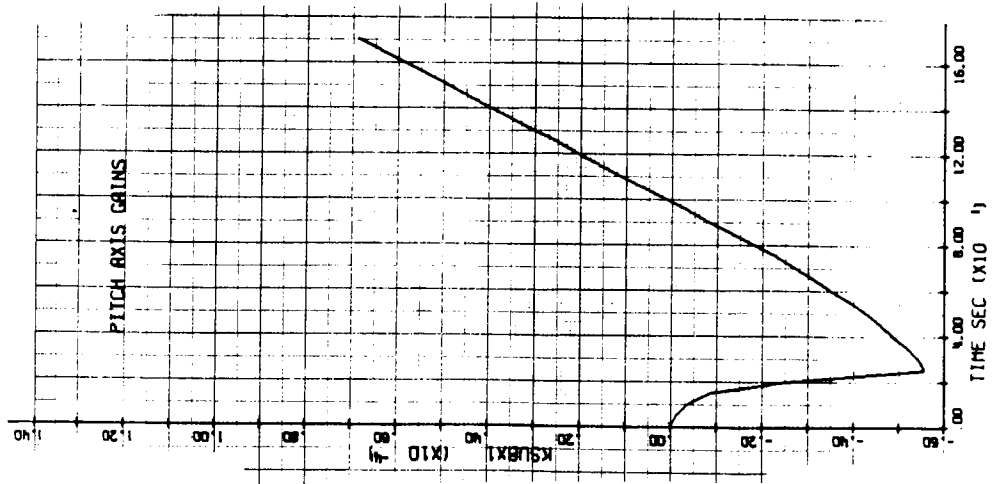
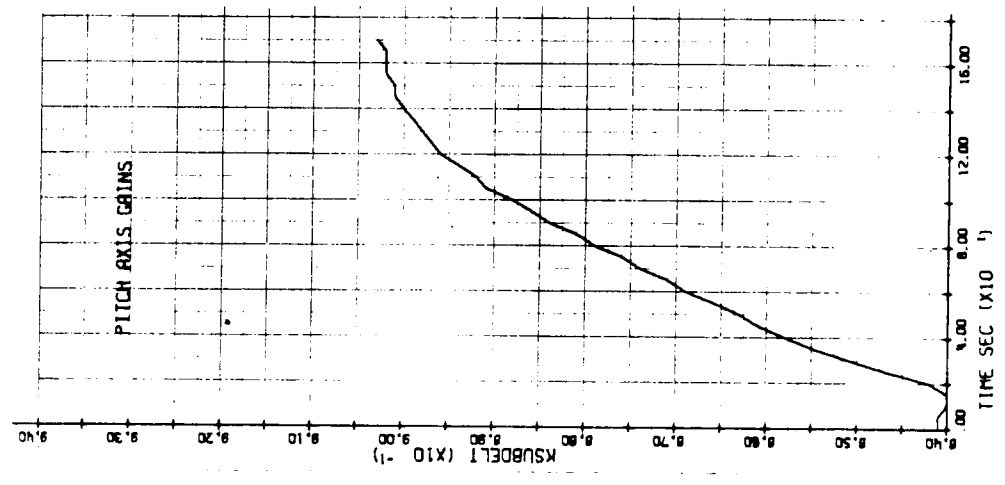
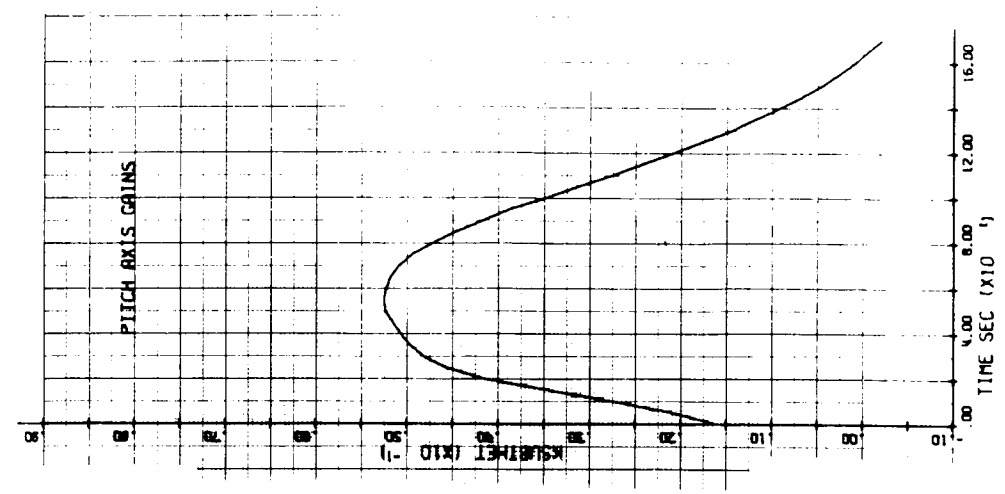


Figure 19. Pitch Axis Gains (Continued)

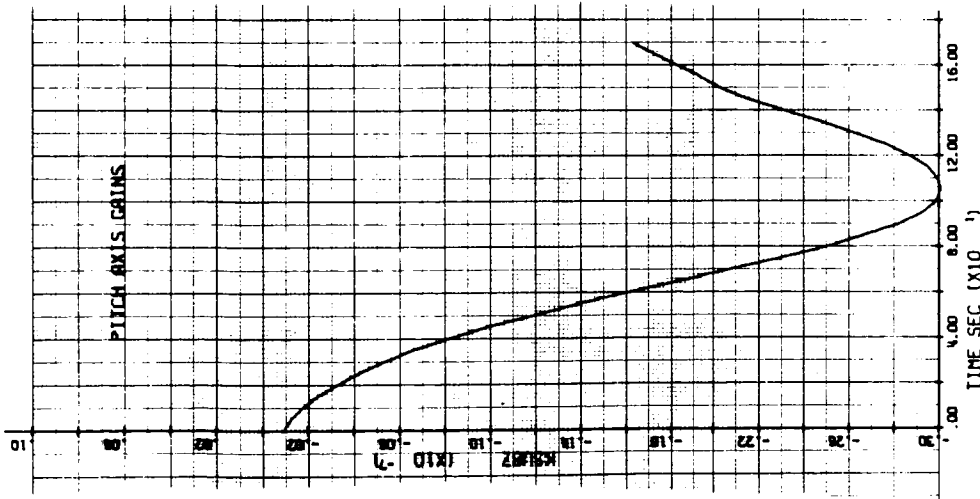
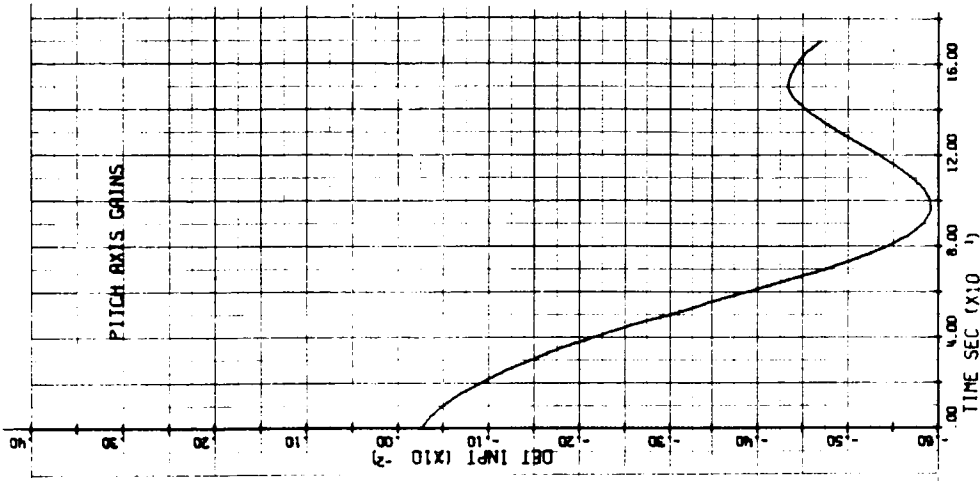


Figure 19. Pitch Axis Gains (Concluded)

SECTION III

LAUNCH PHASE LATERAL AXES CONTROL

Control of the lateral axes during the launch-phase control of Shuttle is examined. The objectives are to determine problems unique to the launch phase of large, winged, rocket-powered boosters and to provide potential solutions.

The major problem is the large amount of gimbal deflection required for roll control. Large roll gimbal requirements are primarily due to the relatively large ratio of dihedral effect relative to roll gimbal torques. The rolling moment due to sideslip is relatively large. Roll torques due to gimbal deflection are relatively small because the rolling moment lever arms are small.

Many solutions are available for the excessive roll gimbal requirements. For each, there are side effects which may be adverse. The rolling moment due to sideslip may be reduced by changing the dihedral. The aircraft may be permitted to roll to large angles to resolve the wind from the side axis into the pitch axis. For vehicles with swept back wings, trajectory shaping should be effective. Gimbal slewing systems different from the ones used might be better. The ailerons can be made operative during the launch phase. The airplane can be flown near zero sideslip during the high-dynamic pressure region where roll gimbal requirements are large. Only the latter two of the above potential solutions are considered in this section.

Ailerons are effective; however, aerodynamicists are having difficulties in developing aerodynamic lateral controls for shuttle craft that have acceptable characteristics during the high-dynamic pressure transonic regime where they are required.

Control of sideslip is considered in this section and found to be very effective in reducing roll gimbal requirements. Time and money restrictions did not permit obtaining results nearly as good as are believed to be available by this means.

The primary objectives of this effort are to determine and resolve problems in following the nominal trajectory. It is necessary to achieve small perturbation loads and terminal drift with small amounts of roll and yaw control.

The primary objectives of this effort are to determine and resolve problems in following the nominal trajectory. It is necessary to achieve small perturbation loads and terminal drift with small amounts of roll and yaw control.

The primary objectives have not been fully achieved. Problems have been identified and partially resolved. Five basic controllers were designed by conventional methodology (with nominal variations) and their capabilities evaluated for meeting objectives. In-flight loads, terminal drift, and gimbal requirements are significantly affected by controller type. The most severe interpretation of results presented here implies minimum yaw gimbal requirements of ± 6 deg and roll gimbal requirements of ± 15 deg; the gimbal systems employed use a ratio of 2:1 roll-to-pitch gimbal to achieve roll control. Hence, the roll gimbal requirement of ± 15 deg adds ± 7.5 deg to pitch gimbal requirements.

It is believed gimbal requirements can be reduced to ± 5 deg each for yaw and roll gimbaling.

Subsequent subsections present an Overview, results of Conventional Analyses, and finally of Covariance Analyses.

OVERVIEW

Salient results are summarized with minimum attention to technical detail. This provides an objectivity for interpretation of detailed discussions in subsequent subsections.

A three-view of the MSFC in-house Vehicle B shuttle used for this investigation is presented as Figure 1.

Figures 20 through 23 provide the summary. Two kinds of analyses were performed to generate these results. The left sets of bars containing both a clear portion for the mean response and a cross hatched portion for the rms response are the results of covariance analyses. A single sample of the random side wind model (cf Appendix A) used to generate the covariance analyses was used in the manner of a synthetic wind for the analog analyses. Figure 7 shows this sample; it is a 1σ wind with a " 3σ " peak at "55 sec." This sample was used to develop the conventional analysis results shown by shading on the right bars:

Gimbal requirements are now discussed. The top portion of Figure 20 expresses the peak roll torque requirement in ft-lb. These roll torques are generated from the gimbal deflections shown in the middle sketch. Yaw gimbal requirements are presented on the bottom sketch. The covariance results are always more severe than those obtained from the analog simulations; this is usually true for other variables. Both the covariance analyses and analog simulation results show marked differences in load severity with controller types but with generally the same trend characteristics.

Maximum in-flight loads are shown in Figure 21. Trend results for controller for the two types of analyses are consistent.

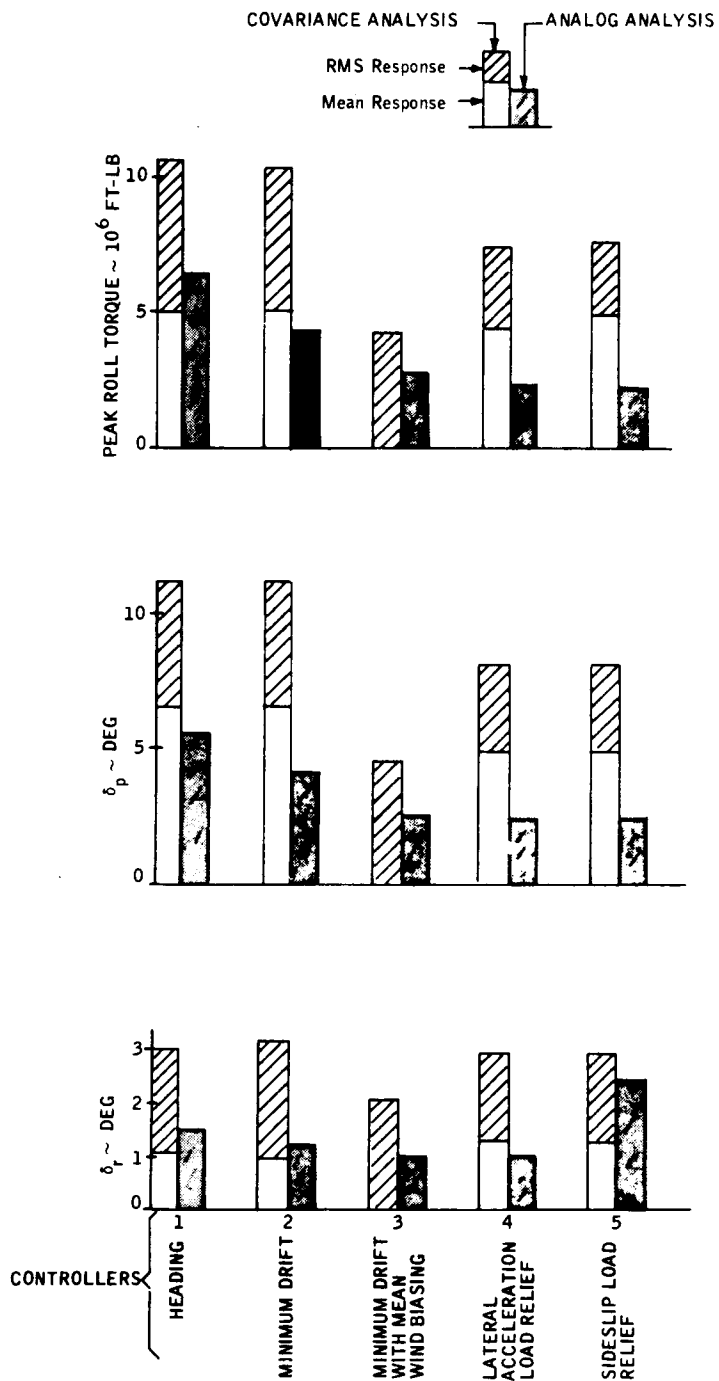


Figure 20. Maximum Gimbal Deflections

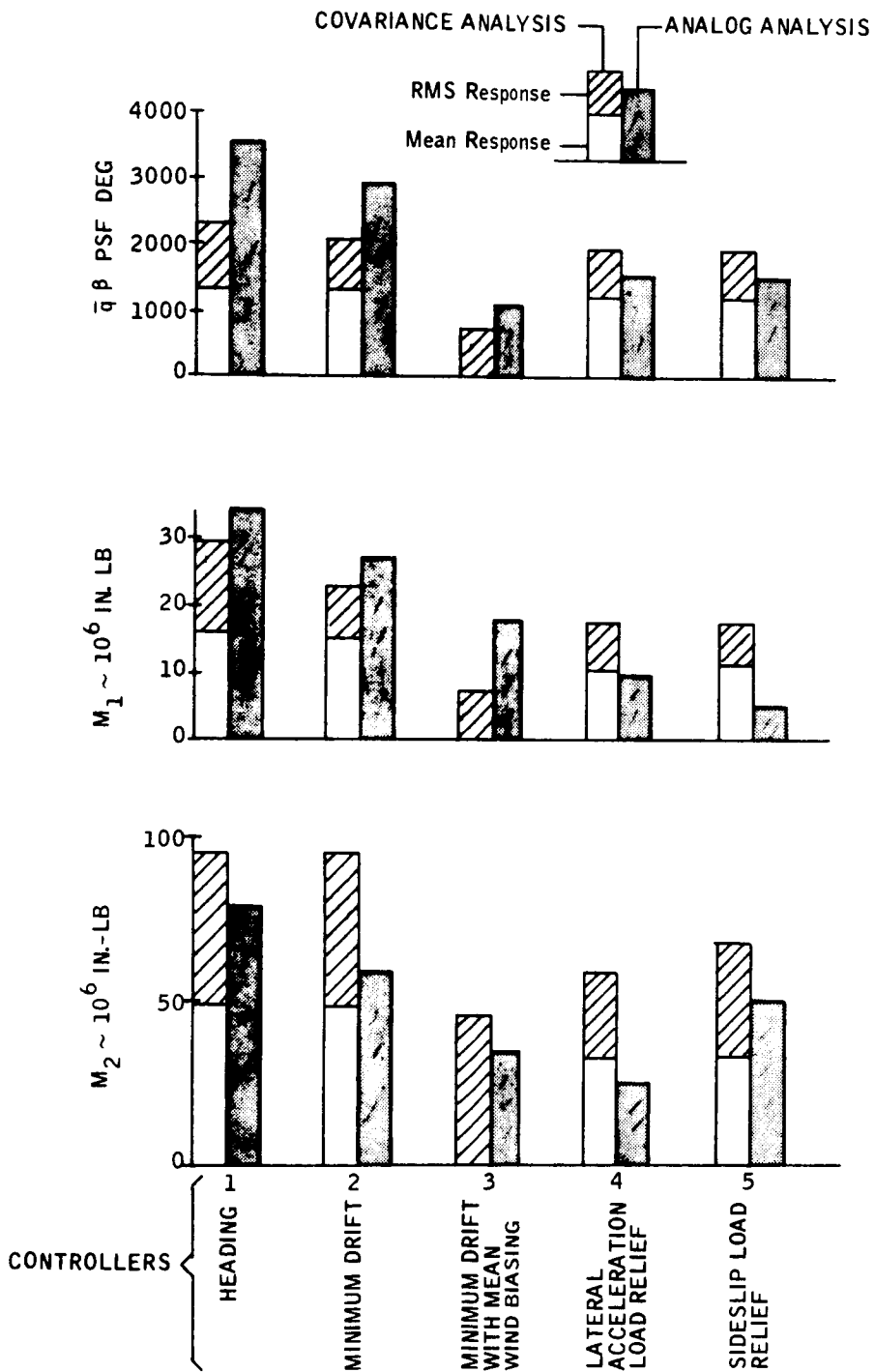


Figure 21. Maximum Inflight Loads

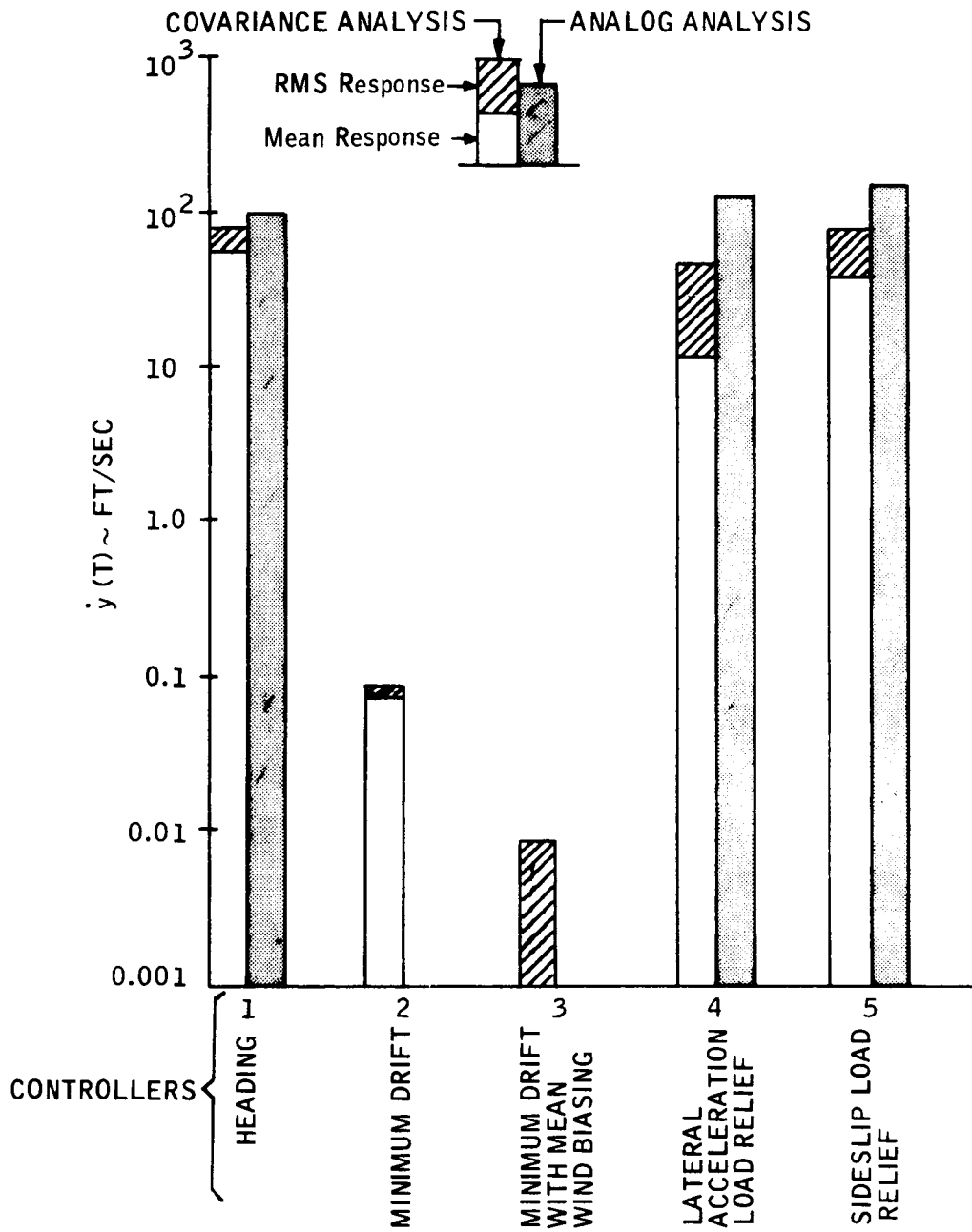


Figure 22. Terminal Drift Rate

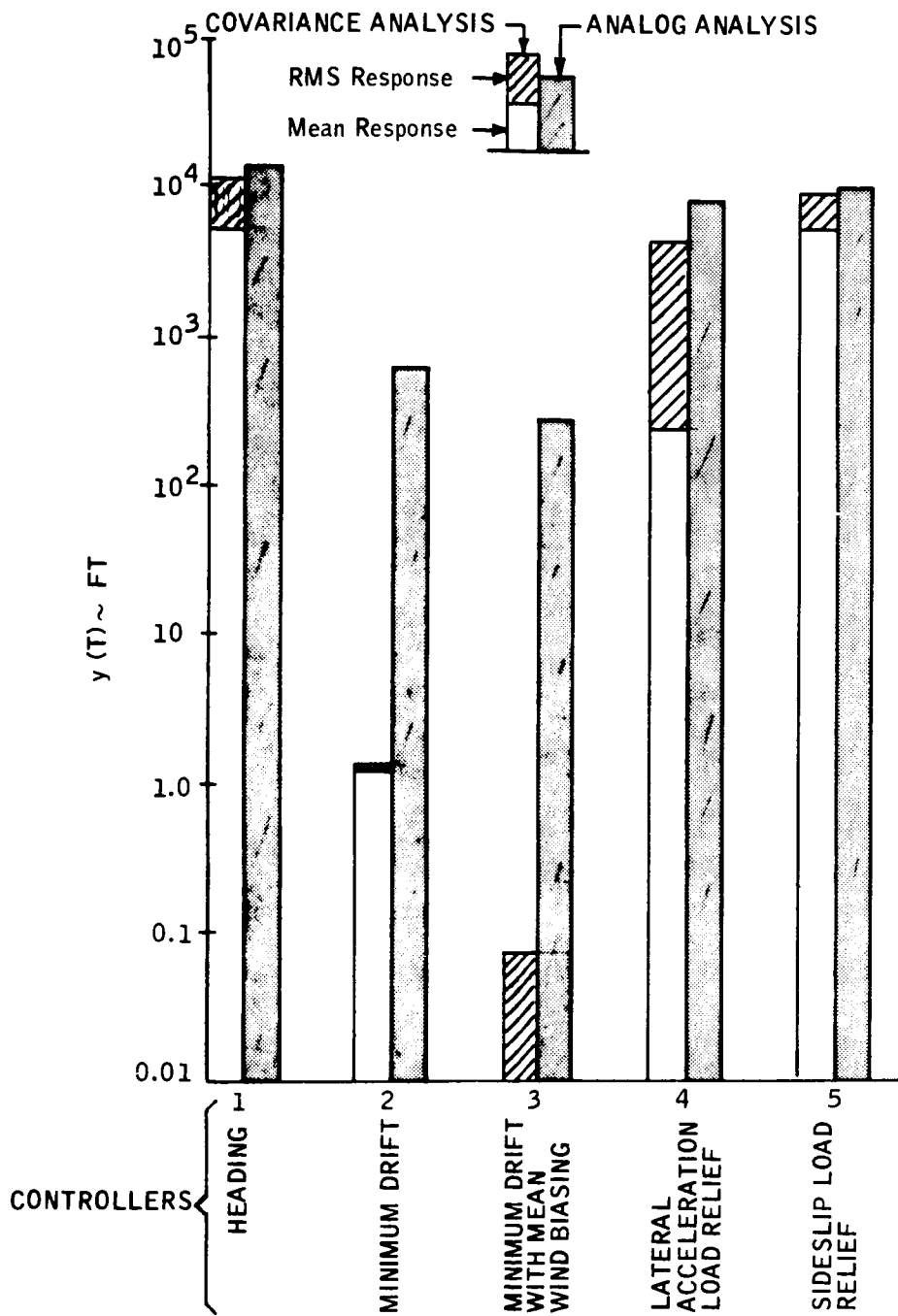


Figure 23. Terminal Drift

Figures 22 and 23 present drift rate and drift results. That there will be small drift rates and drifts achieved from the minimum drift controllers 2 and 3 is to be expected.

This subsection concludes with a rough analysis that attributes the large roll requirements to combination of dihedral effect and small roll moment gimbal arms. This indicates why the load relief controllers are effective in reducing roll gimbal requirements. It will also be shown that yaw gimbal requirements may be decreased slightly by obtaining a reduction in roll gimbal requirements in this manner. Finally, it is observed these load relief solutions reduce bending moments. These conclusions follow from:

$$t = 65 \text{ second}$$

$$\bar{q}\beta_{\max} \approx 3000 \text{ psf deg}$$

$$\bar{q} = 785 \text{ psf}$$

$$\beta_{\max} = \frac{\bar{q}\beta_{\max}}{\bar{q}} \approx 3.8 \text{ deg}$$

$$L'_{\delta_p} = 0.0376 \text{ per deg}$$

$$L'_{\beta} = 0.1190 \text{ per deg}$$

$$N'_{\delta_r} = 0.0247 \text{ per deg}$$

$$N'_{\beta} = 0.00461 \text{ per deg}$$

$$\left| \delta_{P_{REQ}} \right| \cong \left| \frac{L'_{\beta}}{L'_{\delta_p}} \beta_{\max} \right| = \frac{0.1190}{0.0376} 3.8 \approx 12 \text{ deg}$$

$$\delta_{r_{REQ}} \approx \frac{N'_{\beta}}{N'_{\delta_r}} \beta_{\max} \approx - \frac{-0.00461}{-0.0247} 3.9 \approx 0.71 \text{ deg}$$

The time is taken at 65 seconds. This is sufficiently close to the worst case. The $\bar{q}\beta_{\max}$ is taken from Figure 21. Table C8 provides \bar{q} .

Stability derivatives are taken from Table D8; different conclusions will not result from using the data of Appendix B (the major stability derivatives are not markedly different).

The equations for roll gimbal requirements ($\delta_{p_{REQ}}$) show that the roll gimbal requirements are generated by the causes previously stated.

The calculation for the yaw gimbal requirement has significant implications on bending moments. First it is noted the vehicle is directional unstable at 65 seconds (it is unstable for the first 135 seconds of flight). This requires the sideslip (β) and the yaw gimbal (δ_r) to be opposite signs. The bending moment expressions carry the same signs for δ_r and β but for the worst case (aft body) are of equal magnitude (Appendices B or D). Hence, it is safe to conjecture that by forcing the sideslip toward zero during the high dynamic pressure flight regime will

- Reduce roll gimbal requirements
- Reduce yaw gimbal requirements
- Reduce bending moments
- Reduce $\bar{q}\beta$

Drift errors could then be reduced after high dynamic pressure and before burnout.

CONVENTIONAL ANALYSES

Five controllers are synthesized and analyzed. The controllers are analyzed with respect to controller parameters, wind disturbance variations, engine failures, instrument biases, and plant models.

The primary objective is to obtain relative measures of both the effectiveness of controller types and of their complexity. Achievement of best performance was considered to be a secondary consideration; the plant model (Appendix B) is a rigid-body representation containing neither the effects of flexure nor of fuel sloshing.

Stability analyses were performed to provide reasonable values for controller gains and to assist in checking the time-varying analog simulation results that were subsequently obtained.

Stability Analyses

The five baseline controllers are presented in Table 9.

Table 9. Five Conventional Lateral Controls

Roll

$$\delta_x = 3.4 \phi + 10 \dot{\phi}$$

- Directional Heading

$$\delta_z = 3.0 \left\{ \dot{\psi} + 2\psi \left(1 + \frac{0.1}{S} \right) \right\}$$

- Minimum Drift Rate

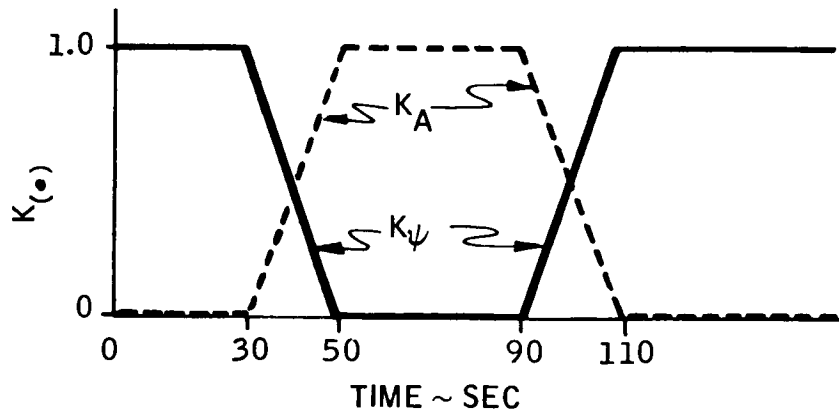
$$\delta_z = 3.0 \left\{ \dot{\psi} + 2(\psi + 0.2 V_N) \left(1 + \frac{0.1}{S} \right) \right\}$$

- Minimum Drift Rate W/O Mean Wind
- Scheduled Attitude and Lateral Acceleration

$$\delta_z = 3 \left\{ \dot{\psi} + \left(2\psi K_\psi + \frac{0.007 A_y K_A}{0.5 S + 1} \right) \left(1 + \frac{0.1}{S} \right) \right\}$$

- Scheduled Attitude and $Y_v v_A$

$$\delta_z = 3 \left\{ \dot{\psi} + \left(2\psi K_\psi + \frac{0.026 Y_v v_A K_A}{0.5 S + 1} \right) \left(1 + \frac{0.1}{S} \right) \right\}$$



Stability analyses were conducted to provide a check on the analog simulation, by comparing response at the selected gains and by checking frequency at neutral gain. The selected roll rate and yaw rate feedback gains both were a factor of 7 below the neutral gain point. The selected gains were (with TWD and DWT)

$$\delta_x = 3.4\dot{\phi}, \quad \delta_z = 4.8\dot{\psi}$$

However, even doubling these gains resulted in a significant reduction in the associated actuator damping ratio (0.36 to 0.20).

The selected roll attitude gain was $\delta_x = 13.6\phi$, a factor of 6 below neutral gain. However, this provided a roll characteristic frequency of 6.3 rad/sec, with 0.8 damping, very adequate. This gain was subsequently reduced to $\delta_x = 10\phi$ due to scaling limitations in the simulation. The selected roll and heading controls were then:

$$\delta_x = 3.4\dot{\phi} + 10\phi$$

$$\delta_z = 4.8 \left[\dot{\psi} + 2\psi \left(1 + \frac{0.1}{S} \right) \right]$$

Stability data (with roll attitude loop open) were obtained at lift off, 64 seconds, and 160 seconds; the lowest gain margin (at 160 seconds) was a factor of 9. At 64 seconds, the margin was a factor of 15. Stability data with roll attitude loop closed were obtained only at 64 seconds; the margin was about the same, a factor of 12. Here the roll/yaw characteristic roots (omitting the actuator) were:

$$(S + 0.105) \left(\frac{\omega = 5.89}{\xi = 0.80} \right) (s+2.3) (s+19.4)$$

\uparrow
 Roll

The heading response to a step required 2 sec to settle within 10 percent

Stability with lateral acceleration (A_y) or sideslip acceleration ($Y_v v_A$) feedbacks was examined only at 64 seconds. Here $A_y = A_{CG} + 55 \dot{\psi}$ (accelerometer 55 feet ahead of the cg). The accelerometer feedback equation selected was:

$$\delta_z = 4.8 \left[\dot{\psi} + \frac{0.007 A_y}{0.5S+1} \left(1 + \frac{0.1}{S} \right) \right]$$

The dominant characteristic frequency was 1.05 rad/sec with 0.57 damping ratio.

The sideslip feedback equation selected was:

$$\delta_z = 4.8 \left[\dot{\psi} + \frac{0.026 Y_{v} v_A}{0.5S+1} \left(1 + \frac{0.1}{S} \right) \right]$$

Here the characteristic frequency was higher, 2.62 rad/sec, with 0.22 damping. The δ_z forward loop gain of 4.8 was reduced to 3.0 when TWD and DWT terms z were removed from the simulation; the negligible effect on performance is subsequently discussed.

Analog Simulations

The effectiveness of the controllers was determined by use of a time-varying analog simulation which is described in Appendix B.

The effectiveness of controllers and effects of parameter changes were determined by performing simulations and in most cases, summarizing the results on bar charts. Figures 24 through 38 present these recordings and bar charts.

The Five Controls -- Figure 24 shows time histories of the five control systems considered disturbed by the reference wind (which peaks at 25,000 feet). The results are summarized in Figure 25. The attitude control has no merit at all; it is worst in every category. It would be used only if the booster had no guidance system. The minimum drift rate system has, by far, the lowest drift. With the mean wind biased out (middle column), roll torque, sideslip, and bending moments of the min drift system compare with those of the two load relief controllers on the right. Mean wind biasing should be used if possible.

The two load relief controllers are comparable except in sideslip and bending moment at station 1800, wherein the sideslip (Y_{v}) controller's increased yaw gimbal activity produces twice as much aft station moment, while reducing sideslip toward zero.

In order of increasing complexity, the five controls would probably be as shown from left to right in Figure 25.

- Attitude
- Minimum drift rate
- Minimum drift rate with mean wind biasing
- Scheduled attitude and lateral acceleration
- Schedules attitude and Y_v (or sideslip)

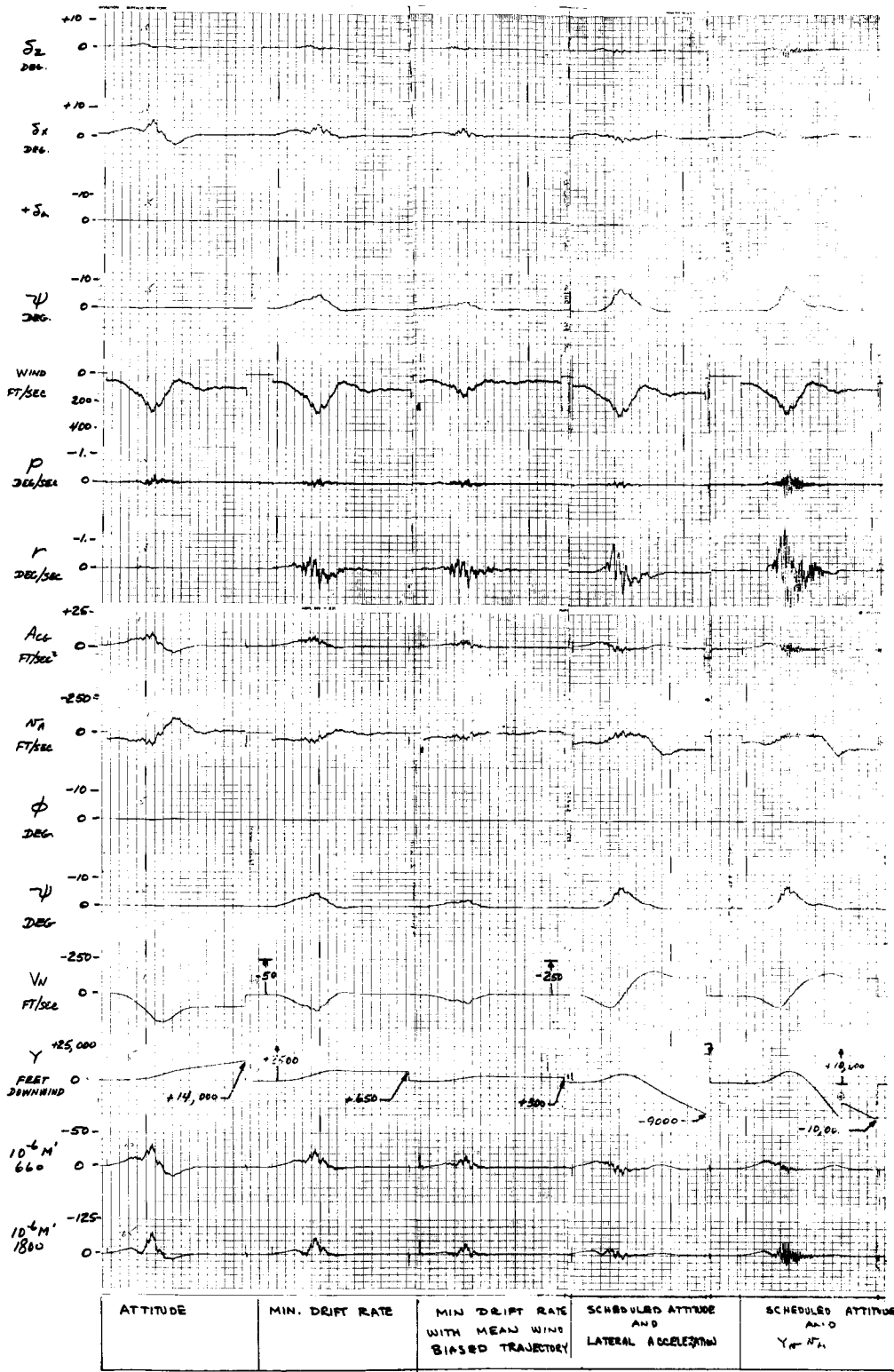


Figure 24. Performance of Five Control Systems

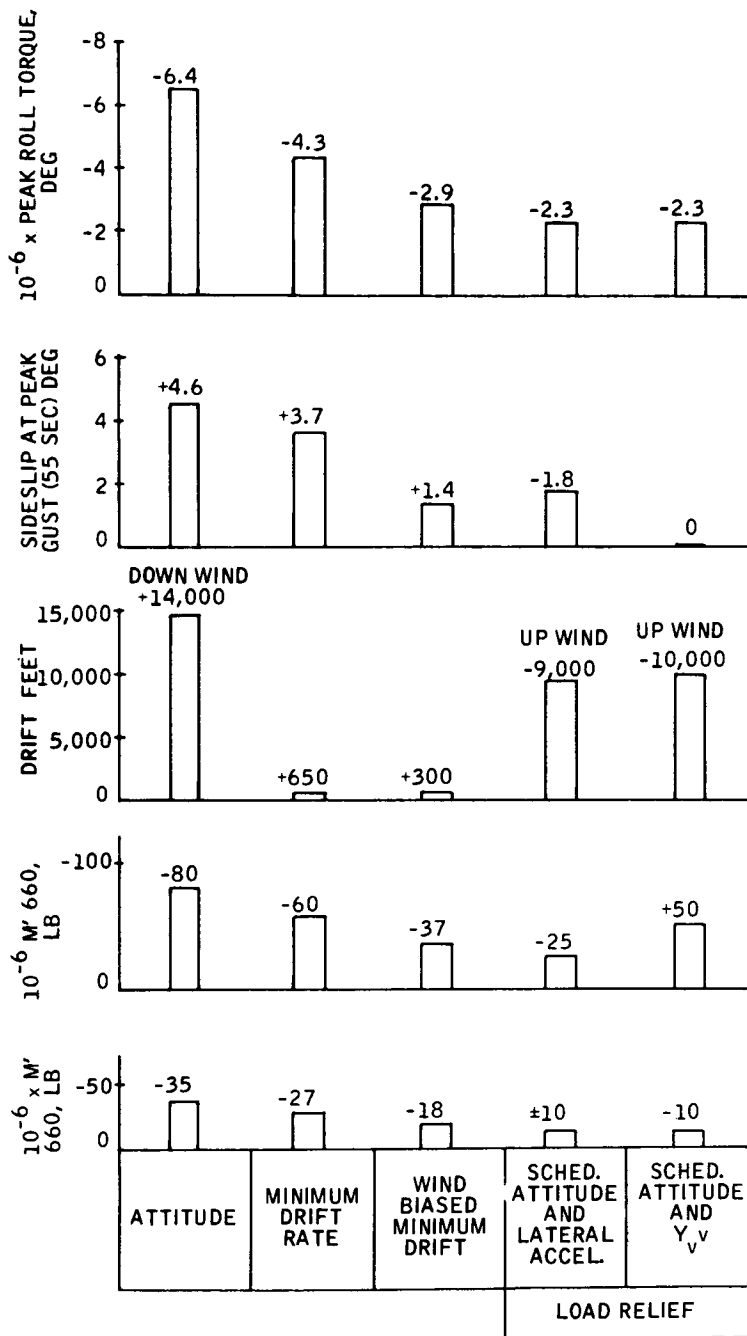


Figure 25. Performance of Five Controls

Load relief implementation requires a major increase in autopilot complexity due to increased sensors and the required variation in guidance and load relief gains. The design objective should be to get by with wind biasing if possible. The initial trade study probably needs to consider only one load relief system; the precise means of load relief can be determined after the need has been established. The load relief system using $Y_{\dot{v}}$ is somewhat fictitious since it is difficult to measure. It was used because it was readily available in the simulation and is comparable to $q\beta$. The ΔP sensor described in (ref. 8), would be one means of mechanizing $q\beta$ (or $Y_{\dot{v}}$); there ΔP is obtained from ports on opposite sides of the nose fairing. \dot{v} ΔP probes are also available. The Rosemount Engineering Company, for example, makes probes with aerodynamic compensation, developed for use in high-reliability angle-of-attack sensing systems.

Effect of Ailerons -- The following table summarizes the simulation results of Figure 26. As expected, there are reductions in roll differential gibal torque required when roll control is augmented with aerodynamic surfaces. It is noted that with attitude control the reduction is not as great as in the minimum drift rate system, because of gibal demands after the ailerons become ineffective due to low dynamic pressure. It is understood there are difficulties in obtaining aerodynamic controls which are effective and do not flutter in the transonic region where needed; the data in the table are near Mach 1.

Yaw Control	Roll Control	$10^{-6} \times$ Peak Roll Differential Gibal Moment, ft lb
Attitude	No Aileron	-5.9 (at 55 sec)
	With Aileron	+3.5 (at 85 sec)
Minimum Drift Rate	No Aileron	-4.1 (at 55 sec)
	With Aileron	-1.2 (at 55 sec)

Effect of Engine Failures -- Figures 27 through 32 show the combined effects of wind and left or right outboard engine failure with two controls; minimum drift rate and scheduled attitude plus lateral acceleration. The wind is from the left so a left engine failure causes a turn into the wind, tending to reduce sideslip.

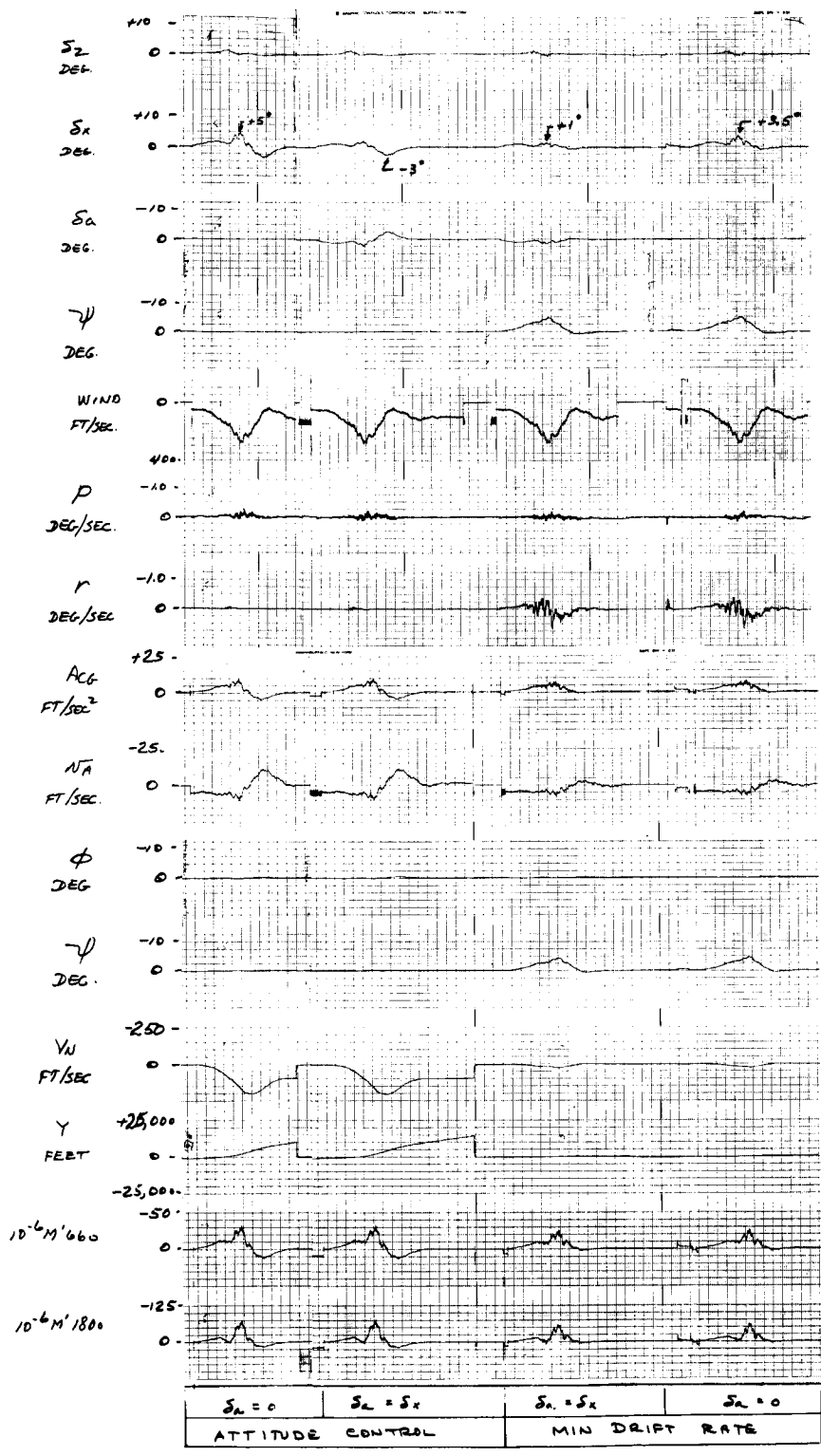


Figure 26. Effect of Ailerons on Peak Differential Gimbal Deflection (δ_x) Required

Figure 27 data, with min drift rate control, are summarized in Figure 28. As expected, left engine failure either at peak gust, 5 sec before, or 5 sec after peak gust causes negligible increases in any parameter. A right failure 5 sec before peak gust produces the largest increases in all parameters.

The lateral acceleration controller was used for the data in Figures 29 through 32. Engine failures are only at peak gust. The low integral gain (T=10) is that used in all other figures in this report. The high integral gain system does not appear again because the low gain was sufficient to handle the wind disturbance. The low integral gain results show the most variation between right and left engine failures, with left failure (turn into the wind) producing the largest disturbances in all parameters except sideslip, which (at 2.8 deg) equals that of right-engine failure. The results with high integral gain show much less variation between right and left-engine failures, and less disturbance than the left engine produced with low integral gain. It is concluded from this engine failure study:

1. Both left and right engine failures must be considered
2. A control system with high integral gain is preferred for rapid trimming of engine failures, a higher gain than dictated by the wind disturbance.

The engine failures were simulated by introducing a step yaw acceleration:

$$\text{left outboard engine out, } \ddot{\psi} = -1.5 \text{ deg/sec}^2$$

$$\text{right outboard engine out, } \ddot{\psi} = +1.5 \text{ deg/sec}^2$$

This magnitude was obtained from physical data at 64 seconds:

$$\ddot{\psi} = \frac{57.3 \ell F}{13 I_z}$$

where

ℓ = 16 ft moment arm, outboard engine

F = 5.87×10^6 lb total thrust

13 = number of engines

$I_z = 270 \times 10^6$ slug ft²

Effects of Wind Variations -- Figure 33 (from the results from Figure 34) shows the effects of wind biasing and the altitude of peak wind on three control systems; scheduled altitude and lateral acceleration, min drift, and scheduled attitude and Y_v . The wind used throughout this section of the

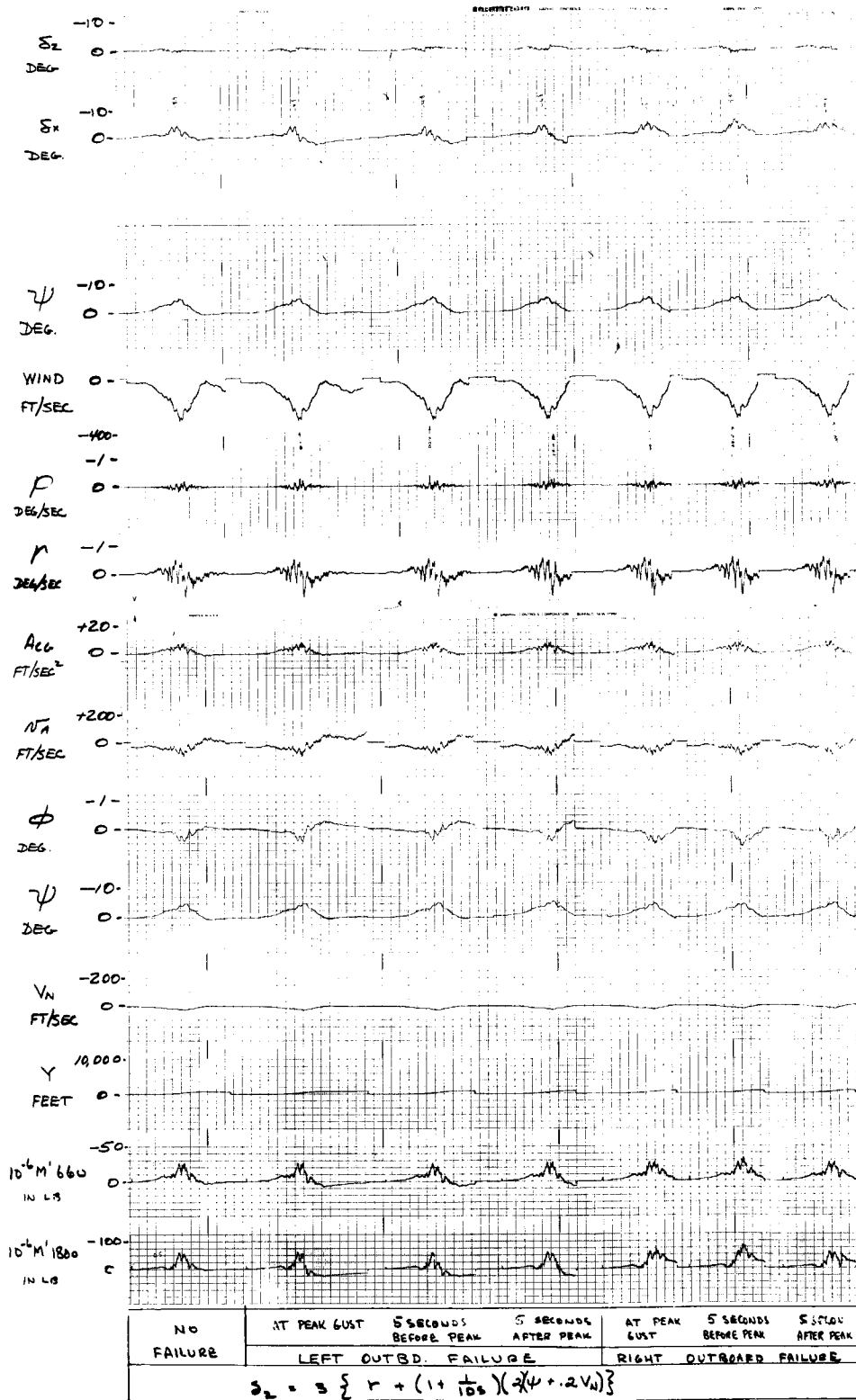


Figure 27. Effect of Wind and Engine Failures with Minimum Drift Rate Control

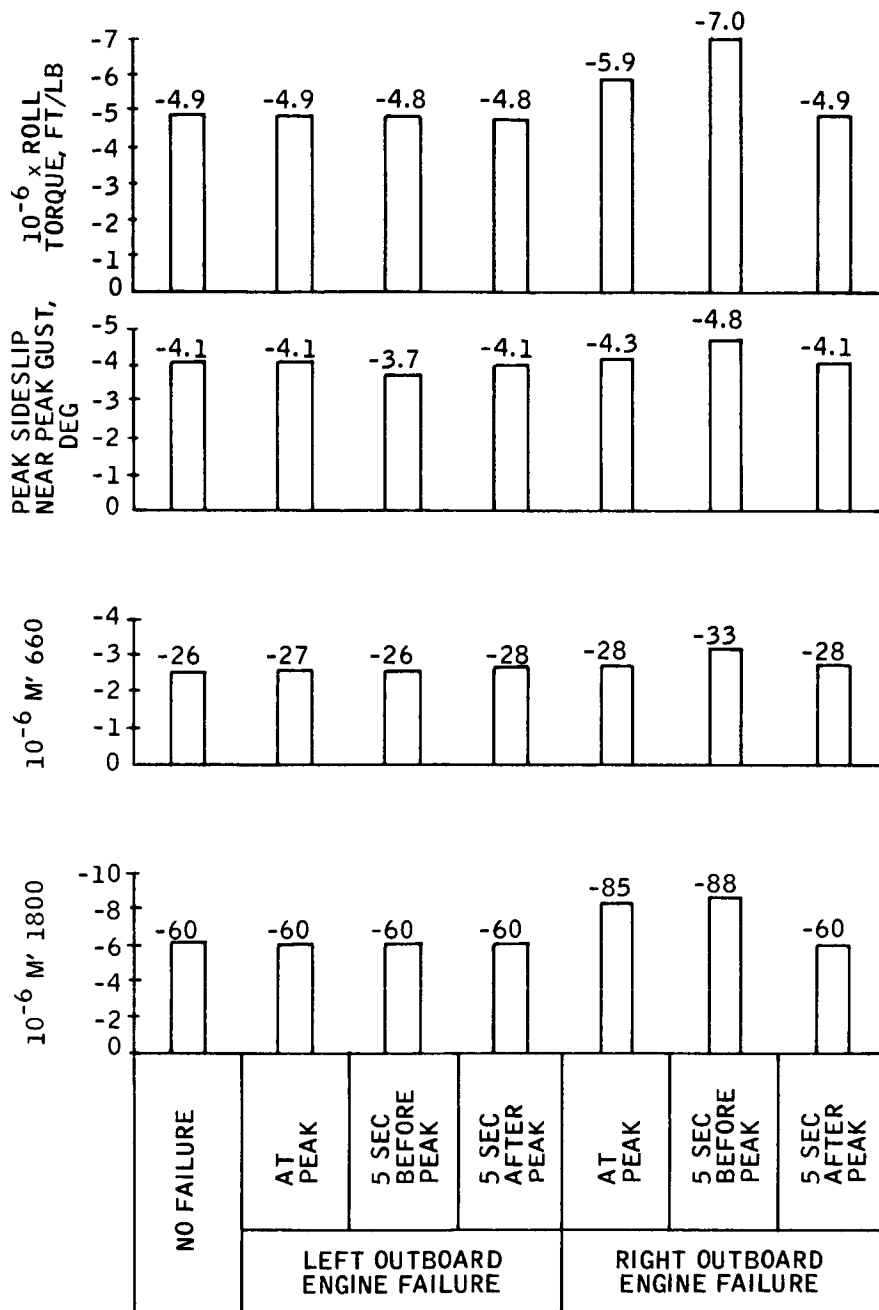


Figure 28. Effects of Wind and Engine Failures on Minimum Drift Control

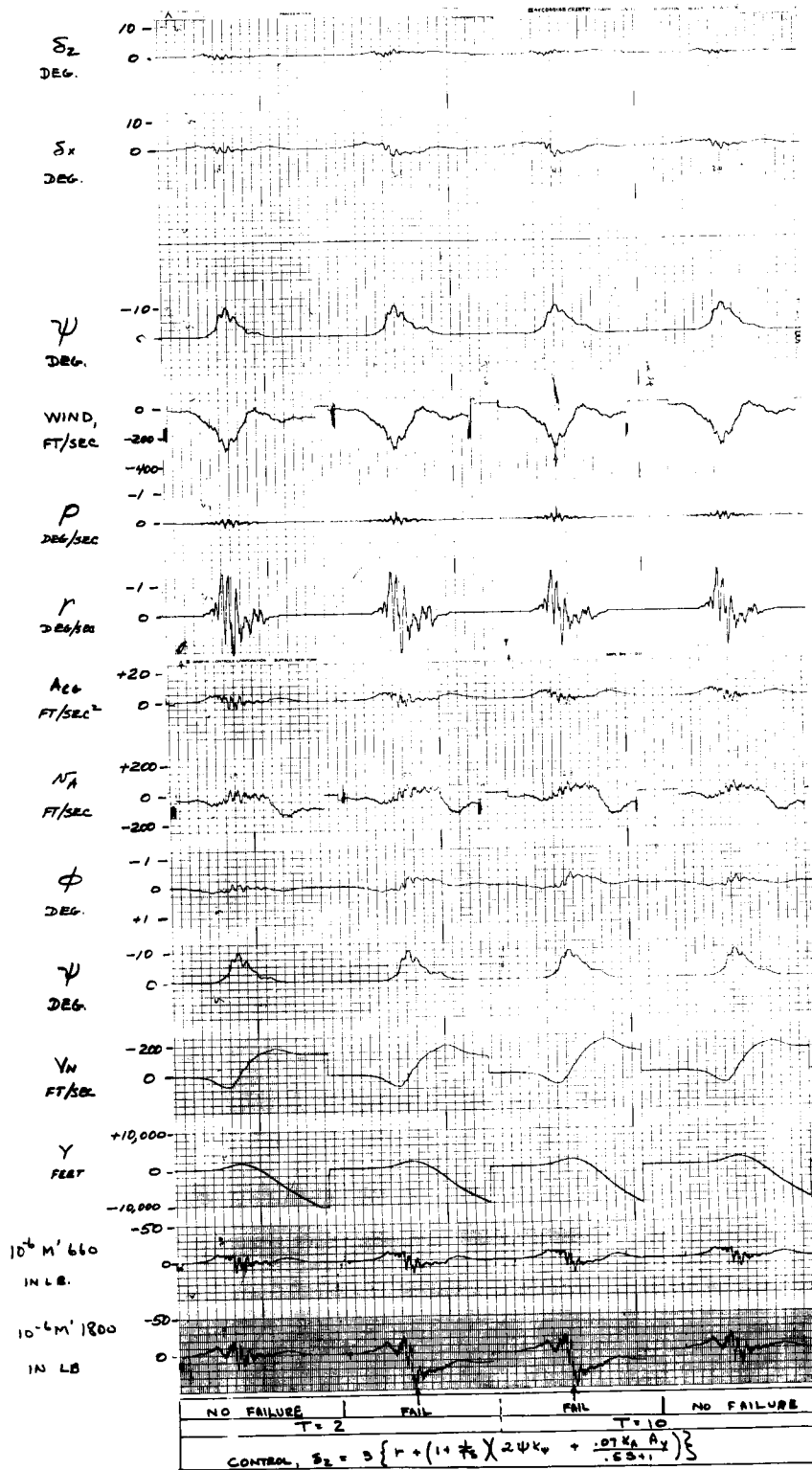


Figure 29. Effect of Integral Gain (T) on Scheduled Attitude plus Lateral Acceleration Control Response to Left Outboard Engine Failure

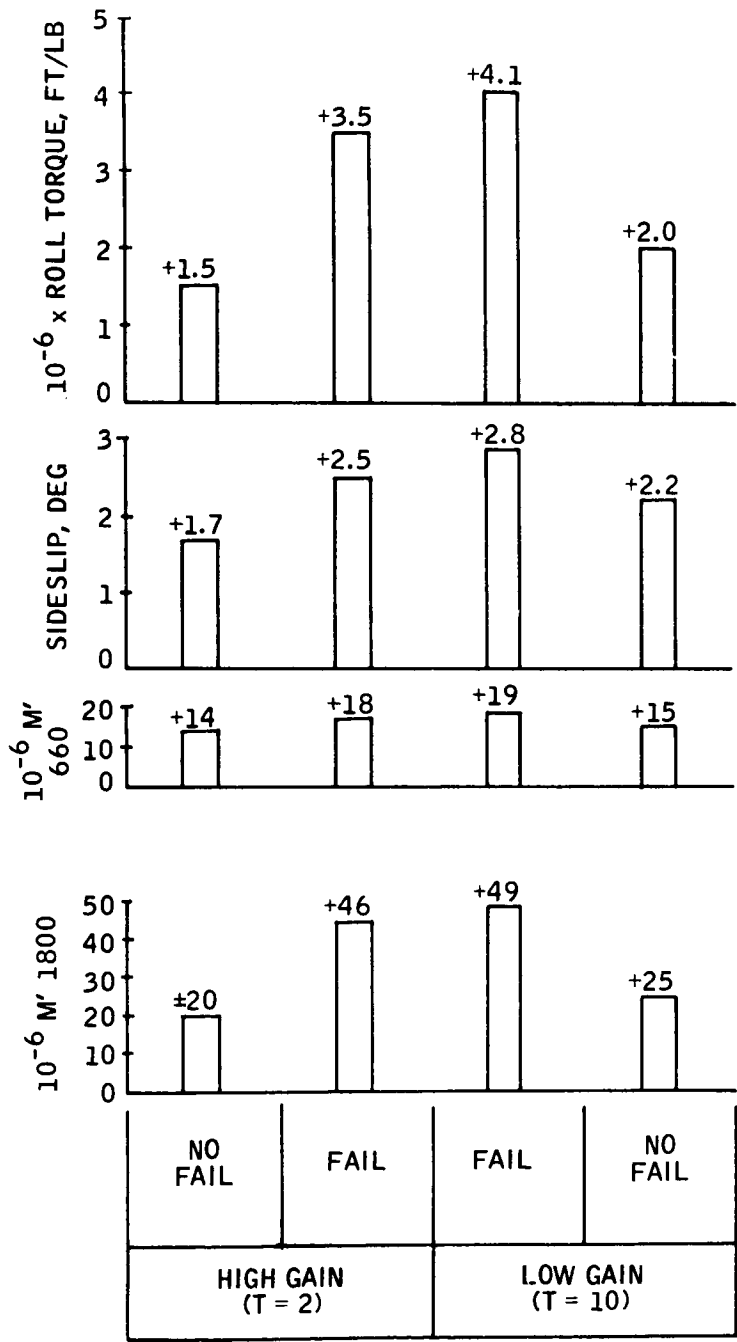


Figure 30. Effects of Integral Gain on Scheduled Attitude plus Lateral Acceleration Control in Wind and Left Outboard Engine Failure

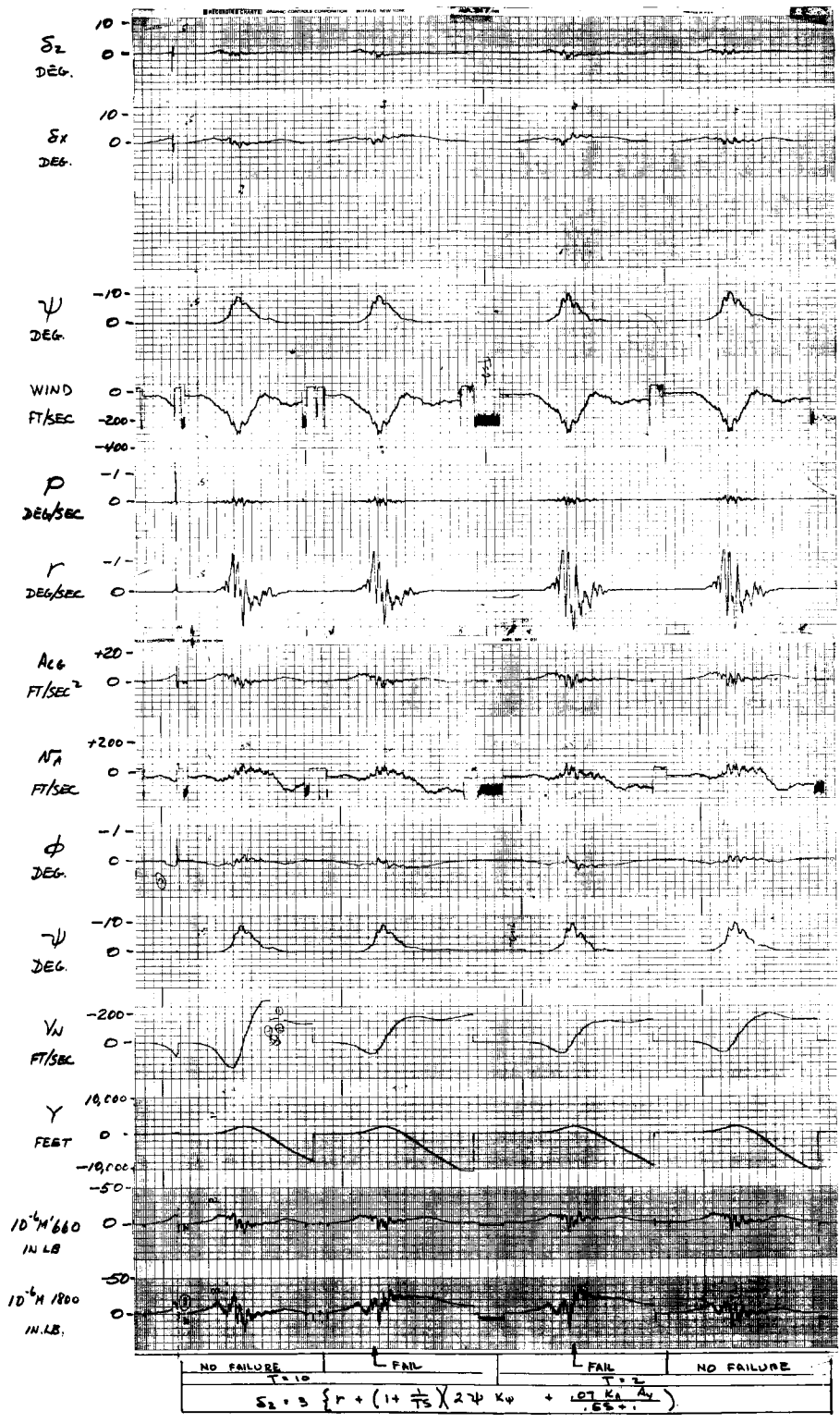


Figure 31. Effect of Integral Gain (T) on Scheduled Attitude plus Lateral Acceleration Control Response to Right Outboard Engine Failure

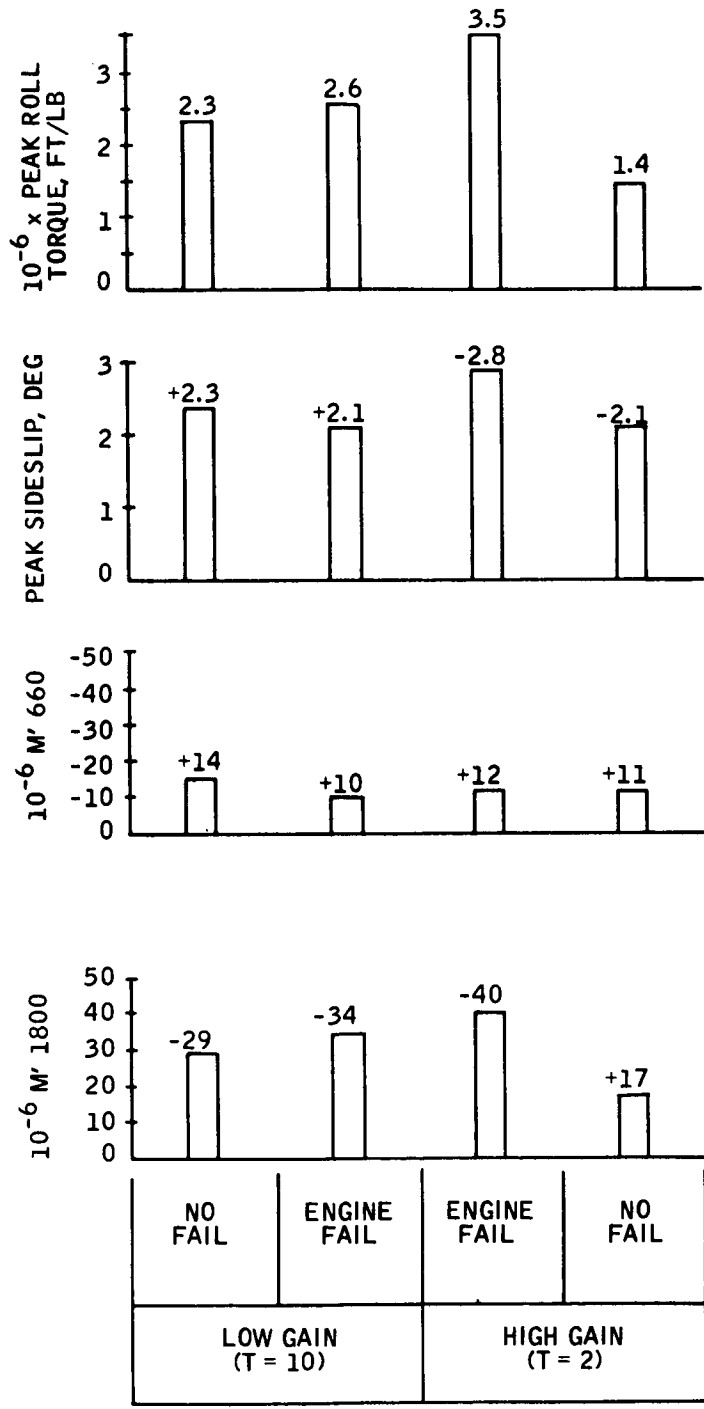


Figure 32. Effects of Integral Gain on Lateral Acceleration Control in Wind and Right Outboard Engine Failure

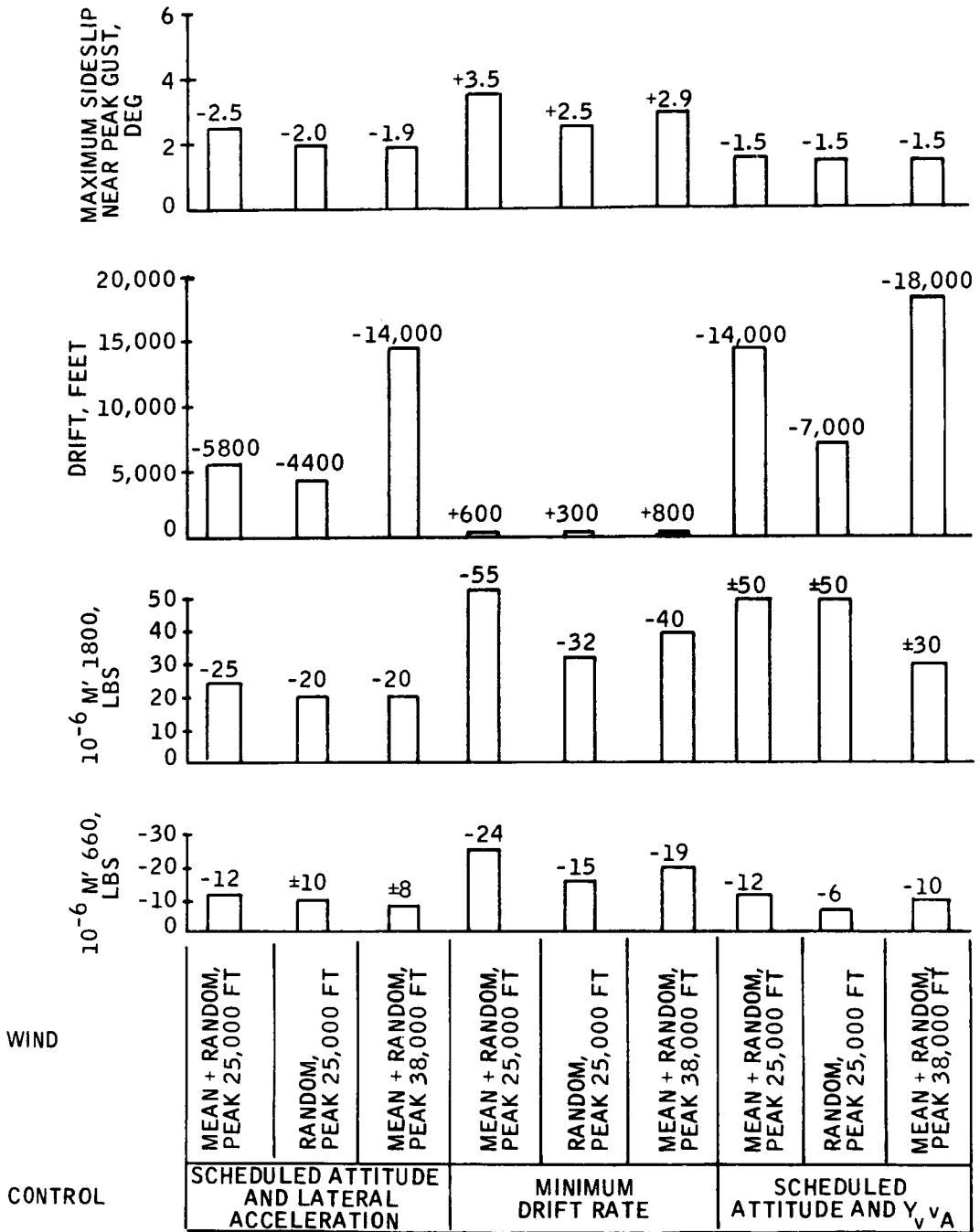


Figure 33. Effect of Wind Biasing and Altitude of Peak Gust on Three Controls

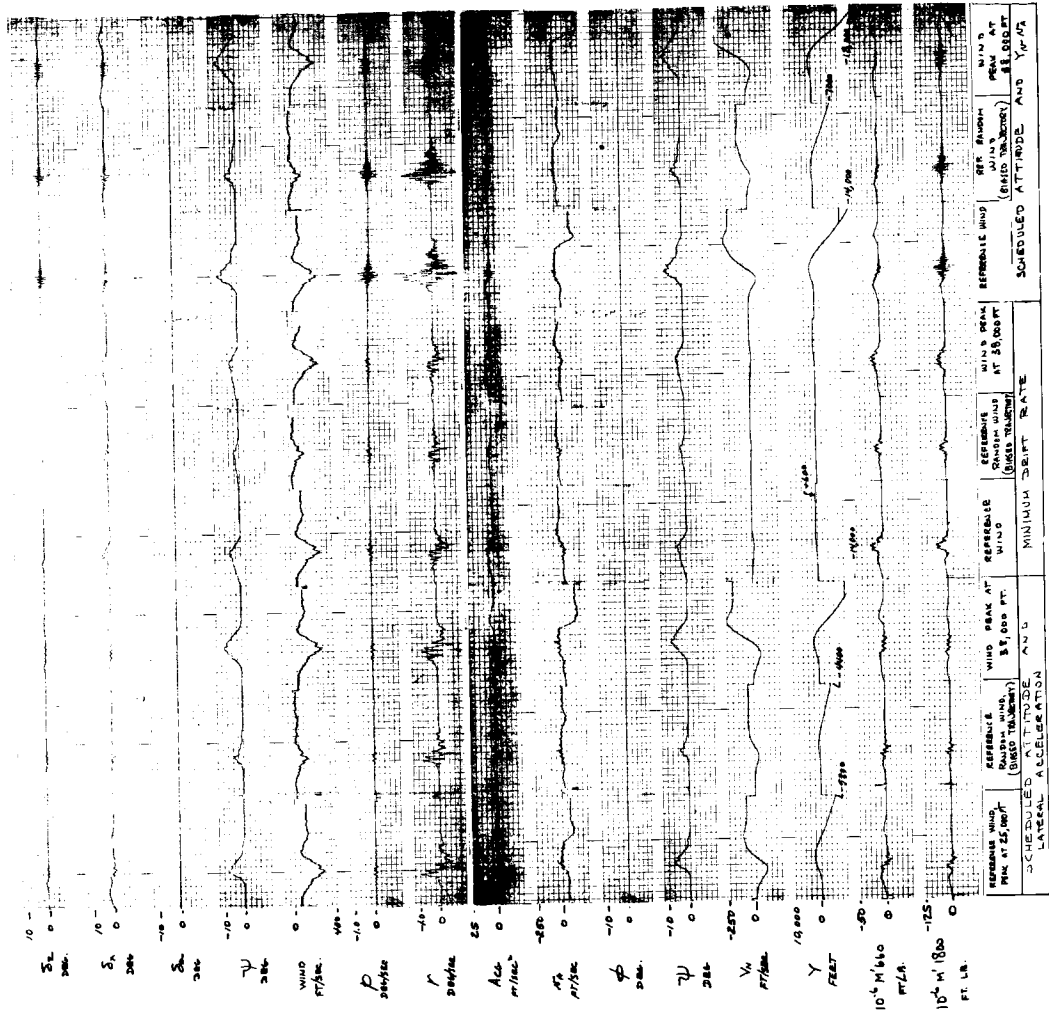


Figure 34. Effect of Wind Biasing and Altitude of Peak Wind on Min Drift and Load Relief Controls

of the report peaks at 25,000 feet (Mach 1) where aerodynamic forces are the largest. Here performance is compared with that in a wind peaking at 38,000 feet (max \bar{q}). The max \bar{q} wind, without exception, produces larger drift and smaller values of all other parameters than does the wind at Mach 1. This, in a small way, emphasizes a conclusion of Reference 8 that performance in a large number of winds (preferably measured) must be obtained to properly evaluate a system.

Effect of Load Relief Control Gains -- Figure 35 (summarizing Figure 36 shows the effect of lateral acceleration proportional and integral gain on performance of the scheduled attitude + lateral acceleration controller. The results agree with intuition; high proportional gain (giving increased static stability) yields the lowest bending moments and the largest drift. Moderate increases in bending moment and a large decrease in drift are obtained by deleting the integral control. This improvement in drift without integral control may be significant, but must be demonstrated in a variety of winds.

Effect of Sensor Bias -- Figure 37 shows the effect of a 1 ft/sec^2 accelerometer bias on performance of the scheduled attitude plus lateral acceleration control. The control was, inadvertently, nonstandard, being low gain without integral control. (This is the same as the third recording in Figure 36. The bias has a small effect on bending moments, but a gross effect on drift, being +10,000 feet with -1 ft/sec^2 and -11,000 feet with $+1 \text{ ft/sec}^2$. This bias is extremely large for an instrument, thus biases of this magnitude must be due to misalignment and consequent sensing of the axial component of acceleration. This misalignment should be small, laterally, because of symmetry.

Load Relief with Drift Rate Control -- Drift rate feedbacks were added to the load relief systems in an attempt to achieve both small inflight loads and low terminal drifts. The results were not successful due in part to lack of flexibility of the analog simulation. The results of simulations are presented in Figure 38.

In the first two recordings of Figure 38 the gain schedules (K_A and K_ψ) used results in large bending moments at the end of the load relief period as control is transferred from relief to guidance. These moments are almost entirely due to gimbal deflection. Clearly a better means of varying gains was needed, to limit gimbal deflection, but difficult to program in the simulation.

The remaining recordings in this figure are the result of manual control of the drift rate (V_N) gain. In the last (extreme right) recording, bending moment at station 660 is finally held to a value less than experienced early in the flight. However, the drift of -8000 feet differs little from the -10,000 obtained without drift rate feedback.

Effects of TWD and DWT -- The effects of TWD and DWT dynamics are of negligible importance, at least for the rigid body dynamics used for this

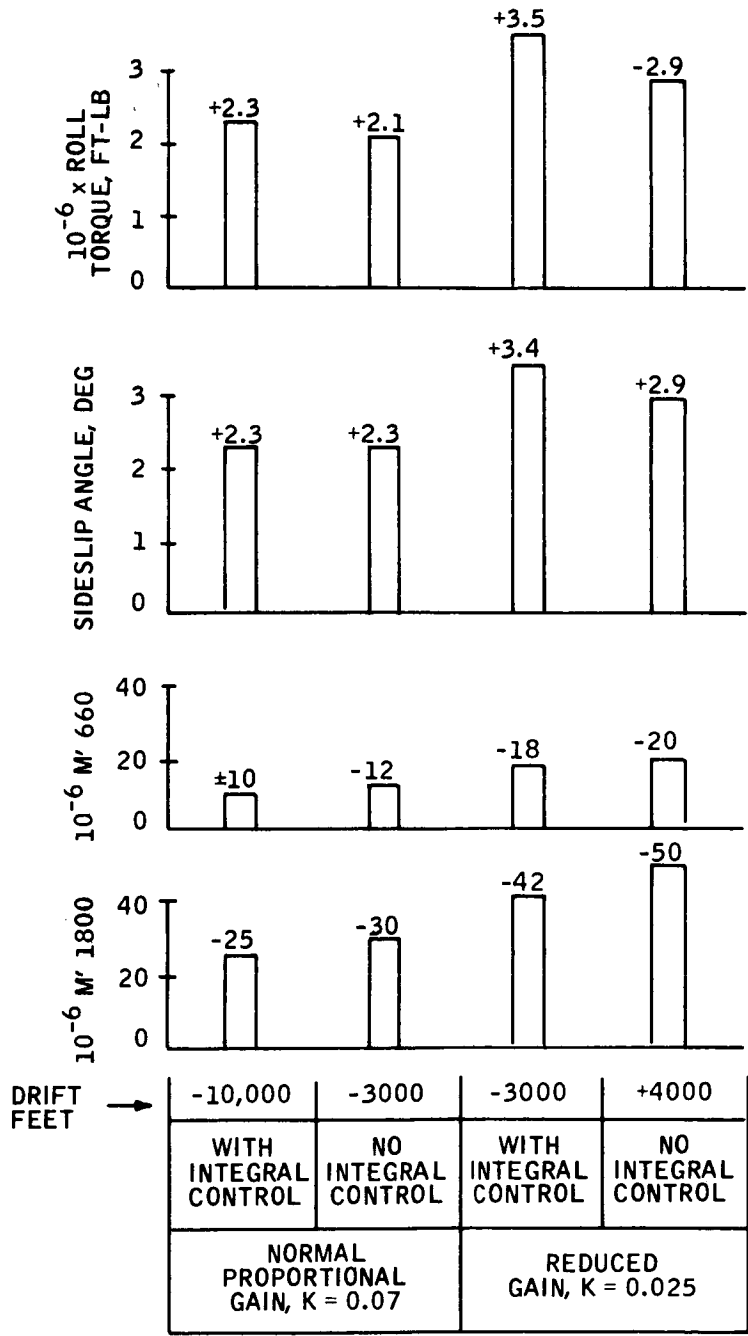


Figure 35. Effects of Integral and Proportional Gains on Lateral Acceleration Control

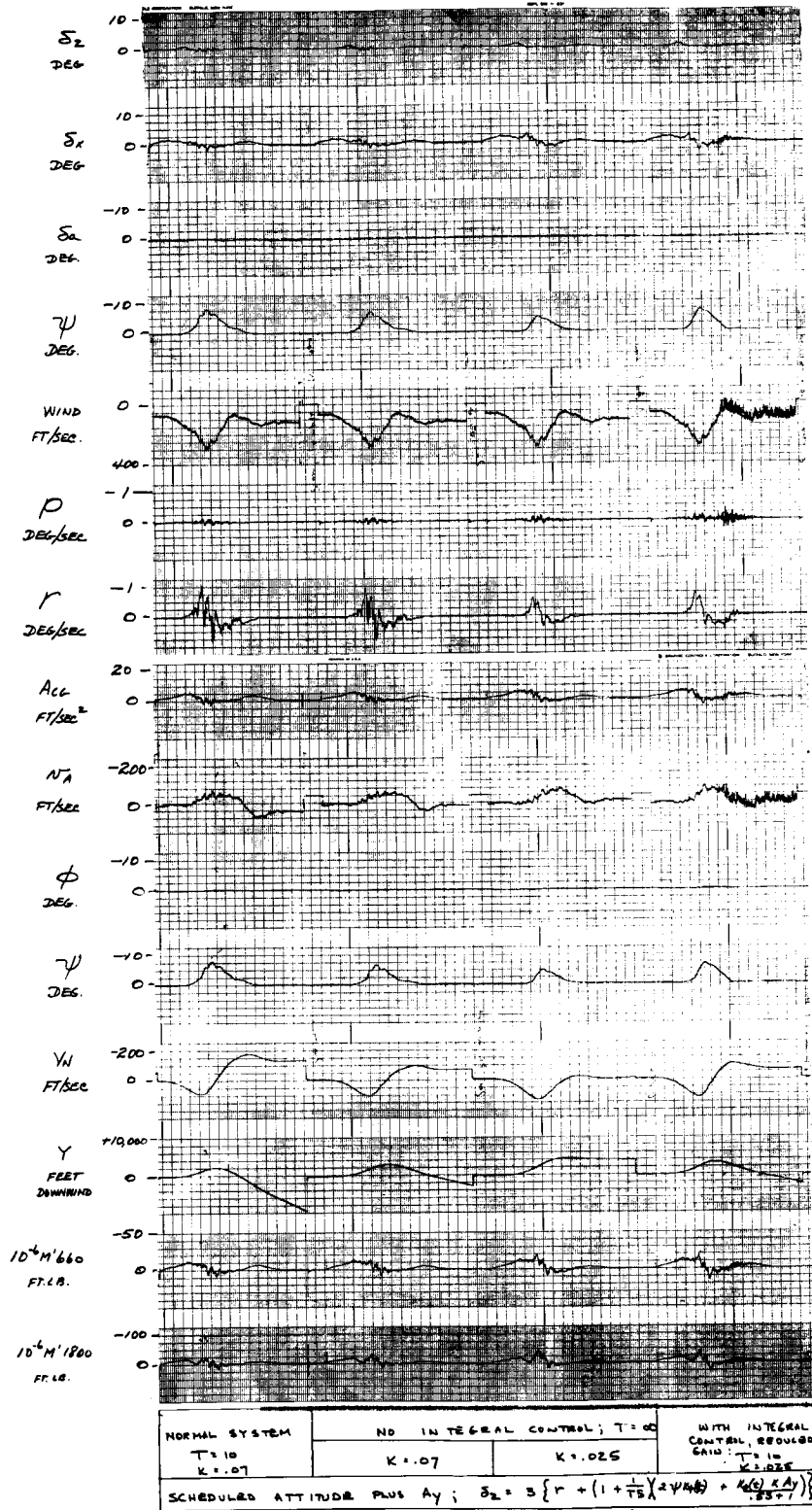


Figure 36. Effect of Integral Control and Accelerometer Gain on Scheduled Attitude plus A_y System METER (STEM)

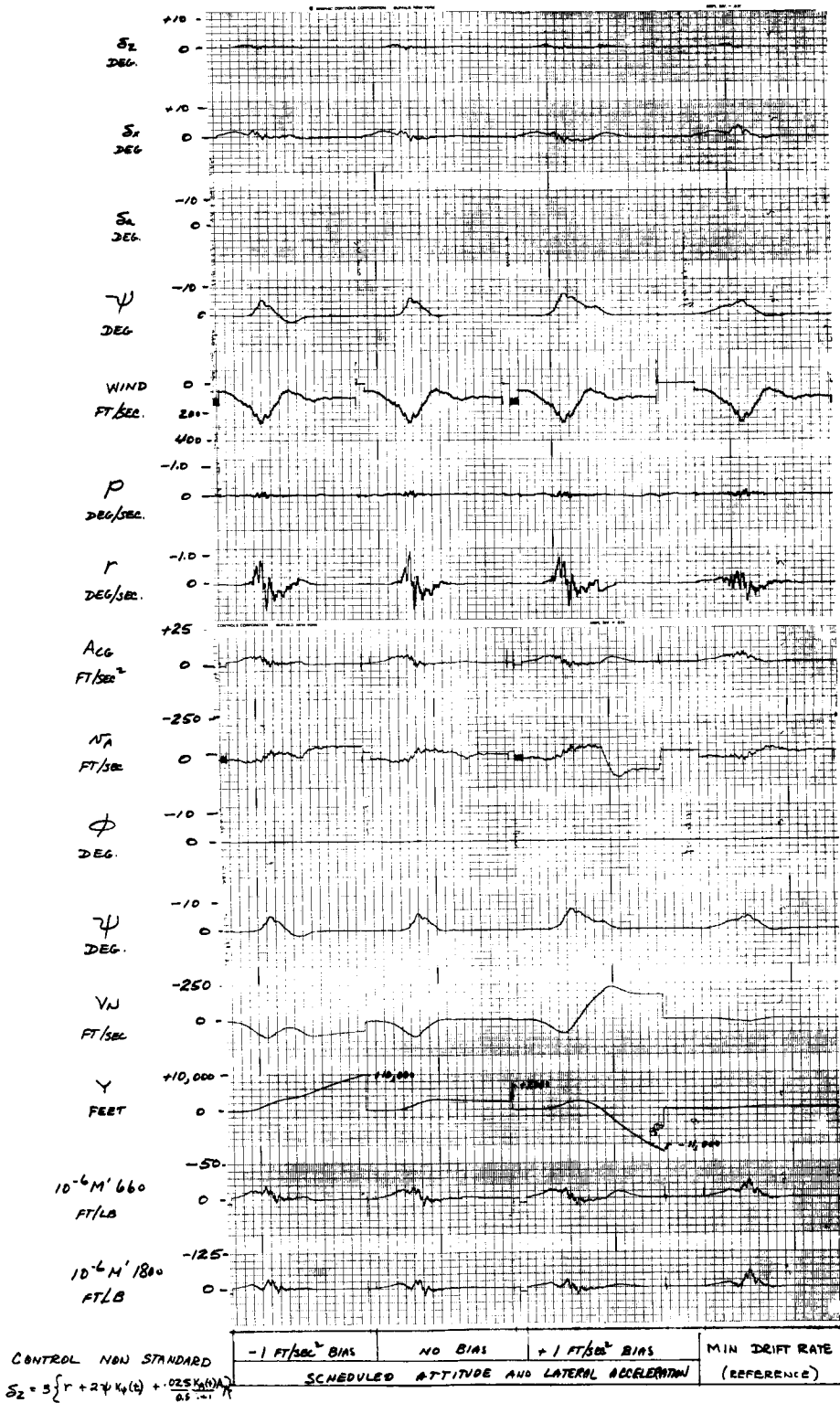


Figure 37. Effect of Accelerometer Bias on Load Relief Controller

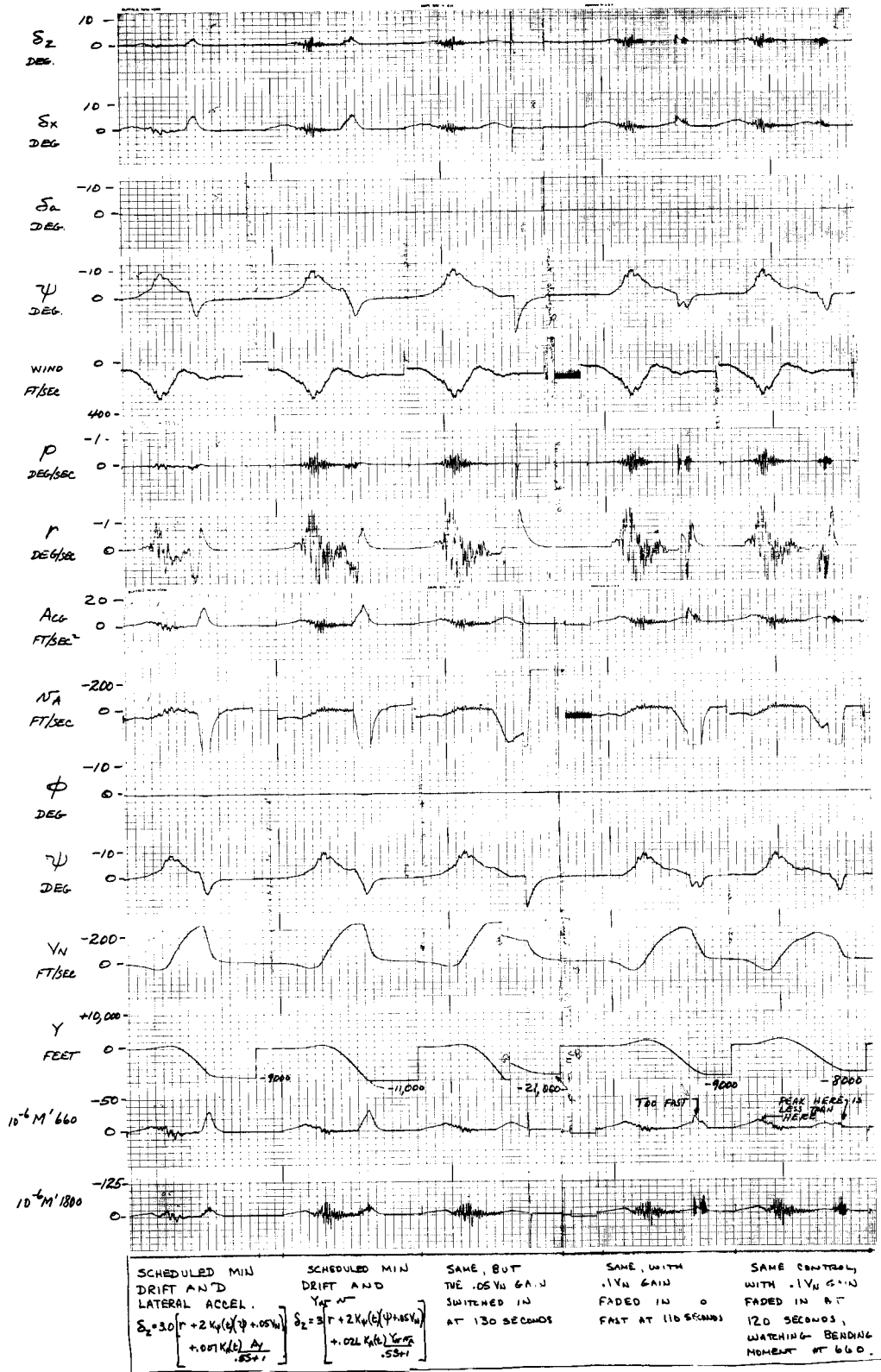


Figure 38. Scheduled Min Drift +Y_v, with Manual Control of the Drift Rate Gain

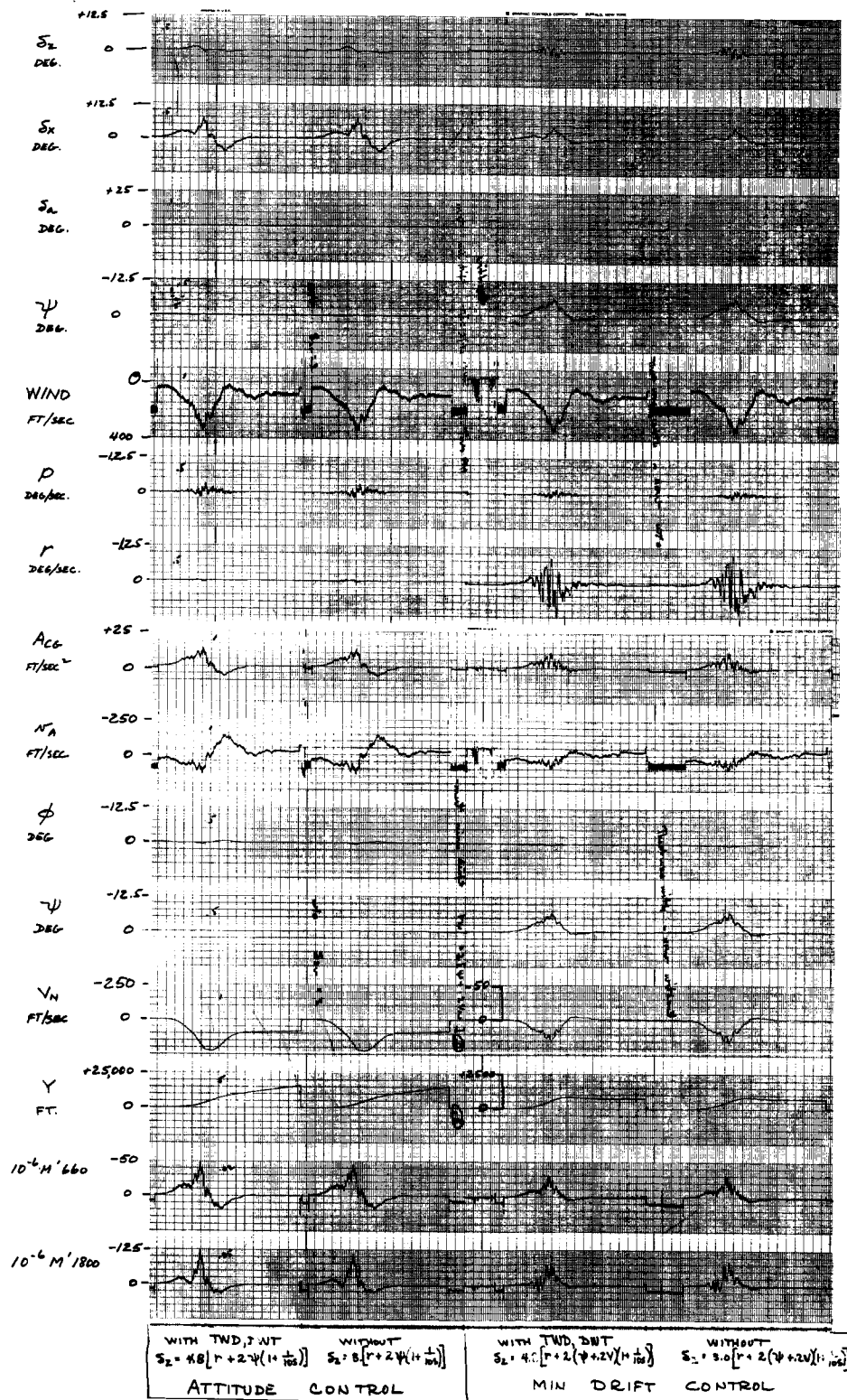


Figure 39. Negligible Effect of TWD and DWT on Attitude and Min Drift Controls; No Load Relief

study. Simulation results presented thus far are without either of these effects included.

Figure 39 shows TWD and DWT dynamics are of negligible importance by comparing simulations with and without these effects. Differences are discernible but are very small.

COVARIANCE ANALYSIS

There are two primary sets of objectives for this subsection. First, to present a comparative analysis of five of the conventional controllers discussed in the previous subsection. Second, to show that the rolling wind gusts neglected in the discussions thus far are of negligible importance. This is based on the hypothesis that the rolling wind gust model used (cf Appendix D) is at least a good first-order approximation.

A check on the validity of the covariance analyses will then be presented.

The Overview subsection presented the major results. It did not consider the major details which are now addressed.

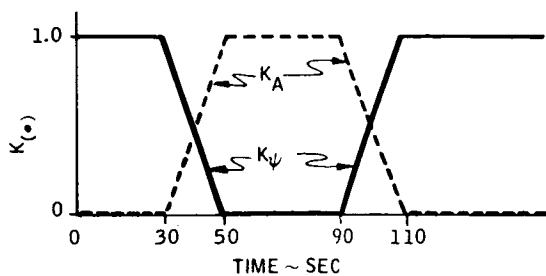
Figures 20 through 24 present comparisons of the effectiveness of five conventional controllers as evaluated by analog simulation and by covariance analyses. Appendixes B and D present the plant representations used for the analog and covariance analyses. Table 10 briefly summarizes the major differences between the plant models of Appendixes B and D. Differences in the simulation of controllers are presented in Table 11.

Table 10. Simulations Compared

Covariance	Conventional
Entire side wind population used	Single sample side wind used
Rolling gusts included	Rolling gusts not included
Revised estimates of stability derivatives	Original estimates of stability derivatives
Conservative gimbal slewing forces	Slightly optimistic gimbal slewing forces
First-order actuators	Second order actuators with TWD & DWT
Gust penetration dynamics	Sudden gust immersion
Accelerometer at 718	Accelerometer at 612
Pitch, roll, yaw	Heading, elevation, roll

Table 11. Controllers Compared

Covariance	Conventional
$u_{11A} =$	$\{3.4\phi + 10\phi\}$
$u_{11D} = 11.15 \left(-\frac{L}{T} \frac{\delta p}{T} \right)^{-1} \{3.4\phi + 10\phi\}$	
$u_{21A} =$	$3.0 \left\{ \psi + 2.0 \psi \left(1 + \frac{0.1}{S} \right) \right\}$
$u_{21D} = \left(\frac{Y}{T} \frac{\delta r}{T} \right)^{-1} \{3.0\psi + 6.0\psi\}$	
$u_{22A} =$	$3.0 \left\{ \psi + 2.0 \left(\psi + \frac{0.2 \sqrt{N}}{57.3} \right) \left(1 + \frac{0.1}{S} \right) \right\}$
$u_{22D} = \left(\frac{Y}{T} \frac{\delta r}{T} \right)^{-1} \left\{ 3.0\psi + 6.0\psi + \frac{1.2 \dot{y}}{57.3} + \frac{0.12 y}{57.3} \right\}$	
$u_{23A} =$	u_{22A} with $\tilde{v} = 0$
$u_{24A} =$	$3.0 \left\{ \psi + \left(2\psi K_{\psi} + \frac{0.007 A_v K_A}{57.3(0.5S+1)} \right) \left(1 + \frac{0.1}{S} \right) \right\}$
$u_{24D} = \left(\frac{Y}{T} \frac{\delta r}{T} \right)^{-1} \left\{ 3.0\psi + 6.0 K_{\psi} \psi + \frac{0.021}{57.3} K_A A_y \right\}$	
$u_{25A} =$	$3.0 \left\{ \psi + \left(2\psi K_{\psi} + \frac{0.026 Y_v v_A K_A}{57.3(0.5S+1)} \right) \left(1 + \frac{0.1}{S} \right) \right\}$
$u_{25D} = \left(\frac{Y}{T} \frac{\delta r}{T} \right)^{-1} \left\{ 3.0\psi + 6.0 K_{\psi} \psi + \frac{0.026}{57.3} (K_A A_{33}) (v + \tilde{v} + \bar{v}) \right\}$	
$u_{31A} =$	$\{3.4\phi + 10\phi\}$
$u_{31D} = 11.15 \left(-\frac{L}{T} \frac{\delta p}{T} \right)^{-1} (1) \{3.4\phi + 10\phi\}$	



The differences in plant models are not large. The analog model was developed relatively early in the program. Quick estimates for stability derivatives not supplied by MSFC were made, the controllers were synthesized, and analog simulated. Covariance analyses are much more demanding of equations and data than conventional analyses. During the time the equations for covariance analyses (Appendix D) were being developed, the estimates for stability derivatives were redone and hopefully improved. Before considering the differences in detail a listing of stability derivatives used near the maximum dynamic pressure flight condition is presented (Table 12).

Table 12. Stability Derivatives

	CONVENTIONAL @ 64 SECONDS	COVARIANCE @ 65 SECONDS
$a_{11} = L'_p$	- .48	- .416
$a_{12} = L'_r$	- .355	- .435
$a_{13} = L'_v$	- .002	- .00436
$a_{1,14} = L'_{\delta_p}$	- 2.3	- 2.164
$a_{1,15} = L'_{\delta_r}$	- 2.9	- 1.468
$a_{1,16} = L'_{\delta_a}$	- 3.5	- .385
$a_{21} = N'_p$	- .07	- .0327
$a_{22} = N'_r$	- .26	- .379
$a_{23} = N'_v$	- .00026	- .000169
$a_{2,14} = N'_{\delta_p}$	- .22	- .2374
$a_{2,15} = N'_{\delta_r}$	- 1.85	- 1.415
$a_{2,16} = N'_{\delta_a}$	- .44	- .0812
$a_{33} = Y_v$	- .07	- .0880
$a_{3,15} = Y_{\delta_r}$	+72.0	+46.3

The a_{ij} 's correspond to those in Table D2. They are equivalent to the stability derivatives listed. Other than for aileron effectiveness, the differences are not large. The reason for these differences is that the first estimate considered the surfaces to ailerons; the second considers them to be spoilers. DATCOM was used for both sets of estimates. Since no covariance analyses are presented with ailerons operative there are no conflicts in results achieved.

The differences in plant models are discussed in the following paragraphs.

Number of Winds

The covariance results use the Skelton differential equation fit (Appendix A) of the Vaughan (ref. 5) E-W Kennedy data for the mean and random components of the side wind. The entire side wind population is used. A set of covariance results is presented which also include rolling gusts of the Dryden form (cf Appendix D). The effects of this rolling are shown to be negligible.

For the analog simulations, the Skelton differential equations were analog simulated. A wind was generated (Figure 7), stored on magnetic tape, and used for all of the analog simulations.

Gimbal Actuators

The analog simulations used second-order actuators with both TWD and DWT dynamics. The previous subsection shows that the effects of both of these sets of dynamics are negligible. First-order actuators were used for the covariance analyses; both simulations have the same break frequencies.

Gimbal Slewing

Both sets of simulations employed slewing schemes to uncouple roll and yaw gimbal moments; there are small detail differences in this aspect. The analog simulations employ a slightly more optimistic set of assumptions in gimbal effectiveness than are used for the covariance analyses. Details are provided in Appendixes B and D.

Accelerometer Location

The accelerometer feedback for the analog simulations is located at station 612. For the covariance analyses it was at the pilot's station. Both stations are well forward of the center of mass.

Gust Penetration

The covariance analyses include gust penetration; the analog used sudden immersion. For the controllers compared, the differences should be minor.

Euler Angles

The analog used a heading, elevation, roll system. Covariance analyses employ pitch, roll, yaw.

Discussion

The comparative performance evaluations of the five controllers previously discussed in the Overview section will not be augmented. Figure 20 through 24 present the comparisons. These data were obtained from Table 13 which includes all data of Figures 20 through 24 plus the times at which in-flight maxima were attained.

The data of Table 13 were obtained by integrating the covariance differential equations for the plant model of Appendix D by digital computer. Tables D8-D11 present these results which were read to obtain Table 13.

Tables D8 and D12 use identical plant and controller models except that the rolling wind is zero for D8 and of Dryden form for D12. The results are within 0.5 percent of each other! If the rolling wind model is even reasonably close to reality it is of no consequence

This completes the technical discussion relative to lateral axes control of the launch phase of shuttle.

A problem in achieving the covariance results is presented as a closure to this section. In a number of applications at Honeywell it has been found satisfactory to use a step size of 0.1 sec in the digital integration of the covariance differential equations. The slightly better accuracy achievable with smaller step sizes has been found not to be warranted because of increased computational expenses. For this application to the lateral axes a divergent oscillation occurred at 0.7 sec per cycle. Step sizes of 0.04, 0.02, and 0.01 were then tried with the heading controller; all produced satisfactory results. For expediency, since these results were obtained near the time of contract termination, 0.02 digital time step was used for all of the lateral axes results discussed thus far. Table D13 presents heading control results with a digital time step of 0.04. They are within engineering accuracy of the comparable results presented in Table D8.

Table 13. Maximum Responses

	δ_p Rad	δ_r Rad	$\bar{q}\beta$ 16 rad/ft ²	M_{660} 10 ⁶ in. lb	M_{1880} 10 ⁶ in. lb	a_y ft/sec ²	$\dot{y}(170)$ ft/sec	$y(170)$ ft
1 Heading	-0.1120 0.0847 0.1967 60	0.0187 0.0328 0.0515 55	23.5 15.8 39.3 60	-16.30 11.18 29.48 60	-50.10 43.90 94.00 60	-3.07 5.89 8.96 60	-58.9 19.58 78.48	-8630.0 3010.0 11640.0
2 Drift	-0.1150 0.0788 0.1938 55	0.0189 0.0361 0.0550 55	22.8 12.03 34.83 60	-15.80 8.75 24.55 60	-49.20 46.00 95.20 55	-3.01 5.73 8.74 60	0.0799 0.00884 0.08874	-1.42 0.0726 1.4926
4 Accelerometer Load Relief	-0.0855 0.0555 0.1410 50	-0.0217 0.0283 0.0500 45	21.3 11.68 32.98 45	-11.00 6.65 17.65 50	-33.20 26.00 59.20 50	-2.95 4.51 7.46 45	11.6 37.0 48.6	-259.0 4510.0 4769.0
5 $\bar{q}\beta$ Load Relief	-0.0908 0.0504 0.1412 50	-0.0217 0.0287 0.0504 45	21.60 11.68 33.28 45	-11.70 6.61 18.31 50	-34.00 34.20 68.20 55	-2.98 4.60 7.58 45	-38.3 38.1 76.4	-5894.0 4640.0 10534.0

Notes:

Row 1 $\mu(\tau)$

Row 2 $\sigma(\tau)$

Row 3 $\text{Max}_t \{ |\mu(t)| + \sigma(t) \}$

Row 4 $\tau =$ time at which row 3 is maximized.

SECTION IV

ORBITER INJECTION

Three-axis attitude (for each of the angular rotations) control systems are designed for a three-engine orbiter (MSFC in-house Vehicle B) and for a two-engine orbiter (North American 134C). Fixed-gain controls provide acceptable performance for normal injection.

For the three-engine orbiter, if the engines are throttled to 50 percent (as might be done in abort), the fixed-gain system is still acceptably stable, even with one engine out; damping is reduced.

For the two-engine orbiter, it is necessary to use reaction controls for roll power during engine out operation. Damping is low but acceptable. Gains should be scheduled with throttle setting to reduce the loss in damping.

Aerodynamic forces are neglected in the analyses because the highest equivalent airspeed is below 25 kt (10 psf).

THE MODELS

Three-view drawings of the orbiters which are presented in Figures 40 and 41 show the gimbaling arrangement. They include tables which give the gimbal hinge line coordinates. The TVCs (thrust vector controllers) for the two orbiters are block diagrammed in Figures 42 and 43. Table 14 presents the equations solved to obtain the characteristic roots. Mass properties data are given in Table 15.

DISCUSSION

The TVC of roll, pitch, and yaw attitude for nominal injection is investigated. Stability with a failed engine with the remaining engines at 50 percent thrust is also considered to obtain information on abort control. This is not a complete resolution of control during abort because aerodynamic effects are neglected. Section V considers TVC control during abort with aerodynamics included.

Single-engine failures are considered. The three-engine orbiter retains sufficient three-axes control. For the two-engine orbiter, it is necessary to provide an additional roll torque force producer. It is assumed the attitude control propulsion system (ACPS) can be used to generate linear roll torques during engine-out operation of the two-engine orbiter.

Stability results are presented in Tables 16 and 17.

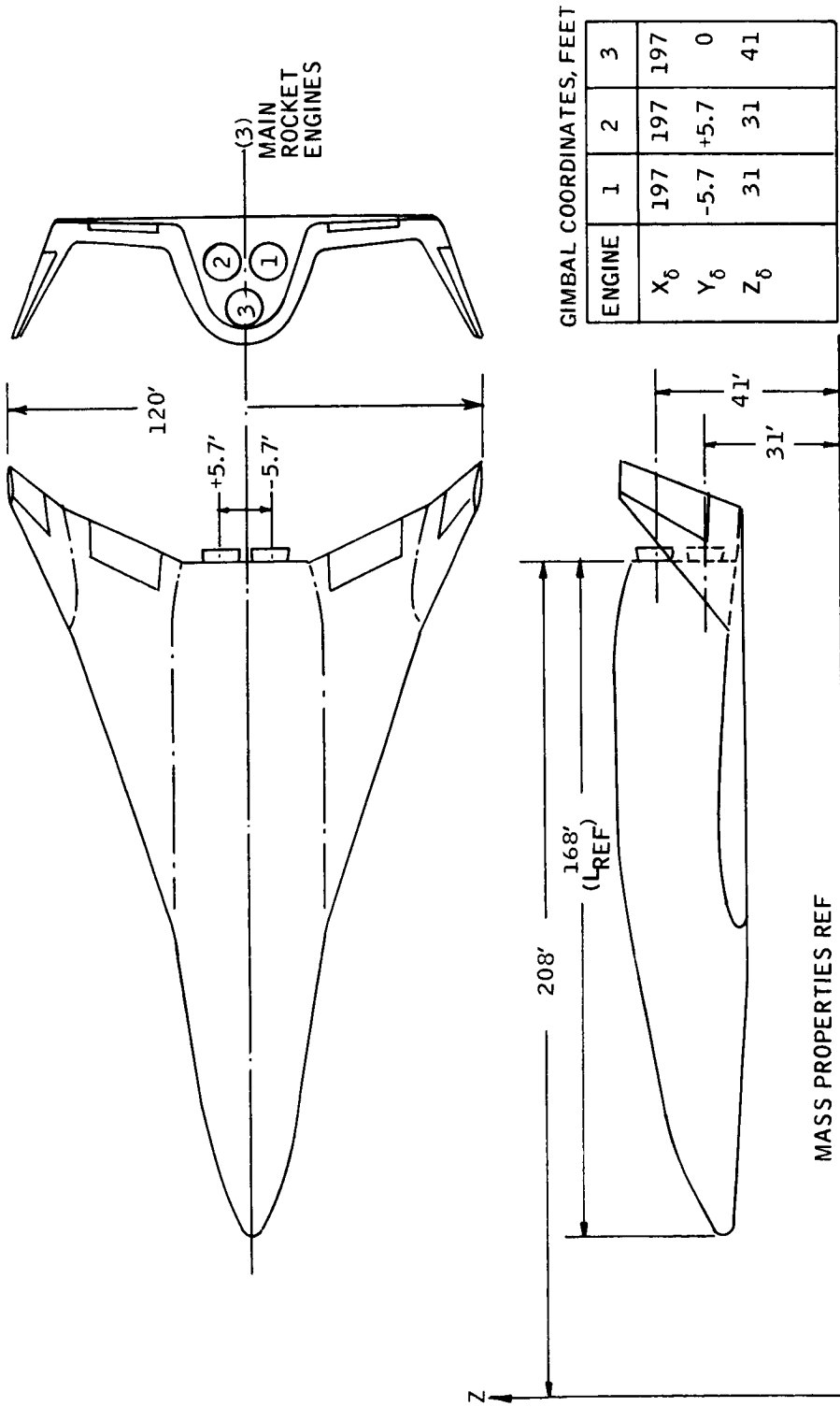


Figure 40. Three-Engine Orbiter

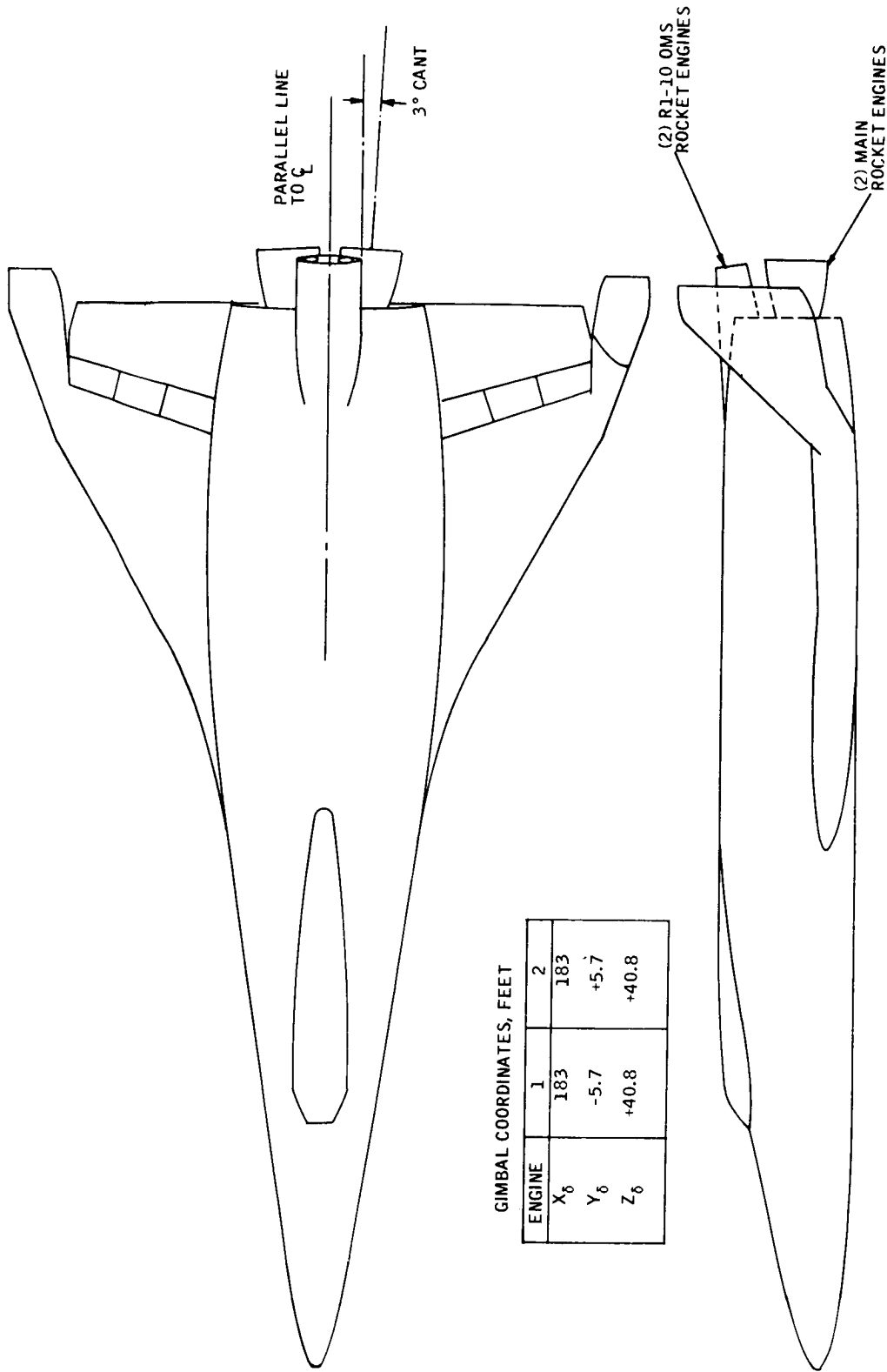


Figure 41. NR 134C Orbiter.

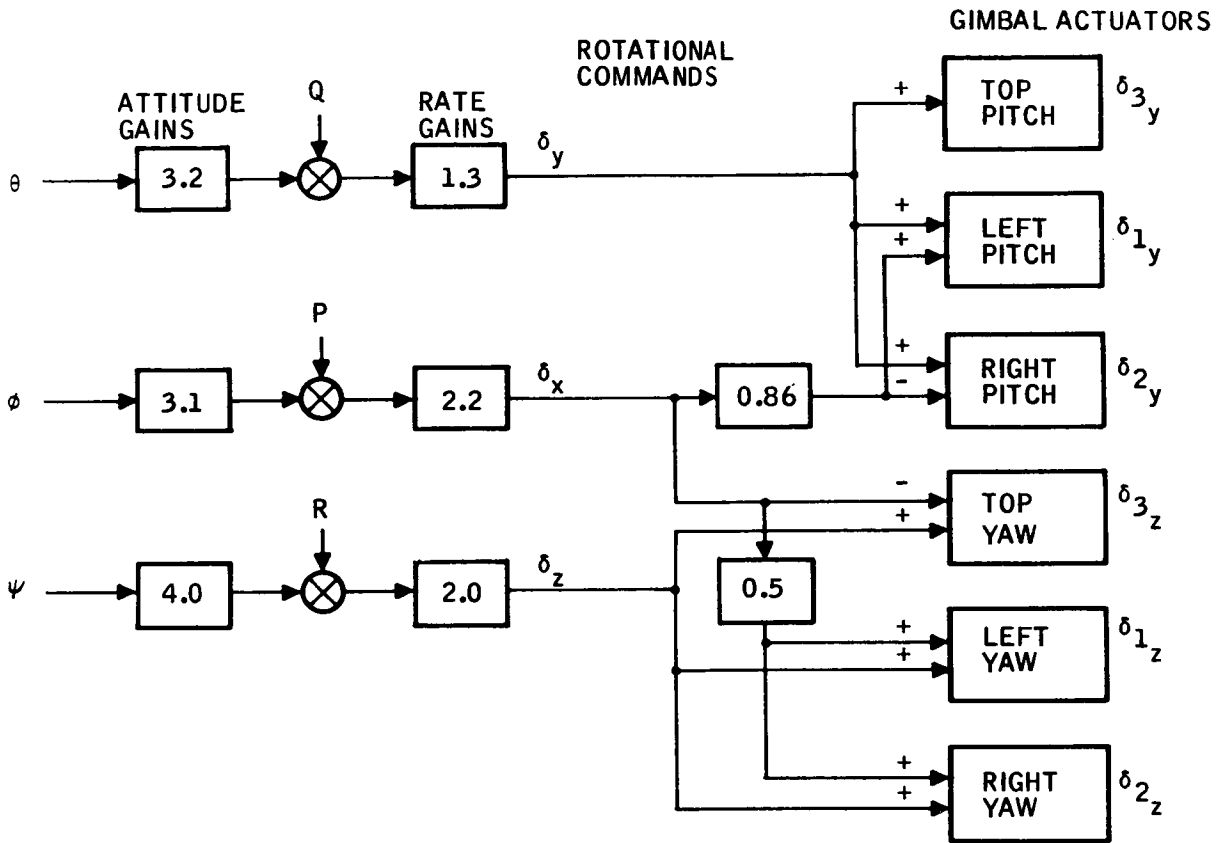
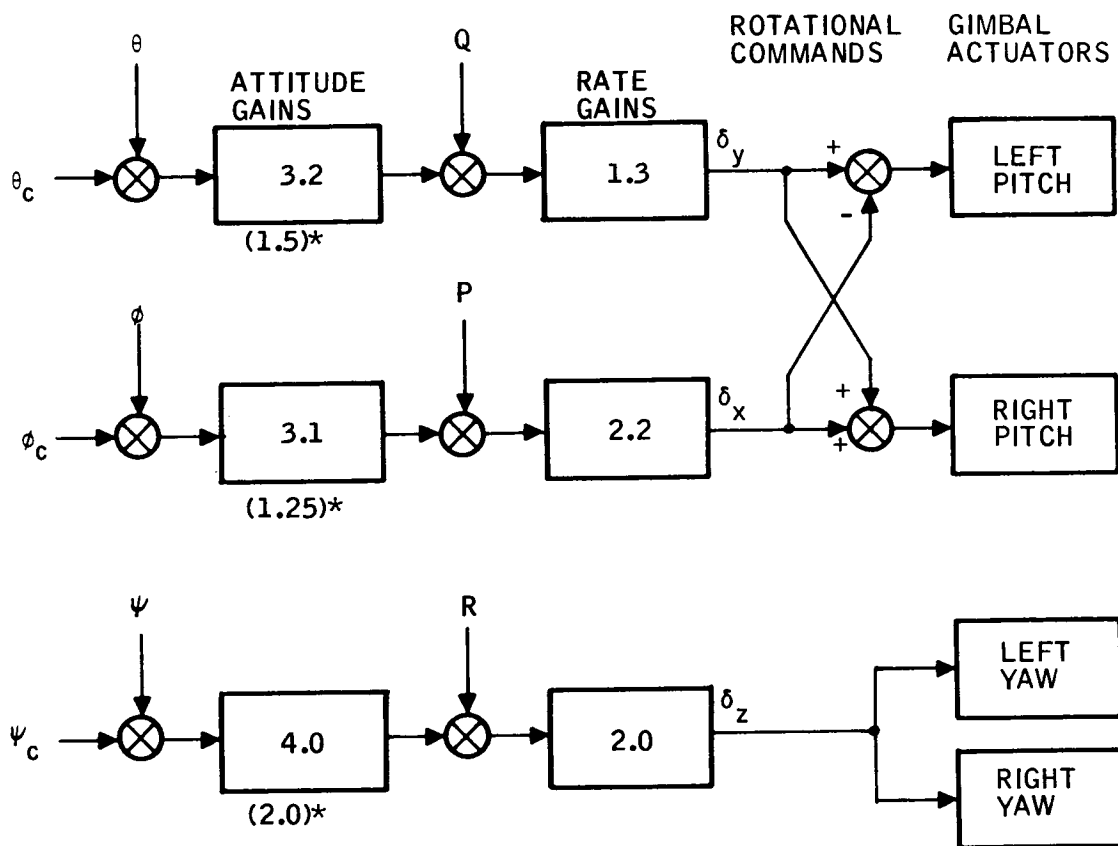


Figure 42. Three-Engine Orbiter TVC Controller



* REDUCED GAINS SELECTED IN 6 DEGREE OF FREEDOM SIMULATION, SECTION V

Figure 43. Two-Engine Orbiter TVC Controller

Table 14. Equations of Motion

Three-Engine Rigid Body Equations	
$I_x \phi s^2 - I_{xz} \psi s^2 - L'_{CG} (460,000 + 313s^2) = 0$	Roll (1)
$I_y \theta s^2 - M'_{CG} (460,000 + 313s^2) = 0$	Pitch (2)
$I_z \psi s^2 - I_{xz} \phi s^2 - N'_{CG} (460,000 + 313s^2)$	Yaw (3)
$mYs^2 - 460,000Y' - 313Y's^2 = 0$	Side force (4)
$mZs^2 - 460,000Z' - 313Z' - 313Z's^2 = 0$	Normal force (5)
Force Equations	
$L'_{CG} = \frac{L}{[460,000 + 313s^2]} = +5.7 (\delta_{1y} - \delta_{2y}) - (z_{CG} - 31) (\delta_{1z} + \delta_{2z}) - (z_{CG} - 41) \delta_{3z}$	(6)
$M'_{CG} = \frac{M}{[460,000 + 313s^2]} = - (x_{CG} - 197) Z' - \sin \delta_o \left[-(CG - 41) \delta_{3y} - (z_{CG} - 31) (\delta_{1y} + \delta_{2y}) \right]$	(7)
$N'_{CG} = \frac{N}{[460,000 + 313s^2]} = (x_{CG} - 197) Y' + 5.7 \sin \delta_o (\delta_{1y} + \delta_{2y})$	(8)
$Y' = \frac{Y}{[460,000 + 313s^2]} = \delta_{1z} + \delta_{2z} + \delta_{3z}$	(9)
$Z' = \frac{Z}{[460,000 + 313s^2]} = -\delta_{1y} - \delta_{2y} - \delta_{3y}$	(10)
Control Laws (cf Figures 42 and 43)	
$\delta_x = 2.2\phi (s + 3.1)$	(11)
$\delta_y = 1.3\theta (s + 3.2)$	(12)
$\delta_z = 2.0\psi (s + 4.0)$	(13)

Table 14. Equations of Motion (Concluded)

Actuator Dynamics	
$[0.001s^2 + 0.032s + 1] \delta_{1_y} - \delta_y + 0.86\delta_x = 0$	(14)
$[0.001s^2 + 0.032s + 1] \delta_{2_y} - \delta_y - 0.86\delta_x = 0$	(15)
$[0.001s^2 + 0.032s + 1] \delta_{3_y} - \delta_y = 0$	(16)
$[0.001s^2 + 0.032s + 1] \delta_{1_z} - \delta_z - 0.5\delta_x = 0$	(17)
$[0.001s^2 + 0.032s + 1] \delta_{2_z} - \delta_z - 0.5\delta_x = 0$	(18)
$[0.001s^2 + 0.032s + 1] \delta_{3_z} - \delta_z + 1.0\delta_x = 0$	(19)
Two-Engine Orbiter Equations	
$L'_{CG} = 5.7 \begin{pmatrix} \delta_{1_y} & -\delta_{2_y} \end{pmatrix} - (z_{CG} - 40.8) \begin{pmatrix} \delta_{1_z} & +\delta_{2_z} \end{pmatrix}$	(6)
$M'_{CG} = -(x_{CG} - 197) Z'$	(7)
$[0.001s^2 + 0.032s + 1] \delta_{1_y} - \delta_x = 0$	(14)
$[0.001s^2 + 0.032s + 1] \delta_{2_y} - \delta_y - \delta_x = 0$	(15)
$\delta_{3_y} = 0$	(16)
$[0.001s^2 + 0.032s + 1] \delta_{1_z} - \delta_z = 0$	(17)
$[0.001s^2 + 0.032s + 1] \delta_{2_z} - \delta_z = 0$	(18)
$\delta_{3_z} = 0$	(19)

*Nominal thrust. For 50 percent thrust 230,000 pounds is used.

Table 15. Vehicle Mass Properties

Condition	3-Engine Orbiter		2-Engine Orbiter	
	Ignition	Burnout	Ignition	Burnout
$10^{-7} I_x$, slug ft ²	0.54	0.32	0.57	0.35
$10^{-7} I_y$, slug ft ²	2.43	1.56	2.29	1.50
$10^{-7} I_z$, slug ft ²	2.83	1.76	2.63	1.61
$10^{-7} I_{x_z}$, slug ft ²	0	0	0.10	0.12
Pitch Trim / $\sin \delta_o$	-0.12	-0.09	0	0
$10^{-7} m$, slugs	0.0028	0.00094	0.00236	0.00077
x_{CG}	151.6	157.6	132.0	137.5
z_{CG}	28.5	31.1	40.4	39.5
Gimbal Coordinates	See Figure 40		See Figure 41	

Table 16 presents the stability of the three-engine orbiter. Stability is adequate under normal operation or with an engine failure. With normal thrust the damping ratios vary from a minimum of 0.48 (for yaw) at ignition to a maximum of 0.71 (for roll) at burnout. Damping ratios are usually reduced by either or both engine failures or thrust level reductions. The failure of the top engine develops more adverse damping characteristics than failure of a bottom engine. Smallest damping (0.12) is attained in the yaw axis at ignition with the top engine failed and with the remaining lower engines at 50 percent thrust. This would be adequate for emergency operation. Stability could be improved by adjusting the gains as a function of throttle setting.

Table 16. Three-Engine Orbiter Stability

Thrust, Each Engine			100%		50%	
Frequency and Damping			ω	ζ	ω	ζ
At Ignition	Normal engines (3)	Roll	3.7	0.52	2.5	0.36
		Pitch	3.5	0.51	2.4	0.35
		Yaw	4.6	0.48	3.1	0.32
	Fail Bottom engine	Roll	1.9	0.26	1.3	0.18
		Pitch	3.1	0.41	2.1	0.28
		Yaw	4.4	0.55	3.0	0.37
	Fail Top engine (worst case)	Roll	2.6	0.49	1.9	0.35
		Pitch	2.8	0.40	1.9	0.28
		Yaw	3.4	0.21	2.3	0.12
At Burn- out	Normal engines	Roll	5.0	0.71	3.3	0.47
		Pitch	4.0	0.58	2.7	0.39
		Yaw	5.6	0.58	3.7	0.38
	Fail Bottom engine	Roll	3.8	0.47	1.7	0.23
		Pitch	2.4	0.33	2.6	0.32
		Yaw	5.4	0.69	3.5	0.45
	Fail Top engine	Roll	3.3	0.48	2.3	0.33
		Pitch	3.2	0.46	2.2	0.32
		Yaw	4.3	0.44	2.9	0.30

Table 17 gives two-engine orbiter results. Stability is again adequate. The worst case is at ignition where the moments of inertia are highest. Loss of one engine reduces pitch and yaw damping from 0.44 to 0.30. At 50 percent thrust, loss of an engine reduces these damping ratios to 0.21. While this might be acceptable, scheduling of control system gains with throttle setting again appears desirable. Normal injection can accept engine-out with a fixed-gain attitude control system.

Section V of this report examines high-altitude aborts in the two-engine orbiter. There the TVC system gains are varied inversely with the power level (PL) of each engine.

Table 17. Two-Engine Orbiter Stability

Thrust, Each Engine			100%		50%	
Frequency and Damping			ω	ζ	ω	ζ
At Ignition	Both engines on ON	Roll	2.2	0.37	1.8	0.25
		Pitch	3.0	0.44	2.1	0.30
		Yaw	4.0	0.44	2.8	0.30
	Fail one (worst case)	Roll*	3.5	0.55	3.5	0.55
		Pitch	2.1	0.30	1.5	0.21
		Yaw	2.8	0.30	1.9	0.21
At Burn- out	Both engines on	Roll	3.4	0.48	2.3	0.33
		Pitch	3.4	0.41	2.3	0.33
		Yaw	4.8	0.51	3.2	0.34
	Fail one	Roll*	4.5	0.70	4.5	0.70
		Pitch	2.3	0.34	1.6	0.24
		Yaw	3.2	0.35	2.2	0.24

* With one engine failed, a pure torque roll control is assumed from ACPS. The roll torque in ft lb, is $L = 10^7 (2.2\phi + 7.0\phi)$

SECTION V

DELTA WING ORBITER CONTROL FOR ABORT

The objective is to determine whether aborts make demands on the orbiter control system which would not be experienced in normal operation. Some differences from normal orbiter flight are immediately apparent; thrust vector control (TVC) in regions of significant dynamic pressure (\bar{q}), single-engine operation, simultaneous operation of TVC with the entry control system's (ECS) attitude control propulsion system (ACPS) and aerodynamic controls; possible staging on the pad for flyaway; and staging in high dynamic pressure regions. Abort guidance trajectories generated by North American Rockwell (NR) in their Phase B shuttle abort studies were used. These trajectories were obtained on a three-degree-of-freedom (point mass) simulation which did not address the control problem. These abort studies use the same steering commands (thrust vector control power levels, angle of attack, bank angle) and initial conditions to fly the delta wing orbiter along the NR trajectories.

SUMMARY AND CONCLUSIONS

This study is primarily of high altitude aborts. Brief attention is given to aborts off the pad and at high \bar{q} . Time did not permit adequate study of high \bar{q} abort.

A North American Delta wing orbiter (DWO) abort trajectory originating at 226,000 feet was selected for analysis of control requirements. This trajectory consists of TVC operation until propellant depletion at 330 seconds. It is followed by normal entry control systems operation for another 1000 seconds. A linear TVC system was designed, similar to the DWO's ECS aerodynamic control, but with gains scheduled inversely with throttle setting, rather than \bar{q} and Mach number. The TVC and ECS are allowed to operate together in this brief study; both received the same angle of attack and bank angle commands as used by NR when generating this abort trajectory.

Figure 44 shows two different trajectories obtained by these programmed commands, one with parallel burn and one with sequential burn of main and orbit maneuver propellants. Sequential burn produces an extreme aft cg location which is aerodynamically uncontrollable following TVC shutdown. In Figure 44 a successful sequential burn trajectory was obtained because, at the very high altitude, the ACPS marginally controlled through the aerodynamically uncontrollable region. Abort initiated at lower altitudes, using sequential burn, would have ended with pitch up at TVC shutdown. Conclusion: parallel burn of main and orbit maneuver propellants is mandatory.

HEAVY LINES SHOW TVC PART
OF TRAJECTORY

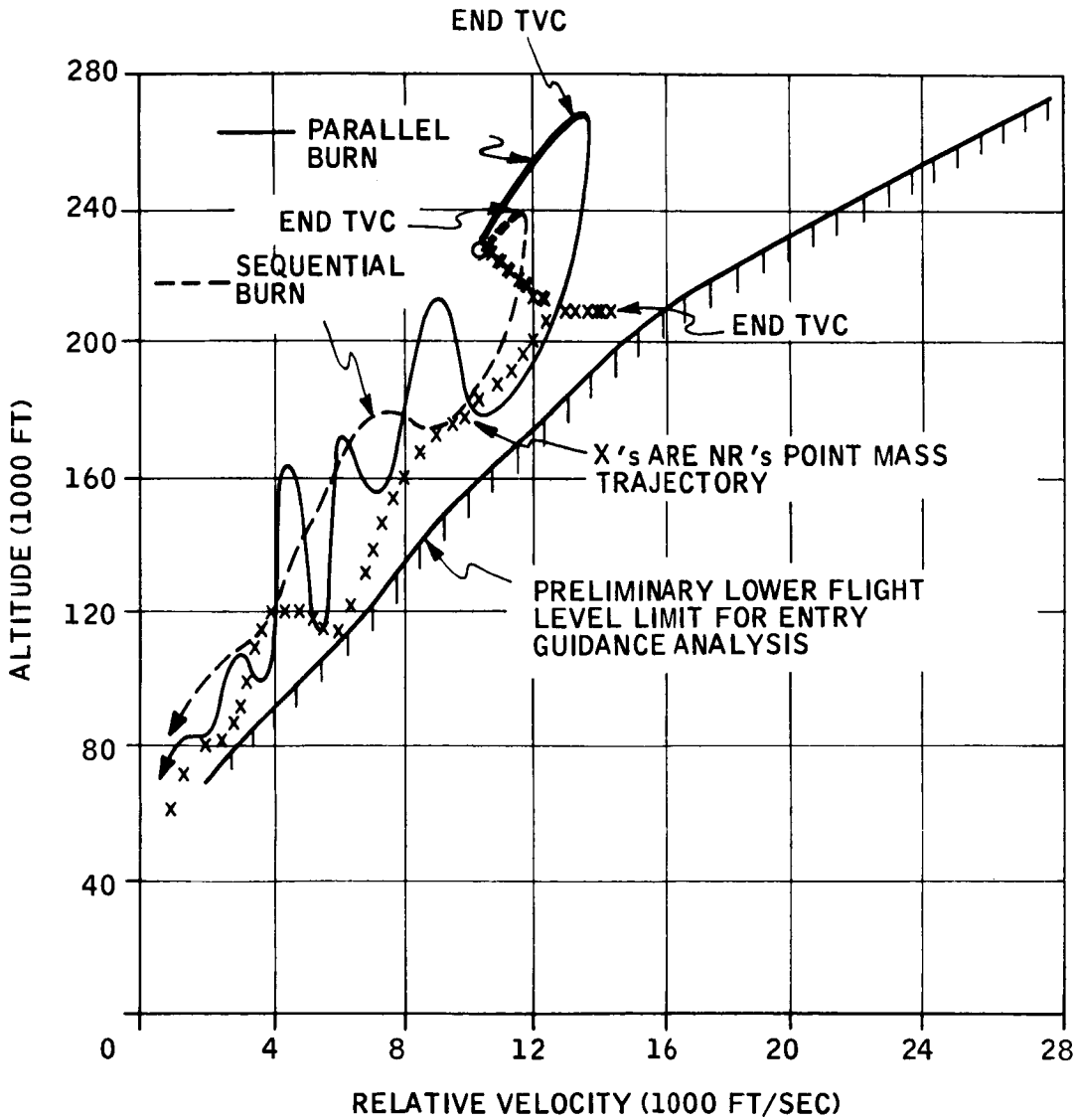


Figure 44. Altitude/Velocity Profiles Comparing NR's Point Mass Trajectory with Honeywell's 6 Degree of Freedom Response to the Same Steering Commands

The TVC system was operated on single-engine for about 190 seconds. The normal gimbal authority of ± 7 degrees is adequate, provided that the null point is in the normal position, canted 3 degrees toward the orbiter centerline.

The angle of attack was 50 degrees in the TVC portions of the abort trajectories, which attained sufficient dynamic pressure to create a significant normal force. The vector sum of aerodynamic and thrust forces could cause the propellant surfaces to tilt as much as 65 degrees from the normal vacuum thrust condition. This poses a slosh modeling and control problem which must be considered in the final design, and which could impact the baffle design.

Some sideslip may be needed to maintain the desired flight path during single-engine TVC. The study found that five degrees sideslip could easily be controlled during TVC, but this presented an initial condition which was uncontrollable following TVC shutdown; the yaw ACPS lacked the necessary control power. If sideslip is needed during TVC, a decrab must be made prior to engine shutdown.

This abort trajectory included simultaneous ECS commands to transition (α from 30 to 14 deg) and bank 30 deg to level. The ECS lost control as the orbiter diverged. This may have been due to an incorrect value for N_{δ_a} (the yawing moment due to aileron). Data received after this study was completely reduced N_{δ_a} to one fourth of the value used. Section VI shows this would have a significant stabilizing effect. Simultaneous maneuvers require additional investigation. If still unstable, these maneuvers must be prevented by guidance logic.

A brief examination of TVC at high \bar{q} results in pitch axis limit cycling of the TVC and ECS, operating together. The tentative conclusion is that the TVC system and the ECS are, conceptually, still acceptable for high \bar{q} operation, but need gain adjustment for satisfactory operation.

The pad abort study considered the effect of a 40-knot wind when attempting orbiter lift off. The two-engine orbiter can lift off without interference with the booster in at least two ways; apply 19,000 pounds thrust at the nose, or tilt the orbiter nose away 4 deg before separation.

PAD ABORT FLYAWAY

North American was considering various pad abort methods at the time of this study. Pad abort is caused by booster failures, such as inability to reach liftoff thrust, fire, or explosion. The primary objective is survival of booster crew, orbiter crew, and orbiter passengers. A secondary objective would be to save the orbiter by flyaway. Flyaway is the only pad abort considered which involves flight control. This study addressed only

the initial phase of pad abort flyaway; how to prevent collision with the booster or with the launch tower. Two methods were considered here. The first would provide a thruster at the orbiter nose (to develop both a normal force and a pitching moment), an alternative is to cant the orbiter nose several degrees about the aft attach point prior to separation.

Figures 45 and 46 present wind force estimates (by use of ref. 12) on a straight-wing and a delta-wing orbiter. Other aerodynamic forces are neglected for this problem of developing a collision-free trajectory.

The forces on the orbiters in a 40-knot wind are summarized from Figures 45 and 46 as follows:

<u>Parameter</u>	<u>Straight-Wing Orbiter</u>	<u>Delta-Wing Orbiter</u>
Negative normal force, lb	41, 000	52, 000
Nose up pitching moment, ft lb	600, 000	130, 000

Pad abort liftoff was simulated with the following equations:

$$\delta = + 1.3 \dot{\theta} + 4 \theta \left[1 + \frac{1}{5S} \right] \quad (\text{gimbal deflection})$$

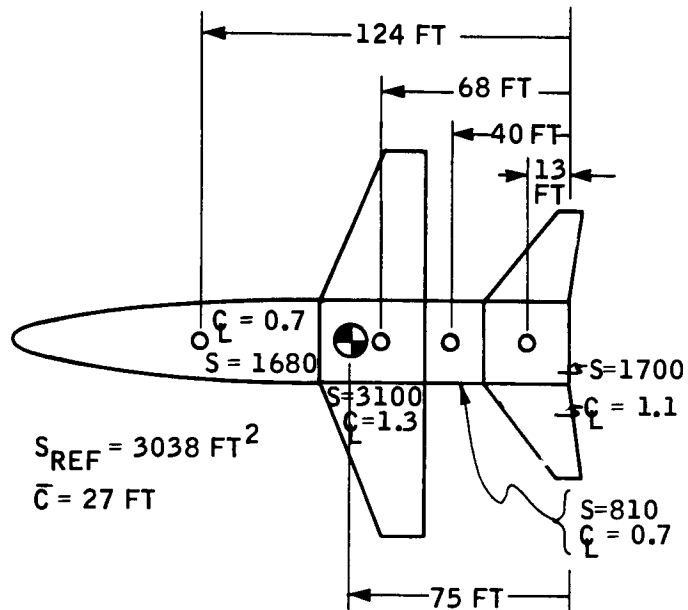
$$I_y \ddot{\theta} = (x_{CG} - x_{\delta}) T \delta - T z_{CG} - Z(x_{CG} - x_{AC}) - Z_j(x_{CG} - x_j) \quad (\text{pitch torque})$$

$$m \ddot{X} = T(\theta + S) - Z - Z_j \quad (\text{horizontal force})$$

$$m \ddot{Z} = T - W \quad (\text{vertical force})$$

Results are shown in Figures 47 through 50. In each case the cross range does monotonically increase upwind. It appears that successful separation is likely. However, Figures 47 and 48 show that, at one second, the pitch angle is increased enough to move the orbiter tail 0.55 feet closer to the booster. A more complete simulation is required to assure that a contact would not be made, or that, with contact, a successful lift off can still be performed.

Thus, the tentative conclusion of this brief investigation is that pad abort flyaway can be accomplished for the conditions investigated by use of a nose thruster or tilt according to the following table:



ESTIMATE C_N AND $C_{M_{CG}}$ (CG 75 FEET FROM BASE)

SECTION	AREA	C_N	$C_N \left(\frac{S}{S_{REF}} \right)$	DISTANCE OF SECTION CENTROID AFT C.B.	$C_N \left(\frac{S}{S_{REF}} \right) \left(\frac{l}{27} \right)$
NOSE	1680	0.7	0.36	-49	-0.65
WING	3100	1.3	1.30	+ 7	+0.34
MIDSECTION	810	0.7	0.17	+35	+0.22
TAIL	1700	1.1	0.61	+62	+1.40

TOTAL $C_N = 2.44$

TOTAL $C_M = +1.31$

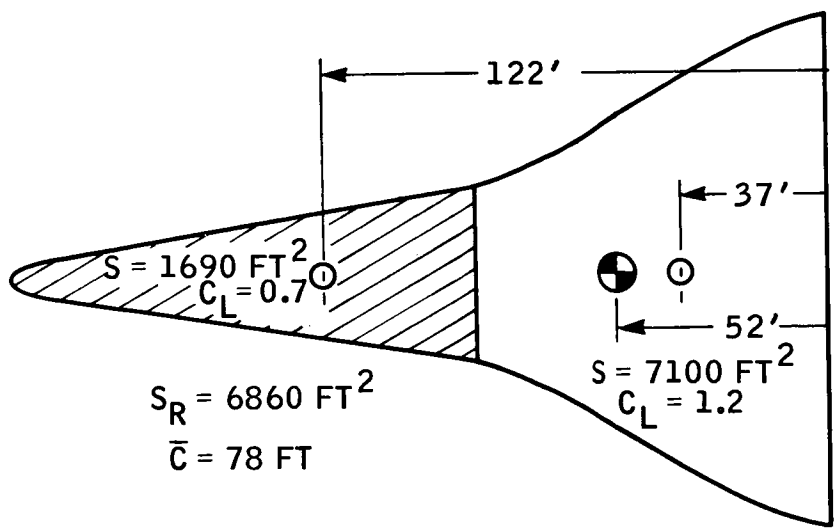
$$X_{AC} = (27) \left(\frac{1.3}{2.44} \right) = 14.6 \text{ FT AFT OF C.G.}$$

FOR A 40 KNOT WIND BLOWING FROM TOP DOWN

$$N = -41,000 \text{ LBS}$$

$$M_{CG} = -14.6 N = +600,000 \text{ FT LB}$$

Figure 45. Wind Force on a Straight-Wing Orbiter



SECTION	AREA	C_N	$C_N \left(\frac{S}{S_{REF}} \right)$	DISTANCE CENTROID AFT CG	$C_L \left(\frac{S}{S_{REF}} \right) \frac{l}{78}$
NOSE	1690	0.7	0.2	-70	-0.18
WING	7100	1.2	<u>1.2</u>	+15	<u>+0.23</u>
TOTAL $C_N =$			1.4	TOTAL $C_M =$	+0.05

$$X_{AC} = 78 \left(\frac{0.05}{1.4} \right) = 2.8 \text{ FT AFT OF C.G.}$$

FOR 40 KNOT WIND BLOWING DOWN:

$$N = -52,000 \text{ LBS}$$

$$M_{CG} = -2.8N = 130,000 \text{ FT LB}$$

Figure 46. Wind Force on a Delta Wing Orbiter

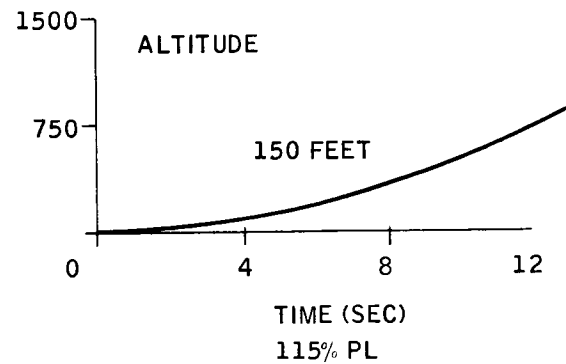
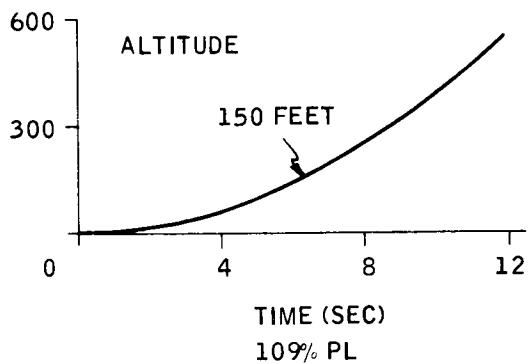
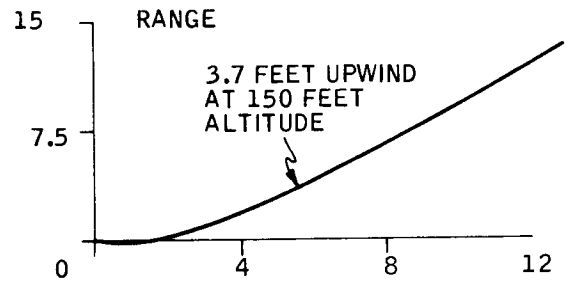
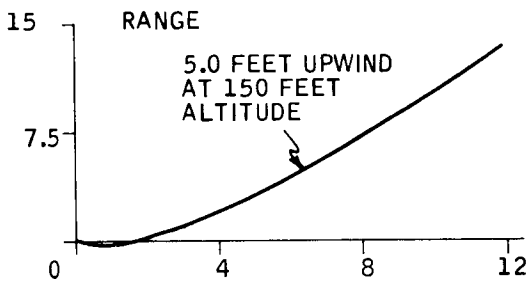
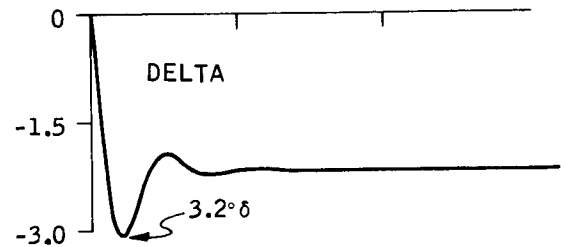
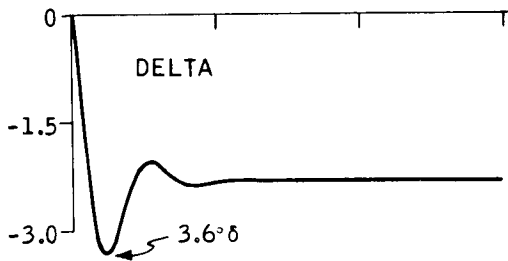
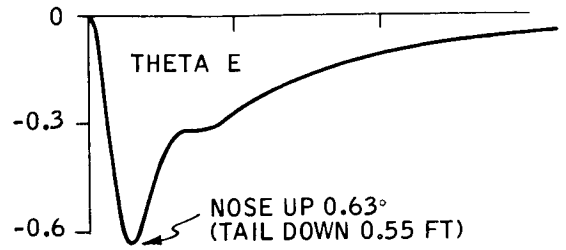
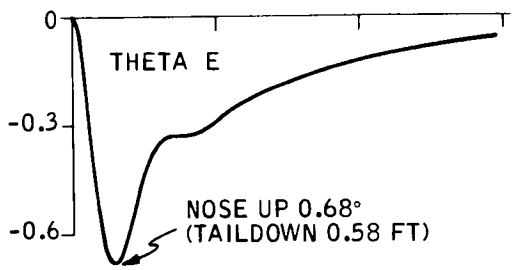


Figure 47. Delta Wing Pad Abort with 19,000 lb Nose Thrust

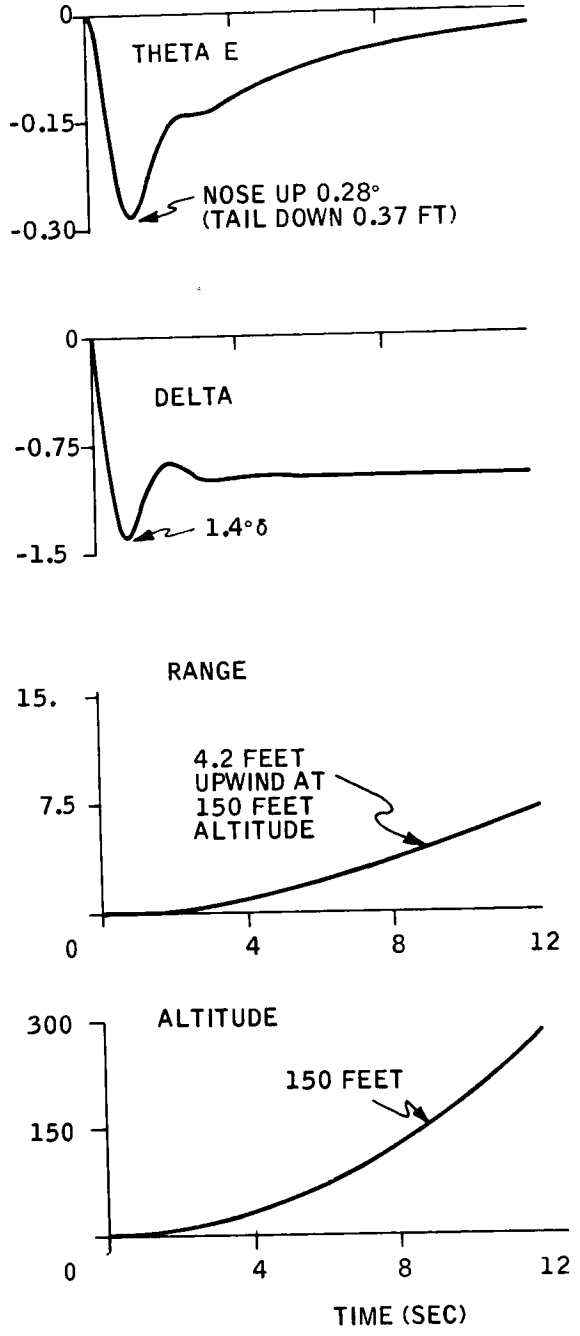
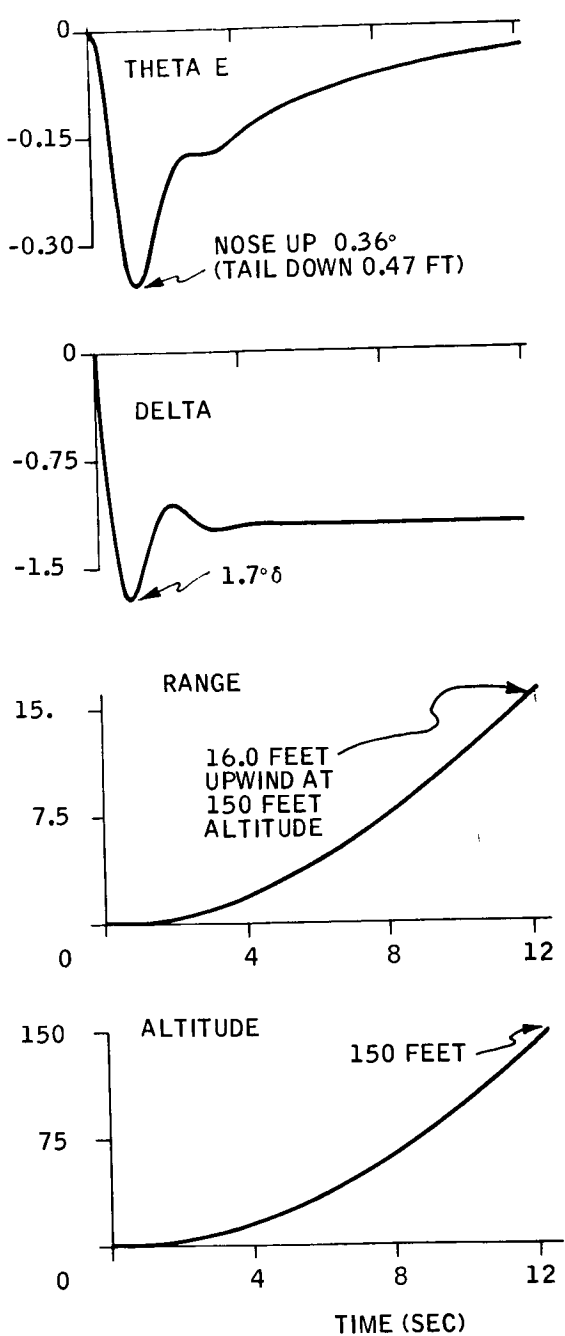
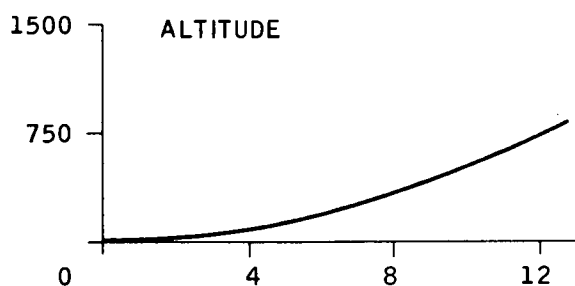
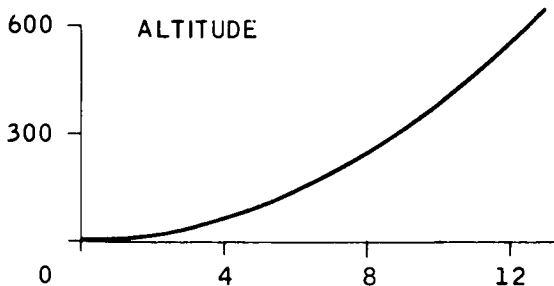
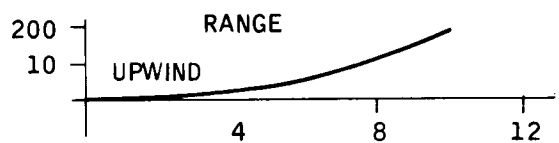
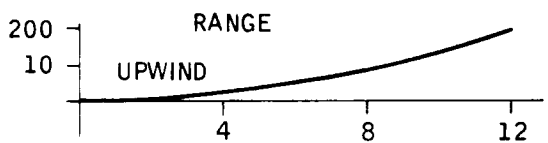
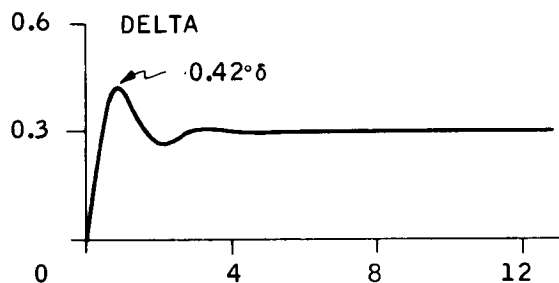
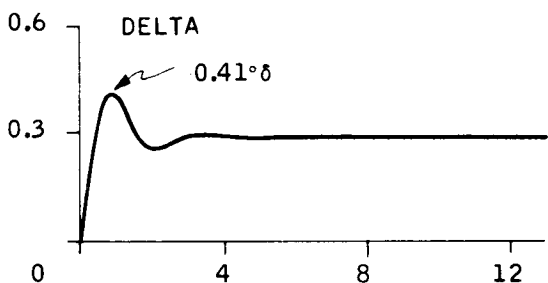
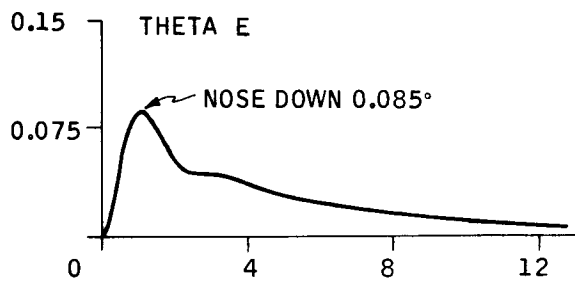
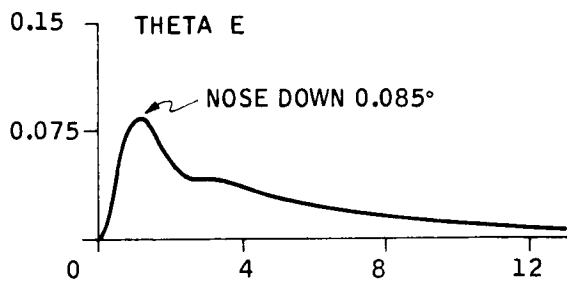


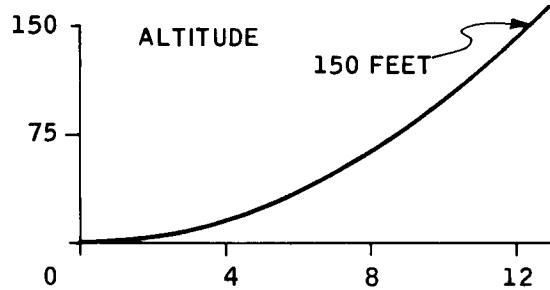
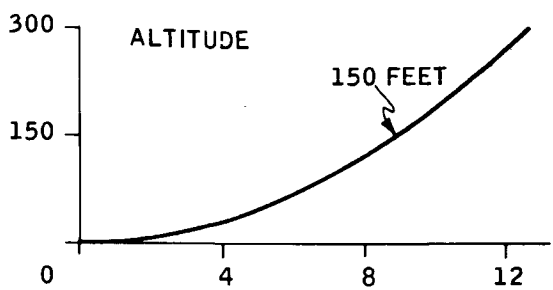
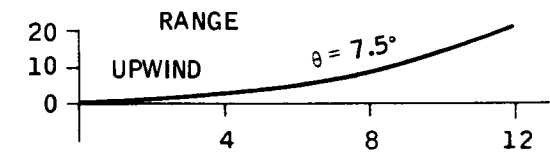
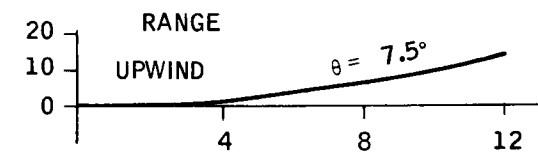
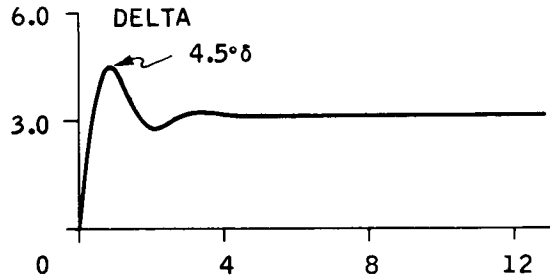
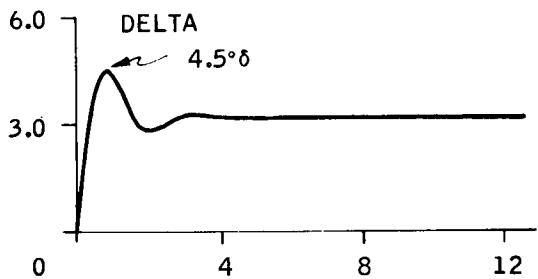
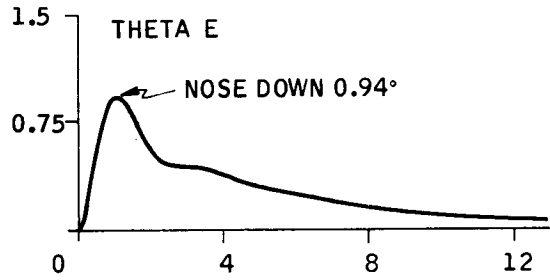
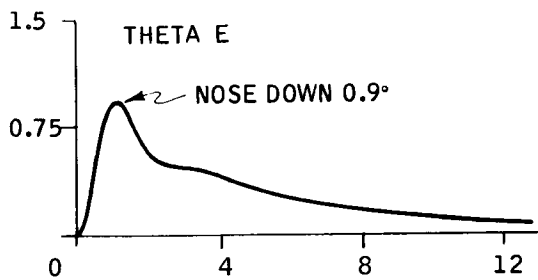
Figure 48. Straight Wing Pad Abort with 27,000 lb Nose Thrust



TIME (SEC)
109% PL

TIME (SEC)
115% PL

Figure 49. Delta Wing Pad Abort with 4.0 Deg Nose Up Tilt



TIME (SEC)
115% PL

TIME (SEC)
109% PL

Figure 50. Straight Wing Orbiter Pad Abort

<u>Separation Means</u>	<u>Delta Wing</u>	<u>Straight Wing</u>
Nose thrust, lb	19, 000	27, 000
Nose tilt, deg	4. 0	7. 5

PRELIMINARY ANALYSIS OF ABORT TRAJECTORIES

Ten trajectories were received from NR. Data on the abort used for these control system studies are given in Figures 51 through 54. Time did not permit study of the other cases. NR is currently generating additional trajectories, including some with staging before max q of mated ascent. Control of these high q abort trajectories needs to be investigated.

Section IV describes a root locus analysis of three-engine and two-engine orbiters in TVC mode in vacuum. This study includes effects of single-engine out, engine throttle settings of 50 and 100 percent, and mass properties at the beginning and end of TVC burn. The study concludes that the fixed-gain controls shown in Figure 43 provide acceptable performance with (a) both engines at 100 percent, (b) both engines at 50 percent, and (c) one engine at 100 percent. The orbiters are still stable, but poorly damped if only one engine is operating at 50 percent throttle. Conclusion, gains should be varied inversely with throttle setting, but engine-out need not be detected to adjust gains.

The NR abort trajectory data (Figure 54) revealed that significant aerodynamic normal force exists when TVC is operating at only 50 percent of available thrust. Figure 55 illustrates the potential problem; the propellant sloshing surface is inclined from the normal expected during orbit injection. This inclination angle would reach 35 degrees during this abort. The pad abort flyaway data includes TVC single-engine operation at 50 percent thrust (25 percent available thrust). Here the inclination angle reached 65 degrees. Conclusion, a unique propellant slosh modeling and control problem exists which must be considered in the final control system design. This could impact the tank baffling design.

HIGH ALTITUDE ABORT SIMULATION

Honeywell's six-degree-of-freedom (6 DOF) entry simulation was used for this abort study. Appendix G summarizes the 6 DOF simulation and presents the vector control (TVC) system added for this study. Figure 56 diagrams the TVC system selected for test. It is modeled from the existing entry control system (ECS) shown in Figure 69 (next section of this report). Figure 56 shows the final gains used; higher gains on α , ϕ , and β were used initially, taken from the roots analysis described in Section IV. See Figure 43 for a gain comparison.

SSV 161 ROCKET POWERED FLIGHT AFTER A BOOSTER FAILURE

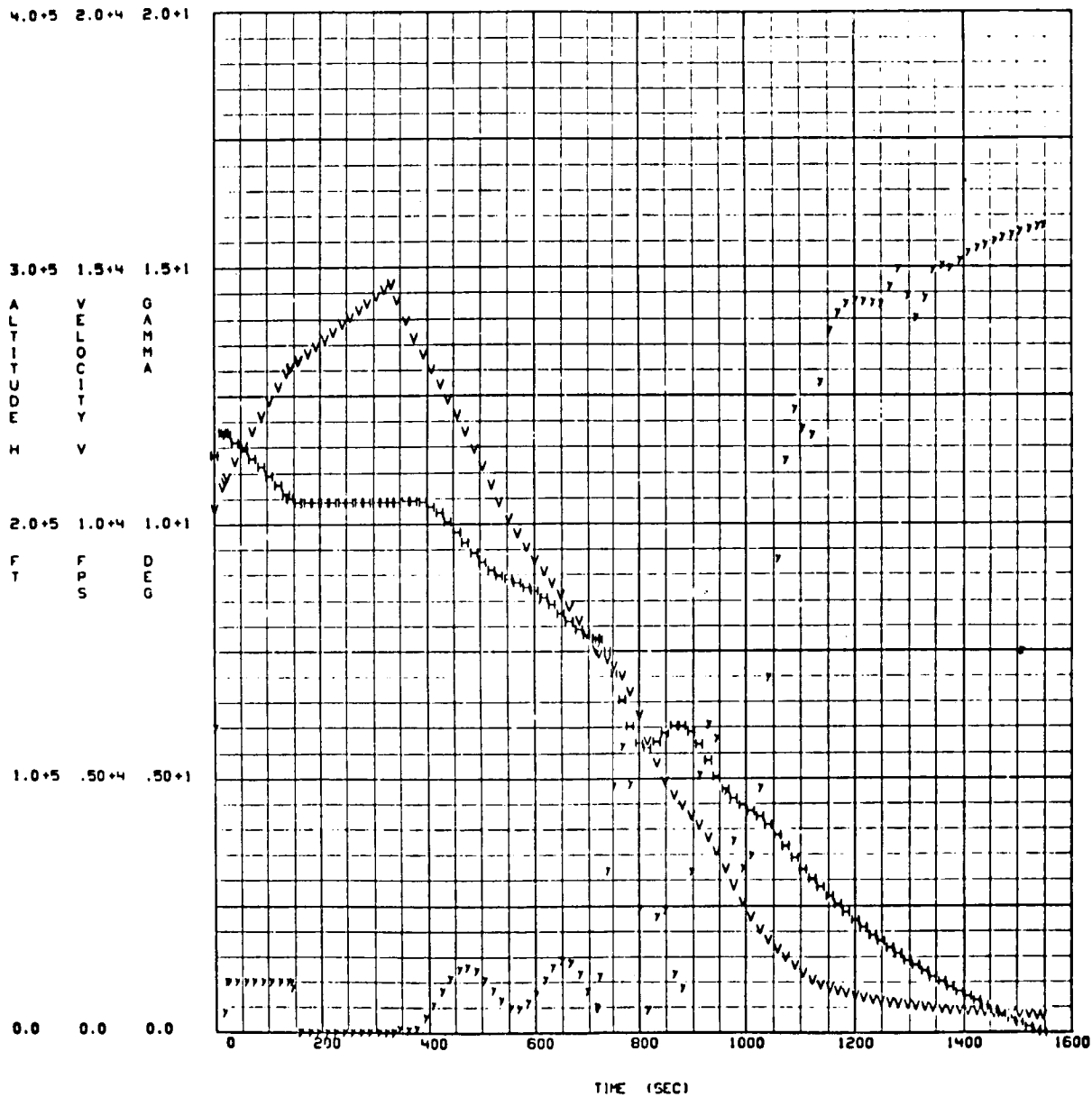


Figure 51. Abort Altitude, Velocity, and Flight Path Angle

SSV 161 ROCKET POWERED FLIGHT AFTER A BOOSTER FAILURE

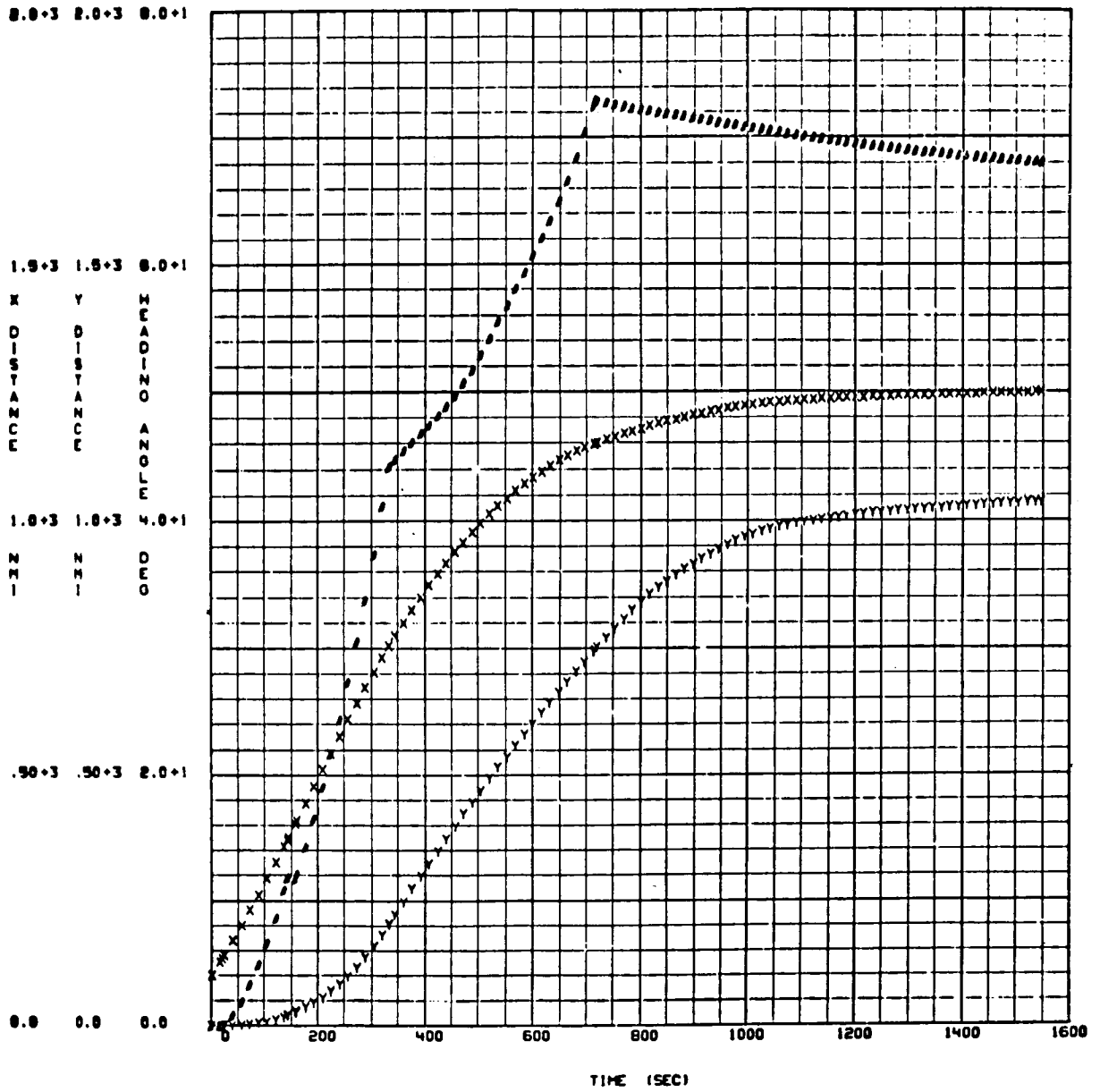


Figure 52. Abort Heading and Range

SSV 161 ROCKET POWERED FLIGHT AFTER A BOOSTER FAILURE

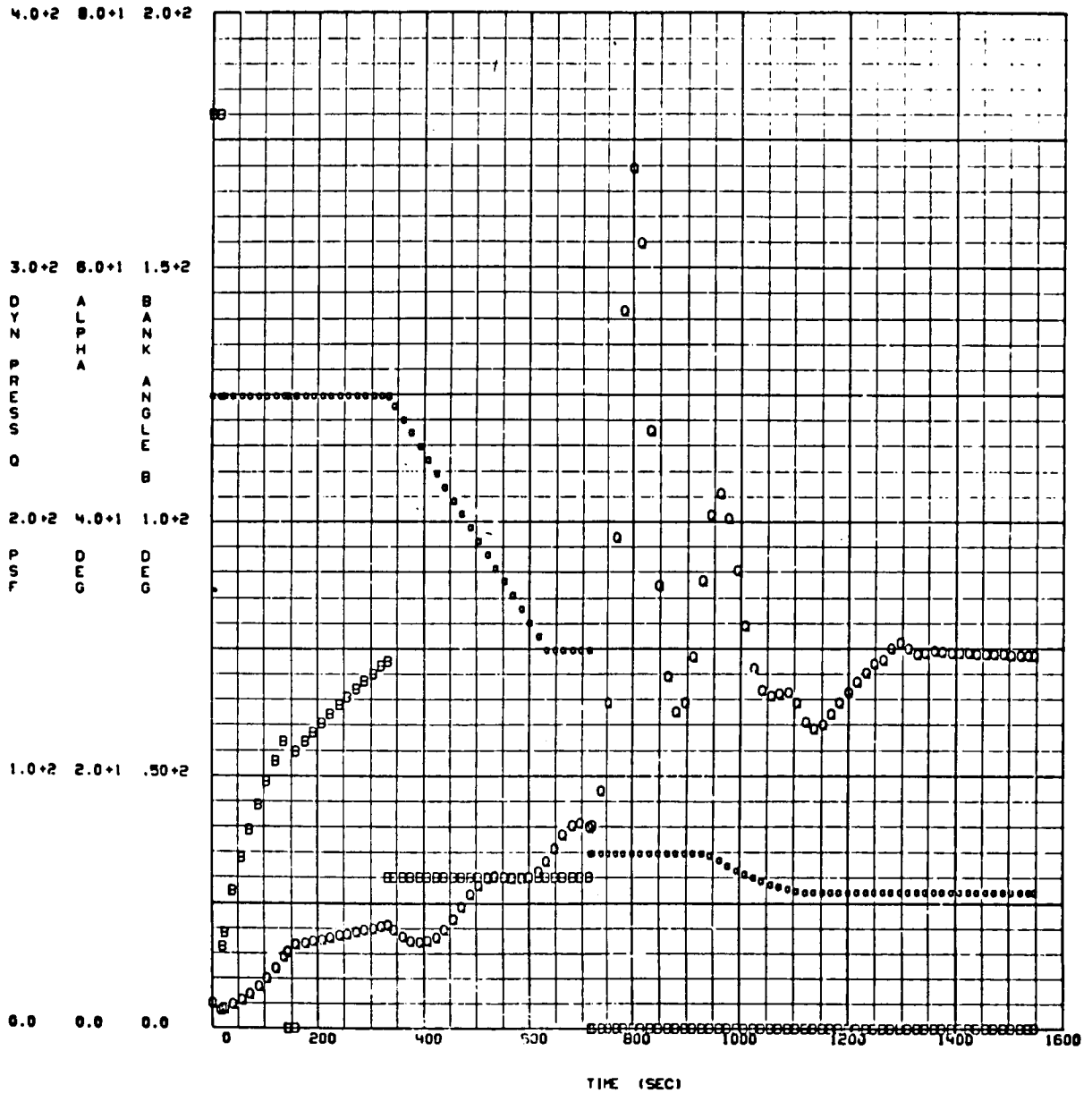


Figure 53. Abort Bank Angle, Angle of Attack, and Dynamic Pressure

SSV 161 ROCKET POWERED FLIGHT AFTER A BOOSTER FAILURE

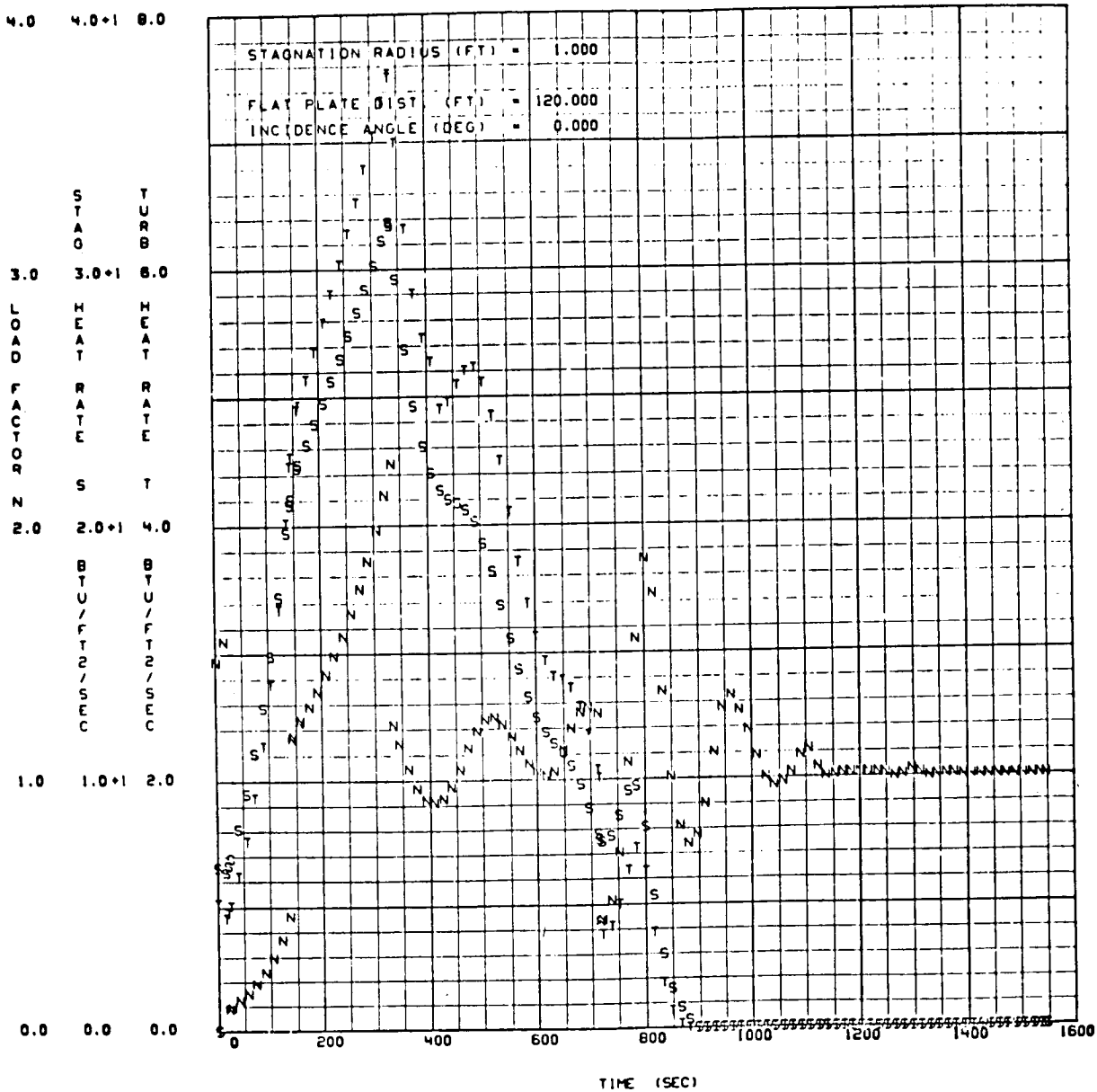


Figure 54. Abort Load Factor and Heat Rates

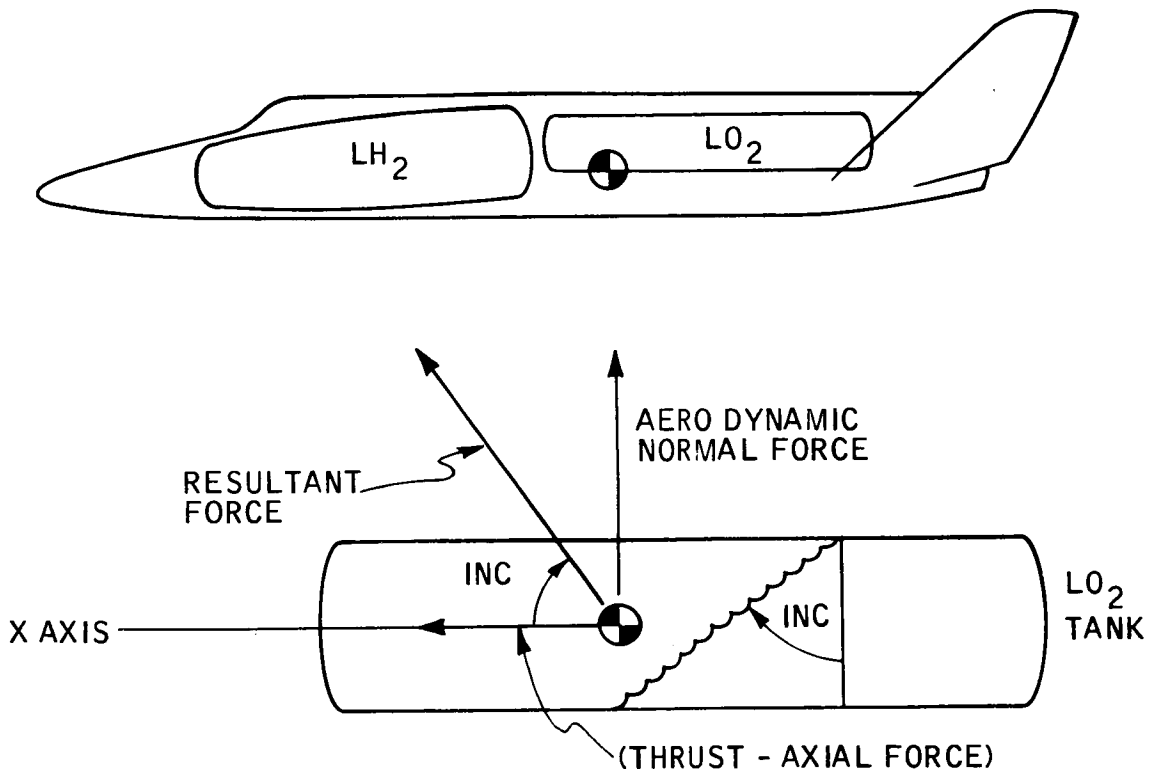


Figure 55. Inclination of Propellant Surface Due to Aerodynamic Normal Force and Thrust

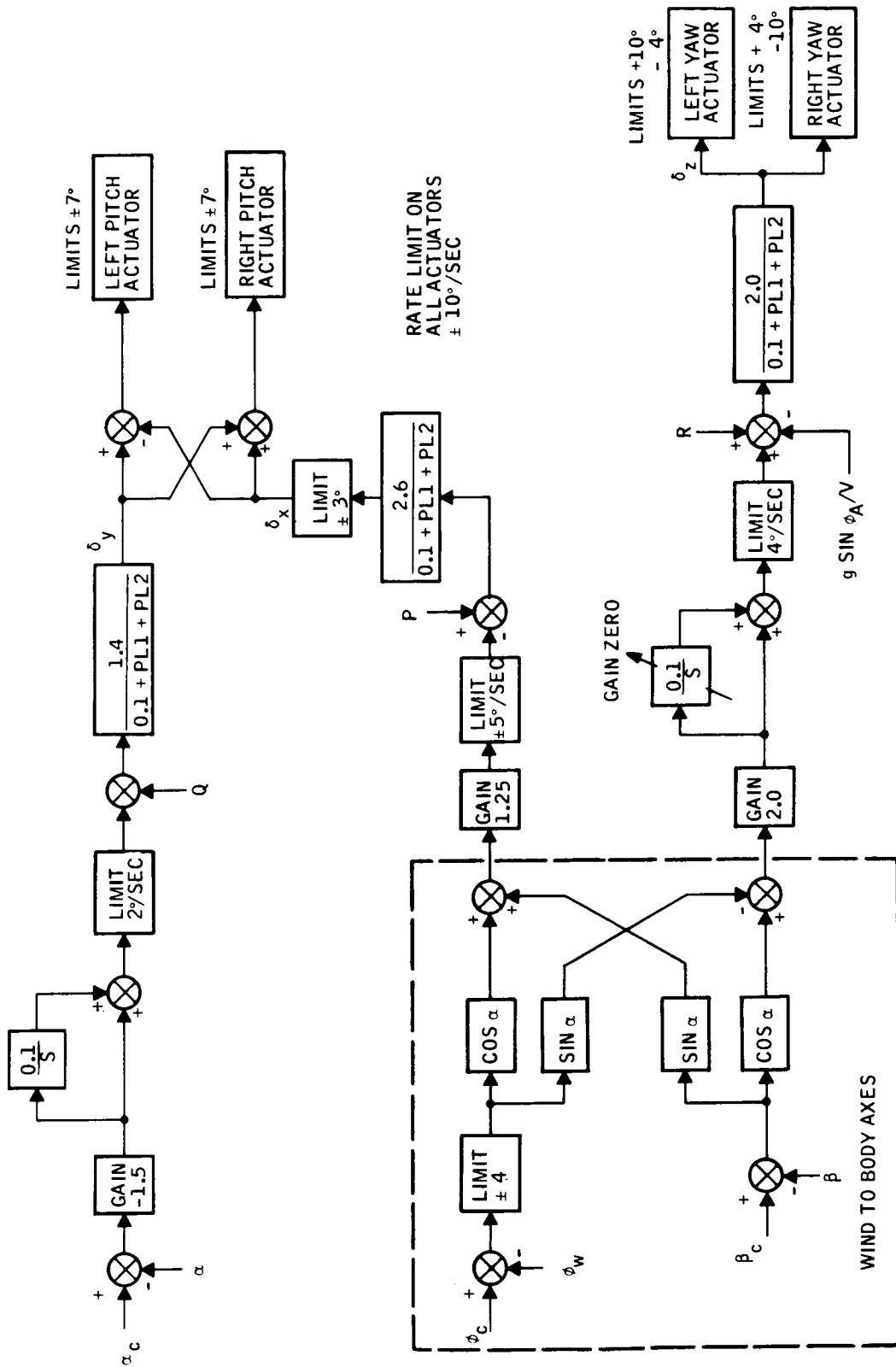


Figure 56. Thrust Vector Control

The ECS was on at all times in the study; it received the same commands as the TVC system. Perhaps more care should have been taken to prevent TVC and ECS conflict, but the primary concern for this investigation was the TVC system. There was reluctance to modify the ECS subroutine because another analyst was simultaneously using the simulation.

Time histories of ACPS propellant consumption were not recorded in these studies, but the total, by axis, was available at the end of each run. Further study is needed to assure ECS/TVC harmony and to determine ACPS propellant consumption versus time. This is of particular concern during TVC single-engine operation when roll must be controlled by the ACPS and aerodynamic controls. The study concentrated on getting a workable TVC system, but was time constrained to the high-altitude region.

The first tests were aimed at defining the TVC system. The process leading to the Figure 56 block diagram is illustrated in Figures 57, 58 and 59, where α and ϕ_w commands were used to test the TVC system. Figures 61 through 63 show the various problems encountered and the solutions when attempting to fly the North American trajectory. Figures 64 and 65 show successful flights along the NR trajectory.

Figure 57 shows TVC performance when commanding an α change from 11 to 50 degrees; there are five recordings marked A through E. Figure 57A has the gains of Figure 43, with a 2-deg/sec pitch rate command limit. Figure 57B attempts to speed up the maneuver with a 5-deg/sec command limit. This triggered an actuator rate limit cycle, which is eliminated in Figure 57C with an unrealistically high limit of 50 deg/sec. The α gain was cut from 3.0 to 1.5 in Figure 57D to improve the damping, with the rate limit again at 2 deg/sec. These pitch gains and limits were used for subsequent tests.

Figures 58 and 59 show TVC roll response at $\alpha = 11$ deg and 50 deg, respectively. In Figure 58A the roll rate command limit and the sideslip gain are too high, leading to the long roll oscillation and the yaw actuator rate limit cycle. The system is finally well behaved (except for sideslip) in Figure 58F, with a roll rate command limit of 5 deg/sec and sideslip gain reduced from four to two. Figure 59 (at 50, degrees α) leads to a reduction in roll attitude gain, from 2.5 to 1.25.

The tests shown in Figures 57 through 59 resulted in:

- Halving the α , ϕ , and β gains selected in Section IV.
- Setting pitch rate and roll rate command limits at values comparable to those in the ECS shown in Figure 69.

The reduced gains are the result of the limit cycles encountered with higher gains and actuator rate limits of 10 deg/sec. Performance with this limit appears adequate.

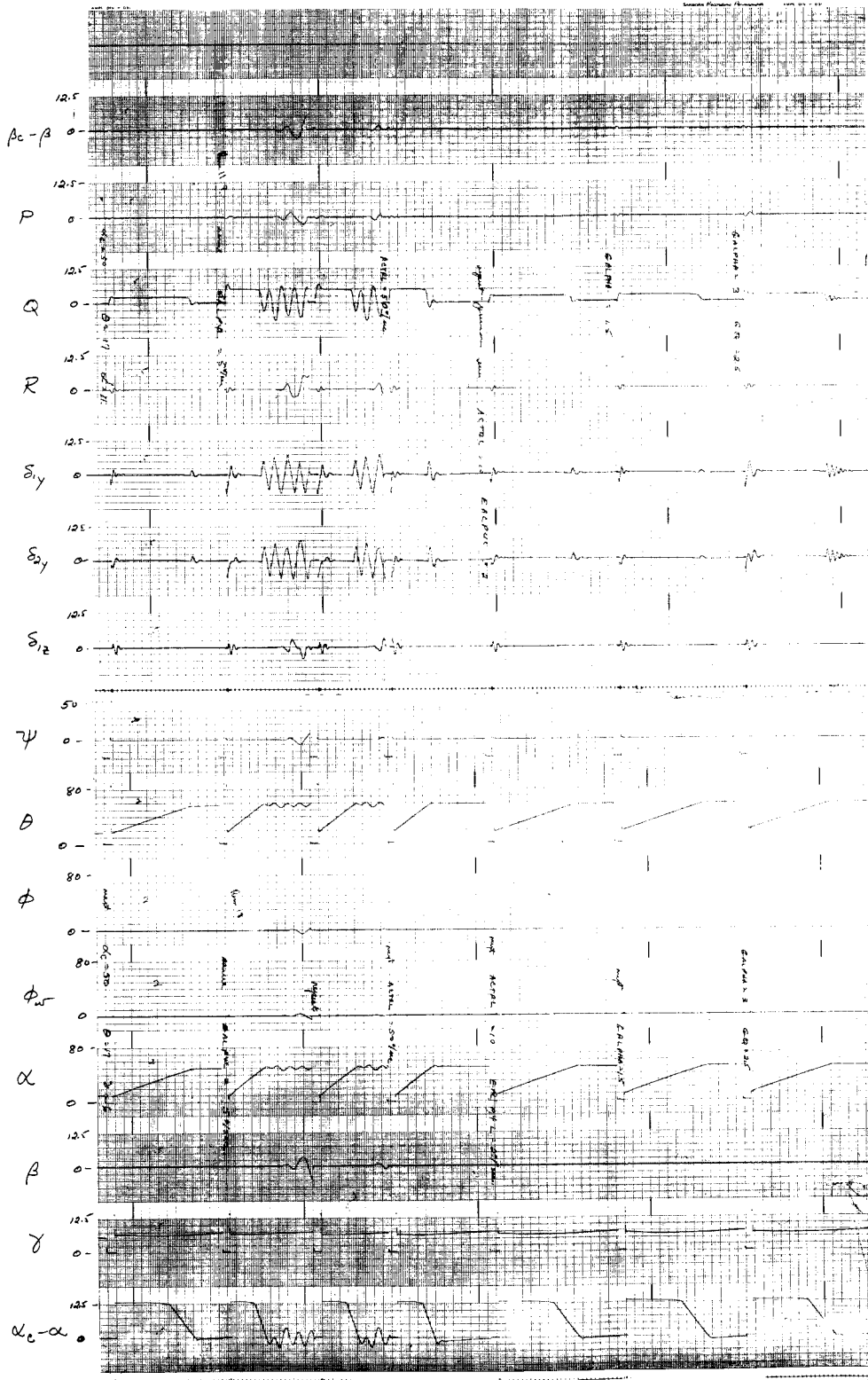


Figure 57. TVC - 11° to 50° α Commands at 226957 feet, Velocity 10308 ft/sec

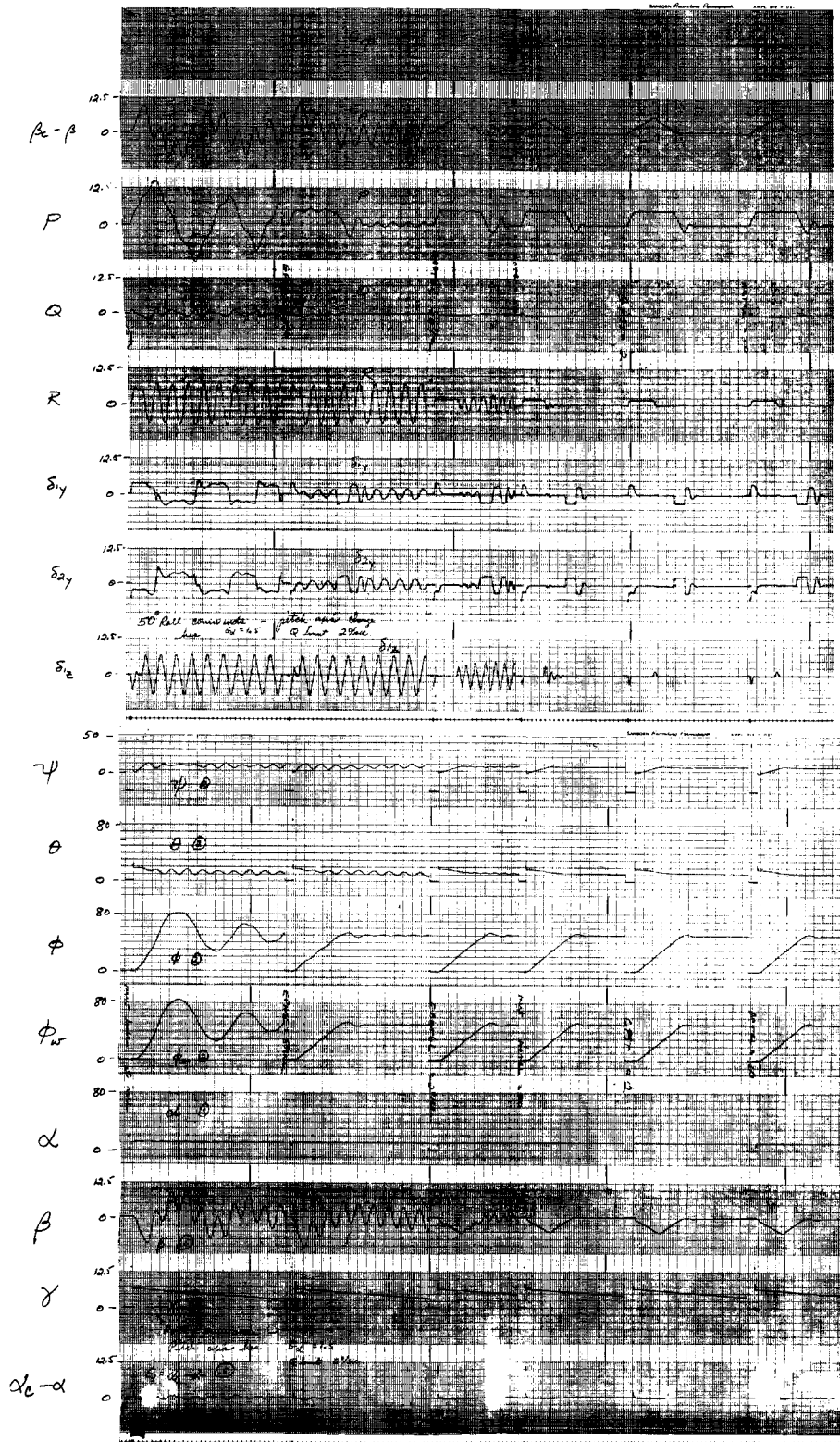


Figure 58. TVC - 50° Roll Commands, ($\alpha=11^\circ$) at 226957 feet

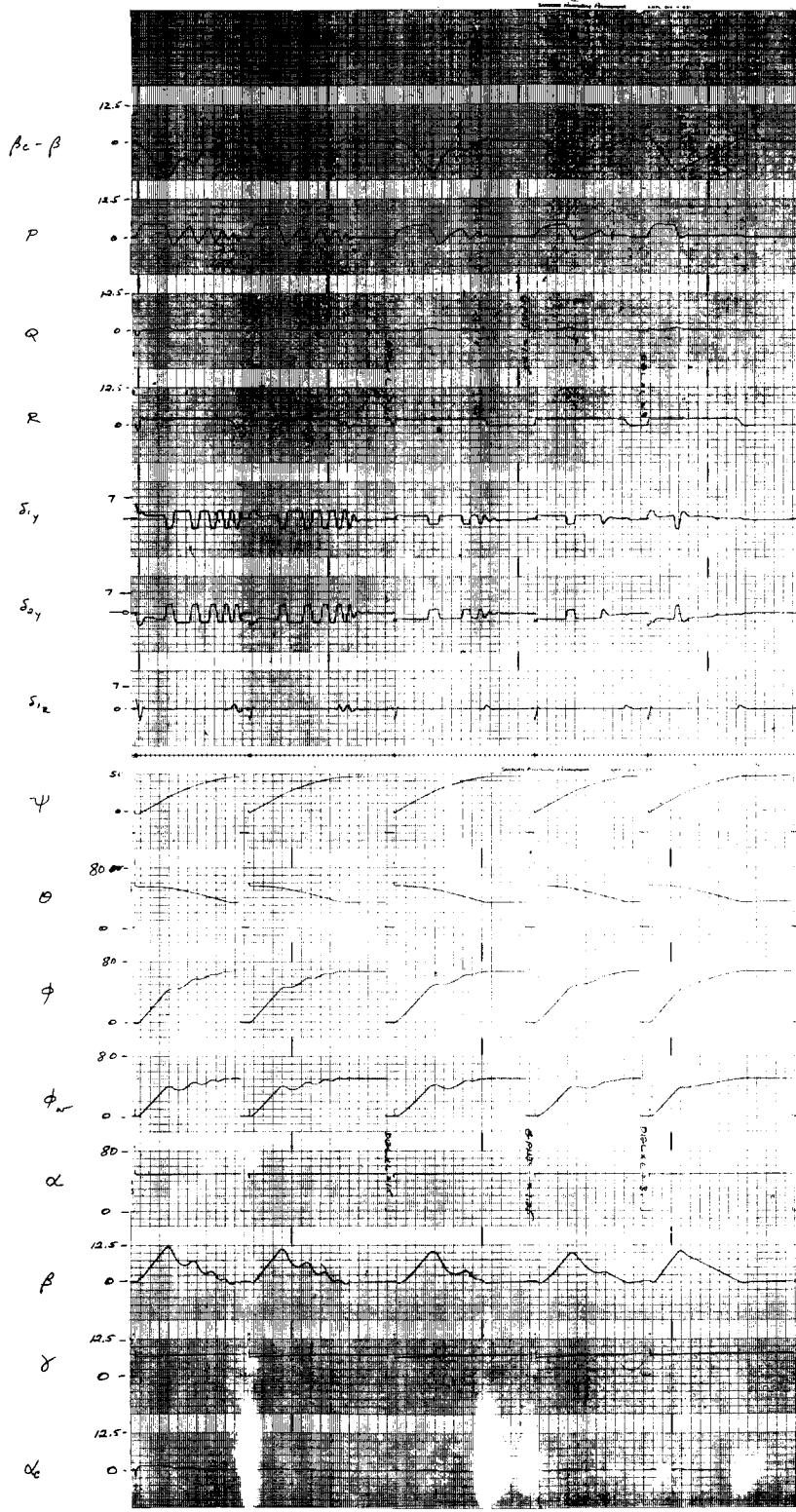


Figure 59. TVC - 50° Roll Commands ($\alpha=50^\circ$) at 226957 feet

Figures 61 through 63 are attempts to fly the North American trajectory. They all begin with the initial conditions for the NR abort; altitude 226,957 feet, velocity 10,308 ft/sec, and flight path angle +6 deg. The steering commands for this abort are shown in Figure 60. Both engines operate for the first 142 seconds. At this time the right (No. 2) engine was shutdown, and the left engine increased to 100 percent, a power level of 1.0, until about 332 sec when the propellant is gone. The same thrust could have been obtained with 50 percent of both engines, but the desire was to investigate the single-engine control problem which is real, due either to failure, or to the need for lower thrust on some other aborts. The initial bank angle is -180 deg, with -16 deg commanded at 20 sec, building to 72 deg at 332 sec to maintain a constant flight path rate, followed by a 30-deg bank turn to 715 sec. The initial angle of attack is 50 deg, followed by a decrease to 30 deg and finally transition at 715 sec.

Figure 61 shows the first problem encountered in attempting to fly this abort. Figure 61A shows divergence at 240 sec during single-engine TVC. Sequential burn of main and on-orbit propellants was used. This results in an aerodynamically uncontrollable situation at TVC shutdown. Figure 61B and 61C use parallel burn of main and on-orbit propellants, a more stable aerodynamic condition. This postpones the divergence until 270 seconds. The problem is insufficient gimbals authority. Figure 61D uses ample gimbals authority. It produces stable TVC to cutoff at 332 sec. This yaw gimbals authority problem was subsequently solved by modifying the simulation to give unsymmetric gimbals limits:

Left yaw	+10 deg,	- 4 deg
Right yaw	+ 4 deg,	-10 deg

This is equivalent to the 7-deg limits currently available, with the null points turned 3 deg toward the c. g. This is shown in Figure 41.

Figures 62 and 63A diverge immediately following TVC operation due to the 5 degree sideslip initial condition; Figure 62 has parallel burn of main and orbit maneuver propellants, but 63A has parallel burn. Even this resulted in unstable yaw operation. The yaw ACPS lacks the control power to stabilize even a mild static instability with 5 degrees initial sideslip. It follows that while sideslip may be needed during single engine TVC, a decrab maneuver must be made prior to TVC shutdown.

Figure 63B, following successful TVC operation, subsequently diverges at 715 sec when the ECS is subjected to simultaneous pitch-down and wings-level commands. This problem was circumvented, in subsequent recordings, by modifying the angle-of-attack program to that shown in Figure 60. Pitch down begins 15 sec before the bank command. Pitch down is virtually completed before the bank command occurs. This is not a good solution to this problem, since it requires some decision and priority logic in the guidance system. New data were received after study completion. The new aileron yawing moment derivative N_{δ_a} is only 1/4 of the old value. Section VI notes the benefits of reduced N_{δ_a} : less tendency to lose control and smaller ACPS fuel consumption. This data change may allow simultaneous pitch and

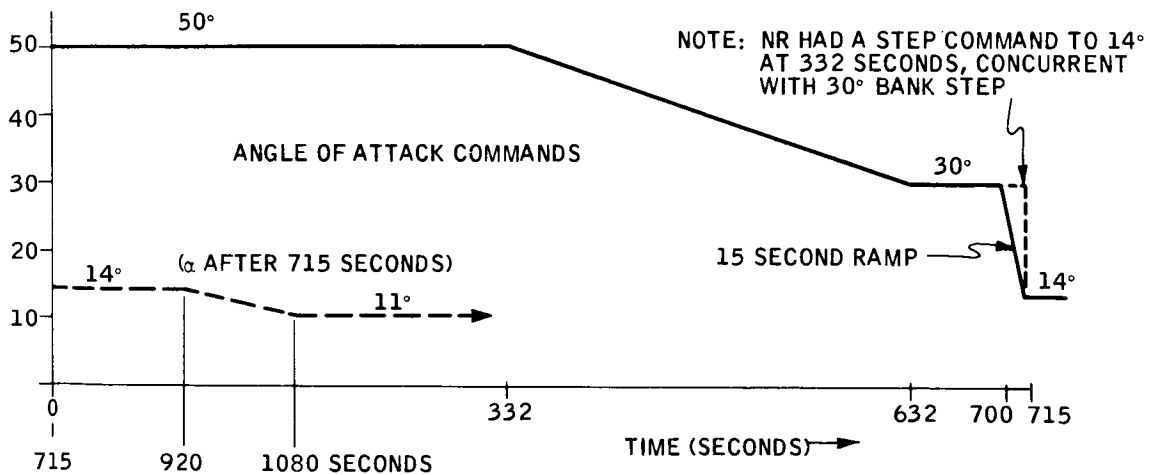
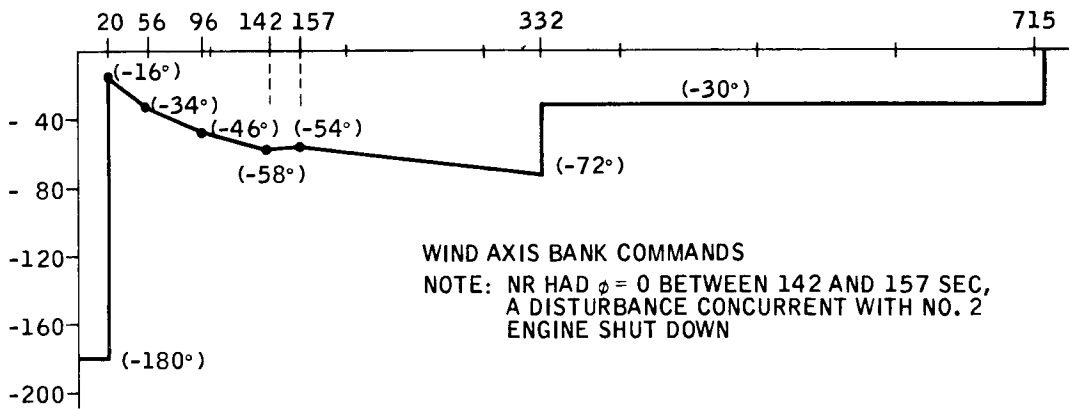
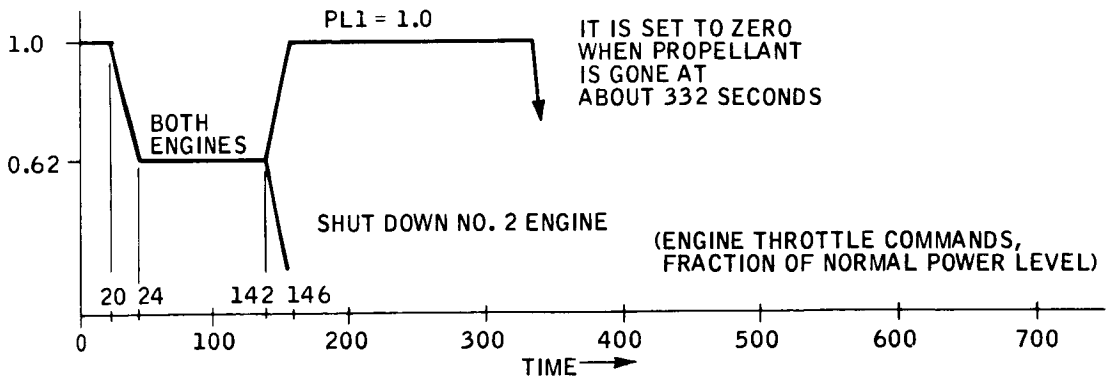


Figure 60. Programmed Commands for Abort at 226957 feet, Velocity = 10308 ft/sec, and $\gamma = +6^\circ$

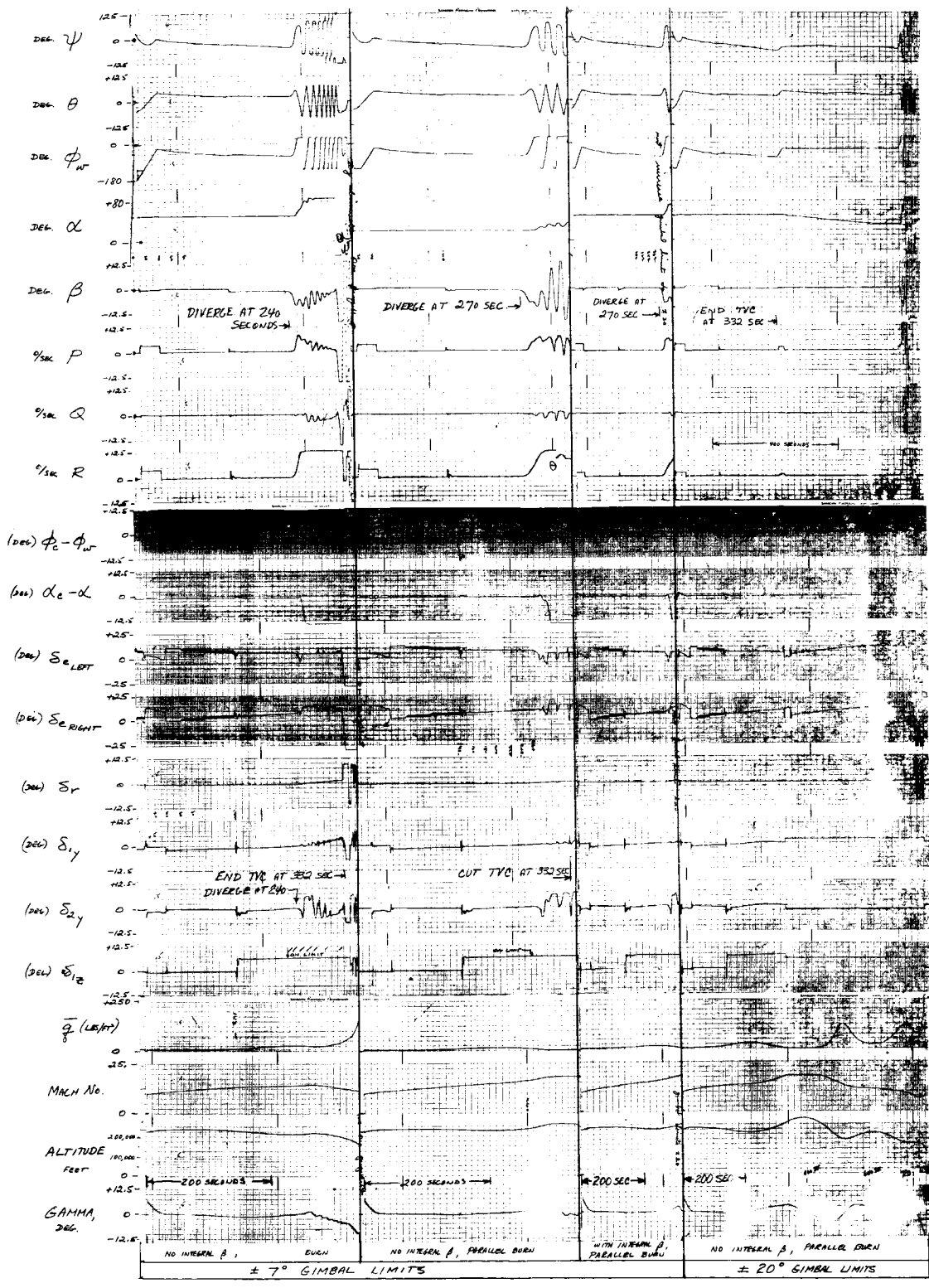


Figure 61. +7° Left Gimbal is not Quite Enough with Right Engine Ou

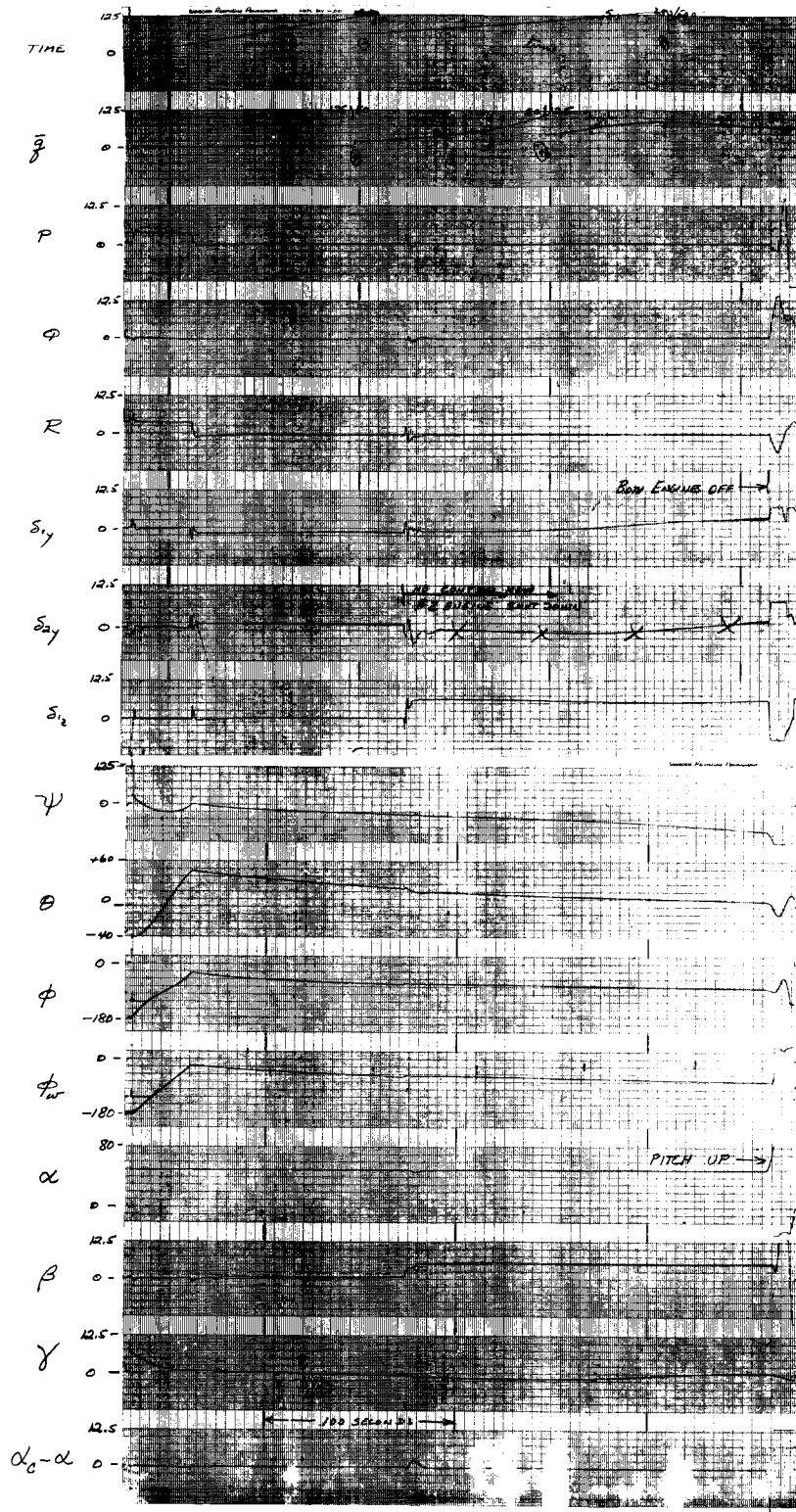


Figure 62. Abort Near Stage - $\beta_c = +5^\circ$ with #2 Engine Out, Normal C.G. Travel

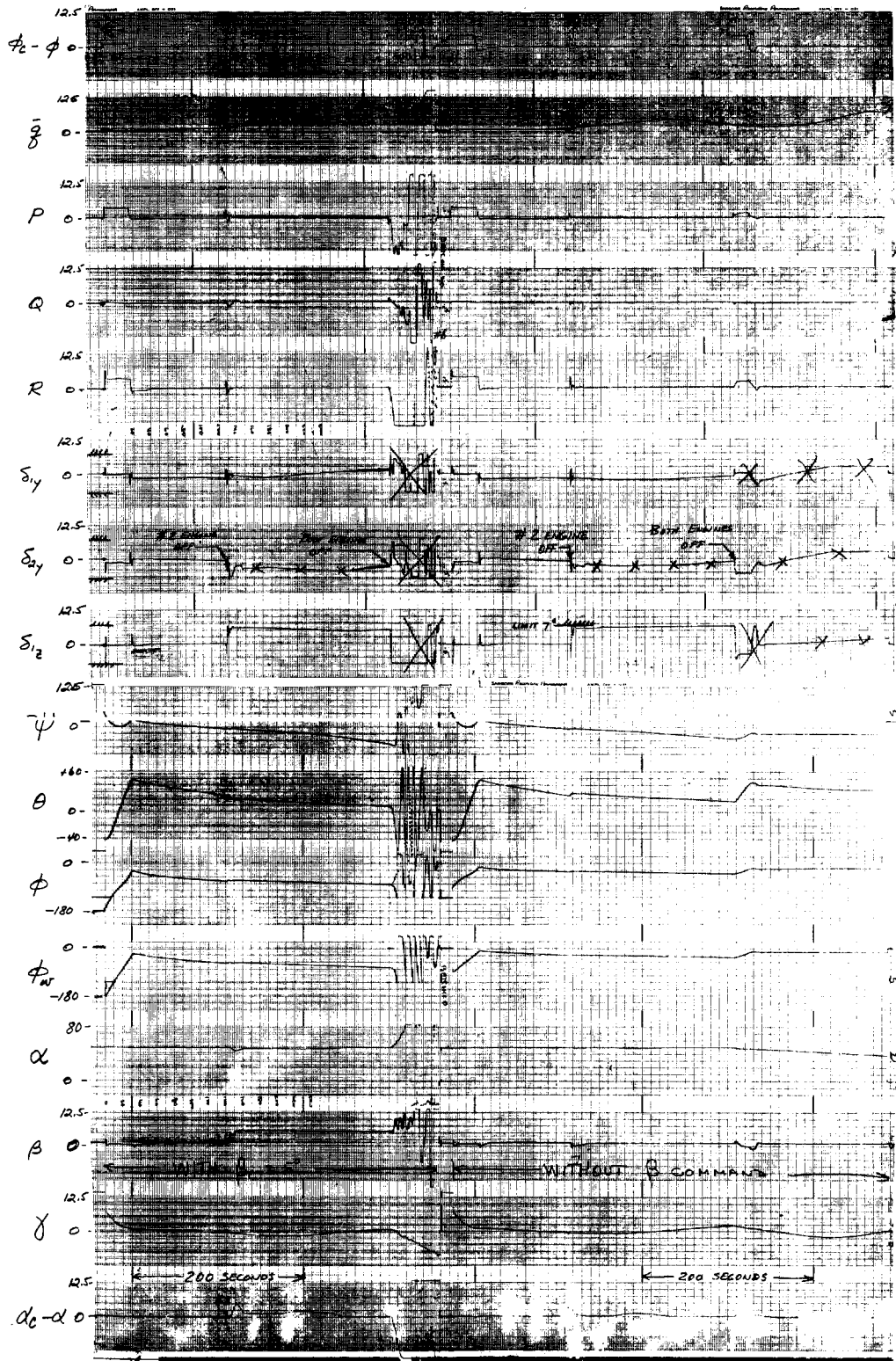


Figure 63. Abort Near Stage with X_{CG} at Burnout and Entry at 1422 inches from Nose (=Station 1633)

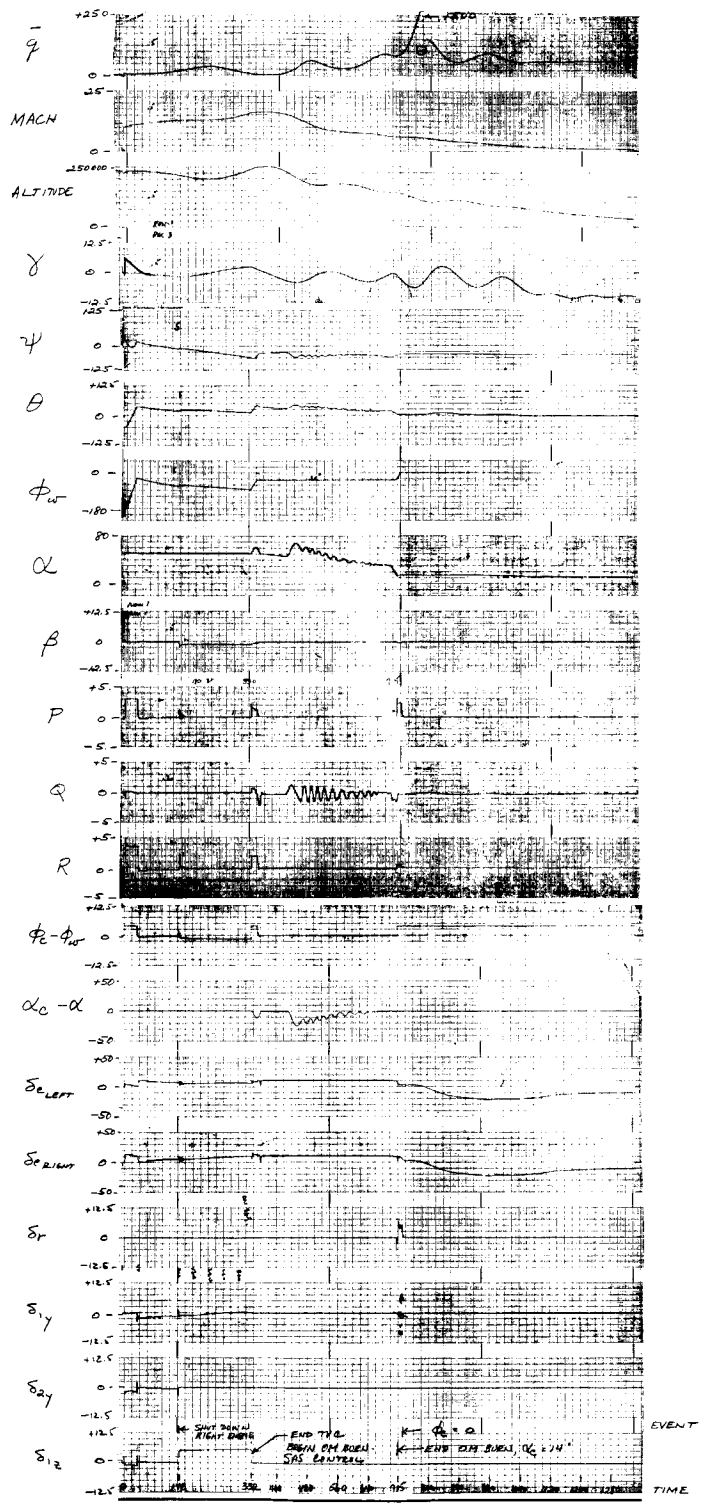


Figure 64. Abort at 225000 feet. Sequential Burn of Main and Orbit Maneuver Propellant

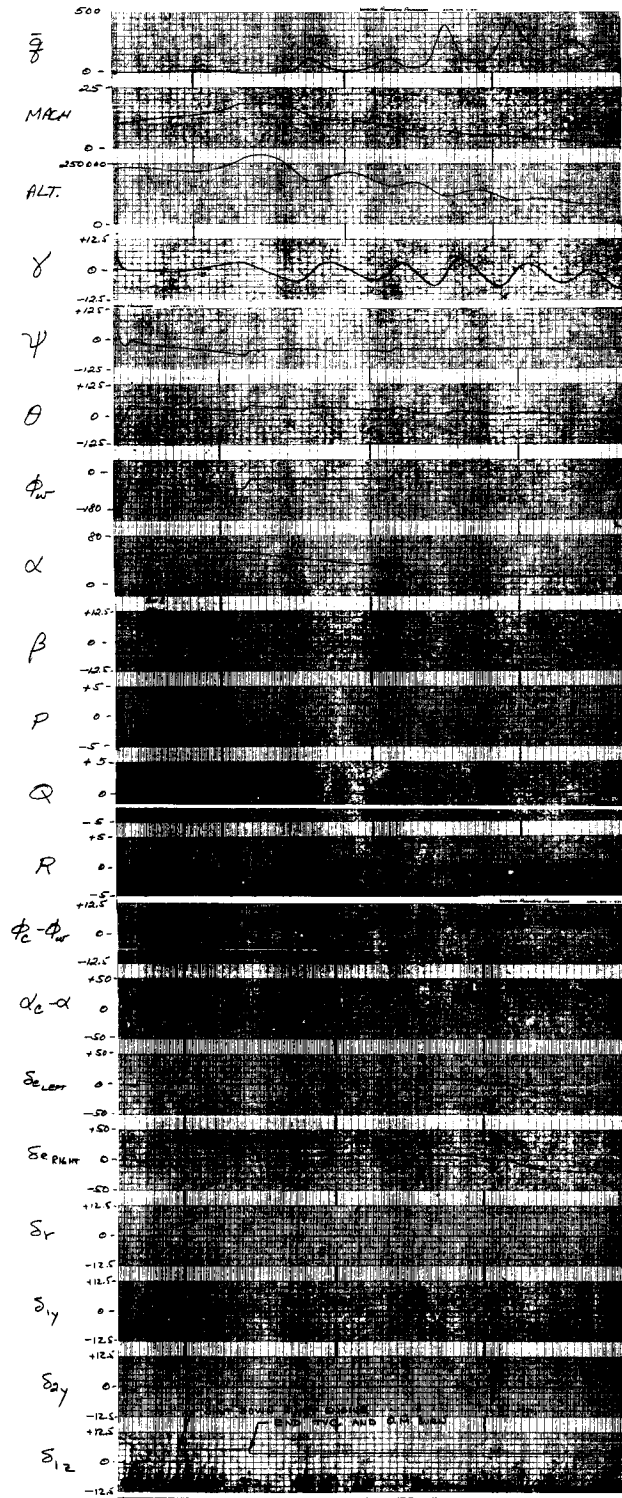


Figure 65. Abort at 225000 feet with Parallel Burn of Main and Orbit Maneuver Engines

roll commands. If not, the ECS needs further study. A design is required which tolerates simultaneous pitch and roll commands.

Figure 64 and 65 are successful time histories covering over 1280 sec of this high-altitude abort. Figure 64 has sequential burn of main and orbit maneuver propellants. Divergence at TVC shutdown was expected but did not occur.

Figure 66 shows the DWO with cg aft to be aerodynamically uncontrollable above 14 deg angle of attack during hypersonic flight. Examination of Figure 64 shows that the dynamic pressure is less than 10 psf at TVC cutoff. It reaches 50 psf 120 sec later, when the cg has moved forward from its aft position. It is noted that the elevons δ_{eLEFT} and δ_{eRIGHT} are hard down (positive) the entire time during the period where a slow pitch oscillation persists. Conclusion: the ECS had just gotten by the aerodynamically uncontrollable region using the ACPS. Higher dynamic pressures would have caused pitch up. The on-orbit propellant should be burned prior to main propellant depletion; it should not be relied on for sustained thrust after TVC shutdown, at least in hypersonic flight.

Figure 65 is this same abort trajectory with parallel burn of main and on-orbit propellant. TVC and ECS operation both appear satisfactory. Figure 44 plots altitude versus velocity from Figures 64, 65, and 51 (which is NR's data). Closer agreement was expected. Figures 64 and 65 were then examined again. The flight path angle breaks up sharply at 142 sec (in contrast with NR's trajectory) when the right engine shuts down. It appears that the left engine trim of about 7 deg toward the cg (see δ_{l_z} at bottom of Figure 64) combined with 55 deg left bank, produces about 48,000 lb of lift. This would not have happened with both engines operating. Further tests are warranted to see if better agreement with the point mass trajectory can be obtained. Figure 51 also shows that these trajectories don't penetrate the boundary. TVC and ECS performance needs to be examined in the boundaries of the flight envelope.

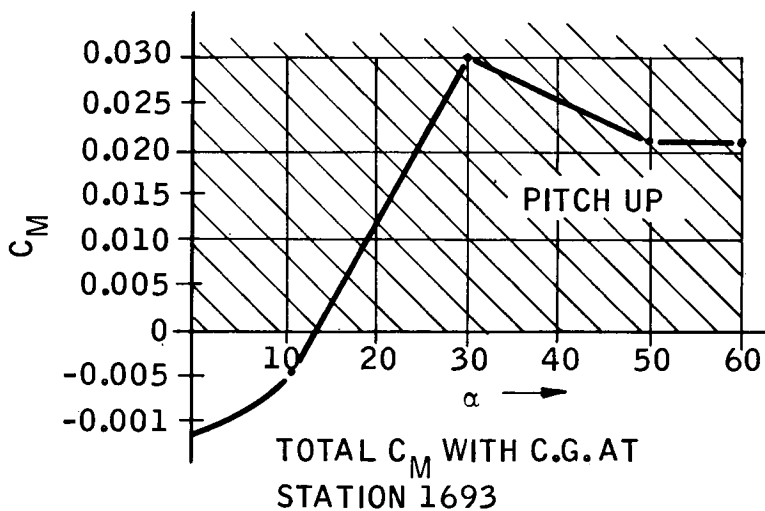


Figure 66. Effect of AFT CG (Due to on Orbit Propellant) on Aerodynamic Trim Capability of 134-C, D, at Mach 10

Figures 64 and 65 both show a differential elevon ring at 142 sec when the TVC right engine is shutdown. Here the ACPS and aerodynamic controls must replace TVC in the roll axis. This ring is of concern, but should be readily eliminated in a detailed design study.

These same figures (near the bottom) also show the ACPS on-times. Totals are 730 sec (about 5800 pounds) in the sequential burn, and 1146 sec (8400 pounds) for the recommended parallel burn. These numbers were obtained from the computer final dump. Both exceed the current 5000 lb budget. Figure 65 consumption was 1020 sec in yaw, higher than in Figure 64. This is believed due to the higher dynamic pressures. This emphasizes the need for TVC/SAS harmonization studies. It is recalled that the ECS operated all the time TVC was on. It is not needed at all with both engines operating, and only the roll ECS is needed for single-engine TVC. These modifications to the ECS should produce a significant reduction in ACPS propellant consumed.

A few additional initial conditions for ECS operation are examined in Figures 67 and 68. Figures 67A through F employ the α command sequence given in Table G3. This precipitates an elevator rate instability at 115,000 feet. This α sequence appeared to be rather demanding, so α holds at 11 deg were tried in Figure 67F through I and also Figures 68A and B. Figures 67G and H show pitch up with cg aft at about Mach 14, $\bar{q} = 50$ psf. Figures 67I and 68A have the cg forward; the ECS controls through peak \bar{q} 's of 600 and 500 psf, respectively.

Figure 68C is a last hour attempt to fly TVC straight up from a low altitude. The flight path angle was 87 degrees with zero α command. The initial conditions were set to produce a reasonably constant flight path. This trajectory starts at about Mach 1.6 at 5000 feet with \bar{q} about 3000 psf. While unrealistic, the resulting trajectory points to an area for further investigation. The aerodynamic controls went into a rate limit cycle. This shows the need for aero and TVC blending and gain considerations at high \bar{q} .

CONCLUSIONS

The tests at high altitude have demonstrate a successful DWO TVC system similar in design to the DWO's entry aerodynamic control. Both are linear, both have scheduled gains, both are gain limited by control actuator rate limits; they have similar maneuver rate command limits. The TVC gimbal position limits of ± 7 deg are adequate with a 3 deg cant. The gimbal rate limits of 10 deg/sec restrict the gains, but acceptable performance is obtained. A single test at high \bar{q} reveals poor control due to aerodynamic control surface rate limiting. While considerable design effort is still needed, it appears that linear TVC and ECS with scheduled gains will prove acceptable throughout the DWO flight regime.

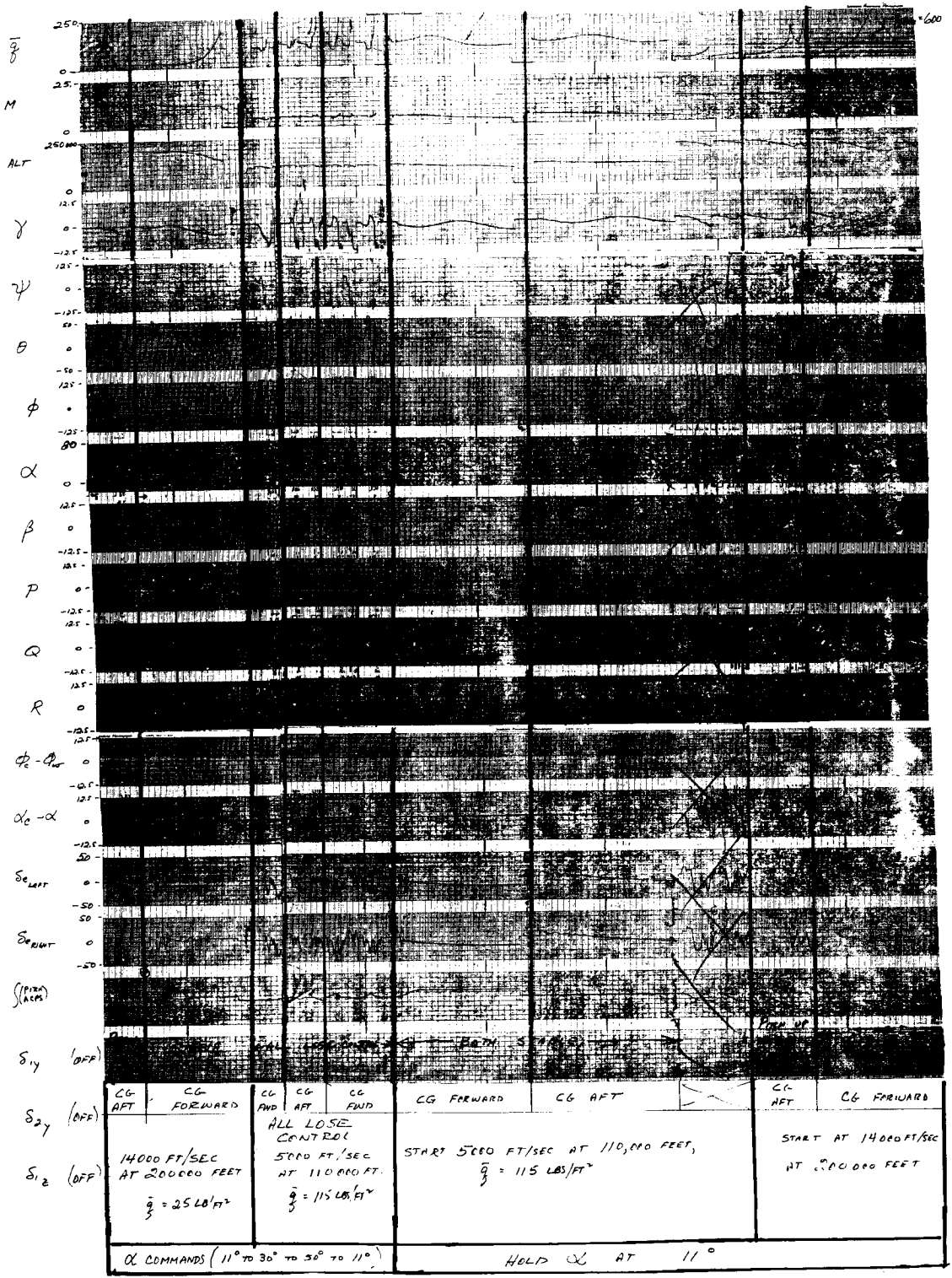


Figure 67. α Control with SAS - No TVC

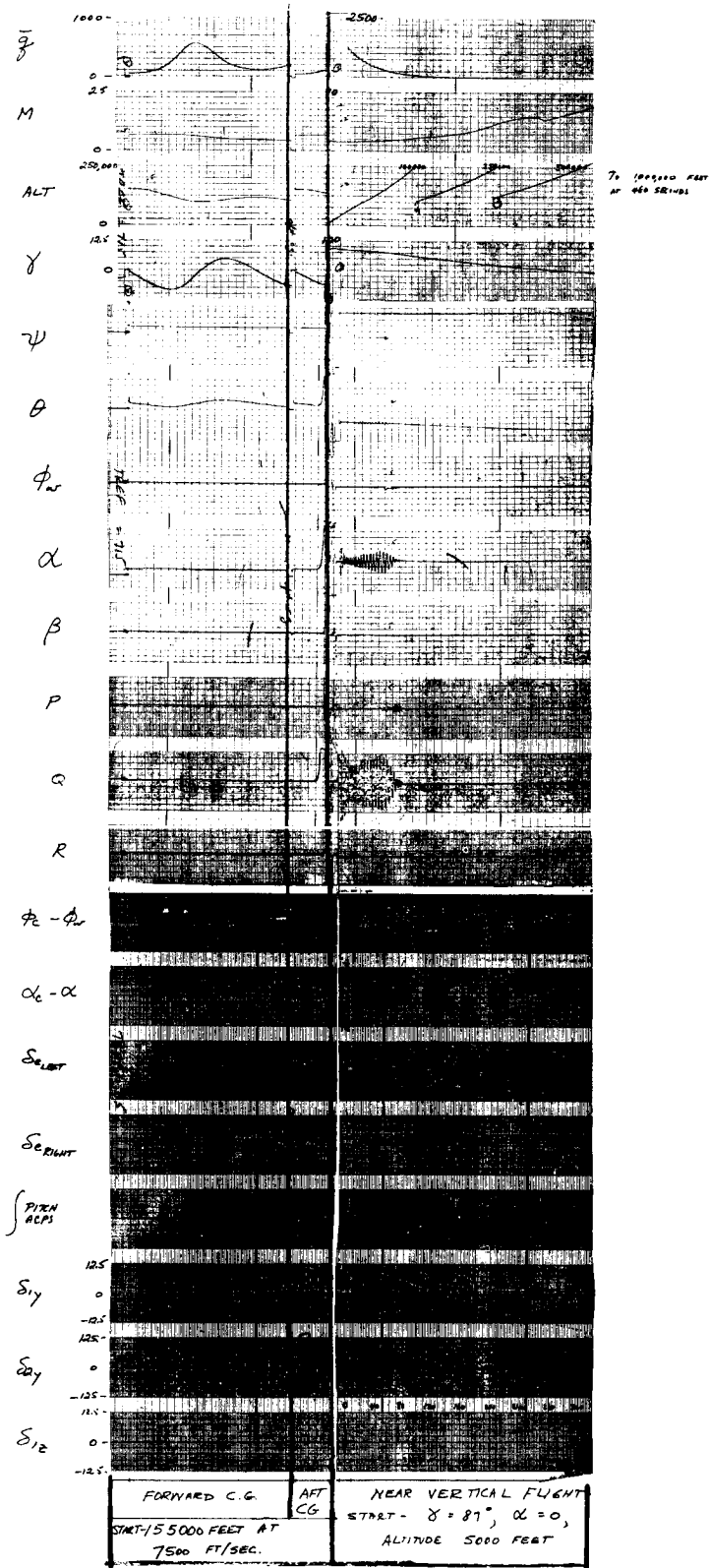


Figure 68. SAS - TVC Control

SECTION VI

DELTA WING ORBITER CONTROLS FOR REENTRY

SUMMARY

This section relies heavily on the DWO reentry studies reported in ref. 1. The results and conclusions of that reference are modified to include the high-altitude abort studies reported in Section V. Described is the ECS block diagrammed in Figure 69, a control for entry covering Mach 20 to 2. Gains and limits are changed at Mach 7. Also discussed are ACPS requirements, fuel usage, and the effects of vehicle parameter variations. Great care must be taken in the 134D, to avoid roll maneuvers which the yaw ACPS cannot stabilize. Reduced values of $C_{n\beta}$ and $C_{n\delta_a}$ would improve the roll capability. Aero data received after completion of this study include a much smaller $C_{n\delta_a}$ which should be beneficial.

Control surface rate and displacement requirements are also discussed. The elevon rate limits are never changed from ± 7.5 deg/sec. The study concerns position limits; more precisely, the differential elevon limits defined as aileron command limits. Ten-degree limits were found to be adequate for normal ECS operation in the Mach 20 to 7 range, while the adverse effects of a large $C_{n\delta_a}$ required a 2.5-degree command limit in the Mach 7 to 2 range. Later vehicle data provided a reduced $C_{n\delta_a}$ which should permit a higher limit. The 10 degree limit may not be adequate for single engine TVC; it must then be reduced at engine shutdown.

Methods for blending and gain adjustment of TVC, aerodynamic, and ACPS controls are discussed. There were no blending methods tested. The normal ECS in the 134D used the elevons for roll and pitch control and the ACPS for yaw at all times. Air data, such as Mach number or dynamic pressure, is suggested as a source to vary aerodynamic surface gains and ACPS deadbands. Satisfactory roll pitch control might also be obtained by using the elevons for trim and the ACPS for perturbation control. Two-engine TVC requires no ECS control, while single-engine TVC can control pitch and yaw, but needs the ECS for roll control.

ENTRY CONTROL SYSTEM (ECS)

Ref. 1 included reentry control studies of two North American delta wing orbiters, the 134C and the 134D. The bulk of this section is taken from this reference. The 134C has tip fins similar to those on the HL-10. The low-speed stability is poor, and the rudders must be in a nonstreamlined position to be effective, creating large hinge moments with consequent large power

requirements. The 134D has a single fin, improving low-speed stability and greatly reducing rudder power consumption. However, the rudder is ineffective at high angles of attack and high Mach numbers. The ACPS is therefore used for yaw control above Mach 2. The 134D was used in the abort studies reported in Section V. Figure 69 from ref. 1, block diagrams the 134D ECS in the Mach 20 to 2 range. Some gains and limits are switched at Mach 7. This control system was used concurrently with TVC in the Section V abort study; both received the same α and ϕ commands. Historically, Figure 69 combines two control systems originally defined by North American, one for Mach 20-7, and one for Mach 7-2. Honeywell's primary emphasis in the ref. 1 Phase B study was to determine effects of vehicle configuration on aerodynamic control and ACPS requirements. Little effort was directed toward control system optimization.

ACPS REQUIREMENTS AND FUEL USAGE

Owing to the ineffective rudder on the 134D orbiter, the yaw axis ACPS must be used during the entire entry trajectory (Mach 20 to Mach 2.0). Furthermore, because of the destabilizing effects of $C_{n\beta}$ in most of this region and the adverse yaw due to aileron characteristics, a small deadband is required. For the nominal trajectory, it appears that a deadband of ± 0.25 deg can be used. However, in order to maintain control during possible additional roll maneuvers in the Mach 7 to 2 range, a deadband of ± 0.1 deg is required.

Even with a ± 0.1 deg yaw ACPS deadband, control can be lost during rapid rolls. A brief analysis indicates that at Mach 6 and a dynamic pressure of 200 psf, the body axis yawing moment due to sideslip is about -140,000 ft-lb/deg. Since the baseline ACPS torque is 160,000 ft-lb, sideslip must be maintained within ± 1.15 deg to avoid loss of control. The problem is compounded by the adverse yaw due to aileron characteristics, which at the same condition produce a yawing moment of about +14,500 ft-lb/deg aileron. This analysis agrees with computer results where even with a ± 2.5 -deg aileron limit, control was lost wherever the roll rate was sufficient to cause more than about 0.75-deg sideslip at this condition. This problem should be somewhat alleviated by using the new, lower yawing moment due to aileron, N_{δ_a} , received after completion of the ref. 1 study.

In addition to utilization of a small ACPS deadband, tighter yaw axis control could be achieved through use of the entire yaw ACPS capability; i. e., four jets for each direction of control for a total moment of 320,000 ft-lb. This would have an impact on the system safety, however, since fully fail-operational requirements could not be met.

Since the 134C orbiter has effective rudder control, utilization of the yaw ACPS in the Mach 7 to 2 region is unnecessary. Furthermore, very brief checks have indicated the rudder to be effective in most of the higher altitude

range. However, the rudder hinge moments are so large that the total energy requirements may be higher using the rudder than the yaw ACPS in the Mach 20 to 7 region.

Both the 134C and 134D orbiters have sufficient aerodynamic control in pitch and roll that use of the ACPS in these axes is not required for following the baseline trajectory. However, because of hinge moments and resulting hydraulic power requirements, it may be advantageous, especially in pitch, to use the ACPS for damping and control inputs, and aerodynamic control only for long term trim.

Maneuvers in addition to those included in the baseline trajectory will result in higher ACPS fuel requirements. Roll reversals from +45 deg to -45 deg (or vice versa) utilize approximately 80 lb of ACPS fuel, both in the vicinity of Mach 6 and Mach 3.

EFFECT OF VEHICLE PARAMETER VARIATIONS

A brief parameter variation study was made to determine the effect of changes in selected aerodynamic coefficients on 134D ACPS fuel consumption. The coefficients $C_{n\beta}$, $C_{l\beta}$ and $C_{n\delta_a}$ were multiplied by constant factors between ± 4.0 . For the Mach 20 to 7 runs, only four variations were considered because of the long computer running times required. Eleven variations were considered in the Mach 7 to 2 range. Results are summarized in Table 18 and indicate that making $C_{n\beta}$ stable (changing the sign) is the single most effective variation for reducing fuel consumption in the Mach 20 to 7 range. In the Mach 7 to 2 range, approximately equally good reductions could be obtained by changing the sign of either $C_{n\beta}$ or $C_{n\delta_a}$. Similar results were observed in the fuel required during roll maneuvers, as discussed below.

CONTROL SURFACE DISPLACEMENT AND RATE REQUIREMENTS

For all studies considered in ref. 1, the elevon rate limits were assumed to be +7.5 deg/sec, a value considered easily obtainable by North American. In the Mach 20 to 7 entry segment, the aileron command limits were set at +10 deg. With these limits, satisfactory operation was obtained throughout the Mach 20 to 7 range. It should be noted, though, that owing to the high angle of attack (53.5 deg) at the initial roll maneuver, the yaw ACPS provides a significant part of the rolling moment.

The abort study, Section V, had examined single-engine TVC which requires the ECS to stabilize roll. There Figure 66 shows TVC operation under these conditions, where a 5-deg sideslip was obtained with this 10-deg limit on

Table 18. Effect of Aerodynamic Coefficients on Yaw
ACPS Fuel Consumption, 134D Delta-Wing
Orbiter in Normal Entry

	ACPS On Time (sec)	
	Mach 20 to 7	Mach 7 to 2
Nominal	141	31
1.5 x $C_{n\beta}$	---	31
2.0 x $C_{n\beta}$	---	30
0 x $C_{n\beta}$	---	34
-1 x $C_{n\beta}$	117	30
-4 x $C_{n\beta}$	---	6.2
2 x $C_{l\beta}$	136	29
4 x $C_{l\beta}$	---	59
0 x $C_{l\beta}$	---	33
1.5 x $C_{n\delta_a}$	---	32
0.25 x $C_{n\delta_a}$	134	
0 x $C_{n\delta_a}$	---	26
-1 x $C_{n\delta_a}$	*	5.6

* Sustained oscillations -- $\pm 1^\circ \beta$

aileron command. The roll ACPS was probably operating here to help control roll; unfortunately it was not monitored. The 10-deg. aileron limit may have to increase to accommodate TVC engine-out. If excessive for the entry control system, the limit should be reduced at TVC shutdown.

Note in Fig. 69, that below Mach 7 the aileron command limit is ± 2.5 degrees; there is no limit on the roll rate command. This limit was established during ± 45 deg to -45 deg roll maneuvers. If roll rate was limited, as in the Mach 7 to 20 range, somewhat greater aileron displacements could be used, although the value used is adequate for control. During parameter variation studies, it was apparent that for the 134D, aileron command limits of ± 5 deg could be used only if the roll rate commands were limited at 2.5 to 3.0 deg/sec. Again, single-engine TVC will very likely require increased aileron command limits, which can be reduced at TVC shutdown.

The effects of selected parameter variations on the 134D rolling performance are summarized in Tables 19 and 20 for maneuvers at Mach 6 and Mach 3, respectively. Parameter changes are evaluated in terms of peak sideslip, time to accomplish the maneuver, ACPS fuel required, and aileron rates and displacements. Peak sideslip values are listed for the initial roll from nominal value ($+15$ deg at Mach 6, 0 deg at Mach 3) to -45 deg ($+45$ deg at Mach 3) and for the subsequent 90 deg roll maneuver. Note that for some cases, the vehicle was unstable when the initial roll occurred at Mach 6.75, but was stable at Mach 6.5. This appears to be explainable by the fact that dynamic pressure is about 15 percent lower at Mach 6.5 than at 6.75, permitting ACPS control of slightly higher sideslip values. For convenience in reducing the data, ± 40 -deg roll angles were selected as end points in measuring the time to roll. In all cases, the aileron deflection reaches the 2.5-deg command limit, but the time it sits at the value changes somewhat with the parameter variations. The peak aileron rates also vary somewhat. Generally, the peak rate occurs when initiating the 90 -deg roll maneuver, although in some cases as indicated, the peak rate occurs when the aileron comes off the displacement limit.

The effects of parameter variations on rolling performance are consistent with the effects on ACPS fuel consumption. That is, reducing the value or changing the sign of $C_{n\delta_a}$ and $C_{n\beta}$ is beneficial, whereas increasing their magnitudes while retaining nominal signs is detrimental. The nominal value of $C_{l\beta}$ appears to be about optimum, although up to a 100 percent increase in magnitude would be tolerable.

The DWO entry study results have indicated that large surface rates are not required for normal entry control, or (in Section V) for high-altitude aborts. Elevon actuator rate limits of ± 7.5 deg/sec proved to be completely satisfactory in both the pitch and roll axes. In the pitch axis, the nominal elevator command limits of ± 10 and -40 deg are satisfactory, and during the course of a normal entry nearly this entire range is required for maintaining

Table 19. Effect of Aerodynamic Coefficient Variations on Roll Maneuvers at Mach 6, 134D Orbiter

Parameter Change	Peak Beta		Time to Roll -40 to +40 (sec)	ACPS on Time (sec)	Aileron Deflection		Peak Aileron Rate (deg/sec)
	1 (deg)	2 (deg)			Peak (deg)	Duration (sec)	
Nominal	+0.3	-0.8	14	30	2.5	7	-10
1.0 x $C_{n\beta}$ *	+0.4	-0.3	14	31	2.5	7	-10
2.0 x $C_{n\beta}$	Divergent						
0.5 x $C_{n\beta}$	+0.3	-0.4	14	29	2.5	7	-10.5
0 x $C_{n\beta}$	+0.22	-0.3	14	27	2.5	7	- 8.5
-0.5 x $C_{n\beta}$	+0.23	-0.22	14	26	2.5	7	- 9.0
-1.0 x $C_{n\beta}$	+0.2	-0.2	14	23	2.5	7	-10.5
-2.0 x $C_{n\beta}$	+0.2	-0.14	14	21	2.5	7	- 9.0
-4.0 x $C_{n\beta}$	+0.12	-0.14	14	17	2.5	7	- 9.5
1.5 x $C_{l\beta}$	+0.3	-0.3	14	31	2.5	7	- 9.5
2.0 x $C_{l\beta}$	+0.32	-0.2	15	32	2.5	8	-10
4.0 x $C_{l\beta}$	+0.2	-0.2	16	41	2.5	11	- 7.5
8.0 x $C_{l\beta}$	Statically Unstable						
0 x $C_{l\beta}$ *	+0.3	-0.3	14	30	2.5	6	- 9.5
1.5 x $C_{n\delta_a}$	Divergent						
0.5 x $C_{n\delta_a}$	0.12	-0.20	14	24	2.5	7	- 9.5
0 x $C_{n\delta_a}$	0.05	-0.12	14	18	2.5	7.5	-10
-0.5 x $C_{n\delta_a}$	< 0.1	< 0.1	13	12	2.5	8	-11
-1.0 x $C_{n\delta_a}$	< 0.1	< 0.1	13	5.6	2.5	8	-10.5
-2.0 x $C_{n\delta_a}$	< 0.1	< 0.1	12	15	2.5	8	- 9.5

* Divergent for roll sequence initiated at Mach 6.75; values shown for sequence starting at Mach 6.5

Peak Betas: 1 Value when rolling from +15° to -45°

2 Value when rolling from -45° to +45°

Table 20. Effect of Aerodynamic Coefficient Variations on Roll Maneuvers at Mach 3, 134D Orbiter

Parameter Change	Peak Beta		Time to Roll +40 to -40 (sec)	ACPS on Time (sec)	Aileron Deflection		Peak Aileron Rate (deg/sec)	
	1 (deg)	2 (deg)			Peak (deg)	Duration (sec)		
Nominal	+0.6	-0.6	15	23	2.5	8.0	9.0	
1.5x $C_{n\beta}$	+0.7	-0.65	15	24	2.5	8.0	9.0	
2.0x $C_{n\beta}$	+1.0	-0.65	15	26	2.5	8.0	9.0	
4.0x $C_{n\beta}$	Divergent							
0.5x $C_{n\beta}$	+0.55	-0.50	15	22	2.5	8.0	8.5	
0	+0.5	-0.45	15	22	2.5	8.0	10.0	
-0.5x $C_{n\beta}$	+0.35	-0.4	15	20	2.5	8.0	9.5	
-1.0x $C_{n\beta}$	+0.3	-0.3	15	20	2.5	7.5	9.5	
-2.0x $C_{n\beta}$	+0.3	-0.3	15	20	2.5	7.5	9.5	
-4.0x $C_{n\beta}$	+0.25	-0.25	15	18	2.5	7.5	10.0	
1.5x $C_{l\beta}$	+0.35	-0.3	15	22	2.5	8.5	8.5	
2 x $C_{l\beta}$	+0.15	-0.25	15	21	2.5	9.0	10.0	
4 x $C_{l\beta}$	<0.1	-0.2	17	24	2.5	12.0	12.0	
8 x $C_{l\beta}$	Very Poor Static Stability							
0.5x $C_{l\beta}$	+1.2	-1.0	15	26	2.5	7.0	9.0	
0 x $C_{l\beta}$	+1.35	-2.5	14	27	2.5	6.0	15 *	
-0.5x $C_{l\beta}$	+1.7	Oscillatory						
1.5x $C_{n\delta_a}$	+1.2	-0.55	16	30	2.5	10.0	10.0	
2 x $C_{n\delta_a}$	+1.7	-0.6	16	45	2.5	10.0	10.0	
3 x $C_{n\delta_a}$	Unstable							
0.5x $C_{n\delta_a}$	+0.1	-0.2	14	17	2.5	7.5	11.5	
0 x $C_{n\delta_a}$	<0.1	-0.2	15	13	2.5	7.5	11.5*	
-0.5x $C_{n\delta_a}$	<0.1	-0.15	15	10	2.5	8.0	11.5*	
-1.0x $C_{n\delta_a}$	<0.1	-0.15	15	8.8	2.5	8.0	11.5*	
-2.0x $C_{n\delta_a}$	-0.1	-0.1	15	8.5	2.5	8.0	11.5*	
-4.0x $C_{n\delta_a}$	Unstable							

* Indicates peak aileron near completion of maneuver

trim. However, no evaluation was made of maneuvering requirements except for the initial angle of attack change from 53.5 deg to 30 deg at 260,000 feet. Consequently, the possibility exists that it may be desirable to limit the short short-term elevator command capability about the trim point to avoid causing an unstable situation should pitch maneuvers be required.

In the roll axis, the problem appears to be one of too much, rather than too little aileron authority. This is particularly true of the 134D orbiter, since the absence of rudder control results in very tight limitations on sideslip to keep destabilizing aerodynamic torques within the 160,000 ft-lb ACPS authority. Consequently, roll maneuvers must be limited if vehicle control is to be maintained. Since $C_{n\beta}$ and $C_{n\delta_a}$ both produce destabilizing yaw torques, consideration must be given to roll rate and aileron displacement during roll maneuvers in the Mach 7 to 2 range. From the study results it appears that the initial aileron deflection is more destabilizing than the subsequent sideslip resulting from relatively high roll rates. Thus, limiting the aileron deflection to 2.5 deg in this region actually permits faster roll responses than can be obtained by allowing larger aileron deflections, e. g., 5 deg, with limits placed on the roll rate command. In the former case, with ± 2.5 deg aileron limits but no roll rate command limits, roll maneuvers are accomplished at average rates of 5 to 6 deg/sec, with peak rates of up to 12 deg/sec occurring. On the other hand, if aileron deflections of ± 5 deg are allowed, the roll rate command must be limited to the vicinity of 2.5 to 3.0 deg/sec with the result that about 30 sec are required for the 90-deg roll maneuvers. The new aero data provided reduced $C_{n\delta_a}$ which will improve the 134D maneuver capability.

A significant impact of these results is that it appears necessary to schedule the aileron command limits since the ± 2.5 -deg limits desirable in the Mach 7 to 2 range will not provide adequate control in other parts of the flight regime, e. g., aerodynamic cruise or landing, nor will it permit single-engine TVC operation, if some sideslip is required by guidance. This would require considerably more than 2.5-deg aileron.

METHOD FOR BLENDING TVC, AERO, AND ACPS CONTROL

No attempt has been made to determine an optimum method of blending TVC, aerodynamic, and ACPS controls. In the normal entry studies either one type of control has been used for the entire entry trajectory or Mach 7 has been used as a switching point between ACPS and aerodynamic control. Mach 7 has also been used as the switching point for discrete changes in some gains, for example K_α and K_ϕ , and for changing the trigonometric crossfeeds between the roll and yaw axes. These crossfeeds could probably be in all the time, rather than switching out below Mach 7. Figure 69 combines separate controls designed for separate mission phases. They were adequate for the studies reported here, assessing vehicle configuration effects.

It was stated that the entry studies to date have not specifically considered blending of the aerodynamic and ACPS modes of control. This does not imply that the method used of arbitrarily switching between modes of control at Mach 7 is considered satisfactory, or that use of aerodynamic controls exclusively in pitch and roll for the entire entry is optimum. In particular, for the range of 400,000 ft down to 300,000 ft and possibly lower, reliance upon the aerodynamic controls would probably not be satisfactory if any disturbances or other control requirements should occur. Furthermore, because of hinge moments, the use of aerodynamic surfaces for high-frequency control in this region might actually require the expenditure of more onboard energy than would be required by the ACPS. Structural and heating problems might also effect the desirability of using aerodynamic surfaces at the higher altitudes, even though their effectiveness is adequate for all necessary control.

In light of the above items, it is evident that any blending scheme must consider more than just the relative effectiveness of the two modes of control at any point in the flight envelope. However, considerable information leading to an ultimate blending concept can be obtained in the absence of hinge moment data and without consideration of structural or heating problems. For example, the feasibility of using the aerodynamic surfaces only for long-term trim and the ACPS for damping and control inputs can readily be determined. It is also possible to determine the crossover point between the relative effectiveness of the two modes of control and evaluate various methods of transferring control between them. Two alternates are simply switching at a discrete point or simultaneously widening the ACPS deadband while increasing the aerodynamic control gains and limits in the vicinity of the crossover area. A major factor in either of these alternates is determining when the crossover point is reached or being approached. It is feasible to assume that this determination can be made based on air data quantities (altitude, Mach, dynamic pressure, etc.) The X-15, for example, had a self-adaptive aerodynamic control system. The adapted gains in roll, pitch, and yaw were summed and compared with the maximum obtainable. If greater than 90 percent, the ACPS was turned on. If below 60 percent, the ACPS was turned off.

For the studies covered in this report, the aerodynamic pitch rate gain was scheduled with dynamic pressure, and control surface effectiveness derivatives were used as scheduling parameters in the aerodynamic roll and yaw rate loops. Other gains were switched by discrete values at Mach 7. Scheduling with dynamic pressure should be feasible, even if this quantity must be generated from inertial parameters at high altitudes. Also, since digital computation is employed, the nonlinear aspect of using the square root is no problem. Similarly, in the roll and yaw axes there is no inherent problem in scheduling with the aerodynamic derivatives, assuming Mach and angle of attack are available. However, a large amount of computer memory will be required to store the aero data, and computation time for table look-ups might be excessive. Also to be considered is the accuracy of the stored data.

Before giving undue concern to these aspects of the gain schedules used in this study, the necessity of using such relatively complex parameters should be evaluated. For example, further study may indicate that scheduling with Mach or dynamic pressure is adequate. In fact, the roll and yaw axis gains vary in a manner very similar to that of the pitch rate gain. Also to be considered is the possibility of using fixed gains, or a small number of discretely switched gains. It is evident that a considerable amount of additional study is required to determine the actual gain requirements. From the block diagrams it will be noticed that the angle-of-attack gain is switched from a value of 1.0 above Mach 7 to a value of 3.0 below Mach 7. The higher value is required below Mach 7 because of the destabilizing sign of $C_{m\alpha}$ at angles of attack below 30 deg and Mach numbers greater than about 5.0.

TVC makes further demands on the ECS, believed to be principally in the mode logic. The following ECS mode conditions have not been tested, but appear reasonable at this time:

- Use normal ECS if both TVC engines are off
- Use the ECS roll control if one engine is on with a larger aileron command limit than used for normal ECS operation
- Shut down the ECS if both engines are on, thus capable of three-axis control

CONCLUDING REMARKS

The major conclusion drawn from this study is that the 134C and 134D delta wing orbiters are controllable along the nominal entry trajectory. However, at this time it is not possible to define in detail a system configuration. Indications are that a preferred configuration would be similar to that in Figure 69, assuming the 134D vehicle as the more representative delta-wing orbiter. Modifications to this basic combination would be expected in the areas of gain switching and scheduling, and the blending in of roll and possibly pitch ACPS control, especially at the higher altitudes. The abort study, Section V, shows additional impact on the ECS, including:

- 1) ECS operation with full propellant
- 2) ECS operation with TVC, with
 - Large aileron command authority possibly needed for engine-out TVC
 - A possibly severe propellant slosh problem during ECS/TVC operation
- 3) Need for a thorough analysis in the abort regions of the flight envelope, not encountered during normal entries.

SECTION VII

LATERAL HANDLING QUALITIES CAPABILITIES OF A STRAIGHT-WING ORBITER IN POST-ENTRY FLIGHT

Lateral handling qualities capabilities of a straight-wing orbiter are examined from the standpoint of meeting flying qualities specifications. The basic unaugmented airframe satisfies specifications except for:

- Marginal roll rate oscillations from aileron commands at moderate dynamic pressure
- Marginal roll effectiveness at landing
- Excessive proverse sideslip during moderate dynamic pressure flight.

The orbiter can be augmented to essentially satisfy all requirements. Level 1 roll control effectiveness is marginal at landing using aileron and rudder controls. Level 3 requirements can be met without the use of aileron through the use of spoilers and rudder. Thus the spoilers provide a natural backup device for the ailerons.

THE BASIC AIRFRAME

A two-sided view of the orbiter is presented as Figure 70. The rudder is conventional. Differential horizontal stabilizer motion is used to provide the primary source of rolling moments. Spoiler ailerons (with extremely slow actuators) are available for generating additional rolling moments:

Linear dynamic models for the basic airframe are developed in Appendix E for flight conditions FC 9 ($h = 20,000$ ft., $V = 674$ ft/sec, $\bar{q} = 287$ lbs/ft²) and FC 11 ($h = 0$, $V = 252$ ft/sec, $\bar{q} = 75.5$ lbs/ft²).

Shuttle handling qualities specifications are presented in reference 13.

Table 21 compares major lateral handling quality parameters of basic shuttle against NASA spec requirements. Numerical values are computed from the roots of the linear models and from free aircraft transient responses (Figures 71-76) according to NASA spec procedures. For example, P_{osc}/P_{avg} for FC 9 is obtained from Figure 71a via the expression

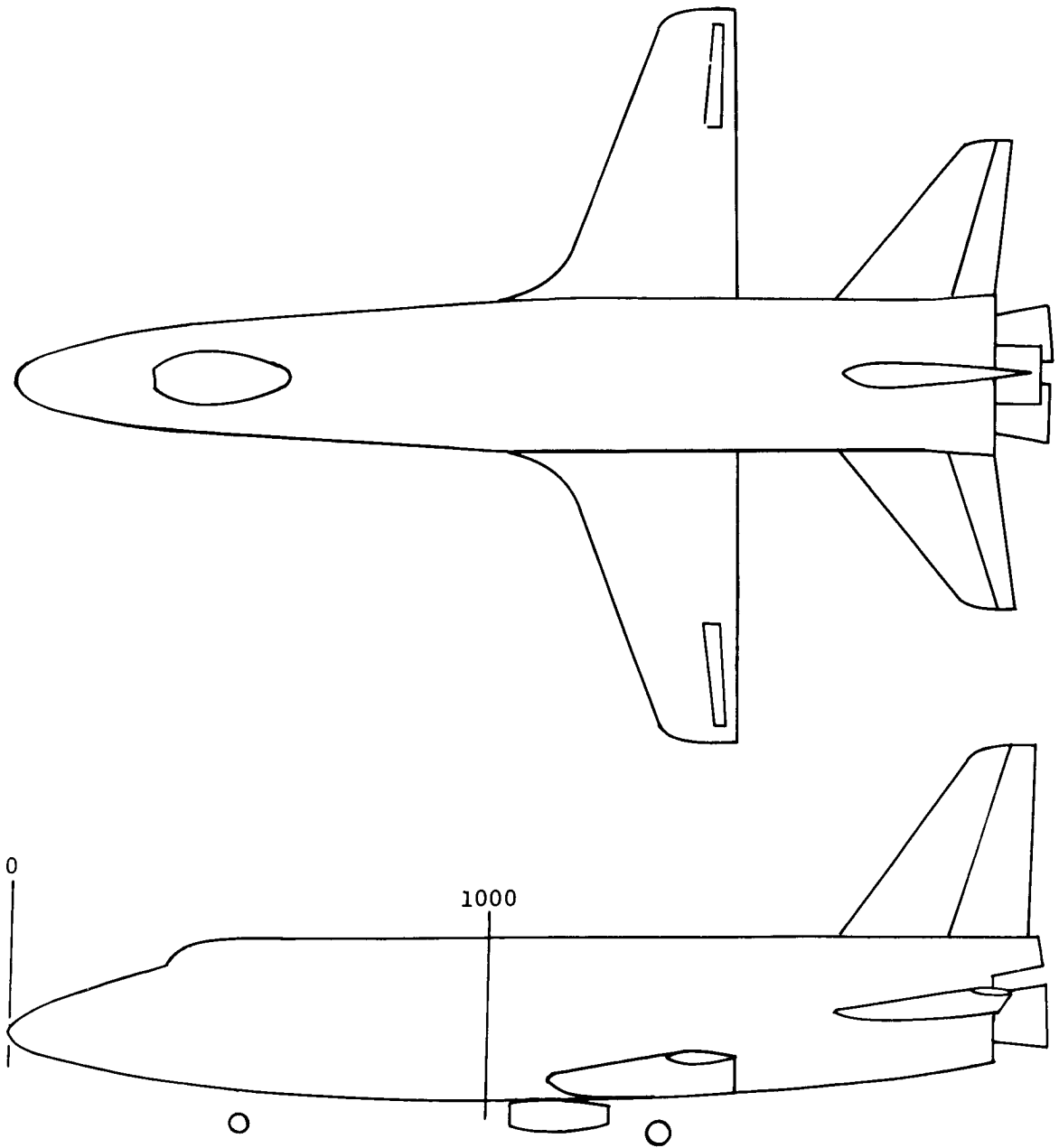


Figure 70. North American 130G Straight Wing Orbiter

Table 21. Lateral Handling Quality Characteristics of Basic Airframe

Parameter	Symbol (units)	NASA Spec Paragraph	FC 9		FC 11	
			Value	Requirement	Value	Requirement
Dutch Roll Frequency	ω_d (rad/sec)	3-3.1.1	1.47	≥ 0.4	0.87	≥ 0.4
Dutch Roll Damping	$\zeta_d^{\omega_d}$ (rad/sec)	3-3.1.1	0.56	≥ 0.35	0.46	≥ 0.15
Roll Time Constant	T_R (sec)	3-3.1.2	0.36	≤ 1.4	0.90	≤ 1.4
Inverse Spiral Time Constant	$1/T_s$ (sec^{-1})	3-3.1.3	0.0053	≥ -0.035	-0.012	≥ -0.035
Roll Rate Oscillations	$(\omega_{\phi}^{\omega_d})^2$ $\zeta_{\phi}^{\omega} - \zeta_d^{\omega_d}$ P_{osc}/P_{avg}	3-3.2.2.1	1.29 -0.18 0.067	≤ 0.05	0.83 -0.13 ≈ 0	≤ 0.60
Sideslip Excursions in Rolling Maneuvers	$\Delta\beta/k$ (deg)	3-3.2.4	9.6 (proverse)	≤ 2.0	6.0 (adverse)	≤ 10.0
Roll Control Effectiveness	ϕ_t (deg in t sec)	3-3.4	32° in 1.5 sec	$\geq 30^\circ$ in 1.5 sec	27° in 2.5 sec	$\geq 30^\circ$ in 2.5 sec

$$\frac{p_{osc}}{p_{avg}} \approx \frac{p_1 - p_2}{p_1 + p_2} = \frac{0.015}{0.225} = 0.067$$

Further, comparison of Figures 71a and 71c shows that the dutch roll component of sideslip lags by $\psi_\beta \approx -40$ deg (i. e., sideslip is primarily proverse) with roll rate leading sideslip by $< p/\beta \approx 170$ deg. The corresponding NASA Spec requirement is therefore $p_{osc}/p_{avg} \leq 0.05$ (Para. 3.3.2.2.1).

Similarly, the sideslip excursion and roll control effectiveness parameters were evaluated from Figures 73c and 73d. These show free aircraft responses to maximum magnitude aileron commands. During the time required to roll to 90 deg., $\Delta\beta$ reaches 10.2 deg proverse. The parameter k has the value

$$k = \frac{(\phi_t) \text{ commanded}}{(\phi_t) \text{ required}} = \frac{32^\circ \text{ in } 1.5 \text{ sec.}}{30^\circ \text{ in } 1.5 \text{ sec.}} = 1.07,$$

so $\Delta\beta/k / 9.6$ deg. The requirement for proverse sideslip excursions is given in Para. 3.3.2.4 of ref. 6.2 as $\Delta\beta/k \leq 2$ deg.

The same data for FC 11 is contained in Figures 74 and 76. Here, however, the roll rate response to aileron exhibits negligible oscillations and sideslip is primarily adverse.

Table 21 can be summarized by noting that the basic airframe at two flight conditions meets all tabulated requirements with the following exceptions:

- Roll rate oscillations to aileron at FC 9 are marginal
- Roll control effectiveness at FC 11 is marginal
- Proverse sideslip excursions due to aileron are excessive at FC 9

THE AUGMENTED AIRCRAFT

Handling quality controllers are designed for both flight conditions to correct the above deficiencies (where possible) and to provide uniform response characteristics for the two conditions. The design procedure used was developed by Honeywell under a recent AFFDL contract (ref. 14) and is illustrated in Figure 77. In essence, the procedure uses quadratic optimal model-following control to cause the aircraft to follow responses of a specified handling quality model for a specified class of pilot commands.

In its full development, the procedure yields practical control systems which are constant over the flight envelope and utilize only realizable measured signals. For the purposes of the present investigation, however,

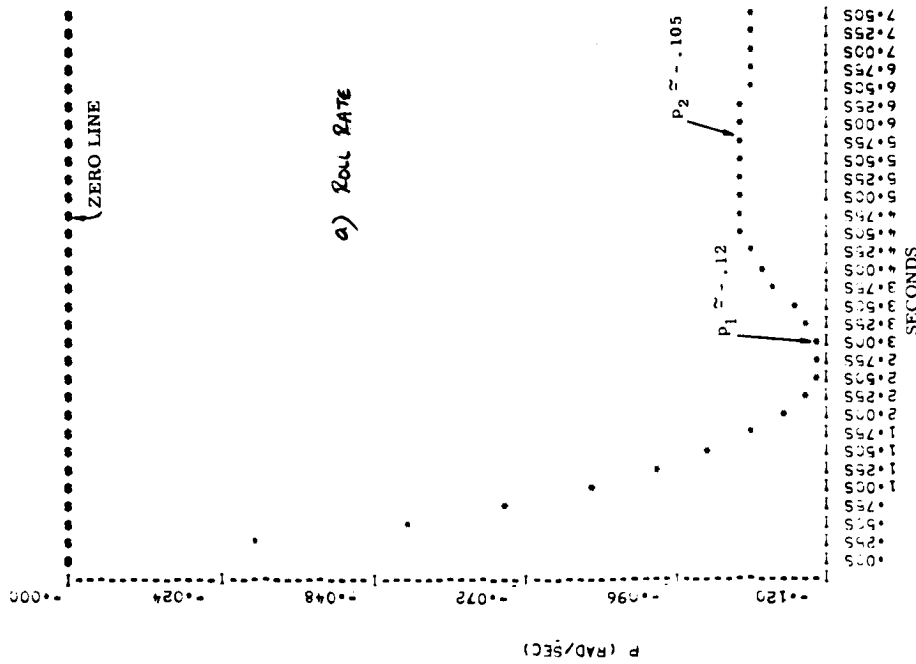
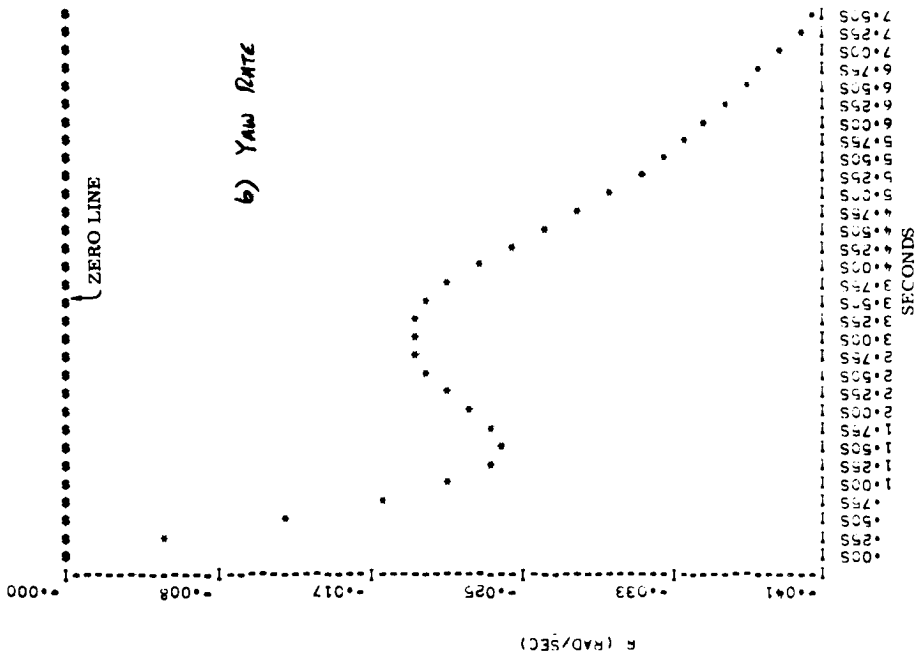


Figure 71. FC9 Step Responses - 0.026 Rad Aileron Actuator Input

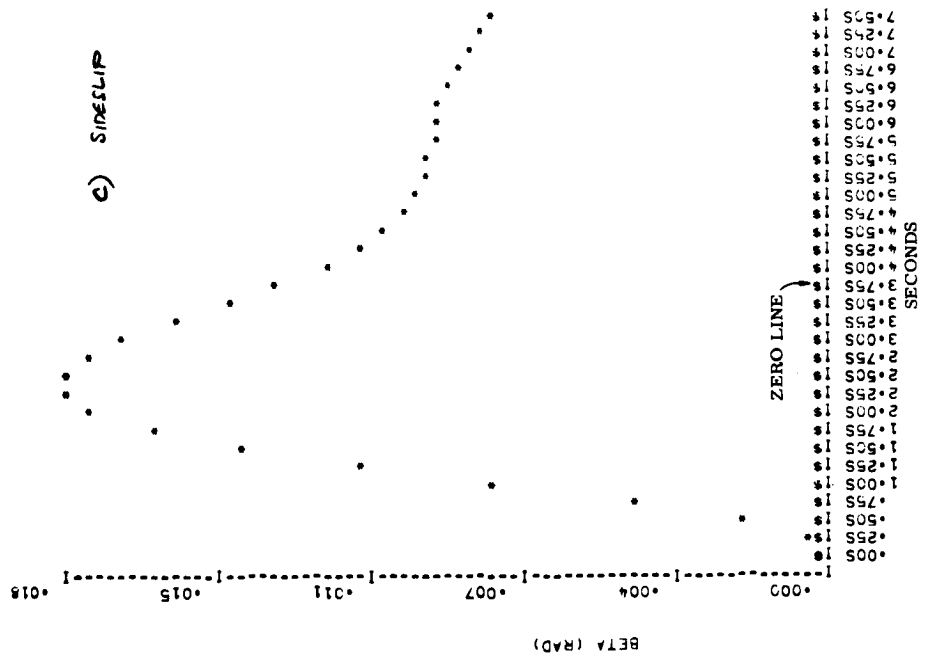
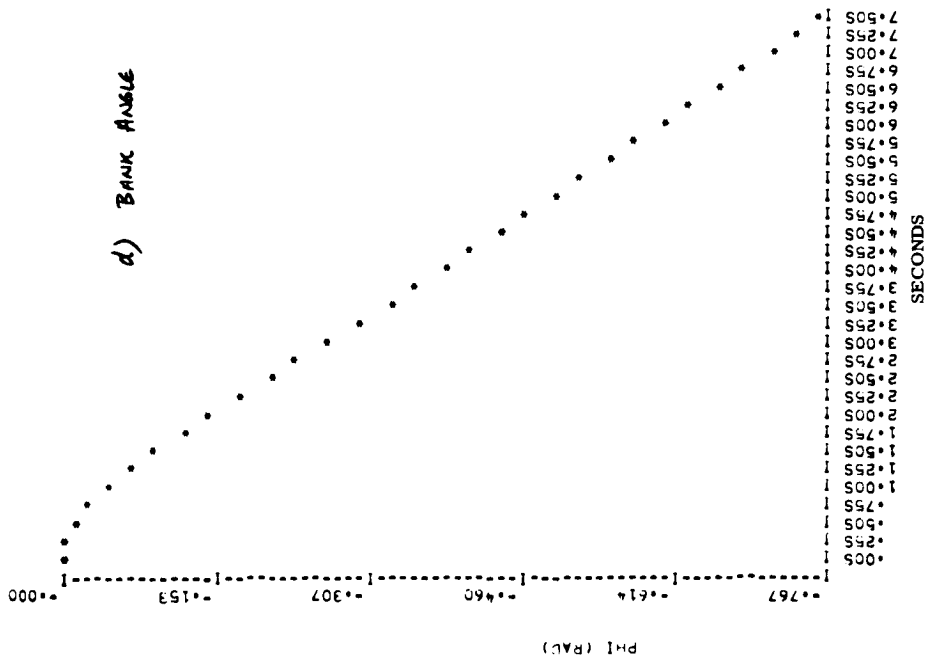


Figure 71. (Concluded)

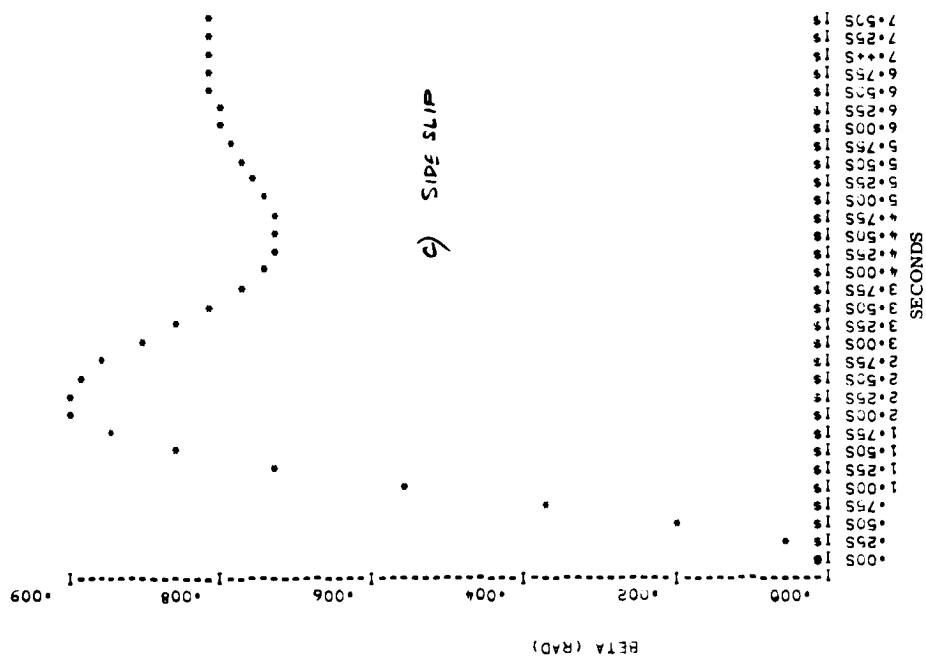
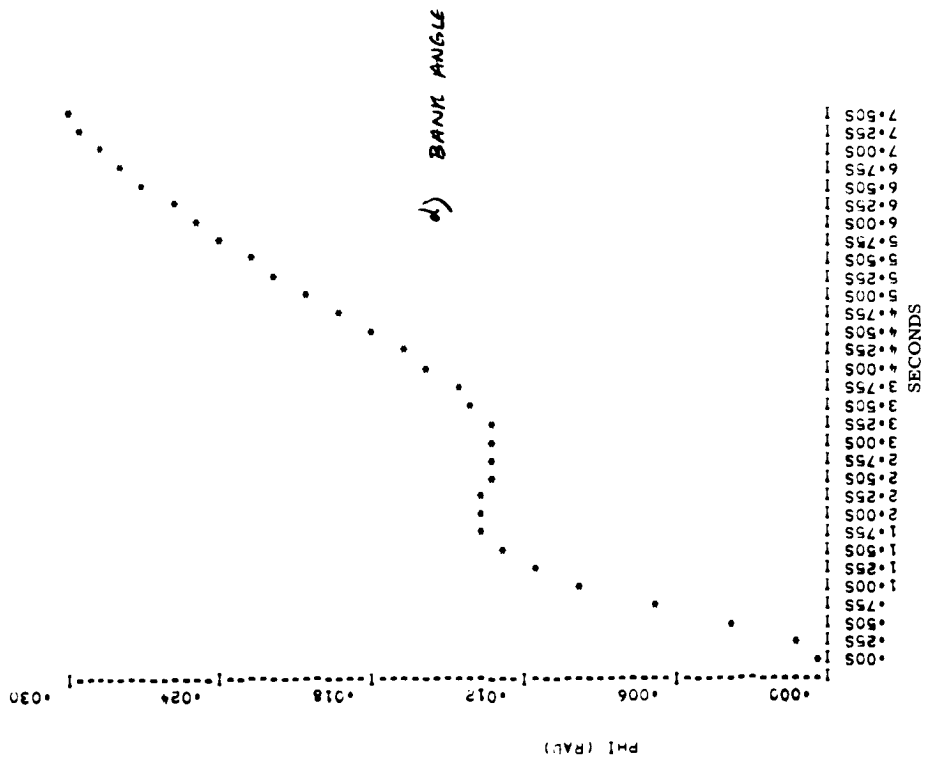


Figure 72. (Concluded)

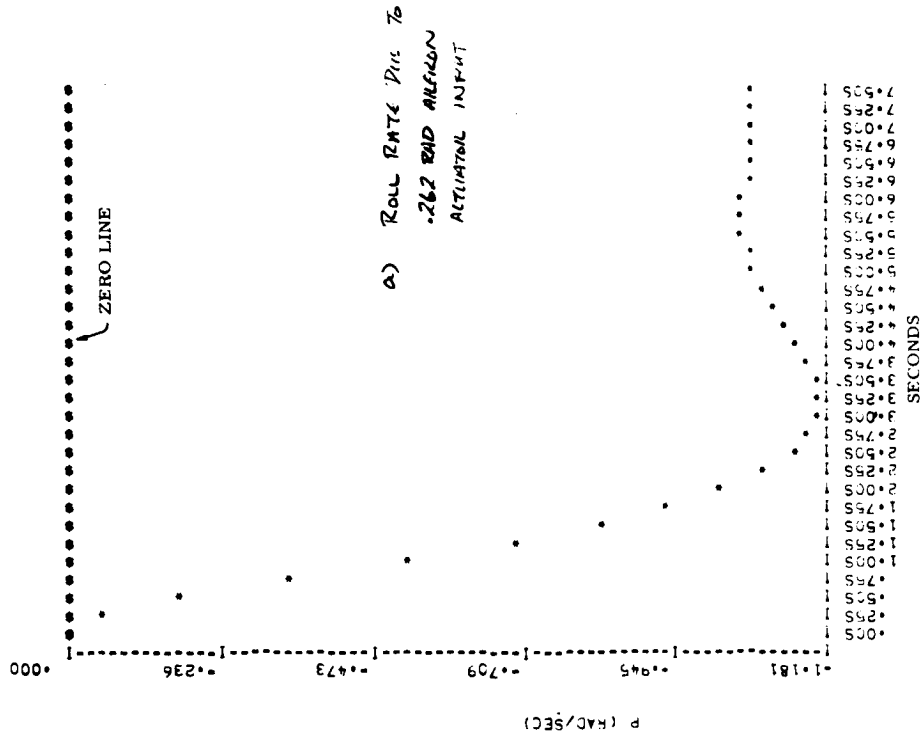
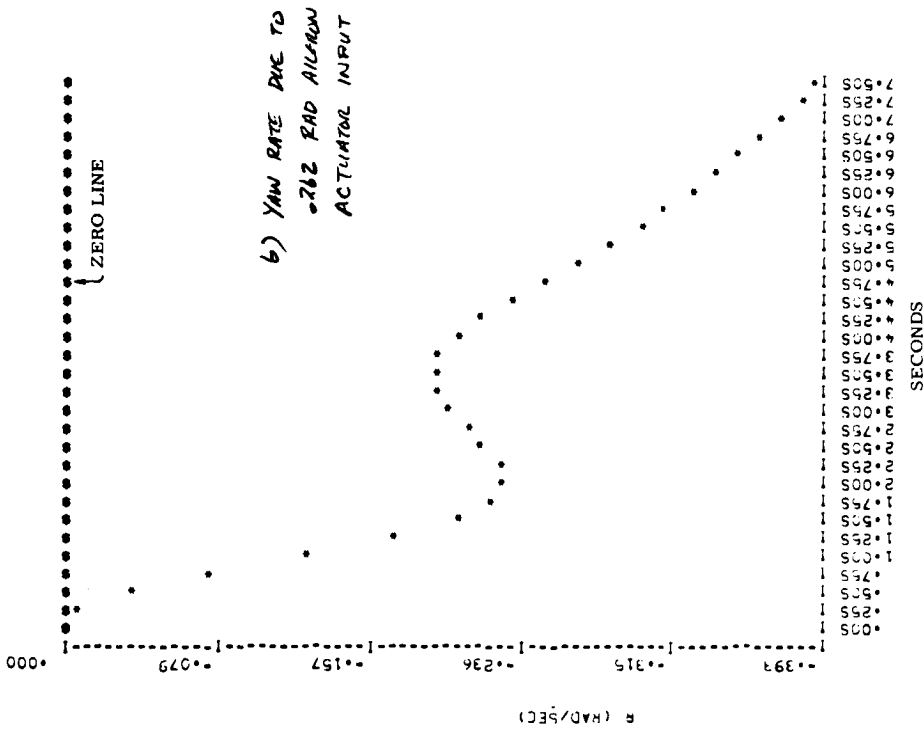


Figure 73. FC9 Step Responses Max Commands

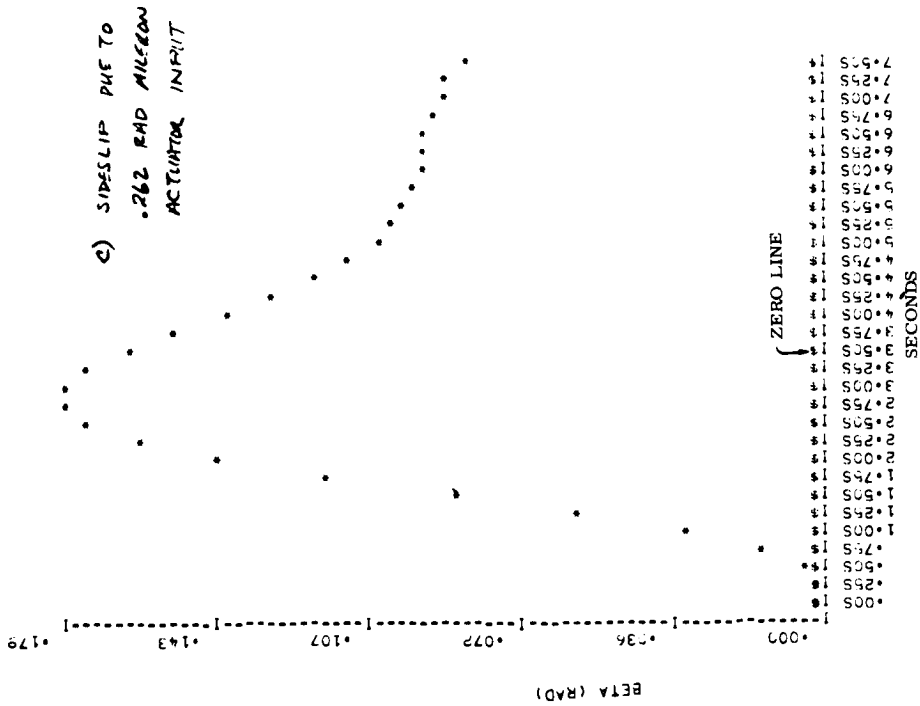
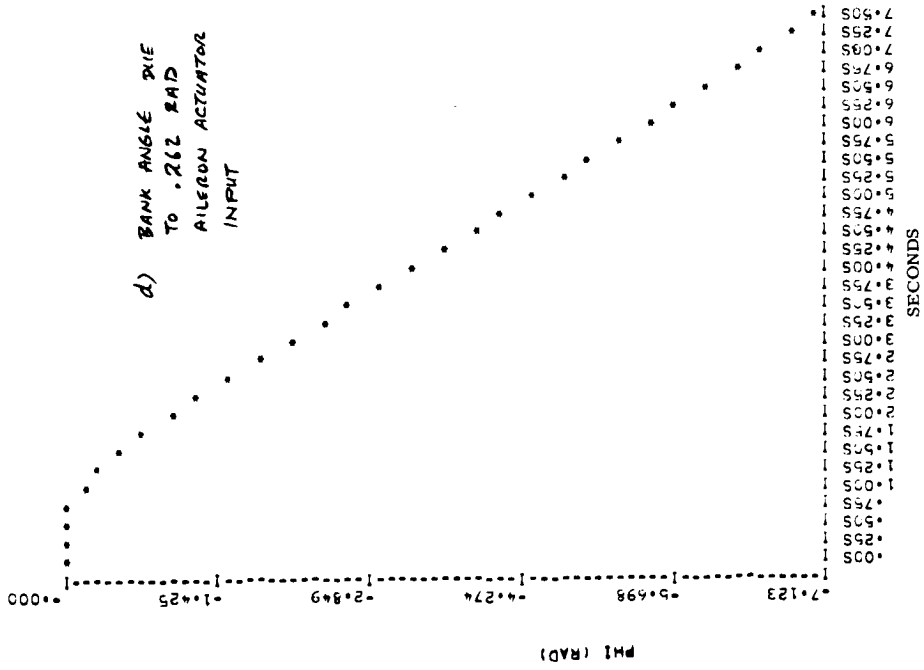


Figure 73. (Continued)

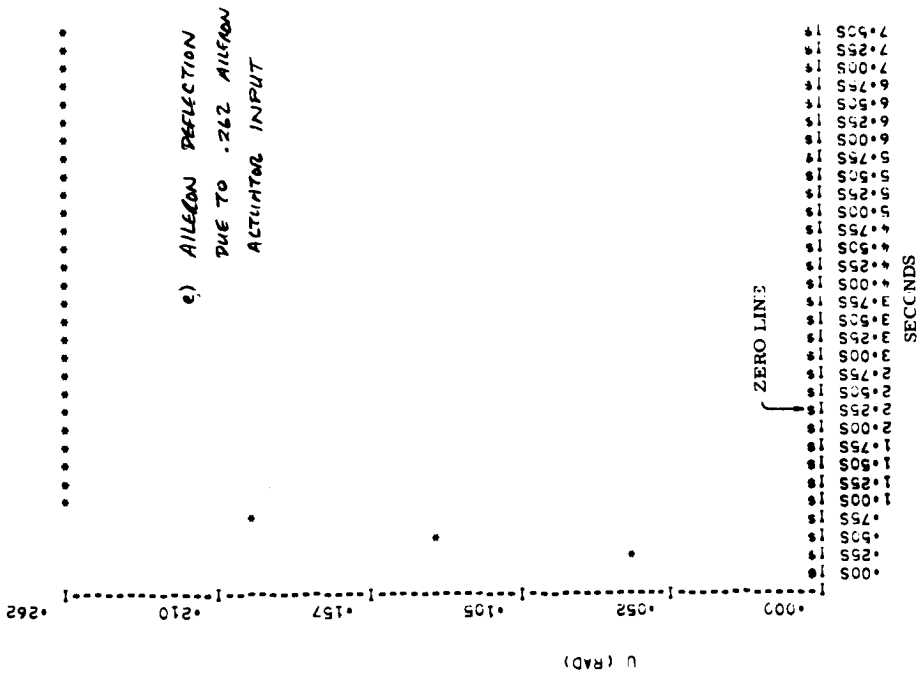


Figure 73. (Concluded)

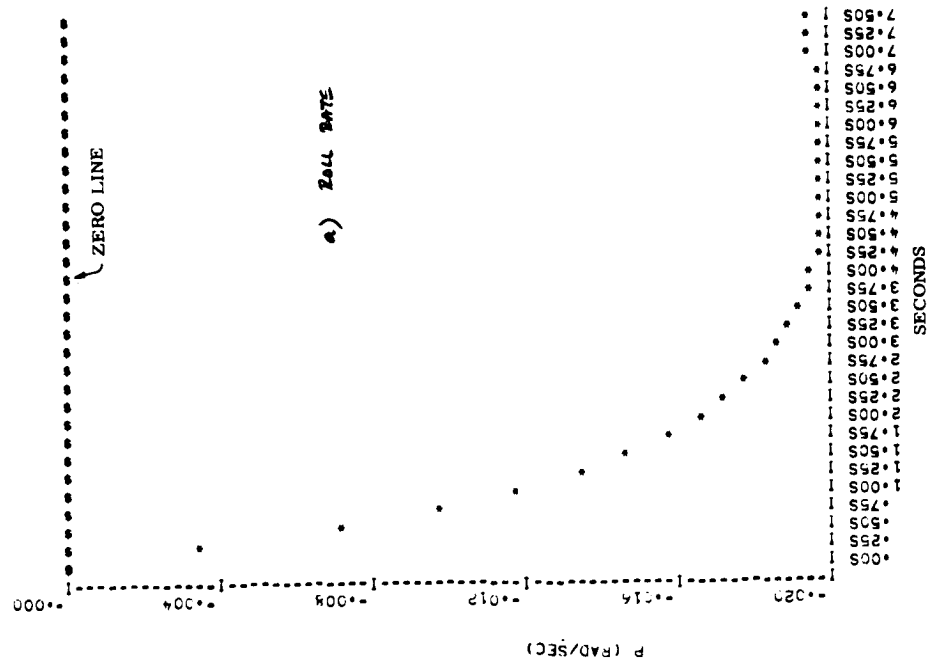
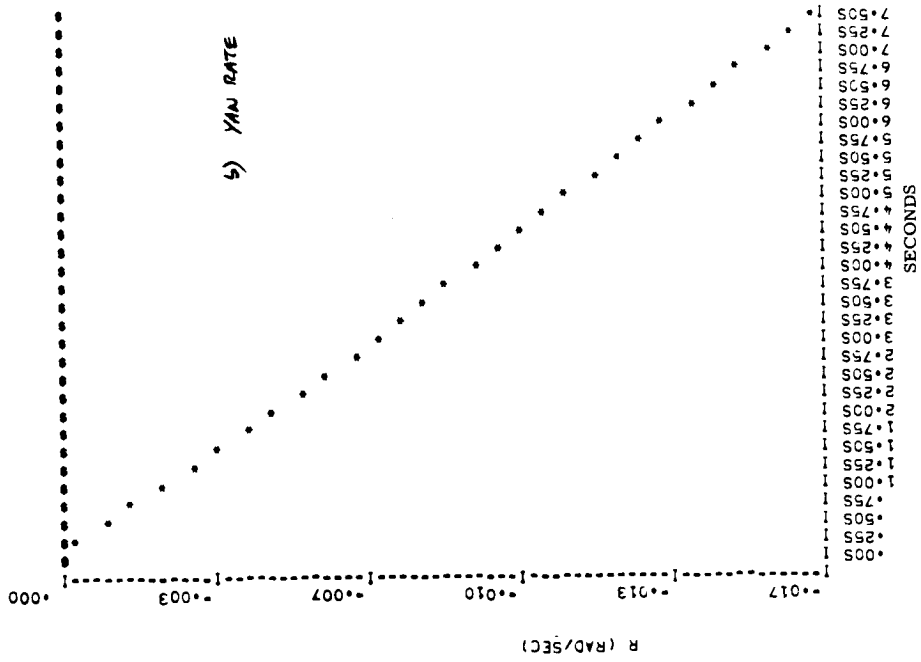


Figure 74. FC11 Step Responses 0.015 Rad Aileron Actuator Input

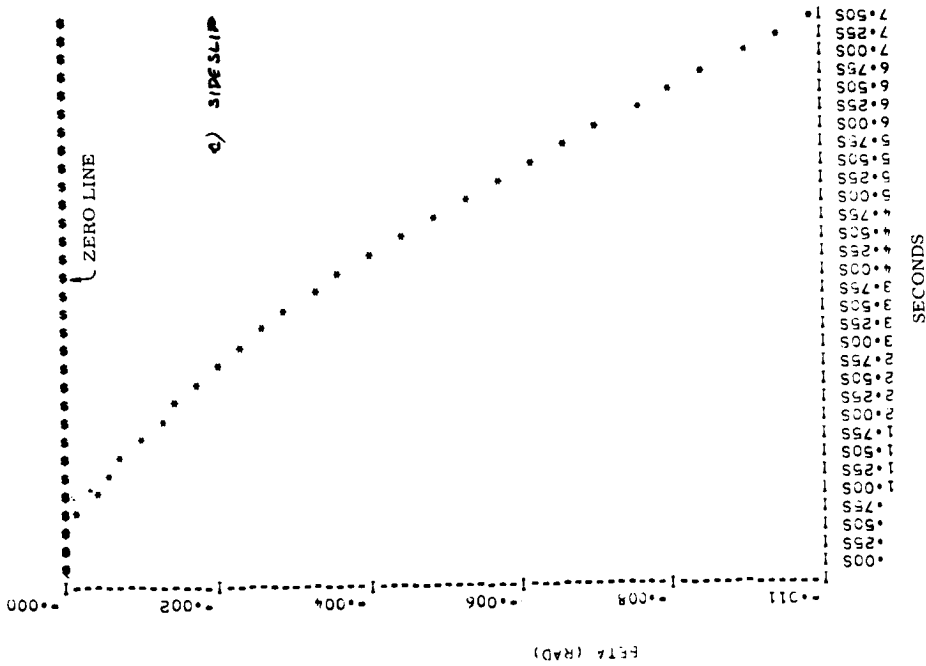
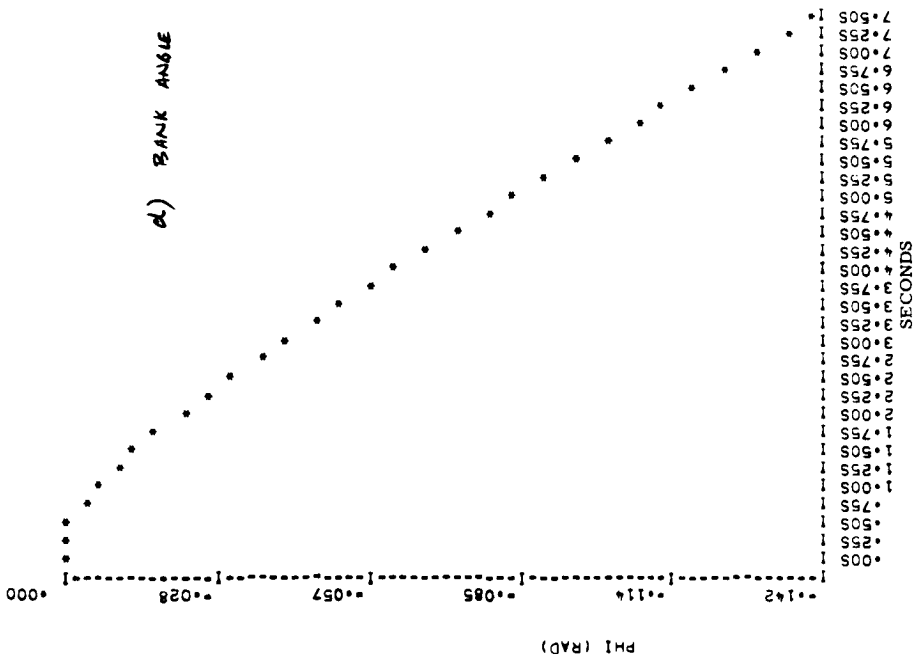


Figure 74. (Concluded)

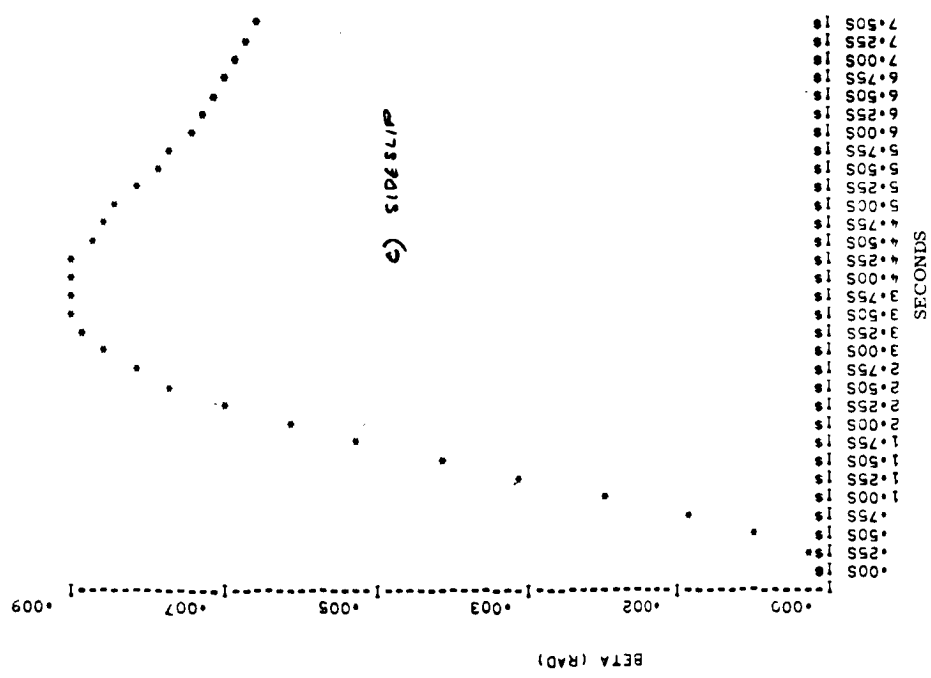
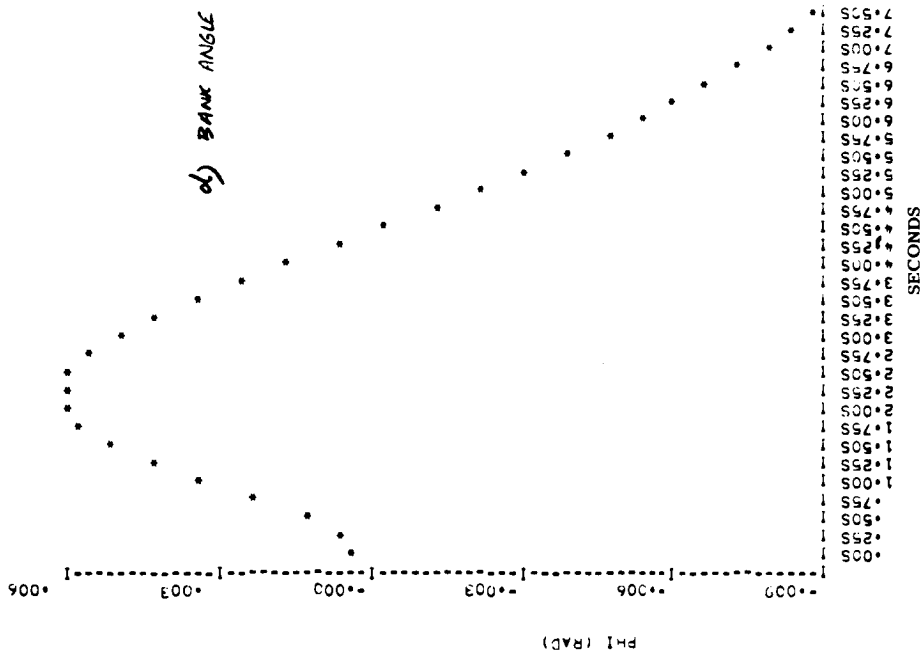


Figure 75. (Concluded)

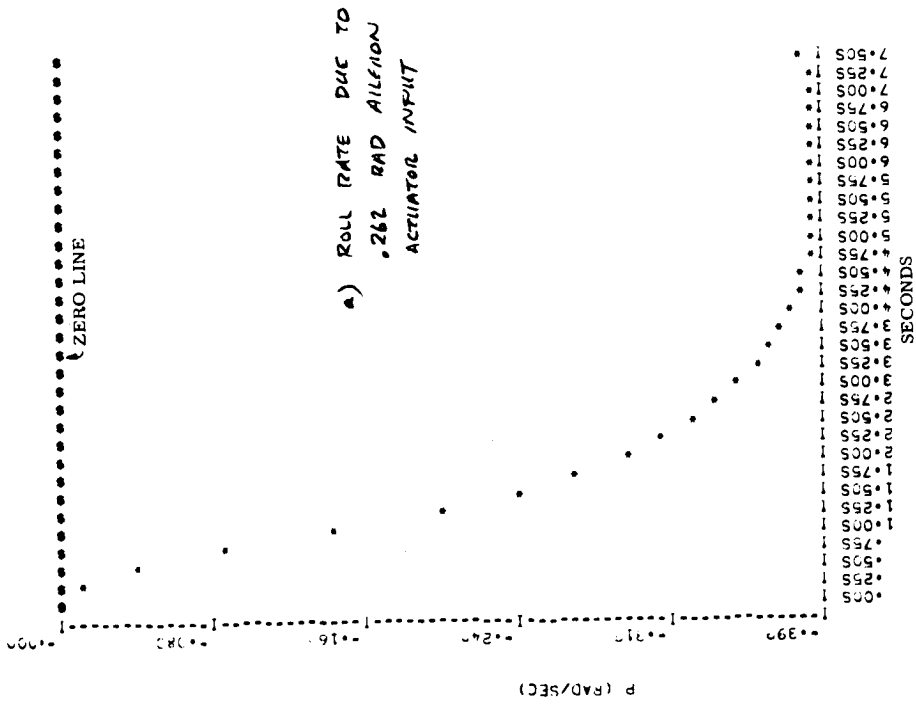
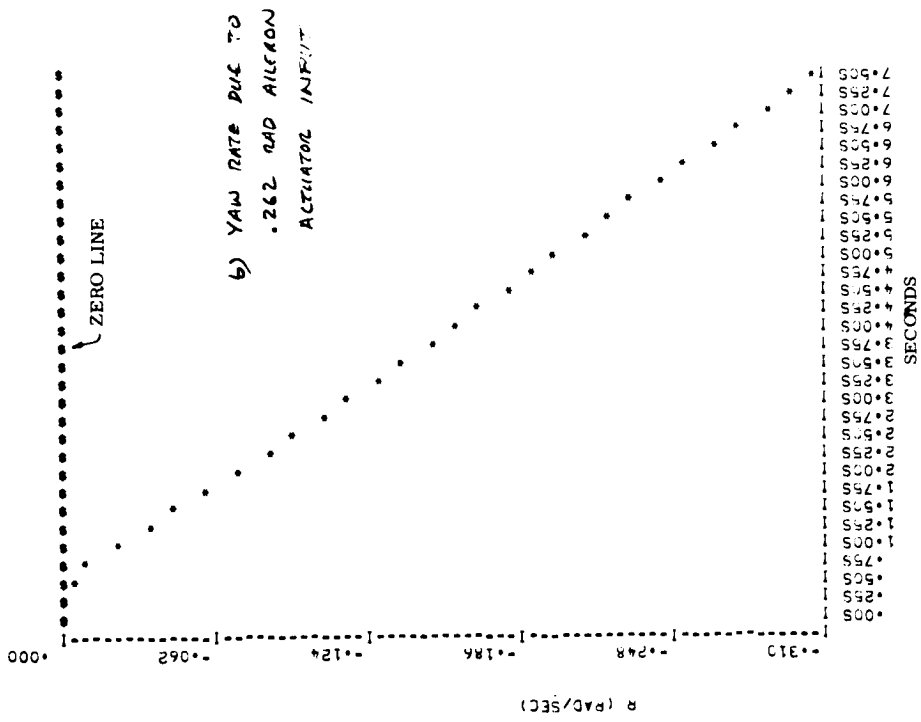


Figure 76. FC11 Step Responses Max Command

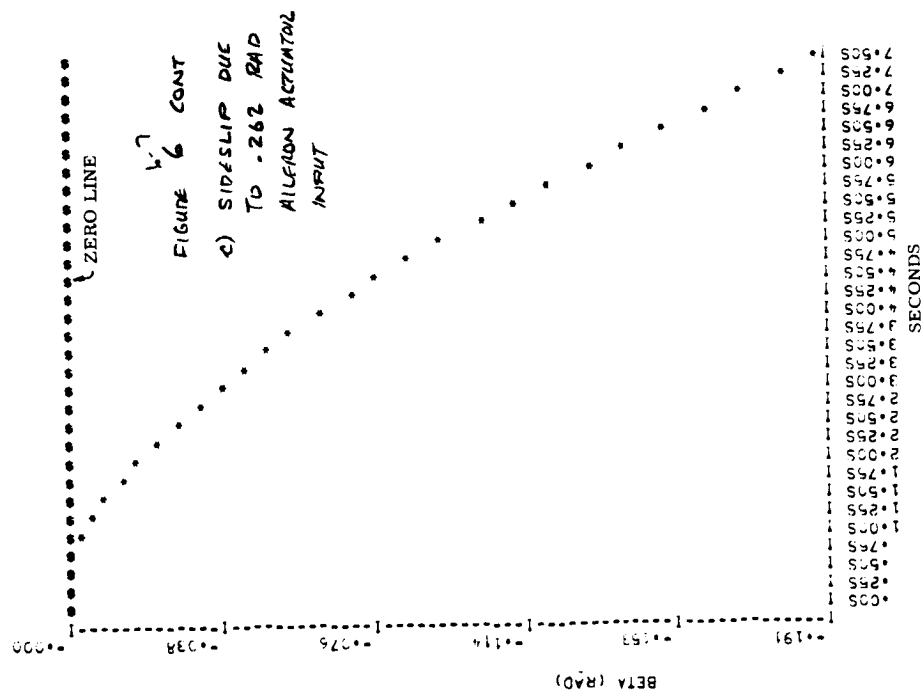
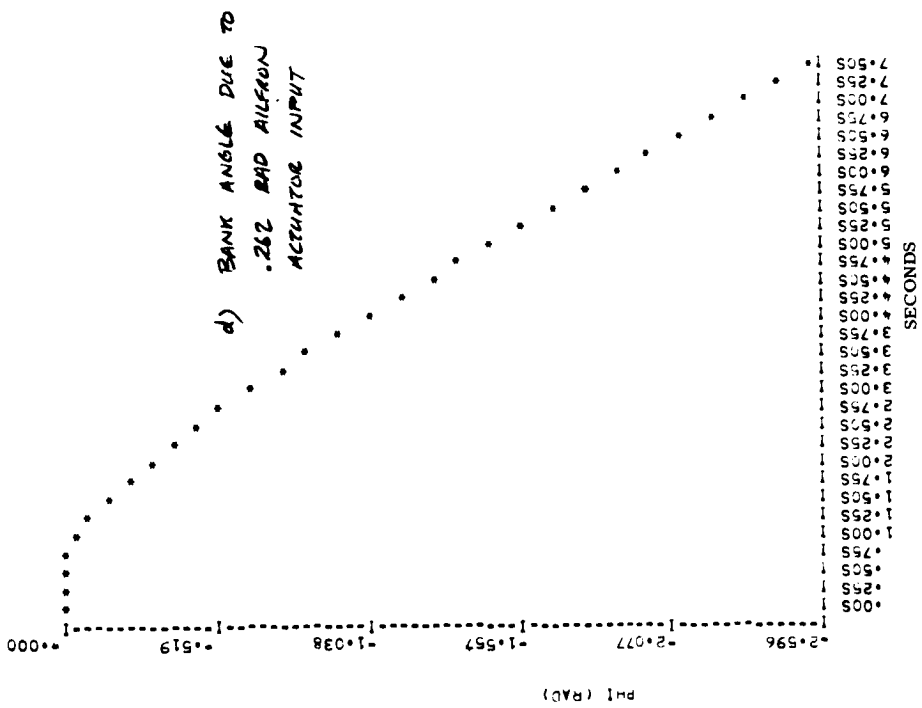
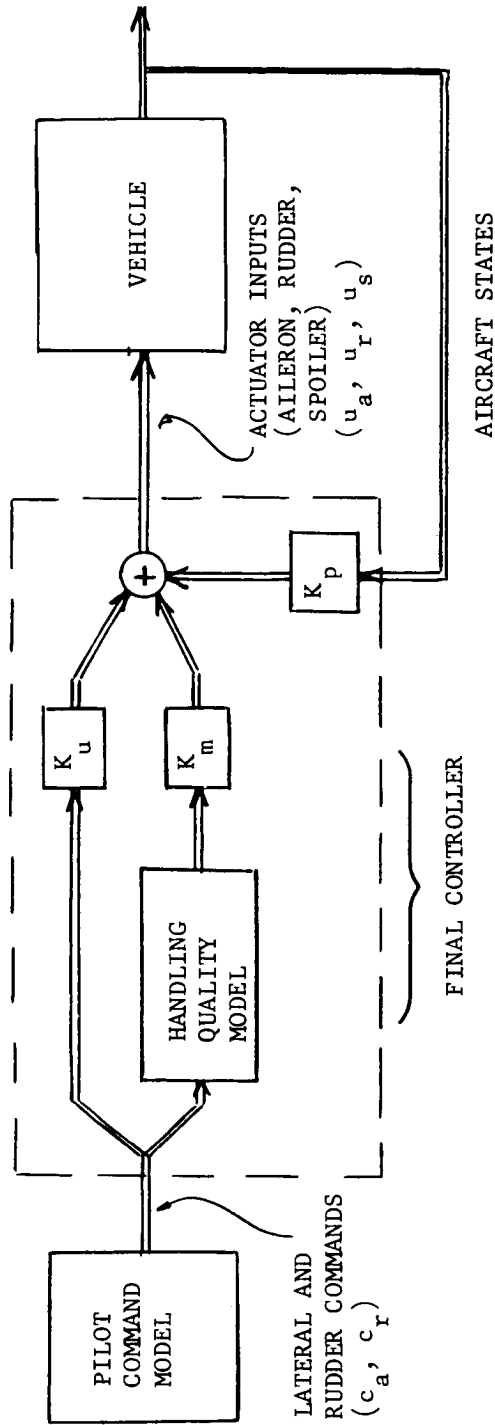


Figure 76. (Concluded)



DESIGN OBJECTIVE: FIND GAINS K_u , K_m , K_p TO MINIMIZE
 $J = \text{QUADRATIC FUNCTION OF ERRORS}$
 BETWEEN VEHICLE RESPONSES AND
 MODEL RESPONSES

Figure 77. Handling Quality Controller Design Procedure

flight-condition-dependent gains and full state measurement are allowed. With these relaxed requirements, controllers can be computed very cheaply yet still provide good indications of performance achievable with practical systems (ref. 15). The handling quality model, command model, and performance index (J) used in the designs are summarized in Table 22.

Control gains for the four quadratic control systems synthesized and their associated quadratic weights are summarized in Table 23.

Controllers are synthesized for ailerons and rudder as primary controls and also for spoilers and rudder only.

FLIGHT CONDITION 9

Step responses for the controller orbiter at FC 9 are given in Figures 78 through 83. The first of these two figures show small command responses for aileron/rudder control. It is evident that roll rate oscillations have been eliminated and that proverse sideslip excursions have been reduced by a factor of five to a level which meets specifications (compare with Figures 71 and 72). The small model-following errors in Figures 78 and 79 verify that the orbiter can be made to follow the handling quality model quite well.

Figure 80 shows maximum command responses for the same controller. These traces indicate that the controller is a little too tight, since it produces some initial actuator rate limit oscillation for large commands. However, the oscillations decay quickly and all responses meet specifications.

Figures 81 through 83 show the same small and large command traces for FC 9 with spoiler/rudder control only. Dynamic responses at small commands are nearly identical to the aileron/rudder system. For max. commands, however, the slow deflection rate of the spoiler actuators makes the 30° in 1.5 seconds requirement unattainable. The system does, however, satisfy the Level 3 requirement of 30 degrees in 3.0 sec. The spoilers are natural roll control backup devices.

FLIGHT CONDITION 11

A similar set of traces for FC 11 is given in Figures 84 through 86 (aileron/rudder control) and Figures 87 through 89 (spoiler/rudder control). The same conclusions are evident. For small commands the transients for aileron/rudder and spoiler/rudder are essentially identical. They also match the FC 9 transients, since the handling quality model is the same for both flight conditions. At large commands, the spoiler/rudder system again falls short of Level 1 roll control effectiveness requirements but does satisfy Level 3. Like the basic airframe, the aileron/rudder roll effectiveness is still slightly marginal for Level 1.

Table 22. Details of the Design Procedure

Handling Quality Model

Ideal lateral directional aircraft equations in stability coordinates

$$\frac{d}{dt} \begin{pmatrix} p_m \\ r_m \\ \beta_m \\ \varphi_m \end{pmatrix} = \begin{pmatrix} -1.33 & 1.55 & -2.50 & 0 \\ .0715 & -.468 & .752 & 0 \\ 0 & -1.0 & -.532 & .0715 \\ 1 & 0 & 0 & 0 \end{pmatrix} \begin{pmatrix} p_m \\ r_m \\ \beta_m \\ \varphi_m \end{pmatrix} + \begin{pmatrix} 1.39 & -2.66 \\ -0.5 & 0 \\ 0 & 0 \\ 0 & 0 \end{pmatrix} \begin{pmatrix} c_a \\ c_r \end{pmatrix}$$

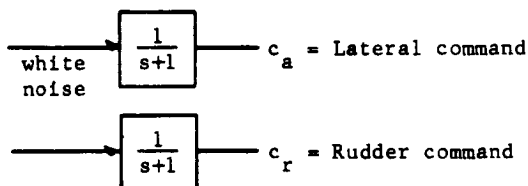
This corresponds to:

$$\omega_d = 1, \zeta_d \omega_d = 1, T_R = .75, 1/T_s = 0., L_\beta = -2.5,$$

$$(\omega_\varphi/\omega_d)^2 = 1, (\zeta_\varphi \omega_\varphi - \zeta_d \omega_d) = 0, \Delta\beta_{\max} = -.035,$$

$$(p_m/c_a)_{ss} = -2., (\beta_m/c_r)_{ss} = -.5, (p_m/c_r)_{ss} = -.2$$

Pilot Command Model



Performance Index

$$J = q_{11}(\tilde{p}-\tilde{p}_m)^2 + q_{22}(\tilde{r}-\tilde{r}_m)^2 + q_{33}(\tilde{\beta}-\tilde{\beta}_m)^2 + q_{44}z^2 + q_{55}u_a^2 + q_{66}u_r^2 + q_{77}u_s^2$$

\tilde{p}, \tilde{r} , etc.: roll rate, yaw rate, etc. with spiral component subtracted out

z : spiral mode component of aircraft

$q_{11}, q_{22}, \dots, q_{77}$: quadratic weights

u_a, u_r, u_s : actuator inputs

Table 23. Gains and Quadratic Weights

FC 9 AILERON/RUDDER CONTROLLER

WEIGHTS: $(q_{11}, \dots, q_{77}) = (10, 10, 100, .001, 1, .1, \infty)$

GAINS:

	p	r	β	φ	δ_a	$\dot{\delta}_a$	δ_r	$\dot{\delta}_r$	δ_s	\tilde{p}_m	\tilde{r}_m	$\tilde{\beta}_m$	c_a	c_r
TO: AILERON	1.7	3.0	-6.3	-0.028	-0.011	-.79	.002	.15	-.14	-2.1	-3.4	6.0	.62	-.08
RUDDER	-6.3	7.2	-15.	-.21	.018	1.6	-.02	-1.7	.17	6.3	-8.6	17.	-.25	.78
SPOILER	0	0	0	0	0	0	0	0	0	0	0	0	0	0

$\underbrace{\hspace{10em}}_{K_p} \qquad \underbrace{\hspace{10em}}_{K_m} \qquad \underbrace{\hspace{10em}}_{K_u}$

FC 9 SPOILER/RUDDER CONTROLLER

WEIGHTS: $(q_{11}, \dots, q_{77}) = (10, 10, 100, .005, \infty, 2.5, .001)$

GAINS:

0	0	0	0	0	0	0	0	0	0	0	0	0	0	0
-.83	2.4	-2.6	-.09	.003	.20	-.006	-.39	-.02	.76	-3.0	3.5	.14	.32	
32.0	122.0	-90.0	-2.3	-.33	-22.0	-.005	-.60	-18.	-55.	-163.0	107.0	61.0	-3.0	

FC11 AILERON/RUDDER CONTROLLER

WEIGHTS: $(q_{11}, \dots, q_{77}) = (10, 10, 100, .005, 1, 5, \infty)$

GAINS:

2.2	3.1	-3.8	.15	-.003	-.23	.0009	.06	-.14	-2.1	-1.8	3.9	1.1	-.37	
-.39	2.4	-2.1	-.08	.0002	.01	-.001	-.07	.006	.15	-2.2	1.7	-.10	.49	
0	0	0	0	0	0	0	0	0	0	0	0	0	0	

C 11 SPOILER/RUDDER CONTROLLER

WEIGHTS: $(q_{11}, \dots, q_{77}) = (10, 10, 100, .005, \infty, .25, .002)$

GAINS:

0	0	0	0	0	0	0	0	0	0	0	0	0	0	0
-2.5	10.4	-14.	.03	.001	.11	-.005	.36	-.06	1.8	-9.0	13.	.30	.89	
101.	330.	-260.	-1.7	-.20	-13.0	-.01	-.81	-18.0	-115.	-285.0	270.	135.0	-26.	

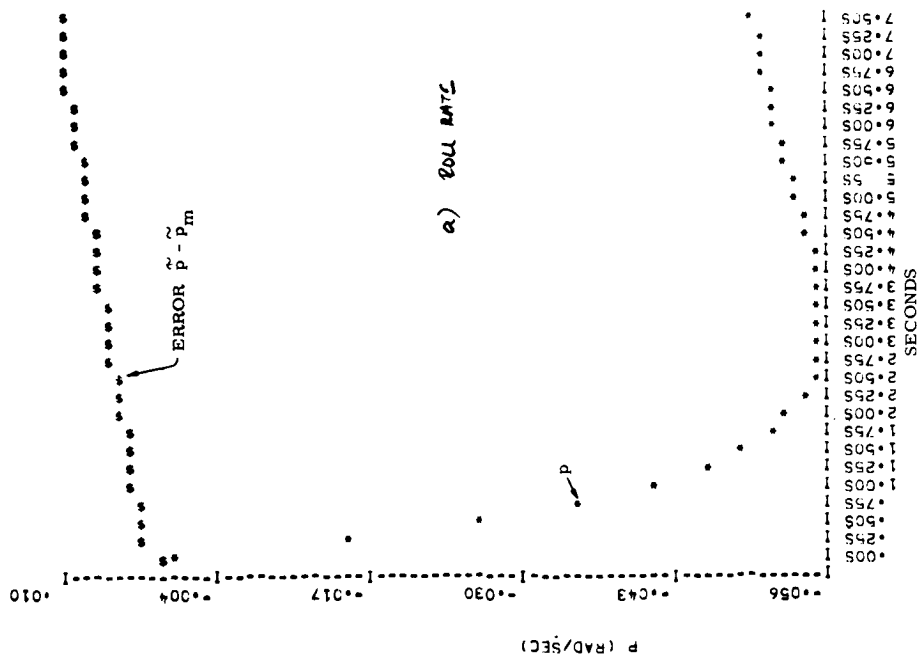
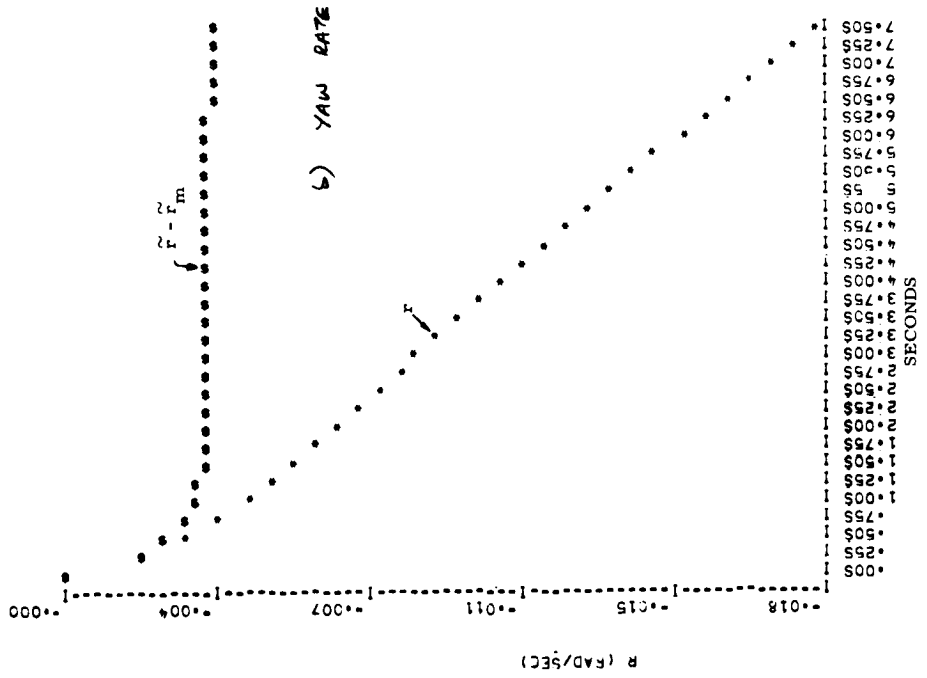


Figure 78. Step Responses, FC9 with Aileron/Rudder Control
015 Rad Rudder Command

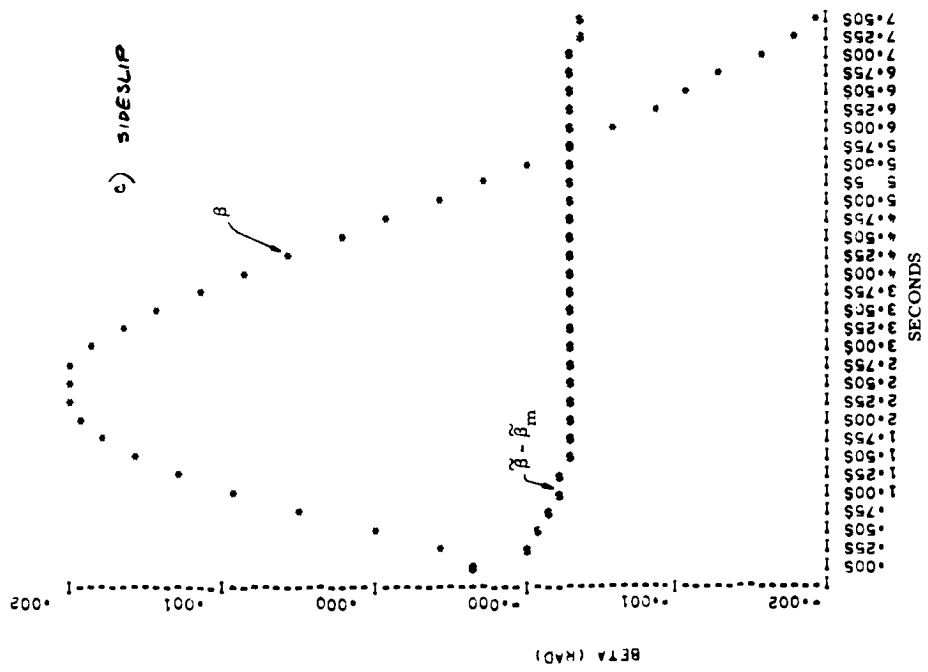
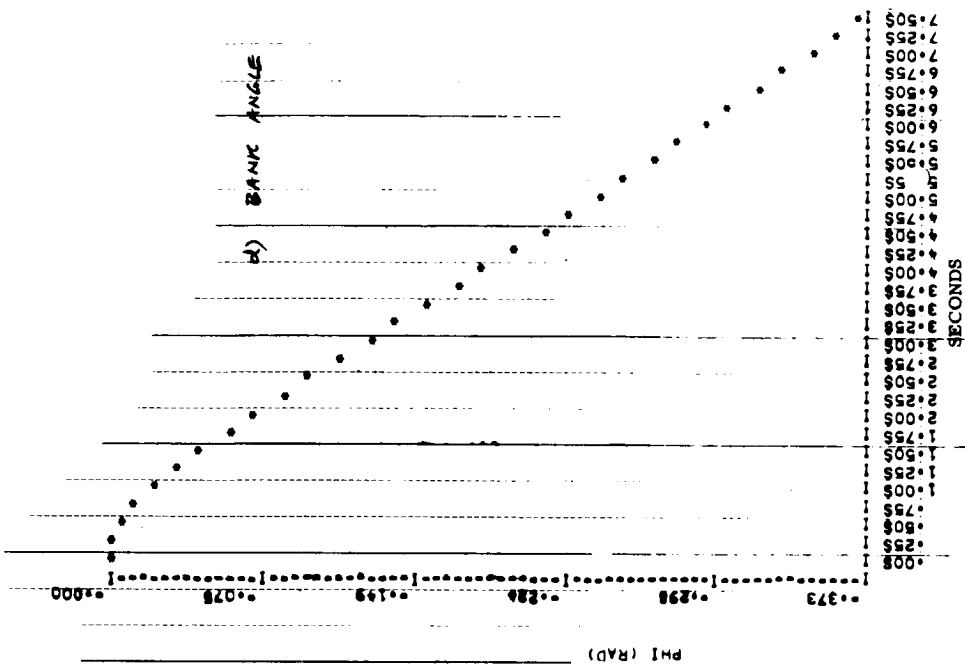


Figure 78. Continued

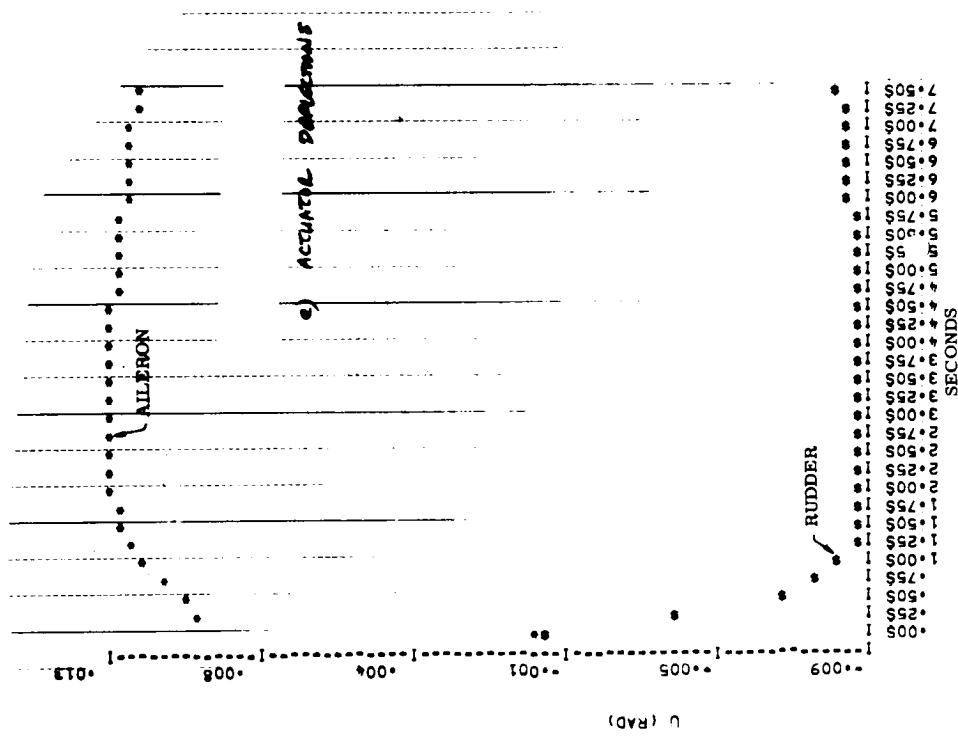


Figure 78. Concluded

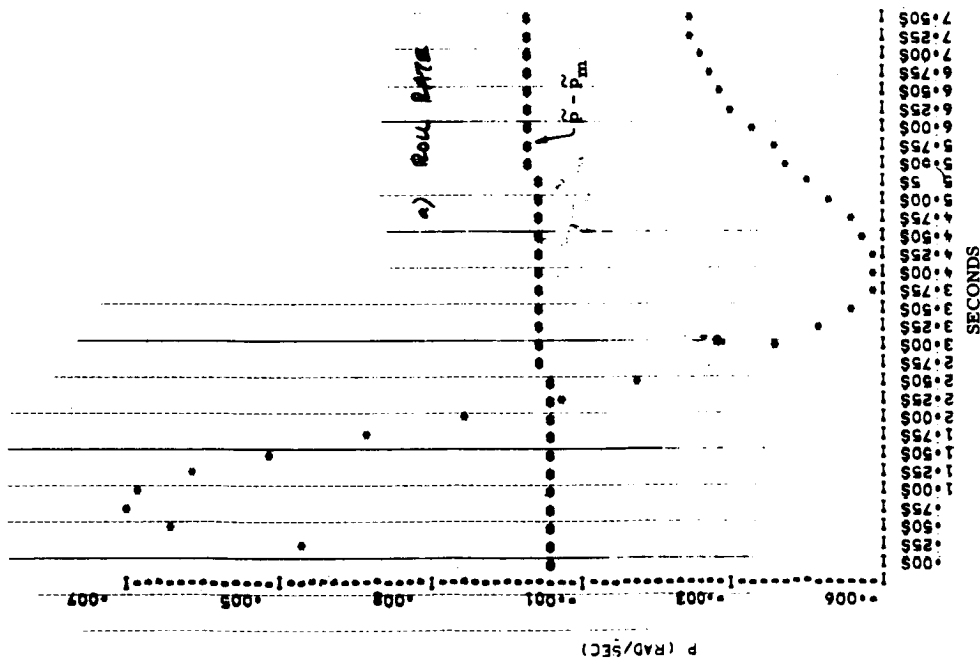
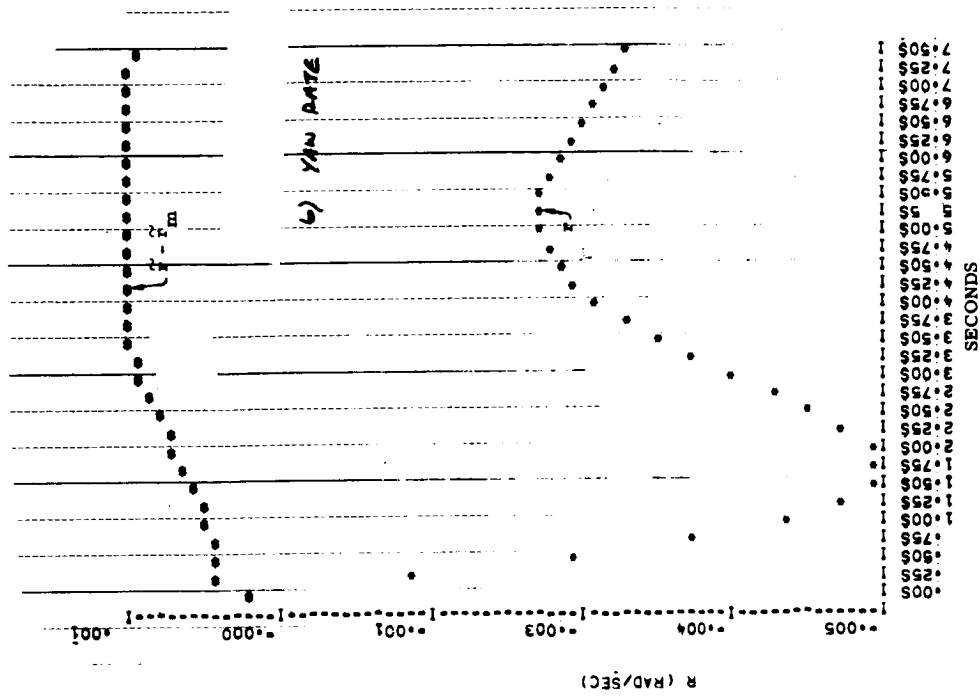


Figure 79. Step Responses, FC9 with Aileron/Rudder Control
0.030 Rad Lateral Command

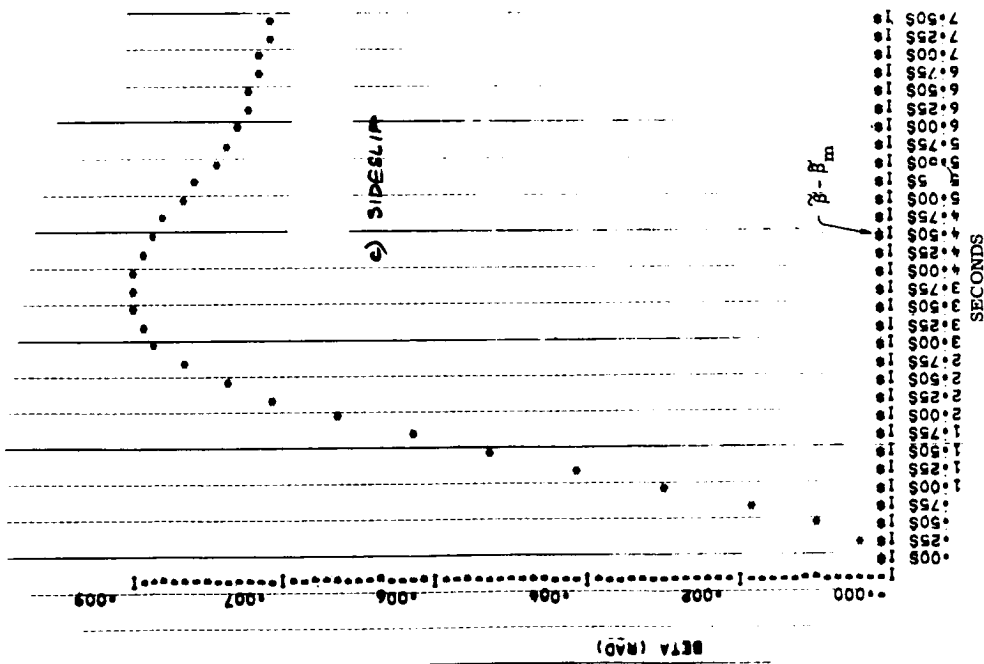
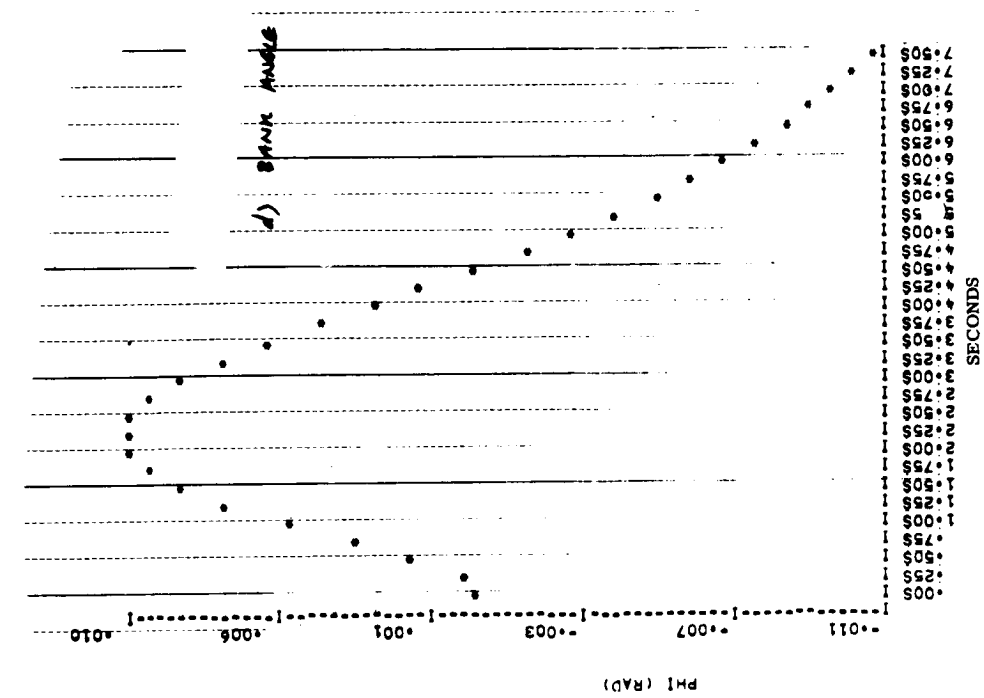


Figure 79. Step Responses, FC9 with Aileron/Rudder Control
0.030 Rad Lateral Command (Continued)

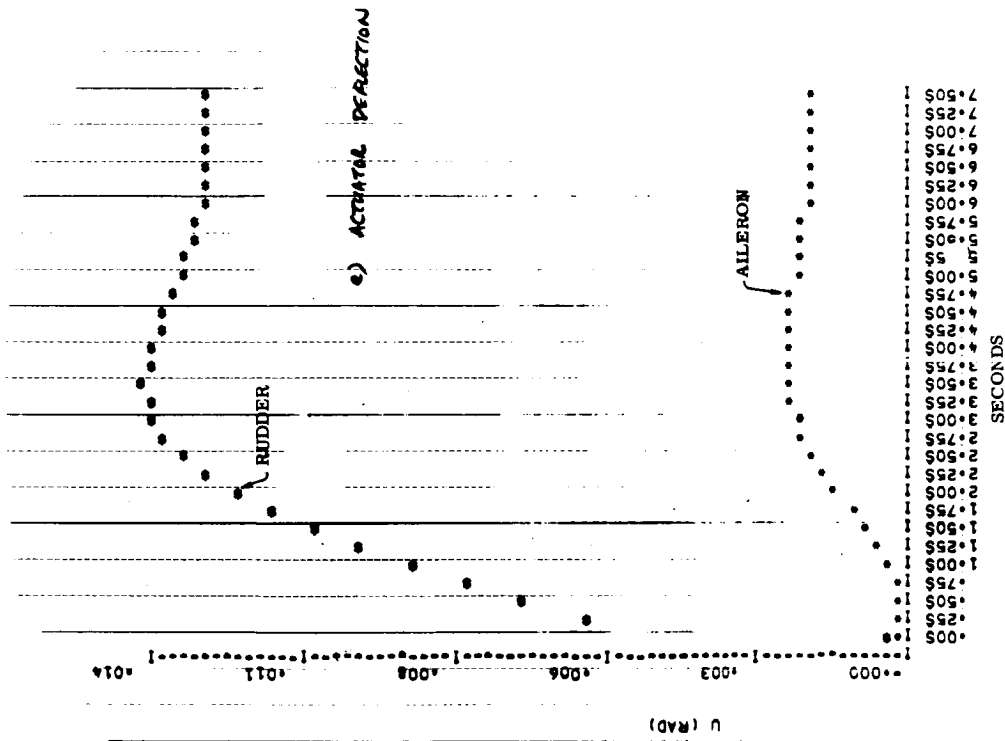


Figure 80. Step Responses, FC9 with Aileron/Rudder Control
0.030 Rad Lateral Command (Continued)

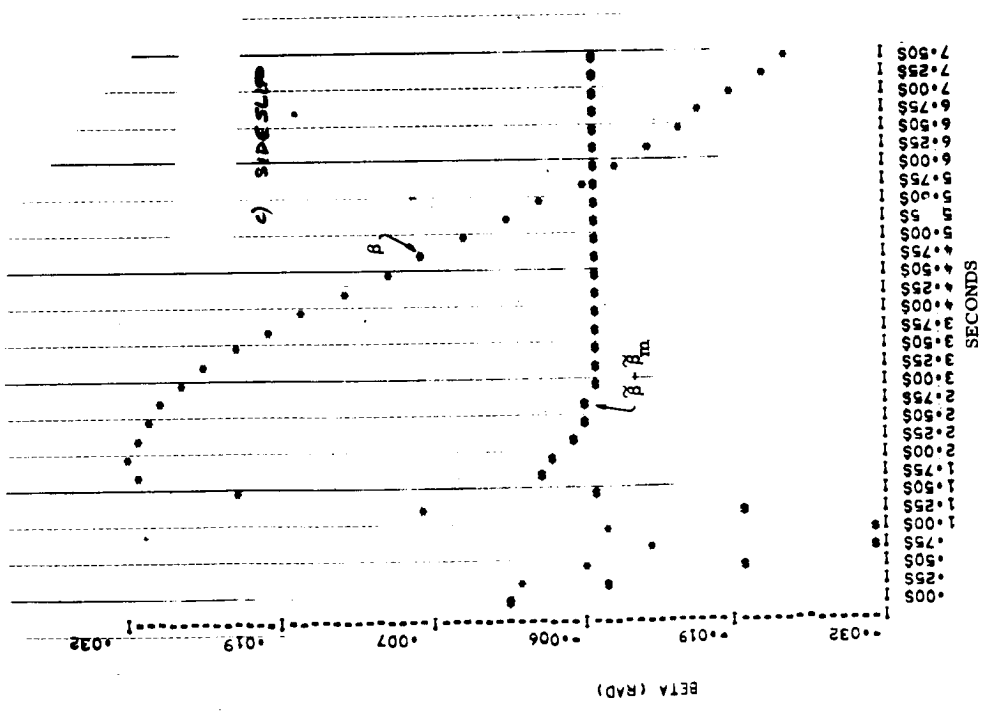
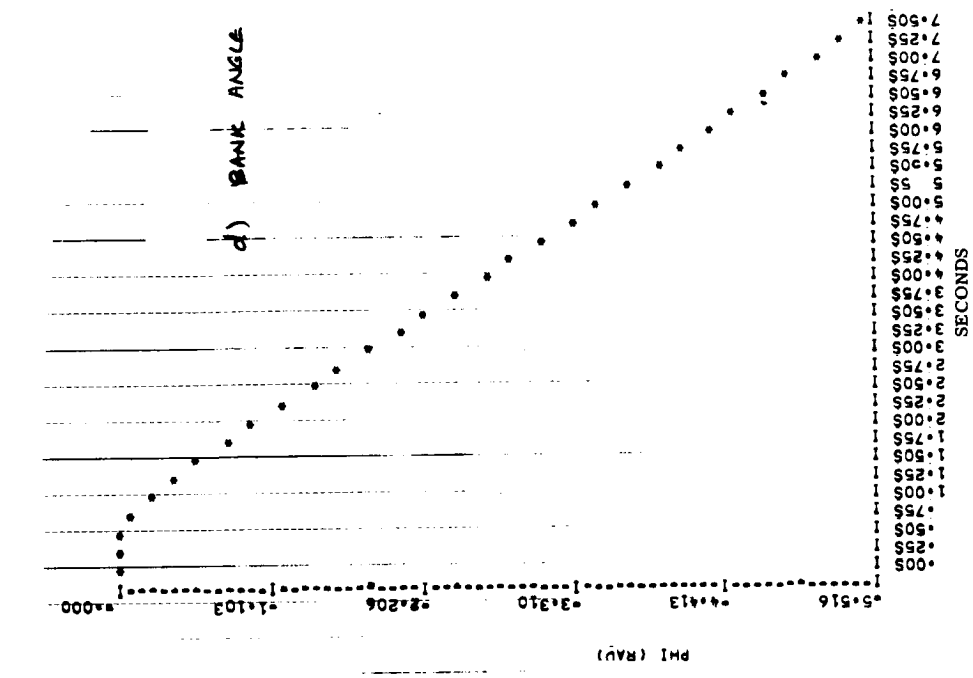


Figure 80. Continued

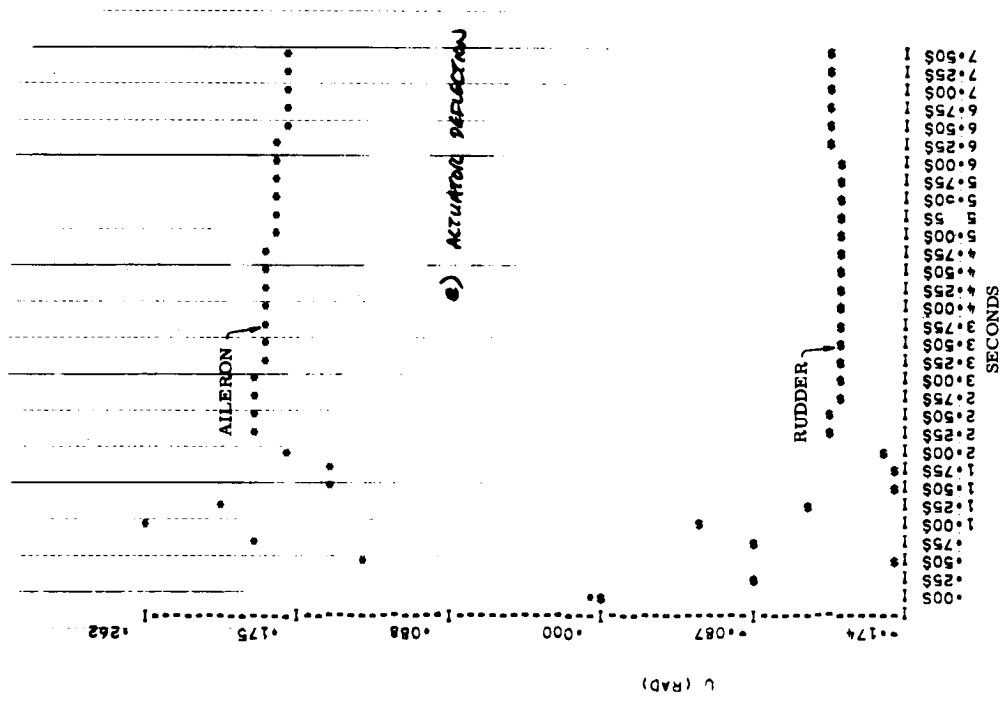


Figure 80. Concluded

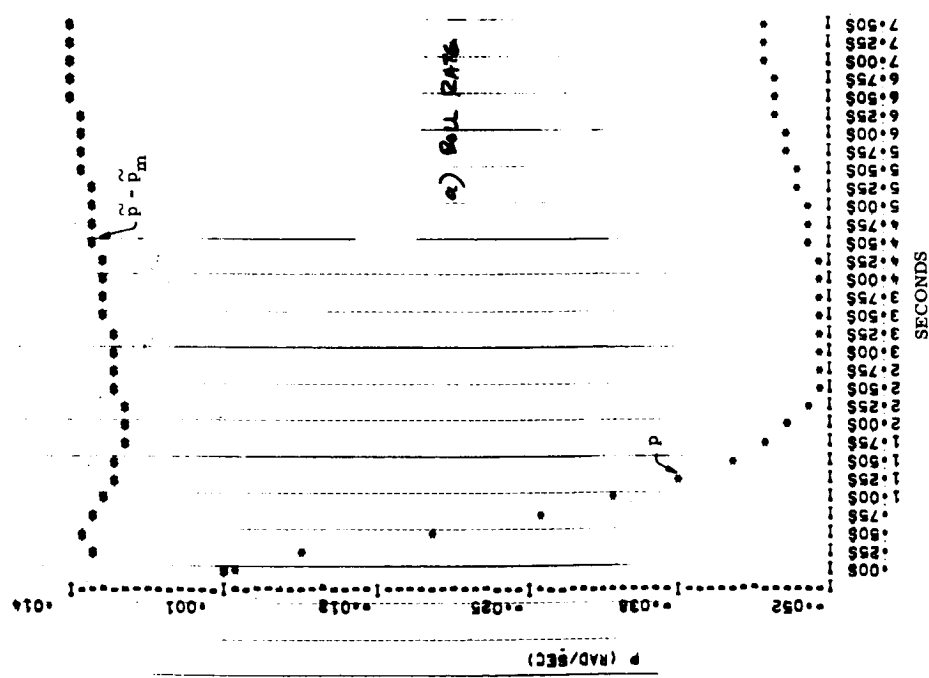
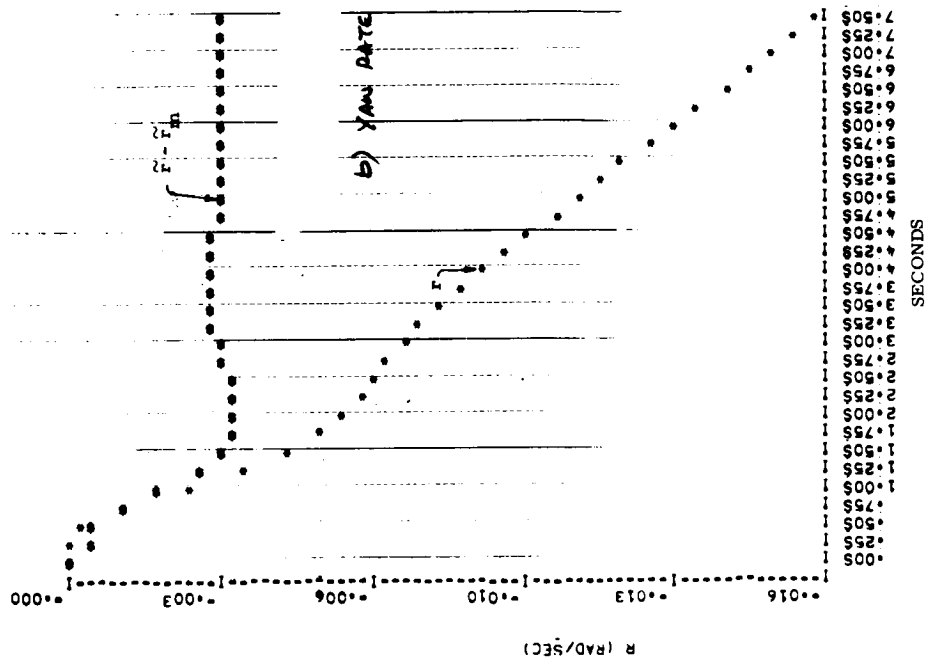


Figure 81. Step Responses FC9 Spoiler/Rudder Control
0.03 Rad Lateral Command

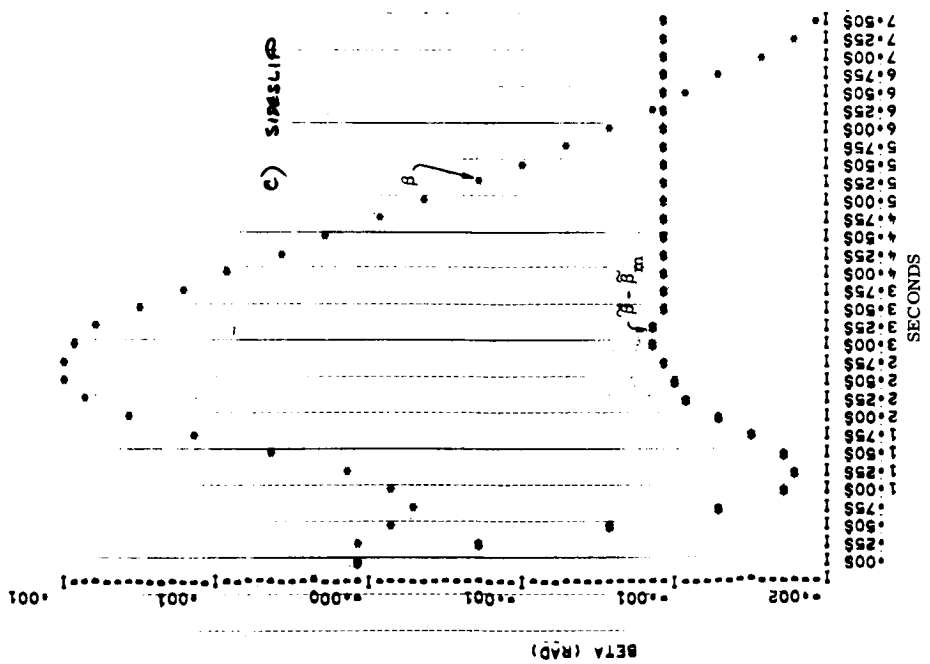
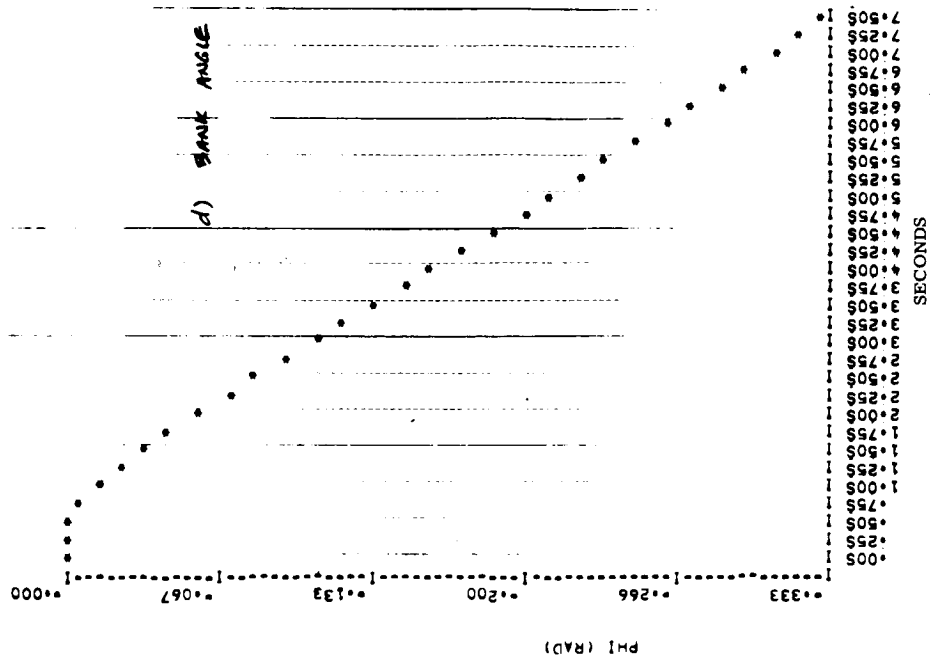


Figure 81. Continued

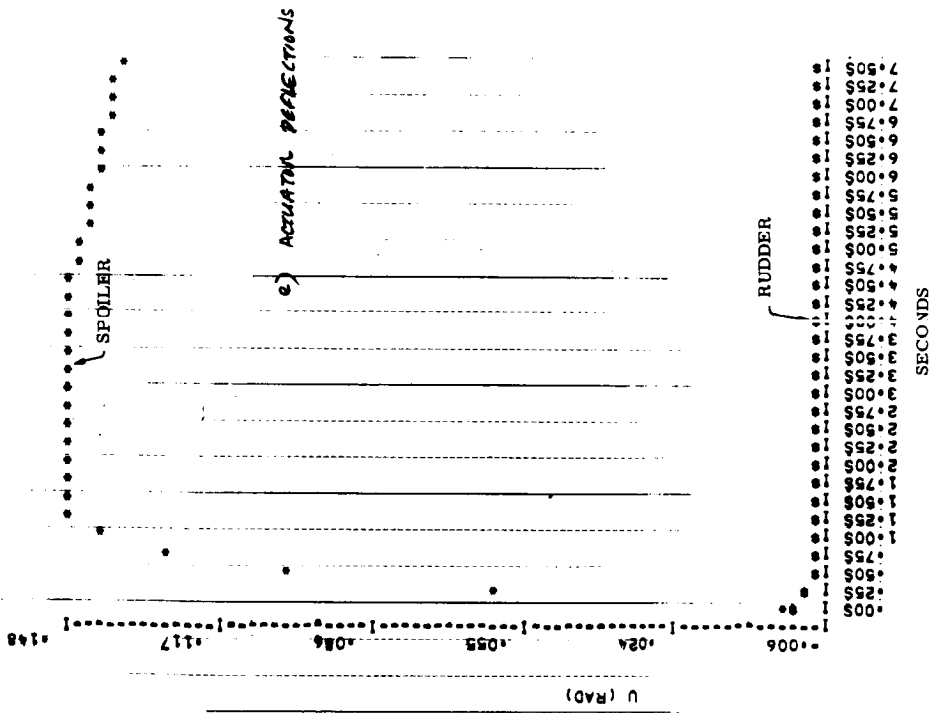


Figure 81. Concluded

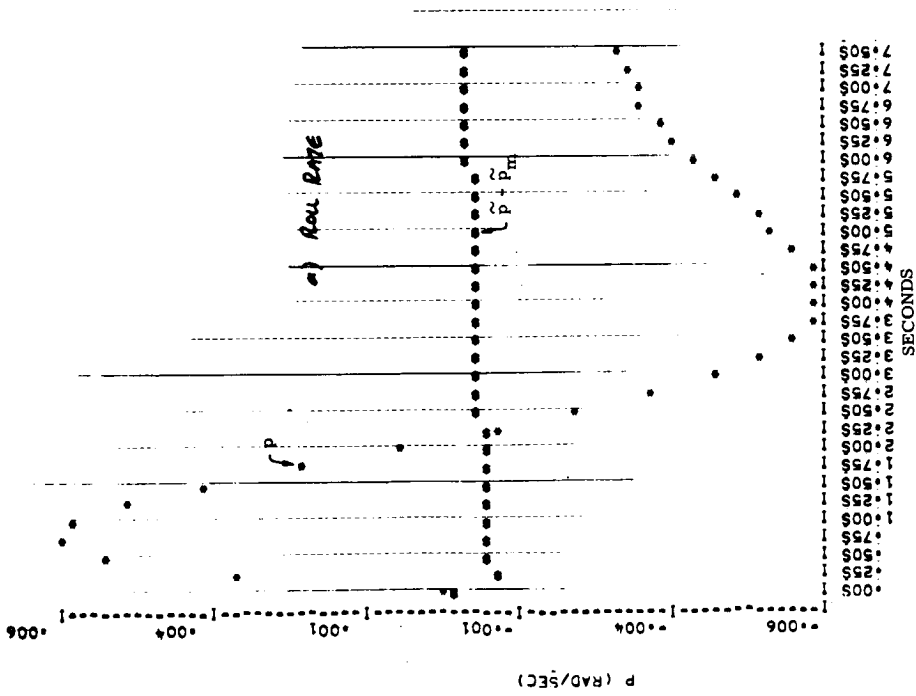
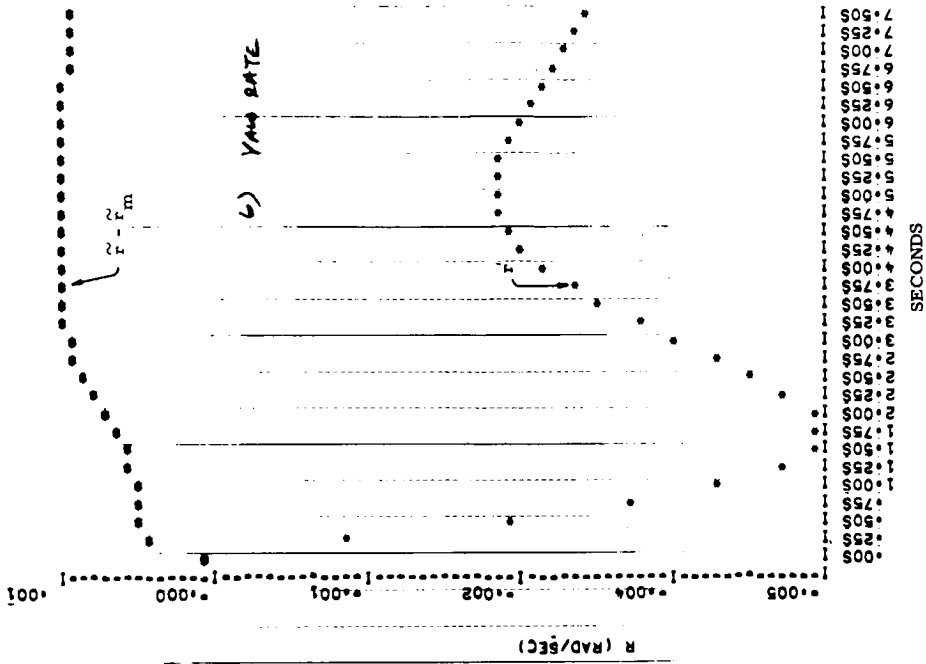


Figure 82. Step Responses, FC9 Spoiler/Rudder Control
0.015 Rad Rudder Command

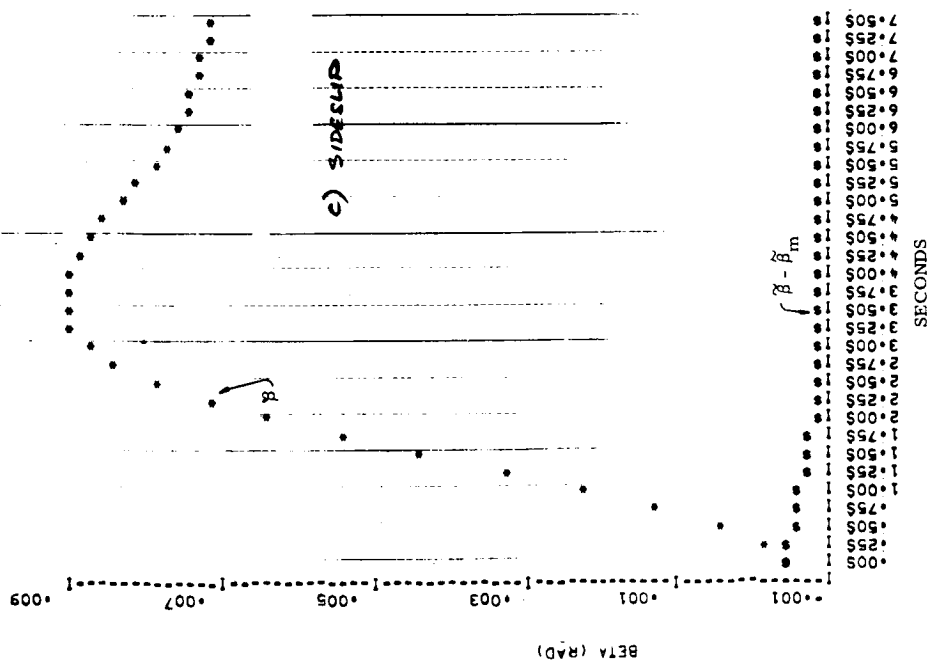
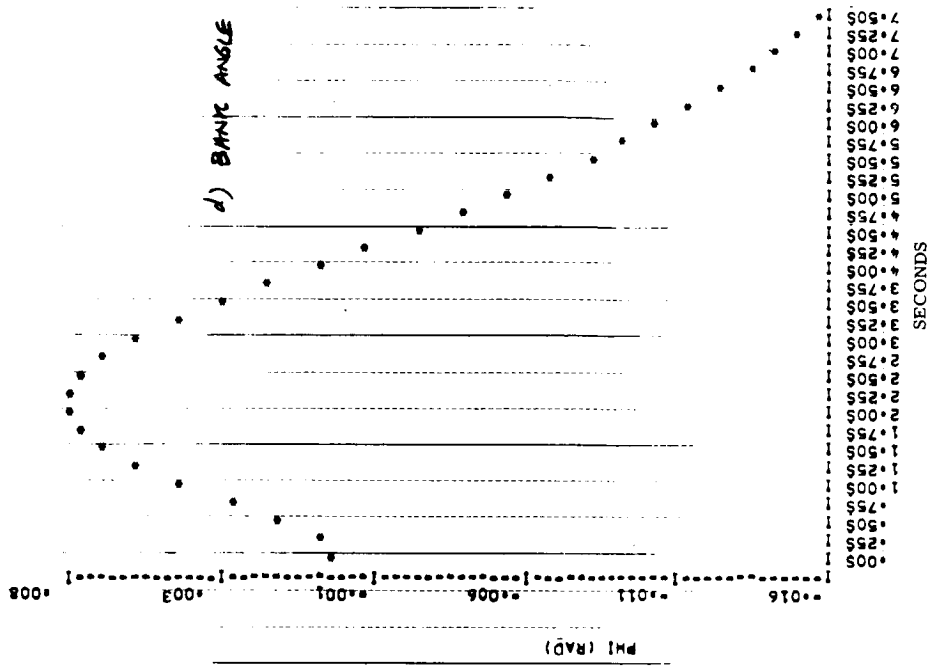


Figure 82. Continued

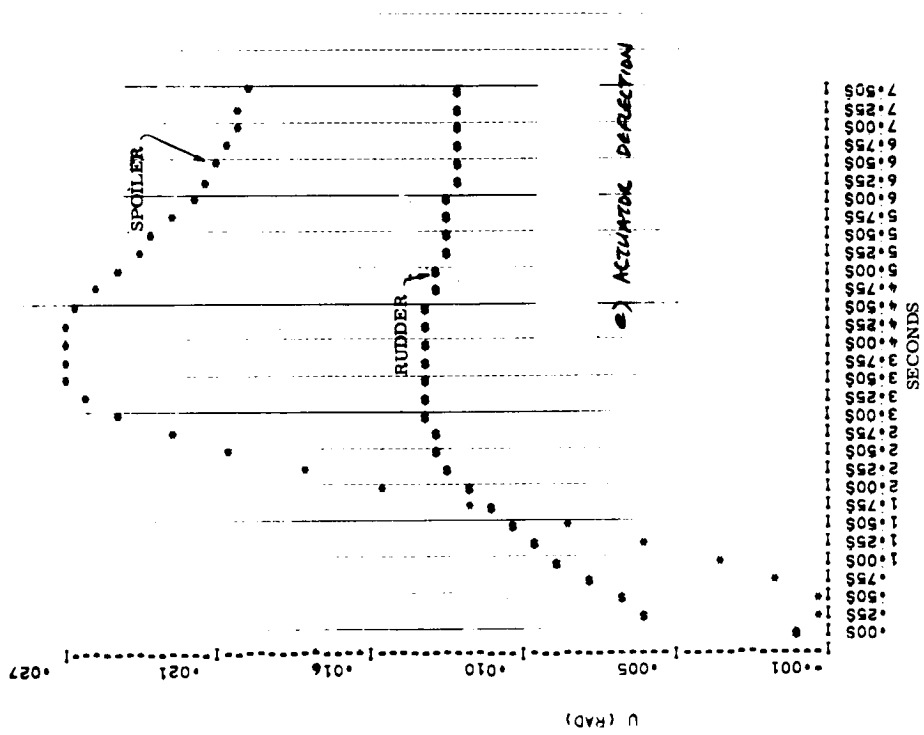


Figure 82. Concluded

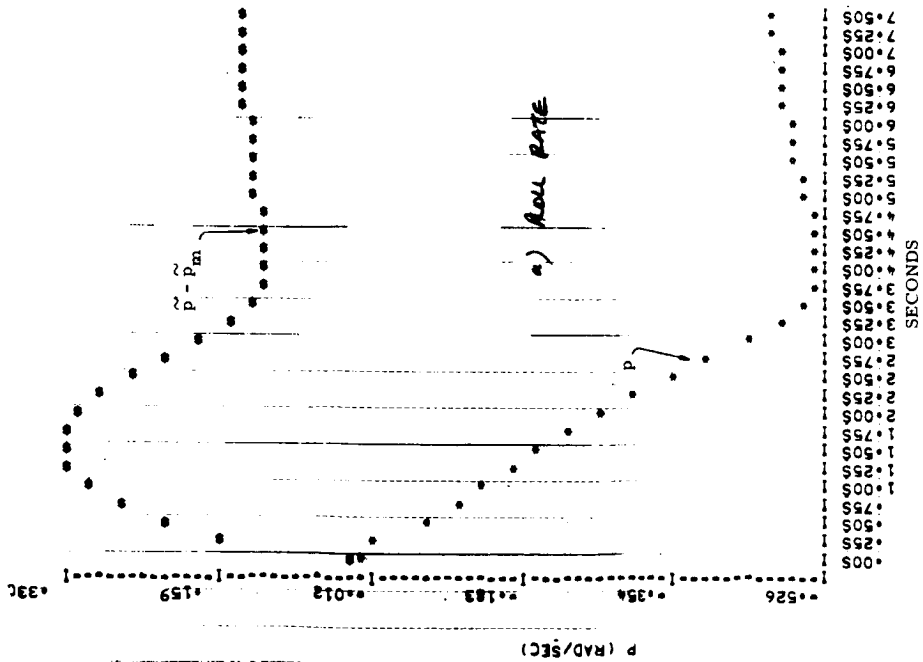
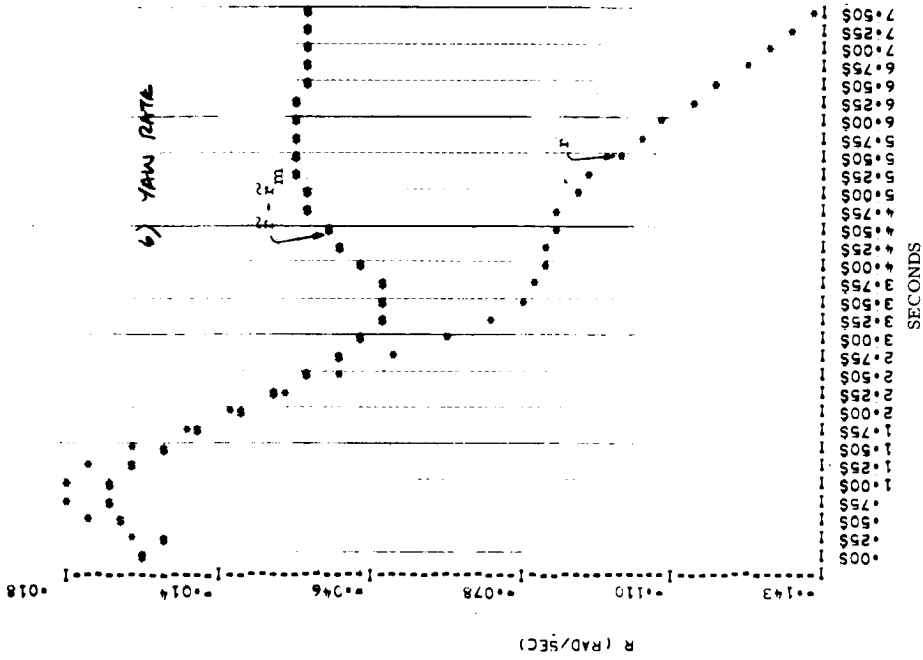


Figure 83. Step Responses FC9 Spoiler/Rudder Control Maximum Lateral Command

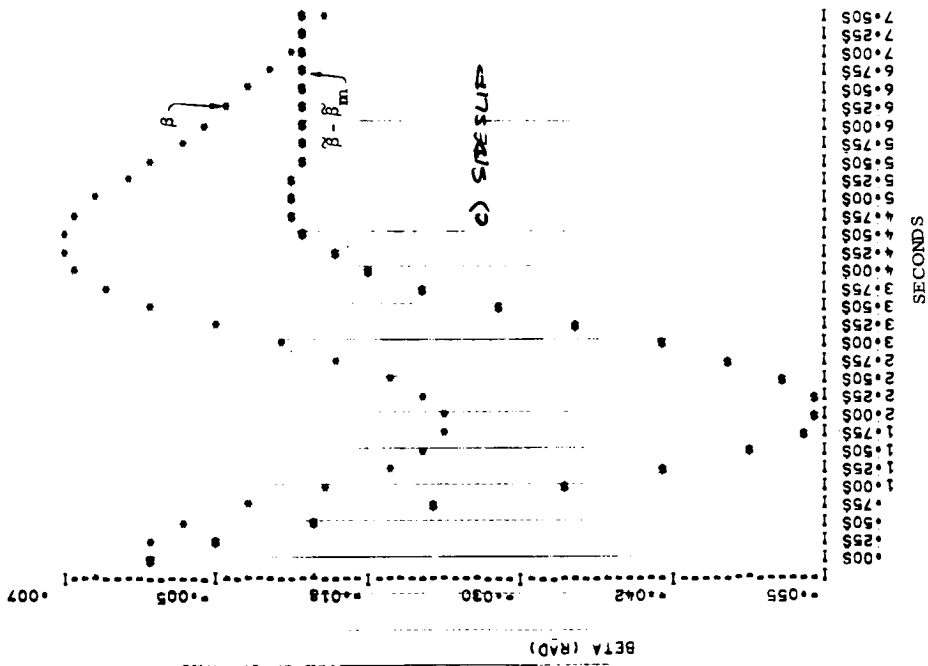
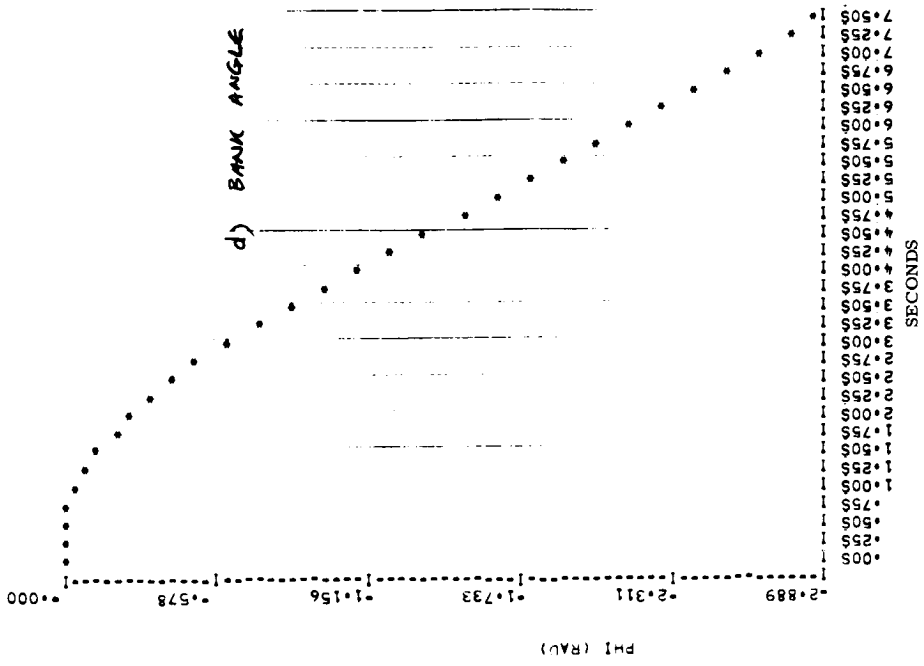


Figure 83. Continued

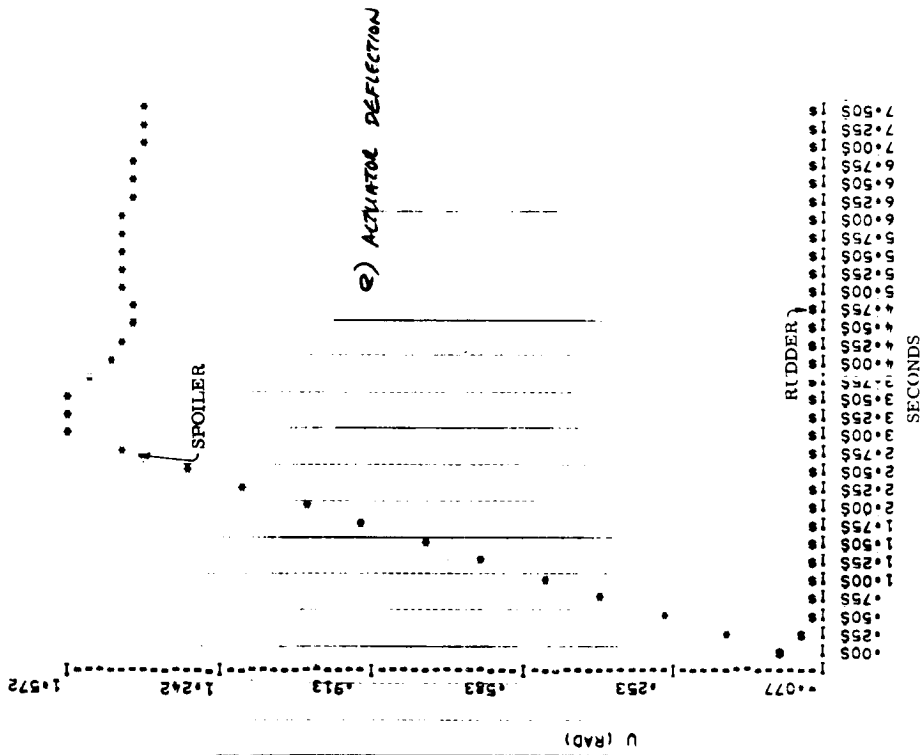


Figure 83. Concluded

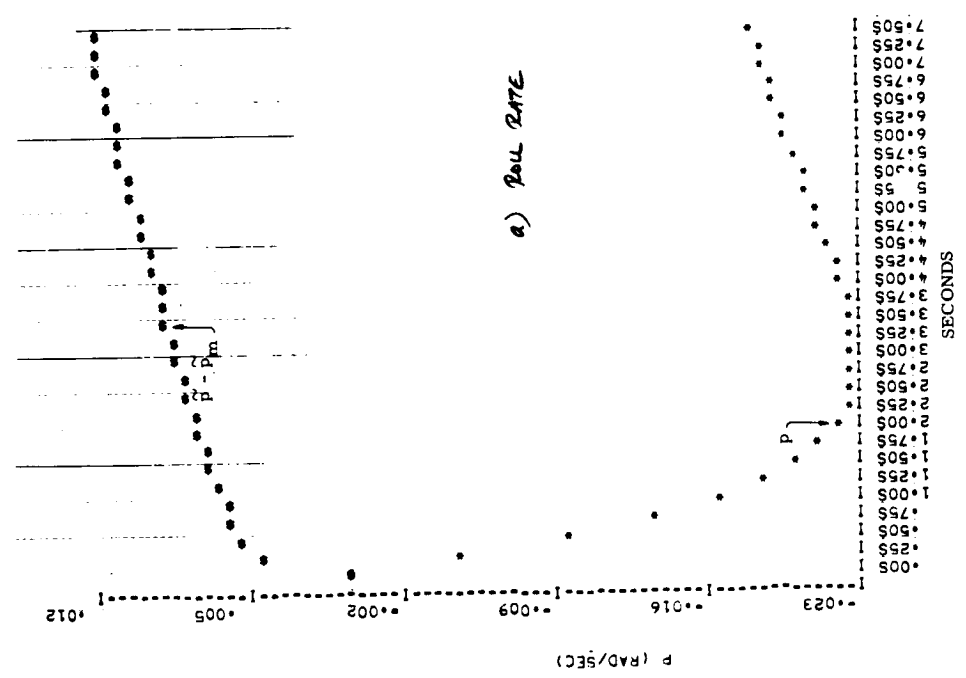
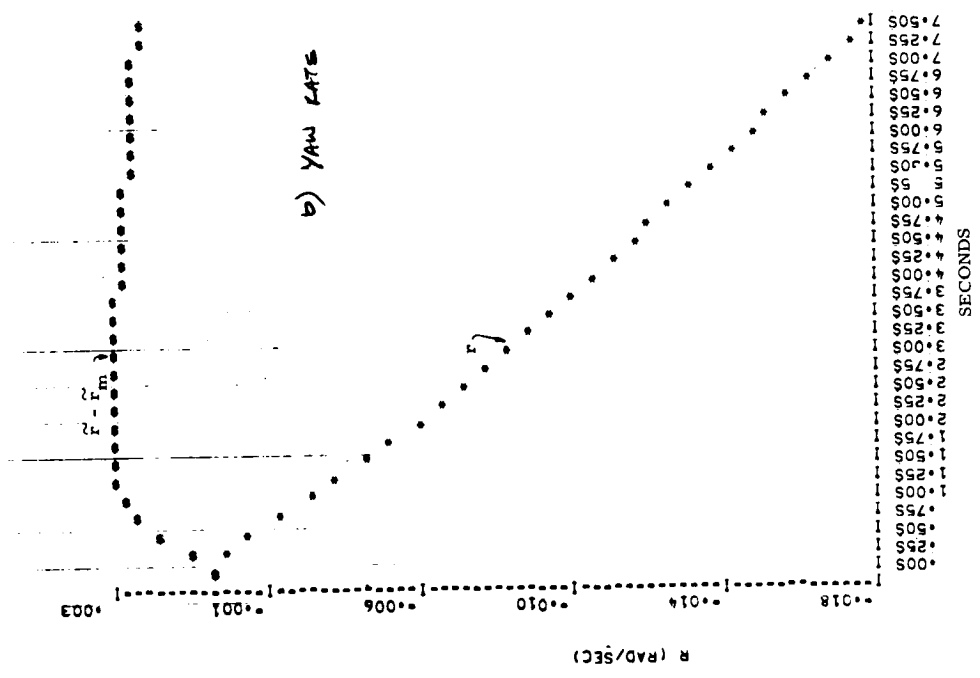


Figure 84. Step Responses FC11 Aileron/Rudder Control
0.03 Rad Lateral Command

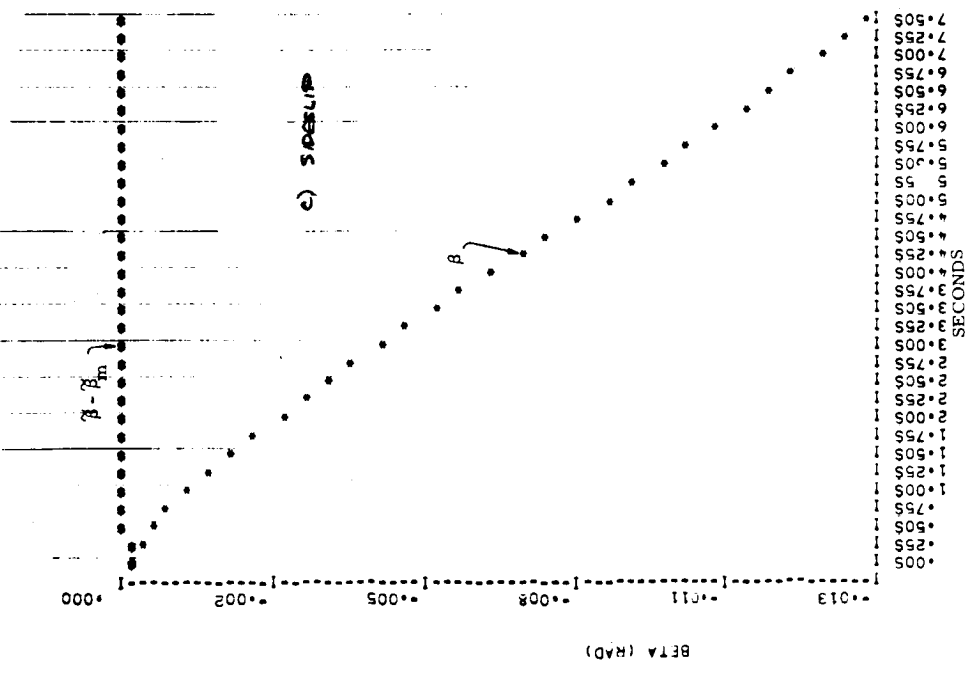
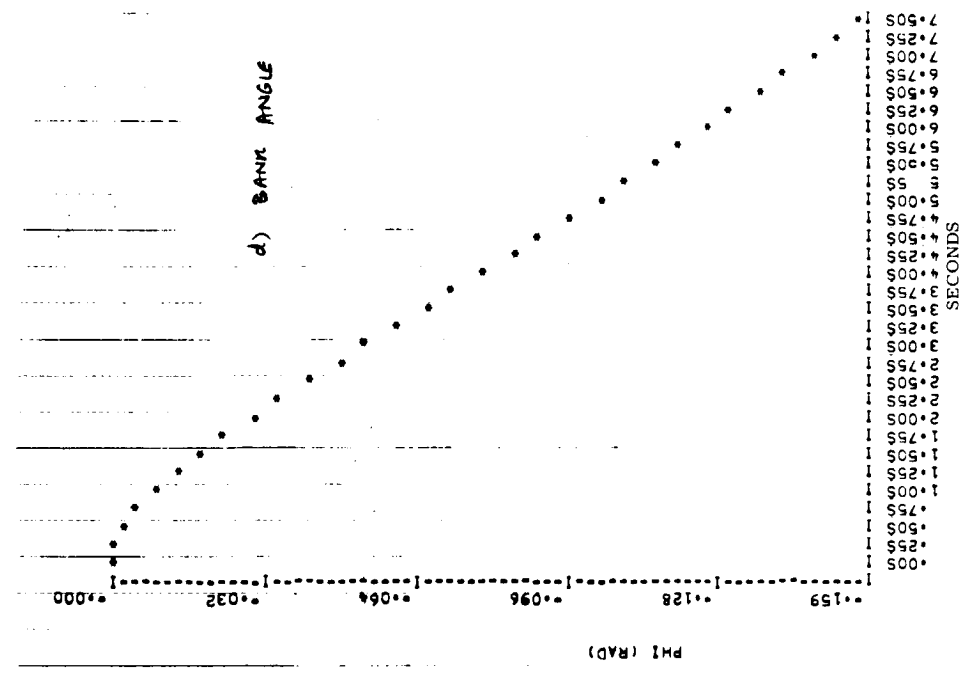


Figure 84. Continued

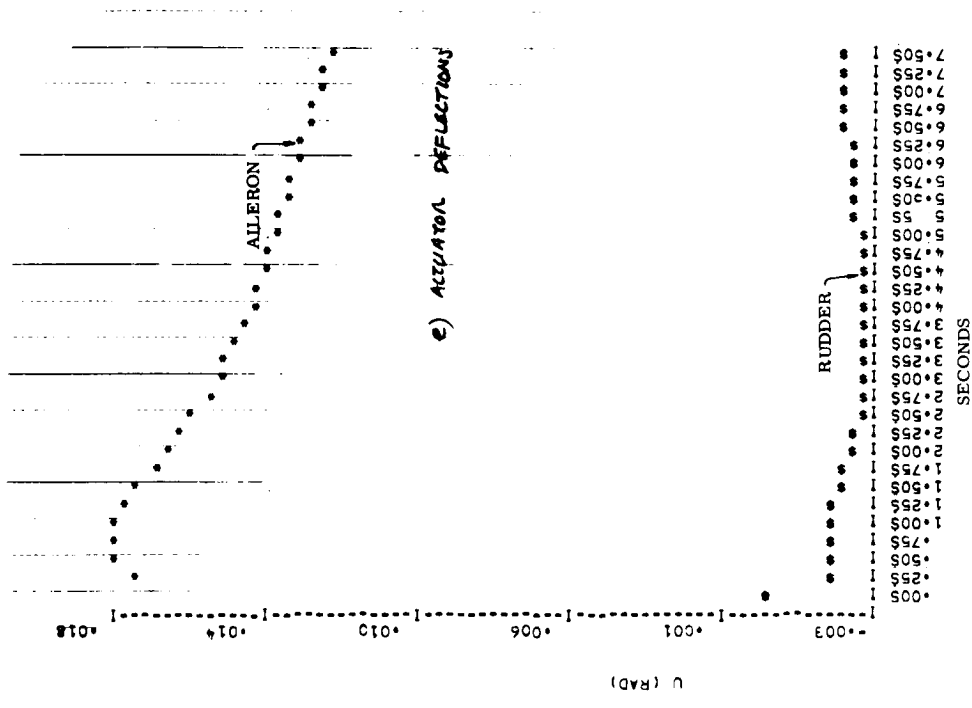


Figure 84. Concluded

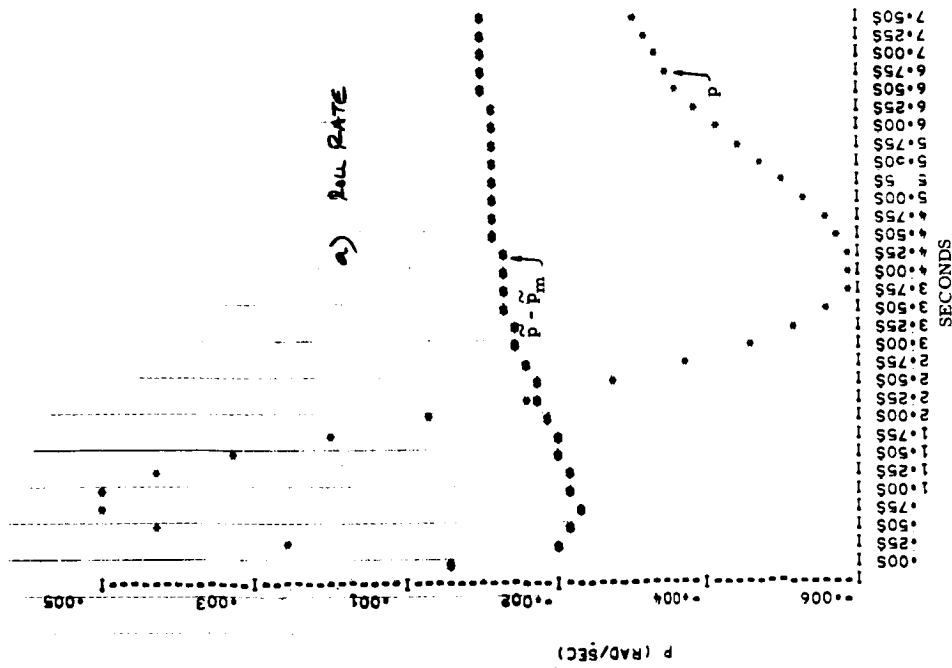
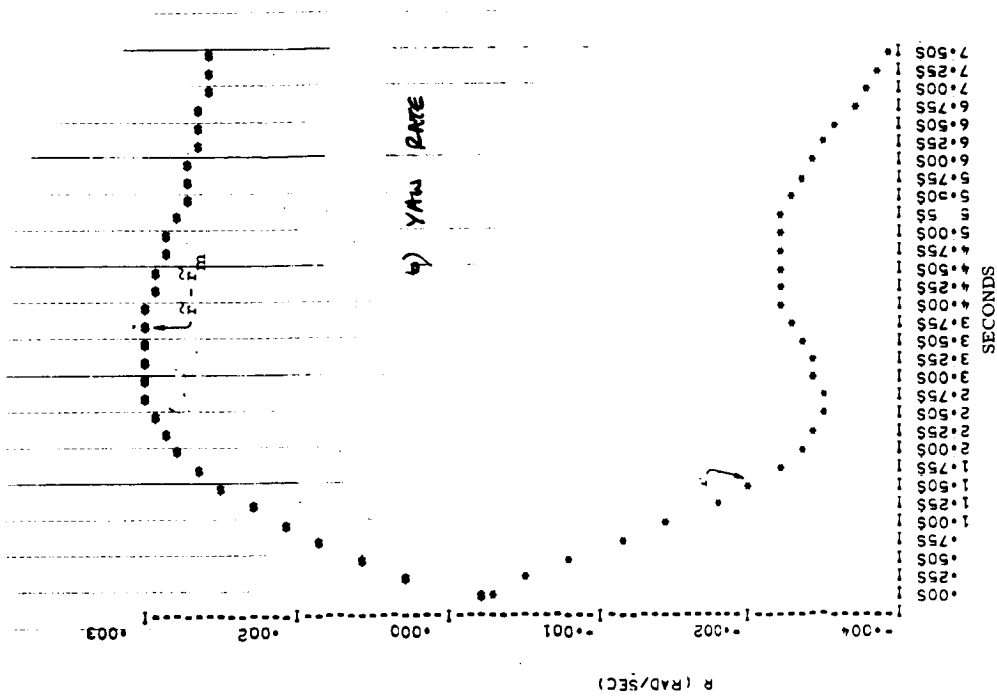


Figure 85. Step Responses FC11 Aileron/Rudder Control
0.015 Rad Rudder Command

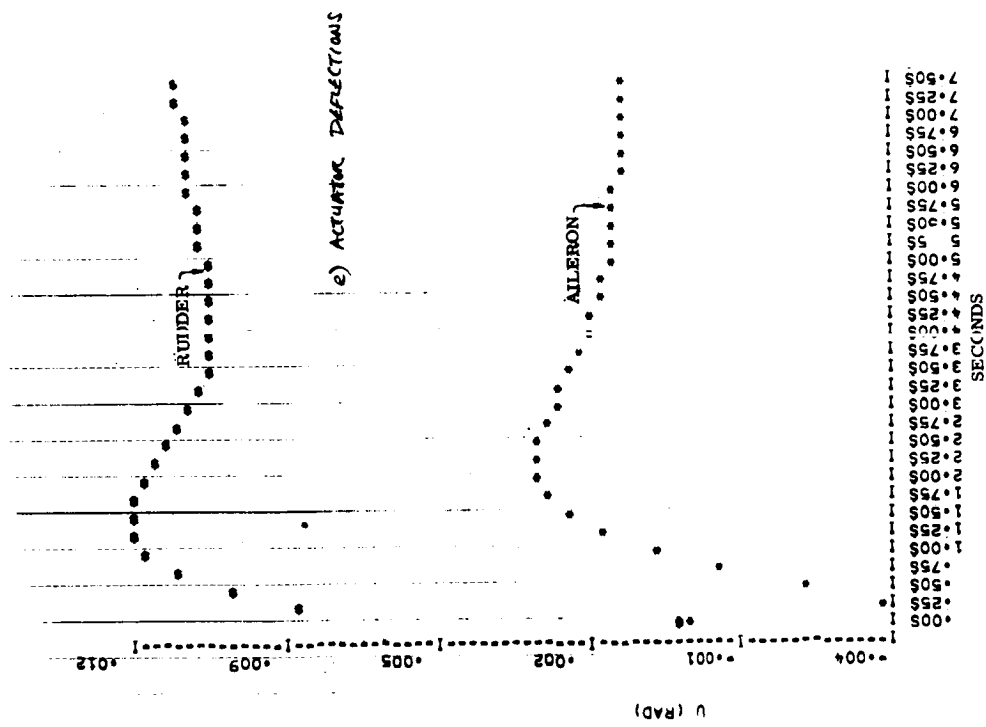


Figure 85. Concluded

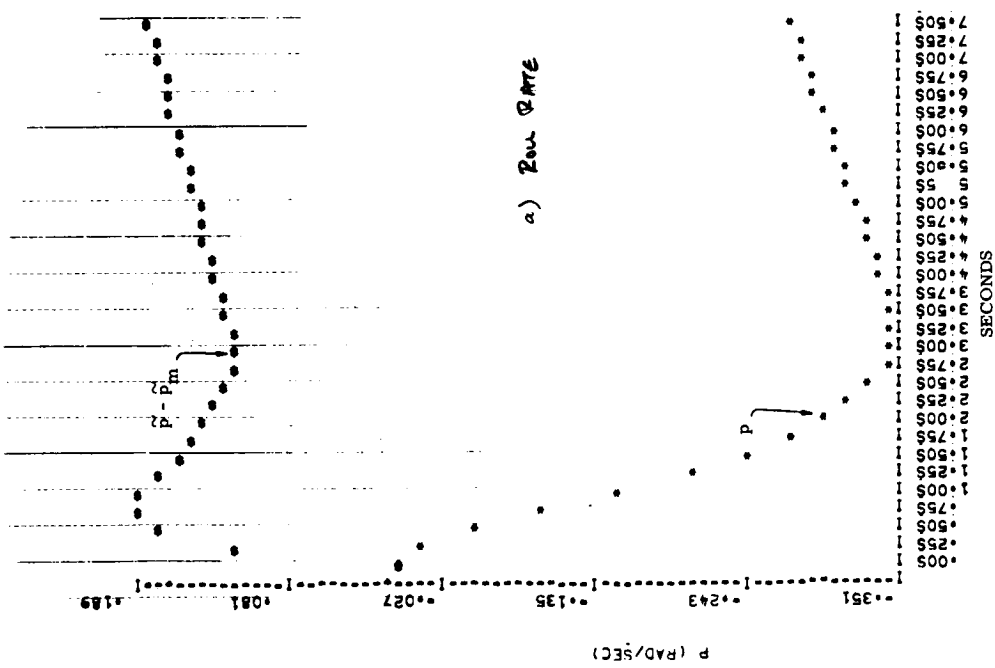
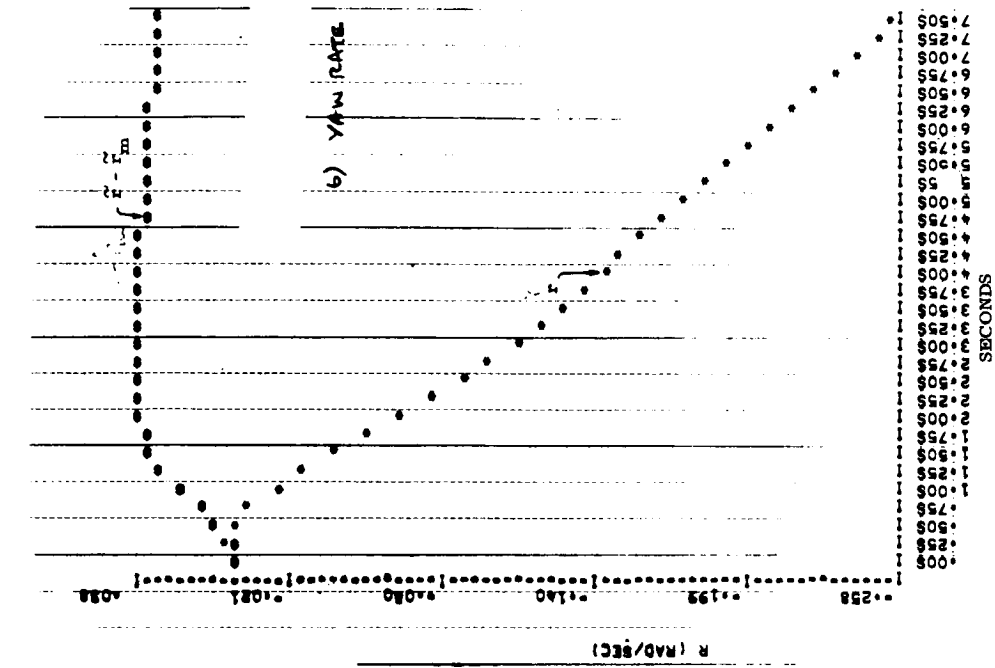


Figure 86. Step Responses FC11 Aileron/Rudder Control Maximum Lateral Command

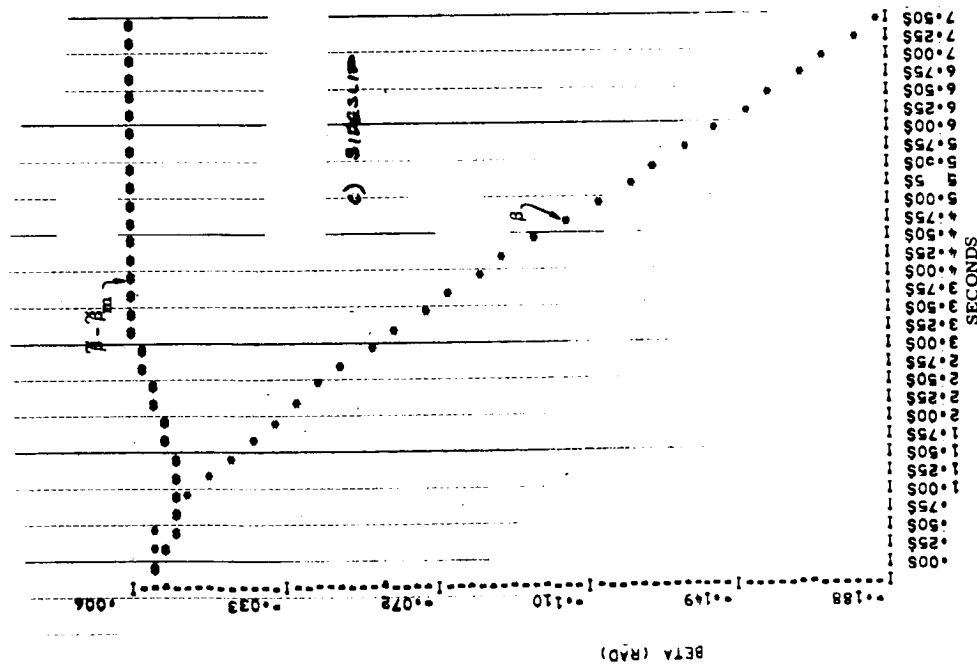
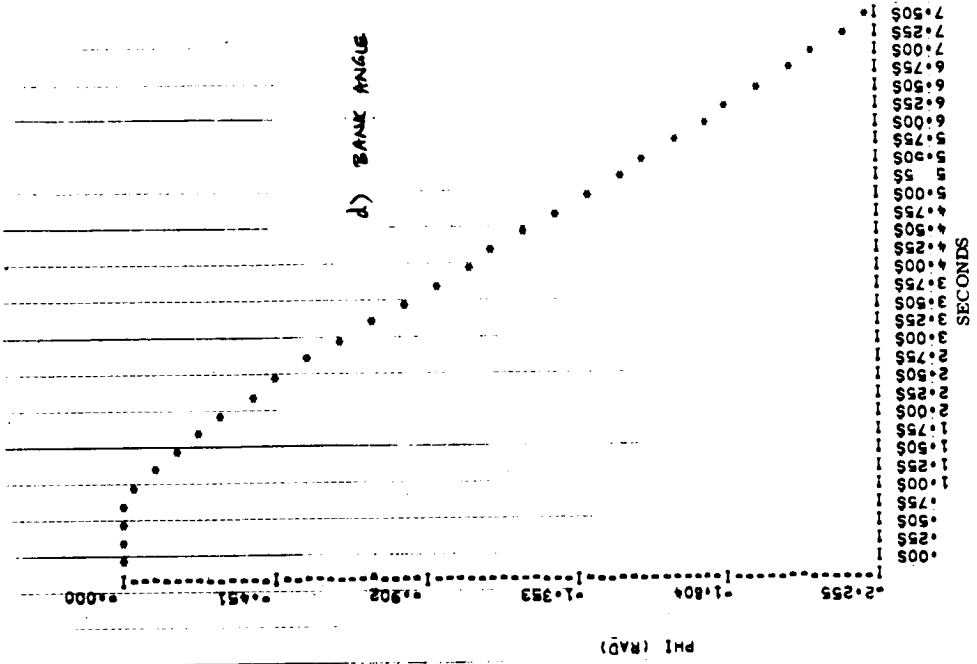


Figure 86. Continued

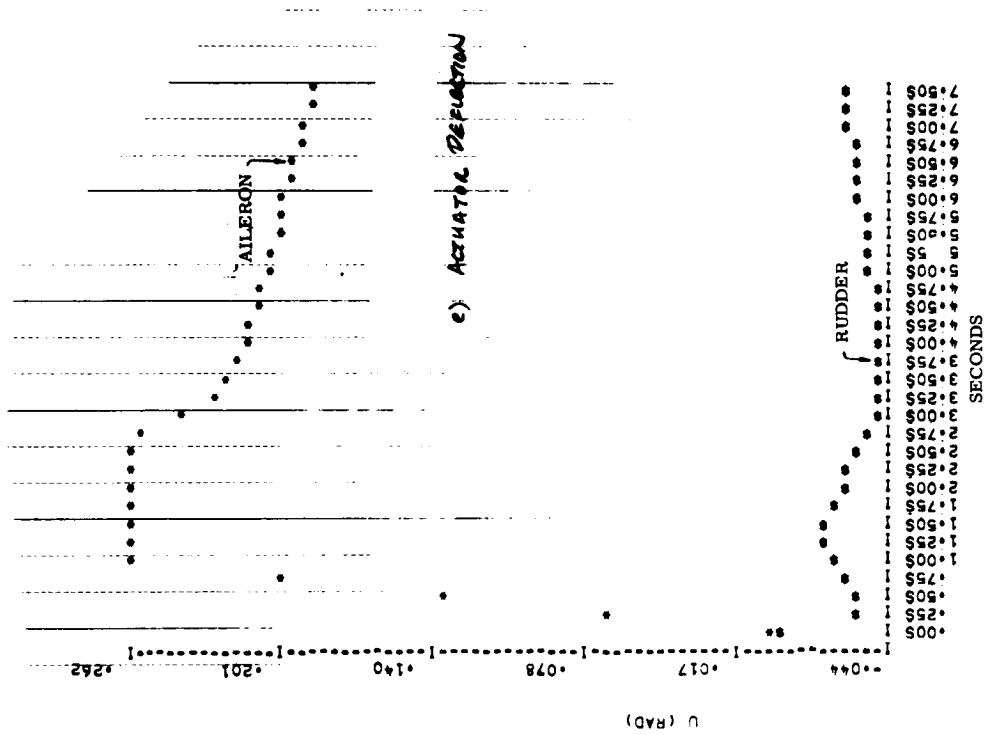


Figure 86. Concluded

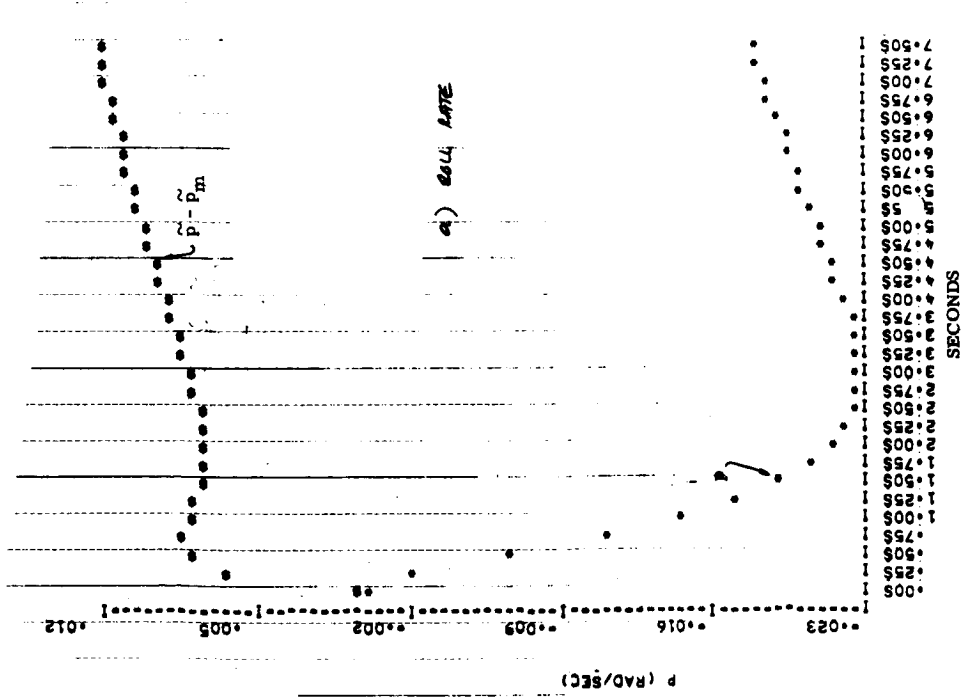
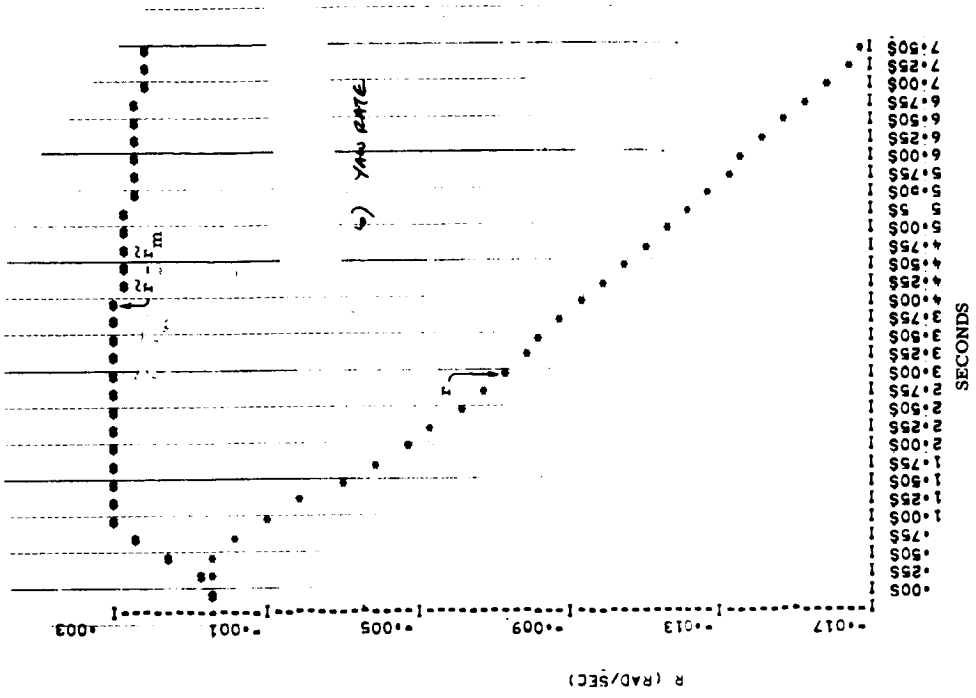


Figure 87. Step Responses, FC-11 Spoiler/Rudder Control
0.015 Rad Lateral Command

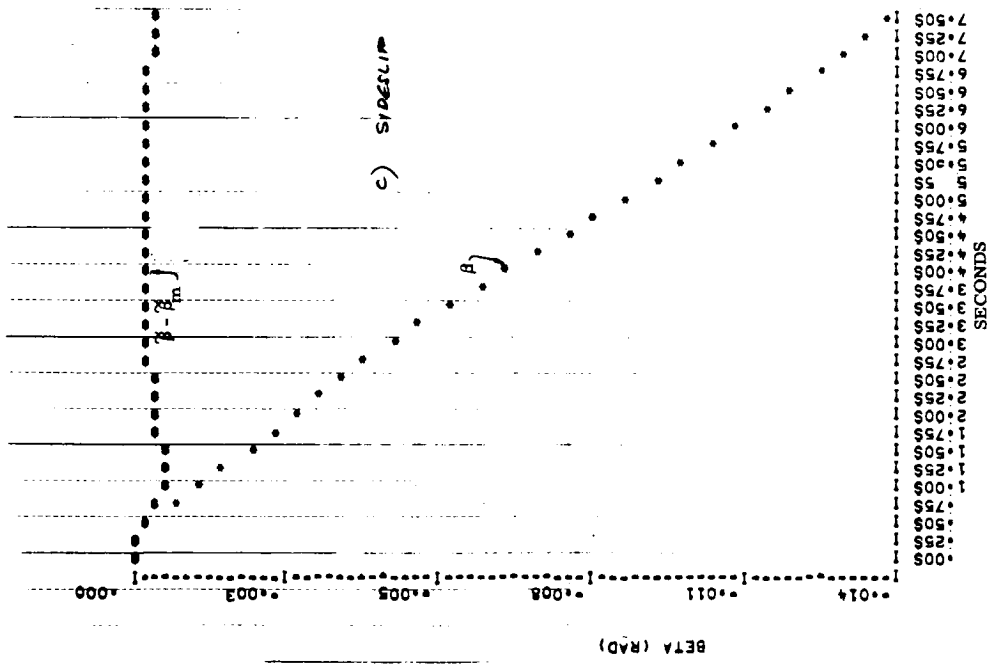
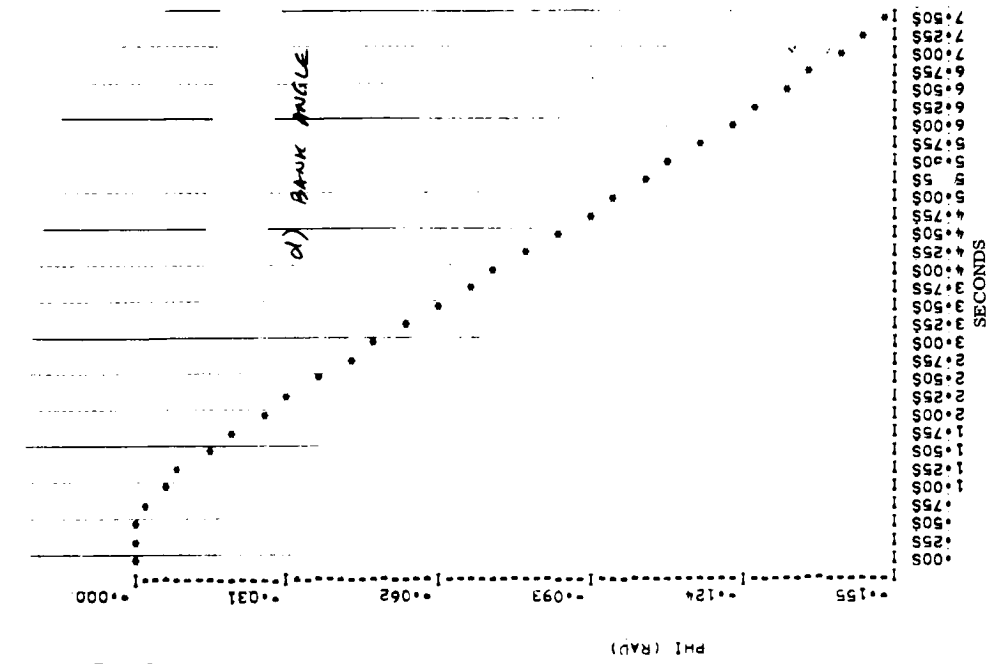


Figure 87. Continued

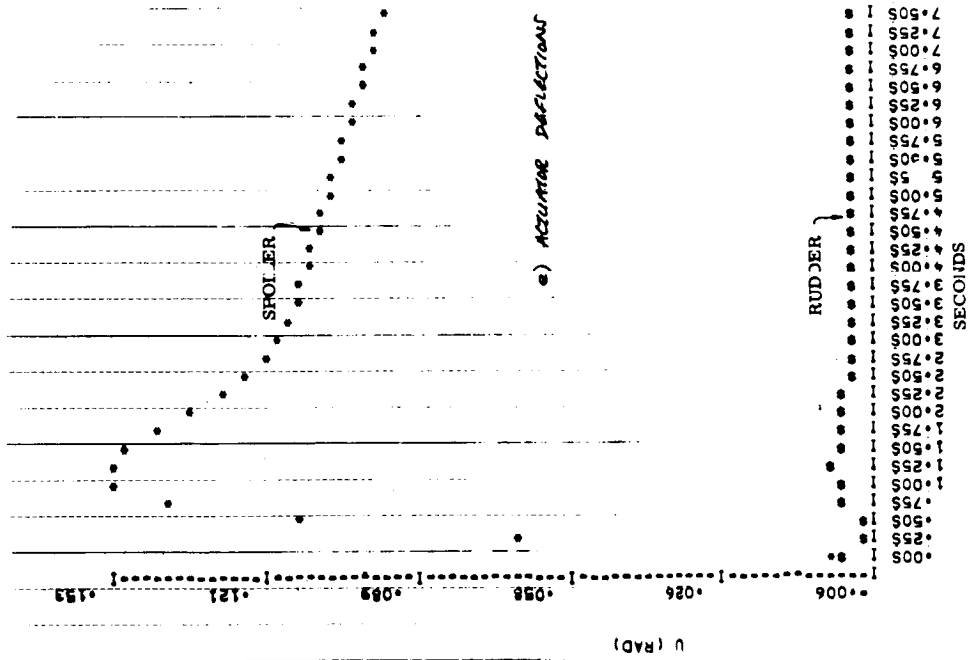


Figure 87. Concluded

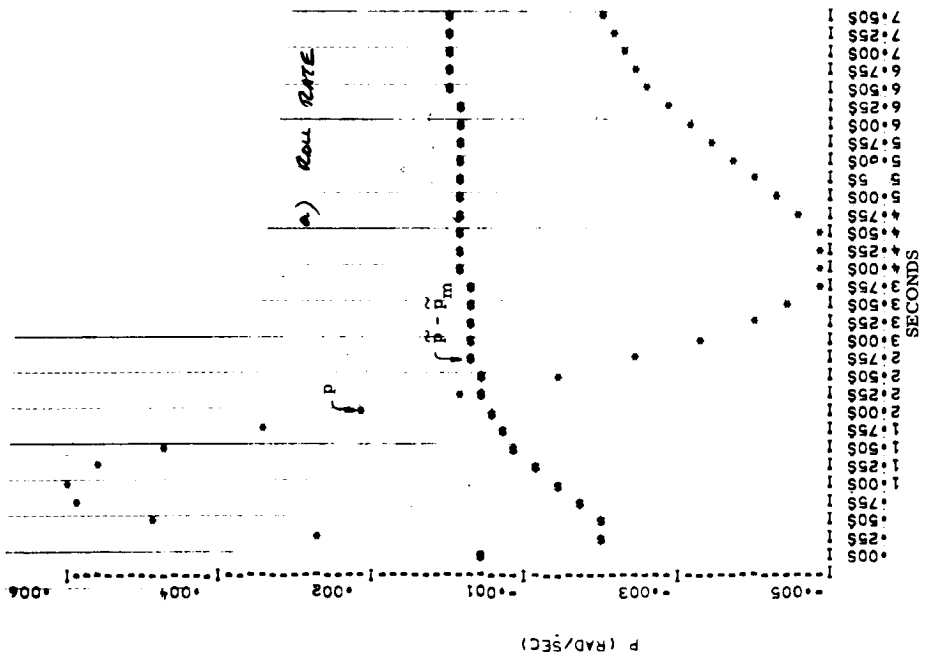
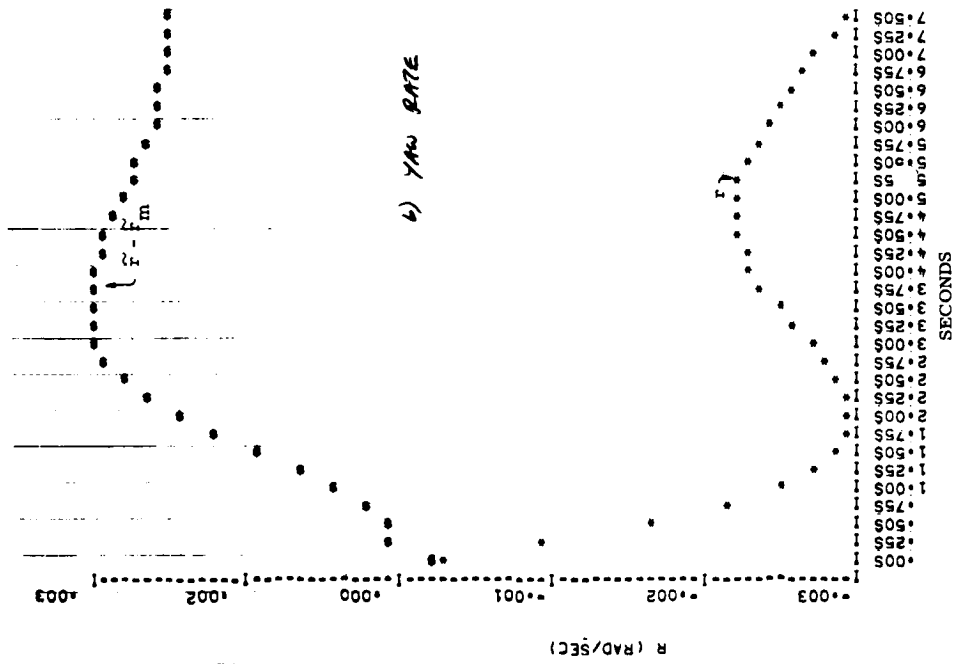


Figure 88. Step Responses FC11 Spoiler/Rudder Control
0.015 Rad Rudder Command

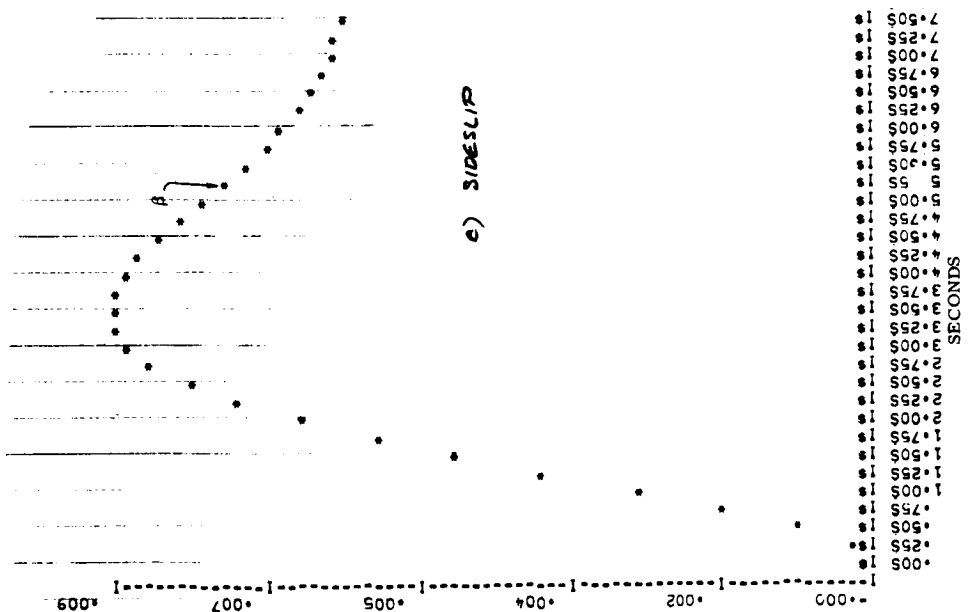
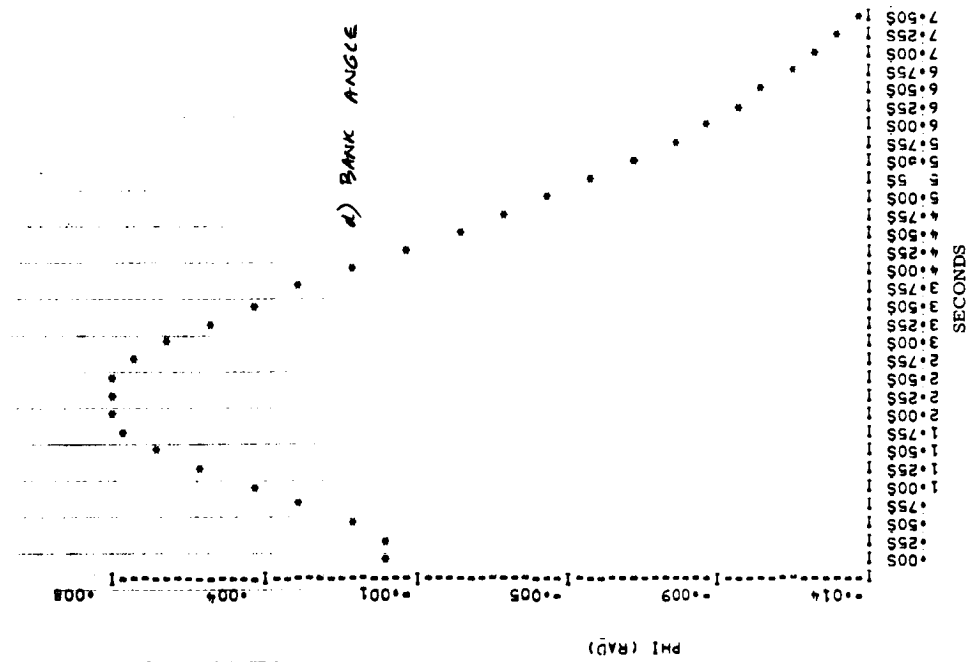


Figure 88. Continued

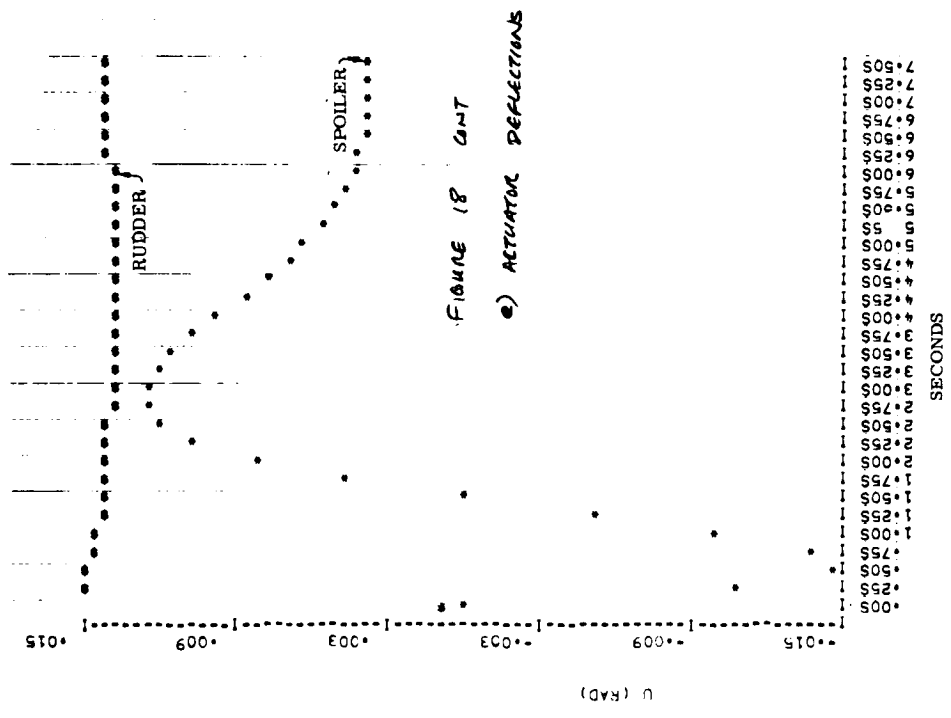


Figure 88. Concluded

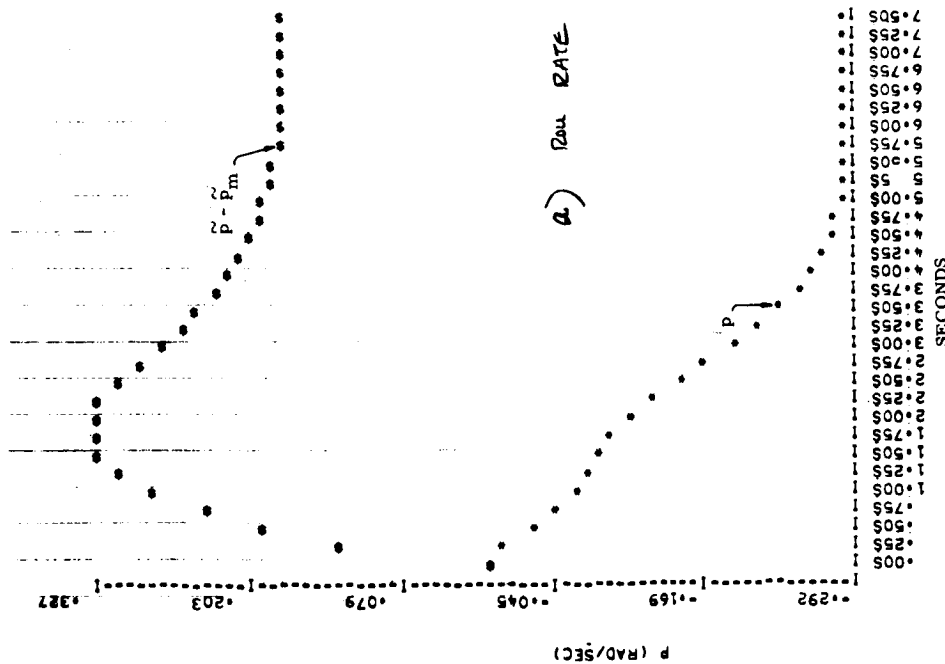
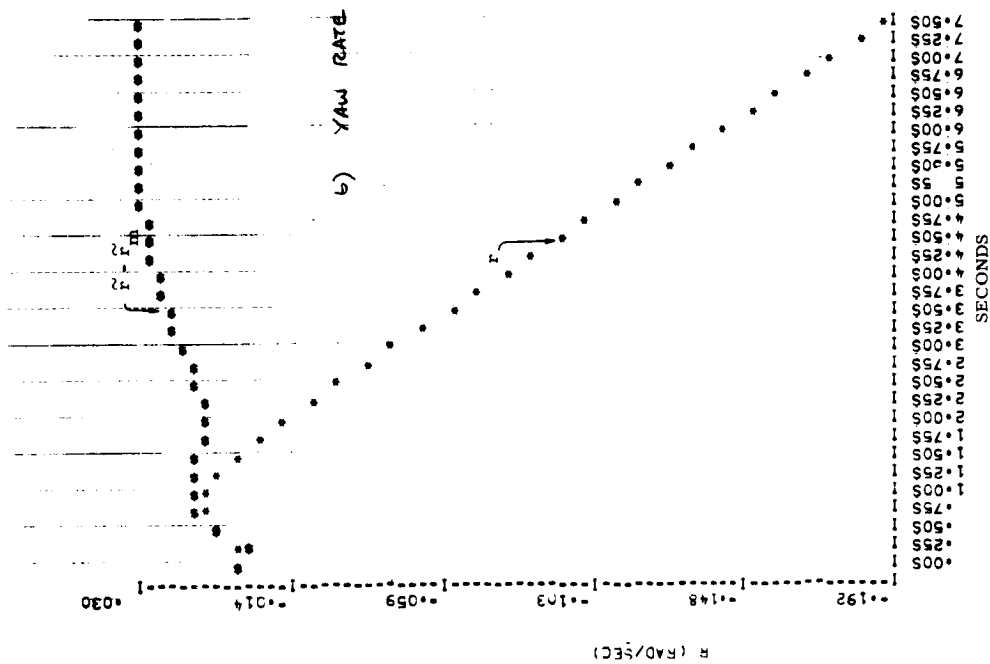


Figure 89. Step Responses, FC11 Spoiler/Rudder Control
Maximum Lateral Command

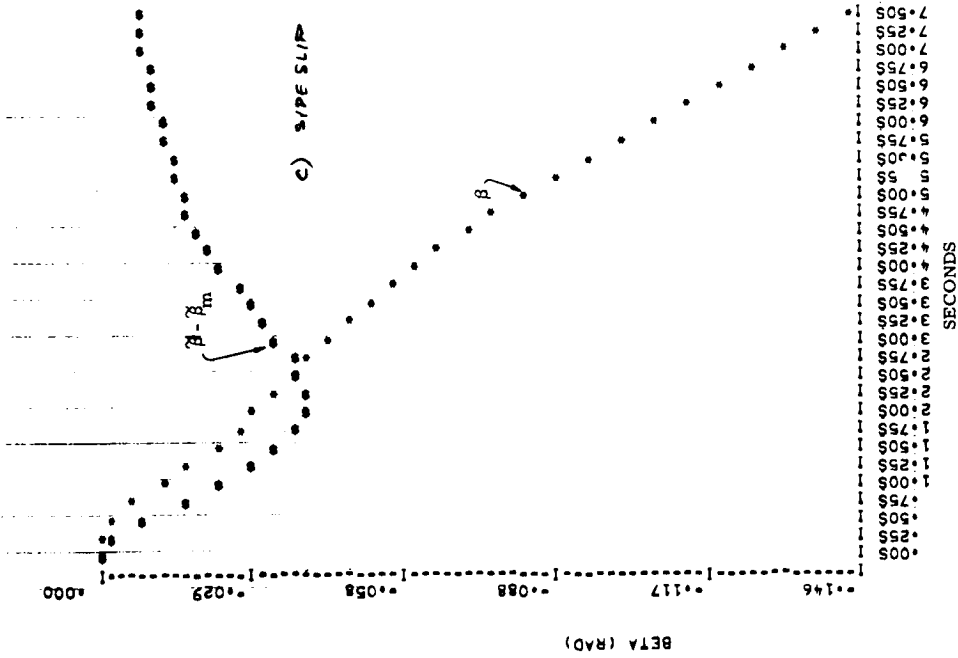
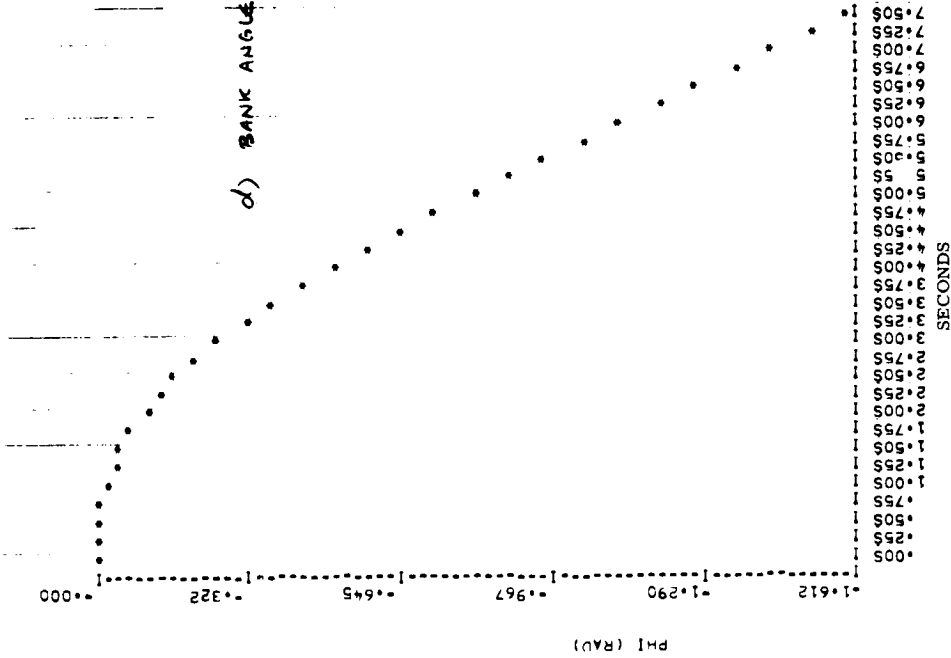


Figure 89. Continued

SECTION VIII

ROLL POWER REQUIREMENTS FOR LANDING

Roll power requirements for a delta wing orbiter are examined from the standpoint of meeting the intent but not the letter of flying qualities specifications. It is shown that by designing to intent, lateral control power requirements can be markedly reduced. It is believed this implies that significant increases in orbital payload can be achieved but quantitative data are not available for these estimates.

An implication of accepting the increase in orbital payload by this means would be the concurrent acceptance of mandatory automatic landings during periods of maximum specification wind turbulence. Pilots would be unable to perform the commonly employed "through the windshield" landings during these periods. Manual landings can probably be performed under high wind turbulence conditions by use of a display system driven by signals derived for fully automatic landings. It is conjectured that most of the time (when wind turbulence levels are moderate) commonly employed manual landing techniques can be used.

NASA specifications (ref. 13) for the landing approach condition require a 30-deg bank response in not more than 2.5 sec. The intent is to provide adequate control in the presence of atmospheric turbulence.

To meet the specification at 172 kt, the North American 134D orbiter (Figure 90) requires 20 deg/sec of aileron rate and 6 deg/sec rudder rate (Figure 3.9-9 of ref. 1).

Three deg/sec each of aileron rate and rudder rate are sufficient to hold the orbiter within 7 ft of the runway centerline, 3 deg of heading, and 2.5 deg of bank angle. This can be accomplished in the presence of specification side and rolling turbulence. This performance shows capabilities sufficient to meet the intent of the specification.

The synthesis, simulation, and the predominance of the analysis that are subsequently discussed were based on using a rolling gust model six times as severe as the specification model. An Erratum at the end of this section discusses the error.

Subsequent discussions, prior to the Erratum, deal primarily with results obtained using the excessive value of rolling turbulence. For this reason the dispersions are from 20 to 50 percent larger than previously enumerated.

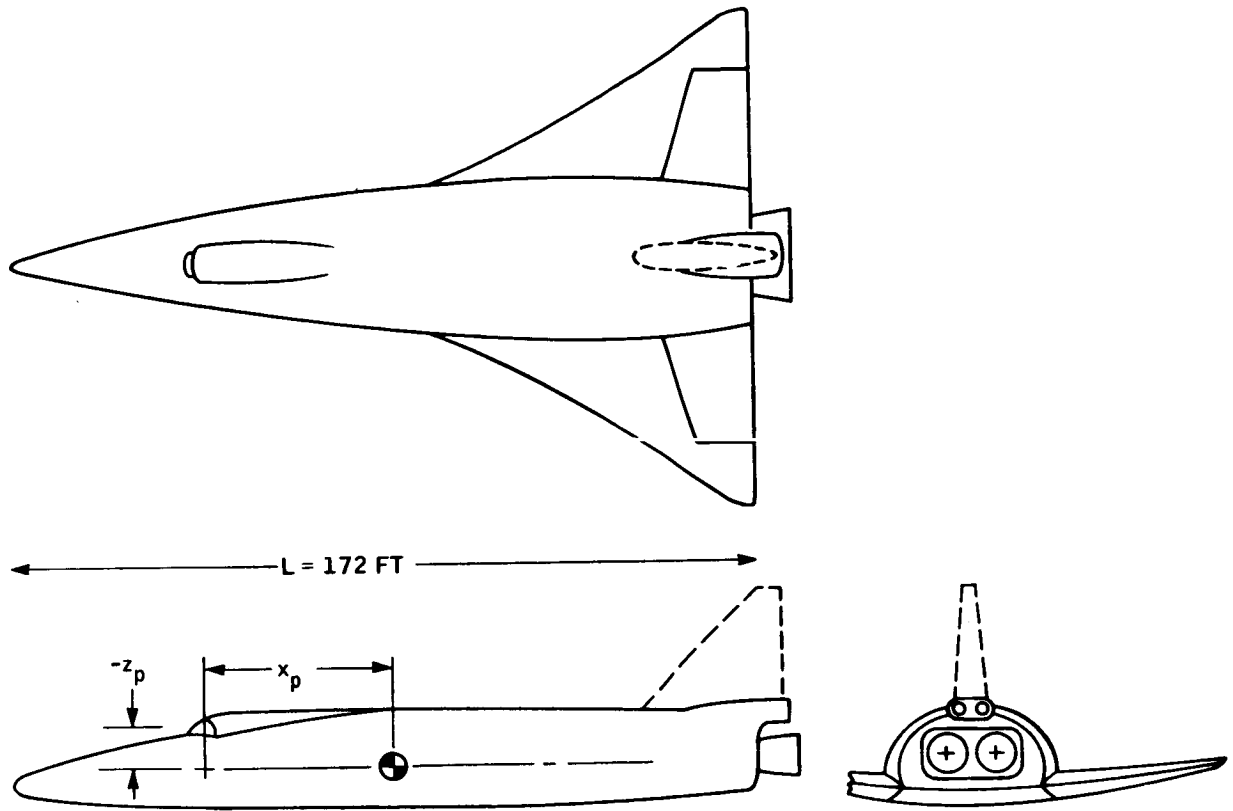


Figure 90. North American 134D Orbiter

NOMENCLATURE

p	Roll rate	rad/sec
r	Yaw rate	rad/sec
v	Lateral velocity	ft/sec
ϕ	Bank angle	rad
H	Heading	rad
y	Cross course displacement	ft
x_1, x_2, x_3	Side gust distribution states	ft/sec
x_4	Rolling gust distribution state	rad/sec
\tilde{v}, x	Side gust states	ft/sec, ft/sec ²
p_g	Rolling gust state	rad/sec
δ_a	Aileron deflection	rad
δ_r	Rudder deflection	rad
a_{cm}	Lateral acceleration at center of mass	ft/sec ²
a_y	Lateral acceleration at the pilot's station	ft/sec ²
x_p	Distance pilot is forward of center of mass	ft
z_p	Distance pilot is below center of mass	ft

TECHNICAL DISCUSSION

The objective here is to establish the feasibility of using small actuator rate capacities to attain the lateral control required. The scope of this study permits only the central question to be addressed and answered. Extensive experience at Honeywell in related studies makes it possible to predict that there will not be undue difficulties or expenses in reducing the results to practice. For example, the controllers synthesized and simulated here

require full-state measurement. The usual complement of sensors and filters is sufficient to extract essentially the same performance as is shown here.

The aircraft model (Appendix F) is set up for 172 kf, 600-ft altitude, -12-deg glide slope, and 14.5-deg angle of attack. The speed is the nominal approach speed for this vehicle and provides a direct comparison with the results previously cited. The 600-ft altitude is selected for two reasons. First, specification wind magnitude increases as the altitude decreases (pg. 51 of ref. 13 but it is within two percent of its maximum at this altitude. Second, the specification wind model is undefined at zero altitude (scale lengths go zero; pg. 52 of ref. 13) and is questionable at very low altitudes. At 600 ft the present model appears to be satisfactory. Subsequent studies should employ a better wind model for lower altitudes. Because of the heavy filtering by the aircraft, results obtained are expected to be quantitatively similar; results are probably much more dependent on turbulence level than on dynamics.

The state and response equations (from Appendix E) are:

$$\dot{x} = Ax + G_1 u + G_2 \eta$$

$$r = Hx + Du$$

where

$$x' = (x_1 \ x_2 \ x_3 \ x_4 \ x_5 \ x_6 \ x_7 \ x_8 \ x_9 \ x_{10} \ x_{11} \ x_{12} \ x_{13} \ x_{14} \ x_{15})$$

$$= (p \ r \ v \ \phi \ H \ y \ x_1 \ x_2 \ x_3 \ x_4 \ \tilde{v} \ x \ p_g \ \delta_a \ \delta_r)$$

$$u' = (u_1 \ u_2)$$

$$\eta' = (\eta_1 \ \eta_2)$$

$$r' = (\phi \ \dot{\phi} \ H \ \dot{H} \ y \ \dot{y} \ \delta_a \ \dot{\delta}_a \ \delta_r \ \dot{\delta}_r \ a_y \ \dot{a}_y)$$

and primes indicate transpose.

The objective is to design a controller that maintains acceptable dispersions of the aircraft with a minimum of control authority. Quadratic control theory methodology is used to accomplish the objective. Fifteen linear state controllers were synthesized; the results for five are presented here. These controllers are referred to as "quadratic" because they are determined from quadratic control theory methodology, the control laws are linear and the control laws are not quadratic.

Table 24 presents the control requirements and desires. Column 3 of Table 24 presents the maximum $1. \sigma$ values that would be tolerated from the controlled aircraft. They are judgements as to acceptable bounds, and are based on the assumption that values above $3. \sigma$ are unlikely to occur and that values less than $3. \sigma$ are acceptable (at touchdown).

For bank angle (ϕ) and cross-course displacement (y), for example, it is assumed that values less than 10 deg and 50 ft are acceptable. In any event, they are plausible guides, except for the lateral acceleration (a_y) at the pilot's station. This value was set sufficiently high such that it would not design the controller. It was hoped the resulting controller would not discomfort the pilot too much. As expected, the controller that protects the aircraft gives a good ride.

The objectives set in column 3 of Table 24 are the results of rough judgments. Subsequent to the completion of this study, Wylie (ref. 32) made a more careful appraisal of touchdown limits which are summarized (with liberties) in column 2. They are more restrictive than those of column 3 but they can be met with control rates of about 3 deg/sec.

Column 4 of Table 24 presents maximum desired rms responses. Column 5 gives the 1σ responses for the "baseline quadratic controller". This narrative account is historically correct. The last column of Table 24 presents estimates of responses for the current wind model.

The precision achieved by the baseline quadratic control might be attributed to a high band pass which would be guaranteed to excite flexure neglected in the analyses; however, this is not the case.

Table 25 lists the open and closed-loop roots for quadratic control. Those roots that can be affected by control are also drawn in Figure 91. The closed loop system is more placid than the open loop system.

Columns 6 and 7 present the 1σ responses with just the rolling gusts and with side gusts, respectively. They are of the same order of magnitude.

Columns 9 and 10 display the control gains for the baseline quadratic controller. The baseline quadratic controller is not the ultimate; it is good enough for present purposes.

Tables 26 and 27 compare the performance and the control gains for five quadratic controllers.

A comparison between columns 2 and 3 of Table 26 shows that in the performance region of the baseline controller, performance achieved is approximately linear with surface rate requirements. In marked contrast is the performance achievable with high surface rates; comparison of columns 2 and 6. In this latter respect, comparisons between columns 2, 4, 5 and 6 show that performance

Table 24. Baseline Quadratic Controller

Response State (1)	Wyllie Max RMS (2)	Required Max RMS (3)	Desired Max RMS (4)	Achieved RMS (5)	Rolling Wind RMS (6)	Side Wind RMS (7)	System State (8)	Aileron Channel Gain (9)	Rudder Channel Gain (10)	Estimate of Achieved RMS With Corrected Roll Gust Model
ϕ (rad)	0.0100	0.058	0.029	0.02005	0.01690	0.01079	P	0.1230	0.03661	0.011
$\dot{\phi}$ (rad/sec)	0.0058			0.01476	0.01181	0.00886	r	0.9569	1.309	0.009
H (rad)	0.0175	0.077	0.0233	0.01434	0.00389	0.01381	v	0.003514	0.006636	0.014
\dot{H} (rad/sec)	0.0058			0.00711	0.00194	0.00684	ϕ	0.05668	-0.1321	0.007
y (ft)	13.2	16.7	16.7	2.965	2.223	1.961	H	1.742	2.504	2.0
\dot{y} (ft/sec)	5.00			1.112	0.7745	0.7985	y	0.001405	0.001412	0.80
δ_a (rad)		0.174	0.087	0.02935	0.02605	0.01353	x_1	-0.002000	-0.001620	0.014
δ_a (rad/sec)		0.116	0.058	0.03441	0.0287	0.01898	x_2	0.0001879	0.0001809	0.019
δ_r (rad)		0.087	0.087	0.02767	0.02692	0.00640	x_3	0.0004218	0.0004028	0.007
$\dot{\delta}_r$ (rad/sec)		0.116	0.116	0.02978	0.02919	0.0058	x_4	-0.04189	-0.04012	0.007
a_y (ft/sec ²)		21.3	0.837	0.7309	0.4575	0.5700	\tilde{v}	-0.001435	-0.0008202	0.58
\dot{a}_y (ft/sec ³)				5.551	3.351	4.425	x	-0.001042	0.001447	4.5
							p_g	-0.2470	-0.2969	
							δ_a	0.6738	-0.06085	
							δ_r	-0.06085	0.5594	

Table 25. Baseline Quadratic Controller System Roots

Open Loop			Closed Loop	
Real	Imaginary	Association	Real	Imaginary
-0.2370		\tilde{v}, x	-0.2370	
-0.2390			-0.2390	
-0.3208		p_g	-0.3208	
-3.8780		x_1	-3.8780	
-3.8250	10.609	x_2, x_3	-3.8250	10.6009
-7.4110		x_4	-7.4110	
-6.0000		δ_a	-1.5001	0.0582
-6.0000		δ_r	-4.4403	0.2557
-1.0350		Roll Subsidence	-3.3877	0.6185
-0.1629	1.4516	Dutch Roll	-0.6494	1.7162
+0.0062		Spiral		
-0.0000	0.0001	H, y		

Table 26. Comparative Performance of Alternative Quadratic Controllers

Response States	1	2	3	4	5	6
		RMS Responses Baseline Controller	RMS Responses Low Gain Controller	RMS Responses High Gain Aileron Channel	RMS Responses High Gain Rudder Channel	RMS Responses High Gain Controller
ϕ (rad)		0.02005	0.02639	0.02205	0.01754	0.01766
$\dot{\phi}$ (rad/sec)		0.01476	0.02338	0.02452	0.01731	0.01820
H (rad)		0.01434	0.01465	0.01413	0.01548	0.01350
\dot{H} (rad/sec)		0.00711	0.00782	0.00808	0.00830	0.00675
y (ft)		2.965	3.948	2.121	2.362	1.700
\dot{y} (ft/sec)		1.112	1.382	0.862	0.922	0.702
δ_a (rad)		0.02935	0.02651	0.05083	0.02154	0.0401
$\dot{\delta}_a$ (rad/sec)		0.03441	0.02373	0.4331	0.02693	0.339
δ_r (rad)		0.02767	0.02818	0.02452	0.02992	0.02650
$\dot{\delta}_r$ (rad/sec)		0.02979	0.02536	0.02549	0.2864	0.1950
a_y (ft/sec ²)		0.7309	0.7182	1.263	0.6631	1.020
\dot{a}_y (ft/sec ³)		5.551	5.216	9.01	4.953	7.29

Table 27. Gain Matrices

Response State	Baseline		Low Gain		High Gain Aileron Channel		High Gain Rudder Channel		High Gain	
	Aileron Channel Gain	Rudder Channel Gain	Aileron Channel Gain	Rudder Channel Gain	Aileron Channel Gain	Rudder Channel Gain	Aileron Channel Gain	Rudder Channel Gain	Aileron Channel Gain	Rudder Channel Gain
P	0.1230	0.03661	0.05120	0.02739	6.438	0.01881	0.1156	3.995	6.205	1.171
r	0.957	1.309	0.5563	0.8544	47.60	1.056	0.7258	98.2	34.60	74.45
v	0.003514	0.006636	0.001641	0.003660	0.4302	0.00585	0.002321	0.5389	0.3578	0.4888
ϕ	0.0567	-0.1321	0.02998	-0.03576	0.7652	-0.1498	0.0857	-14.27	2.631	-16.82
H	1.742	2.504	0.8526	1.400	151.3	2.128	1.273	214.6	124.9	180.5
y	0.001405	0.001412	0.0006584	0.000747	0.1374	0.001128	0.001123	0.1377	0.1230	0.1124
x_1	-0.002000	-0.001620	-0.0009886	-0.001053	-0.09038	-0.001235	-0.001697	-0.1377	-0.0752	-0.0898
x_2	0.0001879	0.0001809	0.0000959	0.0001186	0.01007	0.0001406	0.0001553	0.01445	0.00834	0.01002
x_3	0.0004218	0.0004028	0.0002138	0.0002636	0.02358	0.0003125	0.0003493	0.03221	0.01973	0.02232
x_4	-0.04189	-0.04012	-0.02201	-0.02686	-1.873	-0.03104	-0.03465	-3.169	-1.492	-2.143
\tilde{v}	-0.001435	-0.0008202	-0.000788	-0.000431	-0.0581	-0.0004925	-0.001230	-0.1038	-0.0512	-0.0626
x	-0.001042	-0.001447	-0.0006192	-0.000841	-0.0663	-0.001154	-0.000772	-0.1225	-0.0507	-0.1006
p_g	-0.2470	-0.2969	-0.1475	-0.2134	-10.84	-0.2367	-0.1973	-20.08	-8.08	-14.22
δ_a	0.674	-0.06085	0.8021	-0.0660	-1.925	-0.000623	0.6912	-8.62	-1.917	-0.01775
δ_r	-0.06085	0.5594	-0.06600	0.6781	-4.361	0.588	-0.001232	-19.65	-0.01775	-19.60

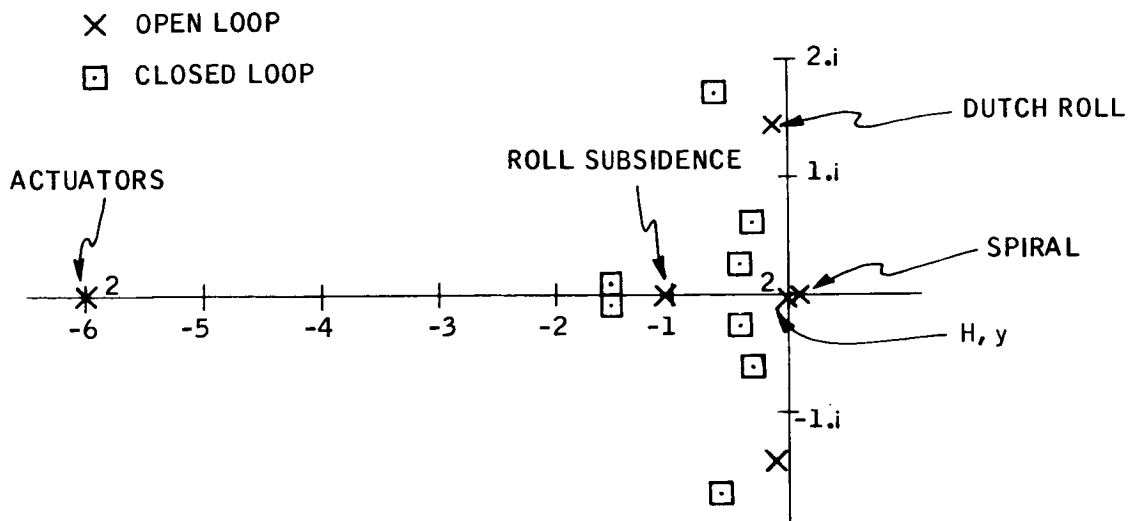


Figure 91. Baseline Quadratic Controller System Roots

comes dearly at the expense of increased surface rates - singly or in combination. Columns 4 and 5 further show that the effectiveness with increased rate capabilities is about equal for rudder and ailerons.

The discussion thus far has dealt with linear controllers on linear representations of the shuttle. Minimal control power can probably be achieved by designing so that saturations occur but do not cause disastrous divergences.

The rule of thumb is that values beyond 3σ occur so infrequently that they can usually be neglected. In particular, it would generally be accepted that surface rate saturations set at 3σ values would be safe; i.e., from Table 24 0.1 rad/sec for the baseline controller. As surface rate saturations limits are reduced, it is to be expected the linear quadratic controller would become unstable. The system was analog simulated to obtain an estimate as to how far the surface rate limits could be reduced before saturation instabilities become intolerable.

Figure 92 shows the response of the baseline quadratic controller without surface saturation limits. The left strip shows the sidestep response in the absence of winds. The right strip presents the capability of the controller for maintaining course in specification winds.

The sidestep response is presented for two reasons: It helps explain the good performance achieved and it provides guides for control system design.

The sidestep response is deadbeat in 8 sec (the smallest visible division is 1 sec; the smallest distinguishable division is 5 sec). This is a relatively short response time for a loop this far out. The good control quality achieved is attributed in part to the good sidestep performance achieved.

Twenty-five feet of sidestep is reasonable for this particular flight condition. Surface deflections, bank angle, and heading excursions are reasonably small. Surface rates are larger than desired but performance would not suffer badly with saturation limits of 3 deg/sec. For 250 ft of sidestep (which might be required at the same dynamic pressure and say 6000 ft altitude) the maneuver would be quite abrupt. This simply implies either signal limiting or gain scheduling must be employed at large distances from landing. Under these latter conditions large sidestep requirements may be necessary.

The right strip of Figure 92 shows the controller without saturation limits in specification winds. Extreme values are close to 3σ (the 1σ values are presented in column 5 of Table 24). The airplane is nicely controlled. There would be no problem in getting down to the ground. The maximum displacement from the runway centerline (y) is only 6 ft. Heading (H) displacements and bank angle (ϕ) are less than 3 deg and 3.5 deg. The maximum lateral acceleration (a_y) at the pilot's station is maintained below 2.5 ft/sec^2 . All these are attained using less than 7.5 deg/sec of aileron rate (δ_a), 5.5 deg of aileron (δ_a), 7.5 deg/sec of rudder rate, and 5.5 deg of rudder (δ_r).

For Figure 93 there are both aileron rate and rudder rate saturation limits of 2.86 deg/sec. Control is unacceptable but it is clear the system is at the edge of acceptability. For the first 370 sec responses are nicely controlled. Extreme values are 60 percent larger than without surface saturation limits. At 370 secs the system breaks into a limit cycle oscillation.

With larger values on the surface rate limits the system remains divergence free.

ERRATUM

After the work for this section of the report had been accomplished and this section drafted, an error was discovered. The effect of the error was the attachment of excessive importance to the rolling gust contribution. This implies the results just presented are unduly pessimistic.

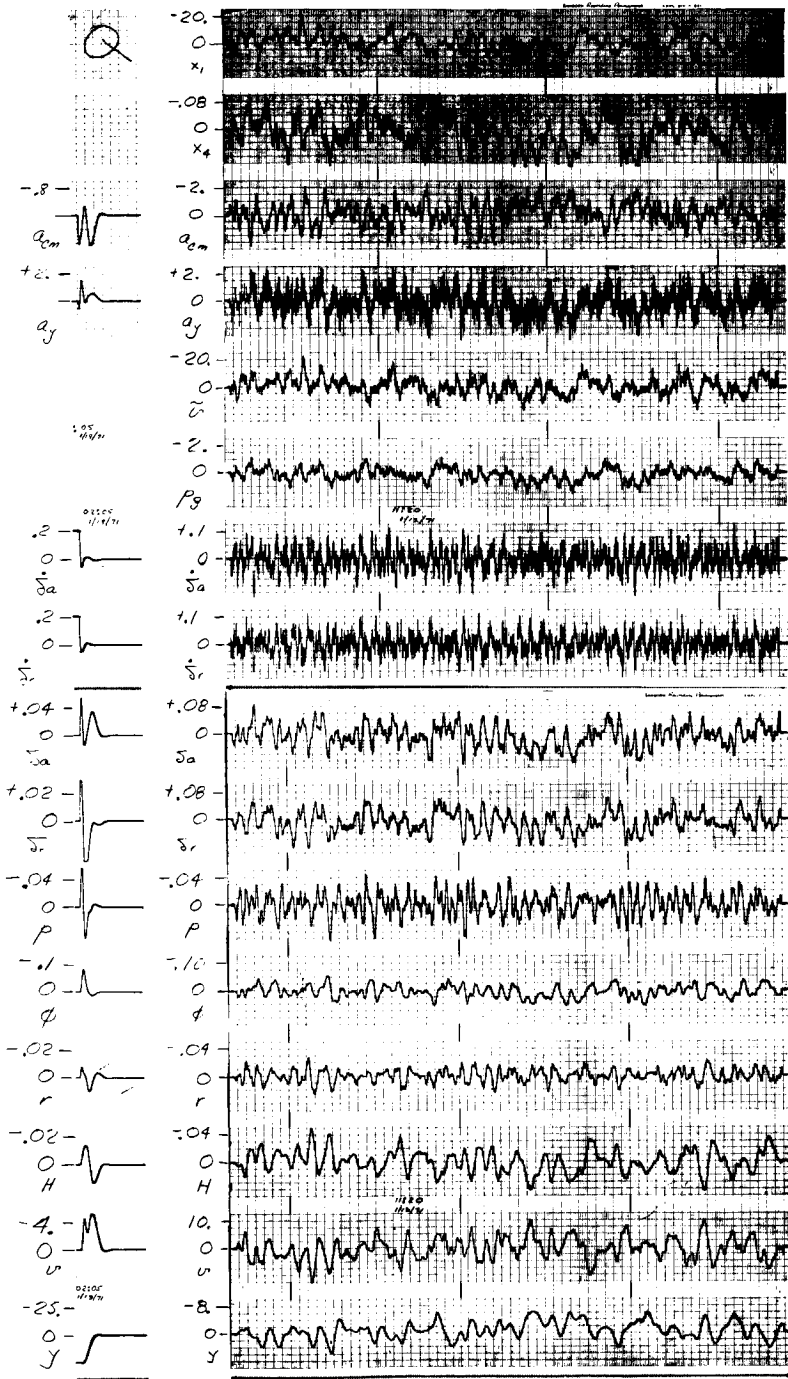


Figure 92. Q Controller

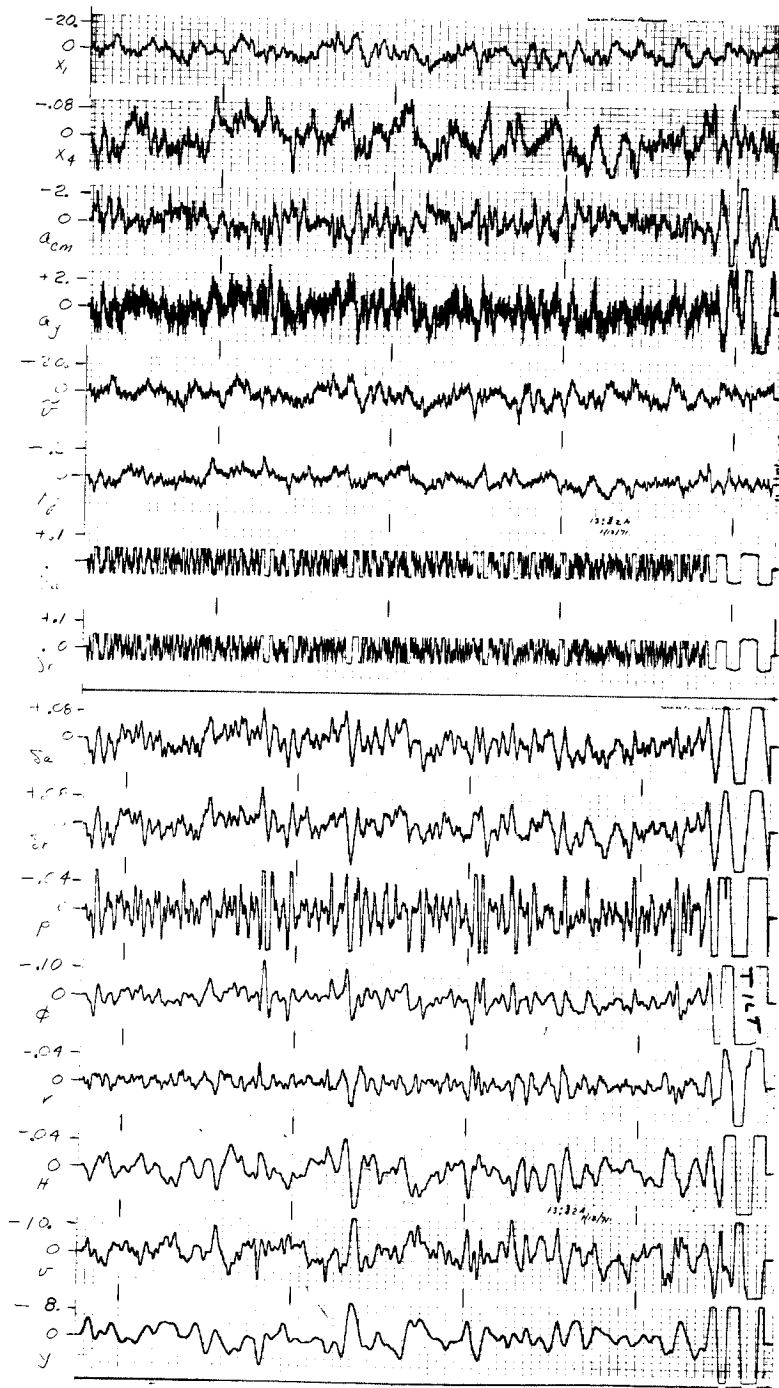


Figure 93. Q Controller $|5a| \leq 0.05$ $|\delta r| \leq 0.05$

From Appendix F the rolling gust model is

$$\dot{p}_g = \frac{\pi}{4} \frac{V}{b} p_g + \frac{\pi}{4} \frac{\sigma_w}{b} \sqrt{\frac{V}{L_w}} \sqrt{0.8 \left(\frac{\pi}{4} \frac{L_w}{b} \right)^{1/3}} \eta_2$$

For the flight condition investigated the differential equations that were simulated and should have been simulated are, respectively,

$$\dot{p}_g = - 0.3208 p_g + 0.0346 \eta_2$$

$$\dot{p}_g = - 1.93 p_g + 0.0346 \eta_2$$

The direct effects of this error are twofold. The rms value for the wind used was $1.93 \div 0.3208 = 6.02$ times the value it should have been. Furthermore, this excessive wind power was "concentrated" over a sixth the frequency band that it should have been.

The overall effect of the error on lateral control power requirements is to reduce them, i.e., the results previously presented are conservative.

SECTION IX

UNPOWERED SHALLOW FINAL LANDING APPROACHES

Shallow final approaches are considered qualitatively. The objective is to present an alternative to the steep path landing methods being investigated. The shallow approach alternative would provide increased orbital payloads (through reduced vehicle weights), lower landing speeds, and shorter field requirements. On the deleterious side are increased difficulties for manual control and a slight (but insignificant for the shuttle application) increase in control complexity. Synthesis of the controls for shallow approaches is well within the state of the art.

Constant-speed shallow approaches typical of conventional aircraft practice are not possible for unpowered orbiter landings. One compromise accepts steep approaches (steeper than 10 deg) at constant speed and a flareout start starting near 600 ft. altitude. For steep approaches the vehicle is powered by potential energy. An alternative is the shallow approach initiated at high speed and terminating after a conventional flareout at touchdown near stall speed. For shallow approaches the shuttle is powered by kinetic energy.

Sperry (ref. 17), under contract to NASA Ames, is investigating the steep approach. They have shown that they can rely on characteristics inherent in the vehicle to maintain speed control on the approach path and thus need only provide height control. Air Force flight test pilots (ref. 18) at Edwards have made strong recommendations for the steep approach option for shuttle based on tests using F-111 and B-52 aircraft. Neither the instrumentation nor control for these flight tests was adequate for good speed control.

NASA MSC (ref 19) has conducted manned simulation studies of unpowered landing approaches for a straight-wing orbiter configuration. The trajectories employ steep approach paths quite analogous to those used by Sperry.

Honeywell (ref. 1) in its contribution to the Phase B Shuttle program is utilizing the steep approach path for unpowered orbiter landings.

There are many good things to be said for the steep approach path. The inherent speed stability with the concomitant reductions in pilot workload and/or the necessity for automatic speed control have already been cited. The resulting high airspeeds increase control effectiveness to provide easier tasks for both manual and automatic control. The higher airspeeds also make it easier to meet flying qualities specifications that are based on manual handling capabilities.

Acceptance, however, of steep approach paths not only gives away significantly lower touchdown speeds naturally provided by the orbiter designed, but it enforces larger brake weights on the orbiter to dissipate the larger energies.

The technical survival of shuttle depends critically on shaving a few pounds here and there to achieve acceptable payload-to-takeoff weight ratios. Shallow approach paths offer another potential that needs to be evaluated against shuttle requirements.

The shallow approach for shuttle landings is not being investigated. It should first be studied with the objective of achieving acceptable touchdown characteristics for a typical shuttle craft. Automatic control, airplane control, and landing gear weight change increments need to be determined. These weights would provide a significant part of the tradeoff for steep versus shallow approach.

SECTION X

CONCLUSIONS AND RECOMMENDATIONS

The "Development of Control Systems for Space Shuttle Vehicles" study is completed with a discussion of results and with a listing of recommendations for future efforts. Our objectives were to identify requirements and to define control logics. Our results indicate the successes in meeting objectives. The recommendations show our deficiencies in meeting all of our desires.

RESULTS

Results are summarized corresponding to the ordering of mission phases.

Boost Pitch

Eight conventional controllers were synthesized and their performance evaluated. Four of them meet control requirements.

Two superior performance quadratic controllers were synthesized. They were not reduced to practical form.

Design guides applicable to conventional synthesis of high performance controllers for Saturn V class vehicles were shown to be less applicable to shuttle.

Boost Lateral

A controller that utilized ailerons in addition to thrust vector control was synthesized and shown to meet control requirements.

Five thrust vector controllers were synthesized. For each the roll gimbal demands are excessive and yaw gimbal deflections are marginal. The two load relief controllers provide direction for synthesizing successful controllers.

Rolling gusts are of no importance. Side wind is the driver.

Orbiter Injection

Fixed gain controllers were synthesized for a two-engine and three-engine orbiter. Control logics are simple and the performance is adequate.

Orbiter Entry

Control logics are presented for entry control of a single-tail delta wing orbiter. Control performance is satisfactory.

Pad Abort

Two methods were determined for successful achieving collision free launches of a straight wing and of a delta wing orbiter.

Inflight Abort

The thrust vector control system was modified to provide satisfactory control throughout an entire abort trajectory.

The ACPS fuel consumption was 60 percent over the nominal allowance. This would require either an increased ACPS propellant budget of 3000 lbs. or redesign of the control system to be more efficient in its propellant utilization.

A unique fuel sloshing problem was identified.

Subsonic Lateral Handling Qualities

A controller was synthesized to enforce a straight wing orbiter to meet level 1 handling qualities requirements with rudder and ailerons.

Level 3 handling qualities were enforced with rudder and spoiler ailerons. This is highly significant because the spoiler rate capability is extremely small. It implies the spoilers can be used as a backup.

Roll Power Requirements

A controller was synthesized to meet the intent but not the letter of NASA specifications. By designing to intent aileron rate and rudder rate capabilities can be markedly reduced. This implies a saving in weight and increased payload.

Shallow Approach Landing

A recommendation was developed to investigate shallow approach landings for unpowered orbiters. There are implications that orbital payloads could be increased by recognizing again that shuttle is not just another airplane. Control design would be the intent rather than the specification.

RECOMMENDATIONS

The results show that further efforts are necessary to remove deficiencies, to eliminate unknowns, and to provide increased payload capabilities. Eight studies are recommended:

- Lateral launch thrust vector control
- Practicalized quadratic launch pitch control
- Abort control of boosters and orbiters
- Maximum orbital payload capability landings
- Handling qualities controllers for booster subsonic flight
- Abort separation
- Effectiveness of alternative gimbal slewing arrangements and ailerons for lateral control during launch
- Control of flexure and fuel sloshing.

The necessity and the objectives for each of these investigations is now discussed.

Roll gimbal demands were shown to be excessive and yaw gimbal capabilities were shown to be marginal for the controllers evaluated. Rolling moment due to sideslip generates the requirement. This suggests that controllers that reduce sideslip during the high dynamic pressure flight will reduce gimbal requirements. Indeed, it was shown that load relief controllers do reduce gimbal requirements. Extrapolating the results from the pitch axis investigation strongly indicates that quadratic control synthesis yields marked improvements. Hence, these controllers should be synthesized, evaluated, and practicalized. Success would yield important benefits to the shuttle program. The solution is more effective than adding ailerons or allowing the vehicle to roll.

The quadratic controllers synthesized for control of the pitch axis during boost were shown to yield markedly better performance than the conventional controls. They require measurement of the full state and also require mean wind biasing. Mechanization requirements are excessive. These controllers need be simplified as much as possible without the loss of essential control performance.

This will provide two benefits. It will define a better control logic. Secondly, it will provide the insight for design of controllers by conventional techniques. Control requirements will be more easily defined.

The abort studies of the twin-engine, single-tailed delta wing orbiter revealed seven unique control requirements. Solutions were provided for five. Peculiar fuel sloshing and excessive ACPS fuel consumption were not resolved. These results were achieved for control over a single abort trajectory. Both the booster and the orbiter need controls designed for satisfactory operation throughout the flight envelope.

Most of the landing investigations consider the shuttle craft to be ordinary airplanes and are designing the landing control systems accordingly. The consequence of this assumption may inflict severe orbital payload penalties due to excessive requirements on the shuttle craft. A good case was made for increasing payload by reducing surface rate requirements. Plausible arguments were presented for reducing vehicle weights by landing closer to the stall point. Both of these items need be explored more completely to assure they can be made operationally reliable. The potential gains in orbital payload demand it.

Lateral handling qualities capabilities of a straight wing orbiter were shown to be adequate. Both pitch and lateral capabilities of a booster need be determined in a similar manner to provide satisfactory manual control.

Our studies did not include abort separation of the vehicles. Collision-free separation is mandatory.

The lateral gimbal slewing arrangement considered in this report provides uncoupled roll and yaw torques. Others use slewing methods that are simpler but the roll and yaw torques are coupled. The primary desire is to achieve more roll authority. Complexity is also an issue. Since roll authority is the issue, the use of ailerons should be simultaneously pursued to develop a trade-off.

Finally, but by no means the least of the requirements, is to include the effects of flexure and fuel sloshing, to determine their significance, and if necessary to provide active control over these effects.

REFERENCES

1. Anonymous, "Guidance Navigation, and Control System: Flight Control Analysis," Honeywell Document 21602-1.3.3.7.3, Circa December 1970.
2. Ellison, D. E. , "USAF Stability and Control Datcom", Air Force Flight Dynamics Laboratory, Wright-Patterson Air Force Base, Ohio, 1970.
3. Anonymous, "Study of Automatic and Manual Terminal Guidance and Control Systems for Space Shuttle Vehicles," First through Fifth Monthly Progress Reports to NASA ARC under Contract NASA2-5804 by Sperry Flight Systems Division; April, May, --- 10 August 1970.
4. Smith, Herbert E. , Jr. , and Walter, Parry M. , "Project Apollo Manned Simulation of a Straight Wing Orbiter Unpowered Approach and Landing", MSC-IN-EG-70-34, NASA MSC, 30 September 1970.
5. Vaughan, William W. , "Interlevel and Intralevel Correlations of Wind Components for Six Geographical Locations," NASA TN D-561, December 1960.
6. Skelton, G. B. , et al. , "Final Technical Report: Design of a Load-Relief Control System," Honeywell report 12-13 FR1 for NASA MSFC, Contract NAS8-20155, St. Paul, Minnesota, 9 May 1966.
7. Harvey, C. A. , et al. , "Application of Optimal Control Theory to Launch Vehicles," Honeywell report 12073-FR1 for NASA MSFC Contract NAS8-21063, 1968.
8. Harris, Robert D. , "Analysis and Design of Space Vehicle Flight Control Systems, Volume XIV -- Load Relief," NASA CR-833, August 1967.
9. Edinger, L. D. , "Saturn V/Voyager Load Relief Study," NASA CR-61956, March 1968.
10. Anon. , "NAS8-25181 Reference Data Package," supplied by MSFC.
11. Etheridge, Orval, "Preliminary Reference Trajectories of the MSFC In-house Space Shuttle," MSFC S and E-Aero-GT-5-70, February 4, 1970.

12. Hoernor, S. F., Fluid-Dynamic Drag, published by the author, 1965.
13. Staff of NASA Flight Research Center, "Preliminary Flying Qualities Specifications for Space Shuttle Vehicles," January 28, 1970.
14. Stein, G. and Henke, A. H., "A Design Procedure and Handling-Quality Criteria for Lateral-Directional Flight Control Systems," AFFDL-TR-70-152, October 1970.
15. Anon., "Study of Automatic and Manual Terminal Guidance and Control Systems for Space Shuttle Vehicles," First through Eighth Monthly Progress Reports to NASA ARC under Contract NASA2-5804 by Sperry Flight Systems Division; April, May, ---, 10 November 1970.
16. Schofield, B. L., Richardson, D. F., and Hoag, P. C., "Terminal Area Energy Management, Approach and Landing Investigation for Maneuvering Reentry Vehicles Using F-111A and NB-52B Aircraft," Technology Doc. No. 70-2, Air Force Flight Test Center, June 1970.
17. Smith, Herbert E., Jr., and Walter, Parry M., "Project Apollo Manned Simulation of a Straight Wing Orbiter Unpowered Approach and Landing", MSC-IN-EG-70-34, NASA MSC, 30 September 1970.
8. McAnnally, R. C., "Preliminary Reference Trajectories of the MSFC Inhouse Space Shuttle," MSFC, February 4, 1970.
9. Thelander, J. A., FDL-TDR-64-70, "Aircraft Motion Analysis," March 1965 (AD 617 354)
0. Nelson, F. R., Koerner, W., and Trudel, R. E., BUAER Report AE-61-4II, Dynamics of the Airframe, September 1952.
1. Edinger, L. D., Hughes, T. W., and Pluimer, M. J., "Data Base Report for Saturn/Voyager Load Relief Study," NASA MSFC Contract NAS8-21171, 30 January 1968.
2. Rheinfurth, Mario H., "Control-Feedback Stability Analysis," Report No. DA-TR-2-60, Army Ballistic Agency, Redstone Arsenal, Alabama, January 11, 1960; AD 232447.
23. Miles, John W., The Potential Theory of Unsteady Supersonic Flow, Cambridge University Press, 1959.
24. Thomson, William Tyrrell, Introduction to Space Dynamics, John Wiley and Sons, Inc., 1962.
5. Anon., "NAS8-25181, Reference Data Package," supplied by MSFC.

26. Anon. , "Simplified Flight Loads Analysis Program," Boeing publication circulation 1964.
27. Space Shuttle Aerodynamics Group, "NR Space Shuttle Program Aerodynamics Design Data Book: Volume 1, Straight-Wing Orbiter," Report 2.1.5-13000-00, SD 70-414, Space Division, North American Rockwell, August 1970.
28. Graham, K. D. , "Kinematic Model for Fire Control," MR 10757, August 7, 1968.
29. Sokolosky, O. M. , "SSV Aerodynamic Rotary Derivatives for the Delta Wing Orbiter (Aero Design Data Book II-DB 2.1.5-13000-10)," NAR, August 31, 1970.
30. Ehlers, H. L. , "Aero Data for 134D Vehicle."
31. Anon. , "Aileron Effectiveness in Roll," NAR 11 August 1970.
32. Wyllie, C. , "Unpowered Orbiter Touchdown State Limits," Honeywell Internal Memorandum, 29 January 1971